Second Report to

The National Science Foundation

AN ENGINEERING FEASIBILITY STUDY OF AN IONOSPHERIC TECHNIQUE TO IMPROVE TSUNAMI WARNING SYSTEMS

Grant Numbers: GI-34973 and ATA 72-03505

Starting Date: June 15, 1972

Ending Date: May 31, 1976

Reporting Date: September 30, 1976

Name and Address of Institute: University of Hawaii
Honolulu, Hawaii 96822

Co-Investigator:

Correspondent for Foundation Mailing

Kazutoshi Najita

Kazutoshi Najita, Professor
Department of Electrical Engineering
Telephone: (808) 948-7249

50272-101

REPORT DOCUMENTATION PAGE	1. REPORT NO. NSF/RA-761702	2.	3. Recipient's Accession No. PB298987

4. Title and Subtitle
Engineering Feasibility Study of an Ionospheric Technique to Improve Tsunami Warning Systems

5. September 30, 1976

6.

7. Author(s)
K. Najita

8. Performing Organization Rept. No.

9. Performing Organization Name and Address
University of Hawaii
Department of Electrical Engineering
Honolulu, Hawaii 96822

10. Project/Task/Work Unit No.

11. Contract(C) or Grant(G) No.
(C)
(G) GI34973
ATA7203505

12. Sponsoring Organization Name and Address
Engineering and Applied Science (EAS)
National Science Foundation
1800 G Street, N.W.
Washington, D.C. 20550

13. Type of Report & Period Covered

14.

15. Supplementary Notes

16. Abstract (Limit: 200 words)

Appropriate interpretation of ionospheric oscillation recordings as a method of predicting generation of tsunami is reported. Such oscillations were observed following the 1968 earthquake in Tokachi-Oki, Japan. They were explained in terms of upward propagating atmospheric acoustic waves generated at the surface of the earth by vertical ground movement during passage of Rayleigh waves from the earthquake. The current investigation presents basic data used in subsequent analyses and calculations; describes the method used to calculate the group velocity for oceanic Rayleigh waves from Dopplergrams and compares these calculations with results reported in the literature; and considers a possible method for inferring the source mechanism of the earthquake from observation of ionospheric motions. The method was applied to earthquakes which occurred in 1968 and 1969. No firm conclusions could be drawn as more accurate information is needed on the relationship between initial phase and source mechanisms. Extensive graphs, tables, equations and references are included.

17. Document Analysis a. Descriptors

Earthquakes
Ionosphere
Ionospheric disturbances
Tsunamis
Seismic waves
Forecasting
Rayleigh waves
Doppler systems

b. Identifiers/Open-Ended Terms

Ionospheric oscillation
Tokachi, Japan
Earthquake mechanisms
Doppler data

c. COSATI Field/Group

18. Availability Statement
NTIS

19. Security Class (This Report)

20. Security Class (This Page)

21. No. of Pages
210

22. Price
A10 - A01

(See ANSI-Z39.18) See Instructions on Reverse

OPTIONAL FORM 272 (4-77)
(Formerly NTIS-35)
Department of Commerce

CAPITAL SYSTEMS GROUP, INC.
6110 EXECUTIVE BOULEVARD
SUITE 2[illegible]
ROCKVILLE, MARYLAND 20852

PREFACE

This is the second report to the National Science Foundation AENV - RANN on a research program designed to establish the feasibility of a tsunami warning system based on data obtained using an HF Doppler technique which measures changes in the upper atmosphere caused by fast Rayleigh waves from a tsunamigenic earthquake. The program was supported by Foundation grants GI 34973 and ATA 72 - 03505.

The first report to the Foundation, dated July 15, 1973, discussed the present Pacific Tsunami Warning System and the need for additional information in order to make the present warning system more effective. It discussed the possible improvements to the tsunami warning system if the source mechanism of the earthquake could be determined and how this information might be obtained by monitoring the ionospheric signatures of the Rayleigh waves generated by the tsunami generating earthquakes. It further described and reported on the design and development of the instrumentation needed to obtain the recordings of these ionospheric signatures in a form useful to the tsunami warning system personnel.

Improvements on the initially-designed system have been carried out since the first report. These improvements have been to make the instrumentation more reliable and to prevent false triggering and recording of data. Although these problems are not trivial and are very time consuming in the development stages, they will not be discussed here because of the technical details involved and because they do not alter the fundamental principles of the instrumentation. Instead, a separate manual for the instrumentation has been prepared and is being updated for internal use.

This report describes the studies carried out to better interpret the ionospheric Doppler recording. The study covers the acoustic waves from the launch point to ionospheric heights through the atmosphere. It reports on the different aspects of determining the accuracy to which one could determine the propagation path and the travel time for these long period acoustic waves. It describes the work carried out thus far on the determination of the initial phases of the Rayleigh waves and points out the extreme accuracy required of the recording and analysis of the data.

ACKNOWLEDGMENTS

This work is the result of the joint effort of many people, some of whom are directly a part of the project and others with whom we have interacted. I wish to acknowledge the participation of: Paul C. Yuen and Augustus S. Furumoto, senior members on the project; Paul F. Weaver, faculty associate; Gaylord R. Miller, Director, Joint Tsunami Research Effort; Tom Soholowski, geophysicist at the Honolulu Observatory; Milton Y. Cha, research assistant; Yinn Nien Huang, Wayne Suenaga, and Lan Pui Wong, graduate research assistants; and Craig Fujimoto, Chi K. Lau, Clyde Kawakami, Paul Matsumoto, and Ralph Yamamoto, undergraduate student laboratory assistants. In addition, I wish to acknowledge the support of the students on the project: Alvin Agena, Jean Chikuami, Keith Ebisu, Janis Fujitani, Dennis Hara, Marjorie Higa, Sandra Ho, Ronald Ibaraki, Brian Kutara, Gajendra Mishra, Earl Yoshino, and Karen Watanabe.

Communication with Katsuyuki Abe, Ari Ben-Menahem, James N. Brune, and Hiroo Kanamori was very beneficial in the evaluation of our results.

TABLE OF CONTENTS

I. INTRODUCTION

Shortly following the occurrence of the May 16, 1968 earthquake in Tokachi-Oki, Japan, the HF Doppler system operated by the Radioscience Laboratory detected fairly rapid oscillatory changes in the radio reflection heights in the ionosphere. These oscillations were explained in terms of upward propagating atmospheric acoustic waves generated at the surface of the earth near the sub-ionospheric point by the vertical ground movement during the passage of the Rayleigh waves from the earthquake (Yuen, et al., 1969). Similar observations were also recorded for the Kurile Island earthquake of August 11, 1969 (Weaver, et al., 1970), and the Kamchatka earthquake of November 23, 1969. This report describes the work carried out to obtain a thorough understanding of the processes involved in the propagation of the released energy from the earthquake's epicenter to the ionosphere.

The major objective of this study focuses on the question of whether one can predict the generation of a tsunami by appropriate interpretations of the recordings of the ionospheric oscillations. This would imply understanding the source mechanism of earthquakes and in particular the initial phase of the epicentral ground motion. In turn, this requires the determination of the propagation time and path of the acoustic waves in the atmosphere. A check on the accuracy of these calculations is obtained by calculating the corresponding group velocities of the Rayleigh waves and comparing them with the reasonably well established values obtained by seismologists.

This report is divided into three parts. The first describes the basic data used in subsequent analyses and calculations. These are: the height in the ionosphere probed by the HF Doppler Array; a collection of Rayleigh wave group velocities obtained from seismogram data and reported in the literature; and the ray path for the atmospheric acoustic waves. The second part describes the method used to calculate the group velocity for oceanic Rayleigh waves from the Dopplergrams. The results from these calculations are compared with the results reported in the literature. The last part is concerned with a possible method for inferring the source mechanism of the earthquake from observation of ionospheric motions. The method is applied to the 1968 and 1969 earthquakes. A discussion of the results is presented.

For simplicity in this report, atmospheric acoustic waves or acoustic-gravity waves with frequencies greater than the acoustic cutoff frequency are called "infrasonic waves", while those generated specifically by the Rayleigh waves are called "R-infrasonic waves".

II. THE DOPPLER DATA AND INTERPRETATIONS

The processes through which the earthquake disturbance excites the ionosphere into oscillation and how this is detected are schematically presented in Fig. 1. The Rayleigh waves from the epicenter of a tsunamigenic earthquake induce vertical ground movements as they pass through the Hawaiian Island chain. This movement generates infrasonic waves of the same period, which then propagate upward to at least the F1 and F2 regions of the ionosphere (the 180 - 350 km heights). These infrasonic waves produce up-and-down motions in the neutral particles (rarefraction and compression of the neutral gas). The positive ions follow the neutral gas particles because of elastic collisions and the electrons closely follow the positive ions because of the Coulomb attraction. Thus, as the pressure wave propagates through the lower ionospheric region, the height of the electron density layer moves up and down accordingly. The HF radio wave whose frequency is equal to the plasma frequency of the particular electron density layer is reflected back towards the ground and is received by our Doppler frequency detection system.

Fig. 2 is a map of the Hawaiian Island chain with the locations of the HF Doppler receivers and the corresponding sub-ionospheric points for the three-station array operated by the University of Hawaii. The HF Doppler detector used for the present project is located at Manoa, Oahu, with the sub-ionospheric point indicated midway between Barking Sands and Manoa. The location of the Honolulu Observatory, where the Pacific Tsunami Warning System is headquartered, is also indicated on the map.

There are several distinct but inter-related processes through which energy from the epicenter is transferred to the ionosphere: (1) transfer of the stress energy in the earth's crust into the seismic and water waves; (2) propagation of Rayleigh waves over the surface of the earth; (3) launching of the infrasound at the ground-air interface; (4) propagation of the infrasound waves in the atmosphere; and (5) ionospheric perturbations produced by the infrasound. The R-infrasonic waves of different periods generated near the sub-ionospheric point do not travel along the same atmospheric path and do not necessarily produce ionospheric effects at the same time. Therefore, the different frequency components observed at the ionospheric heights are, in general, not launched at the same point along the path of the seismic wave.

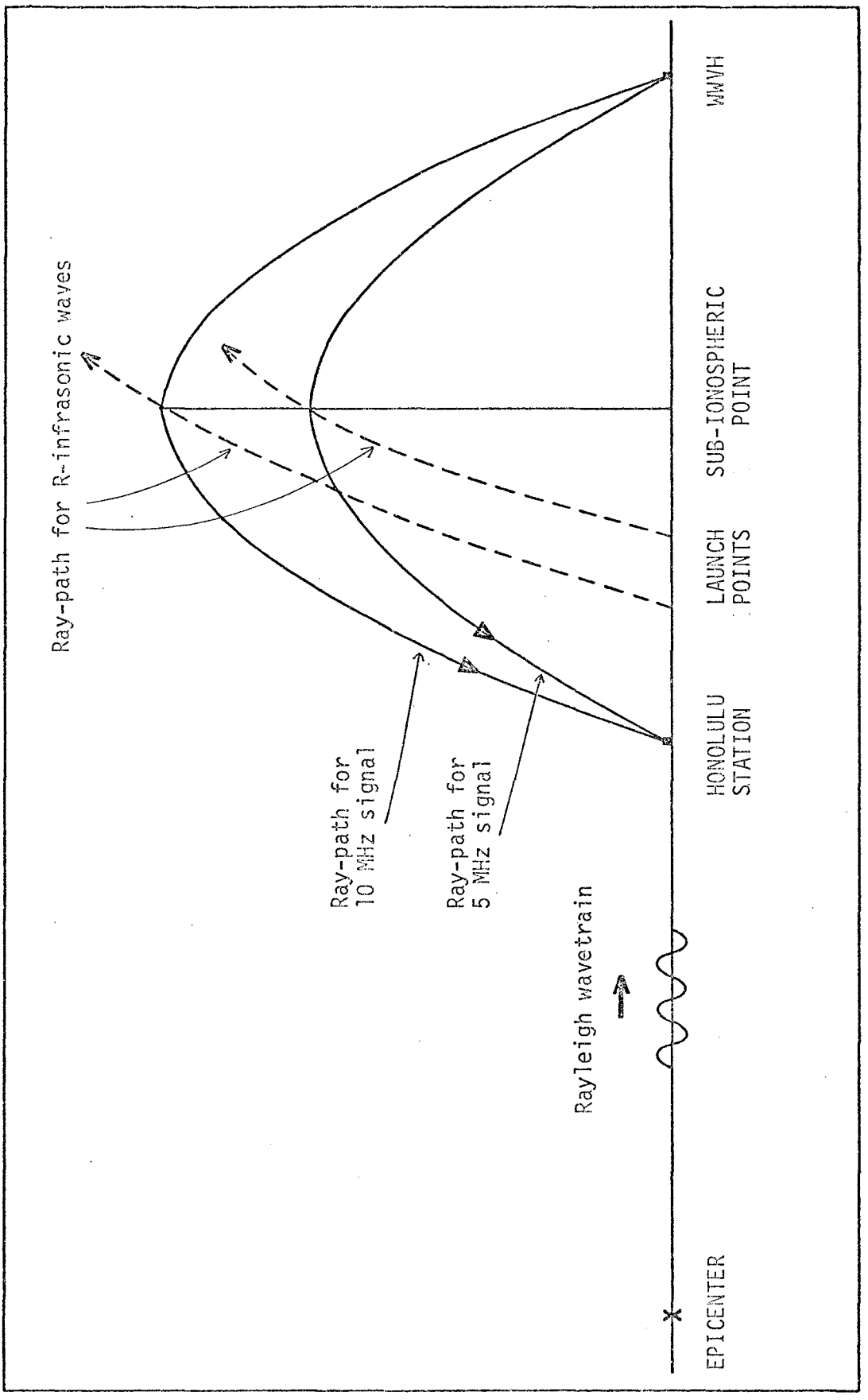

Figure 1. Schematic diagram of physical processes by which earthquakes produce distant ionospheric disturbances.

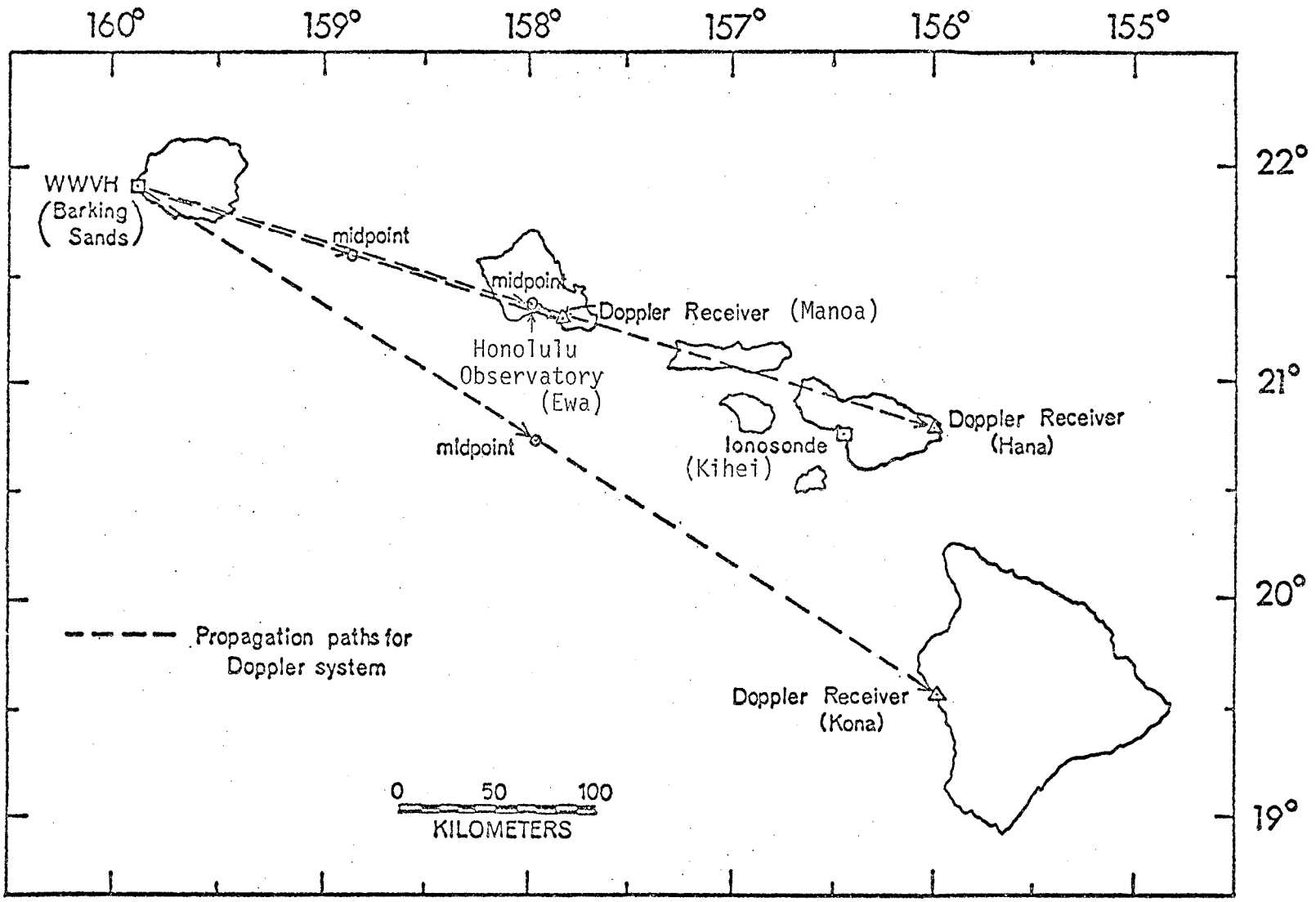

Figure 2. Three-station HF Doppler network in Hawaii.

A. The HF Radio Wave Reflection Height

In order to trace the observed wave motion from the ionospheric height to the ground, it is essential that the height of reflection be accurately known. This height is dependent on the electron density, which in turn is dependent on the ionospheric temperature (dependent on the geomagnetic activity, solar activity, season, and solar cycle).

A computer program was developed by Huang (1973) as part of his doctoral dissertation to determine the reflection height of radio waves. The program uses the electron density distribution as input data and follows the ray path of the radio wave as it travels from a ground-based transmitter up to the ionosphere and back to a ground-based receiver. The reflection height and the coordinates of the ray path are printed out. If the electron density distribution (profile) is not available, another computer program, also written by Huang (1973), allows one to determine the electron density profile corresponding to the ionogram for a particular day and time. The latter is written in the right format for use in the former program. Descriptions of the method and the programs are given in Appendices 4 and 5 and listings of both programs may be found in Appendices 4A, 4B, 5A, 5B, and 5C.

For the 1969 disturbance, a composite ionogram was calculated from ionograms made at 11:45, 12:00, 12:15, 12:30, and 12:45 Hawaiian Standard Time (HST), and the reflection height was computed from the corresponding electron density profile. For the 1968 disturbance, however, the reflection heights were computed from the electron density corresponding to ionograms made at 12:15 and 12:30 HST; then the reflection heights were averaged to give a representative height.

The reflection heights for the 1968 and 1969 earthquake-related disturbances for the 5 MHz and 10 MHz radio frequencies are listed in Table 1 below.

Table 1 Reflection Heights

Event	Reflection Height (km)	
	5 MHz	10 MHz
May 16, 1968	178.2	287.2
August 11, 1969	153.5	332.4

Some error is expected in these estimates because of changes in the ionosphere during the day, especially in the case of the May 16, 1968 earthquake because of the time difference between the event and the ionograms. The period during which the ionospheric oscillations were recorded is from 0120 to 0140 UT.

B. The Ionospheric Doppler Data

The Doppler records of the ionospheric oscillations induced by the earthquakes of 1968 and 1969 are shown in Fig. 3 and Fig. 4, respectively. These oscillatory traces, beginning at about 0124 UT on the 10 MHz records and at 0121 UT on the 5 MHz records in the former, and at about 2201 UT in the latter, represent Doppler shifts in the frequency of the radio signals from the time standard station WWVH.

Several characteristic features of these Doppler records can be readily recognized in Figs. 3 and 4:

1. The oscillations in the 10 MHz signal drift toward longer periods as time progresses. This suggests that the R-infrasonic wave trains are propagating in dispersive media.
2. The short period oscillations of about 20 seconds are observed in the 5 MHz (≈150 km height) but not on the 10 MHz (≈300 km height), thus the infrasonic waves are filtered as they propagate toward greater heights.
3. The amplitude of the oscillations on the 10 MHz signal has its largest amplitude at about the third peak and not at the beginning or end of the train.
4. The 10 MHz waveforms appear to be congruous to that of well-dispersed wave trains with quasi-sinusoidal oscillations, corresponding to the stationary phase approximation to a Fourier integral. However, the 5 MHz waveforms are very similar to the seismic oscillations at about 20 to 40 seconds period.

Table 2 contains a list of the periods of the maximum upward and downward excursions in the waves. These excursions correspond to variations in speed with which the ionospheric layer at the radio reflection height moves downward or upward, respectively. The periods were determined by means of the peak and trough method (Ewing and Press, 1954). To determine the period of the extrema in displacement, which correspond to the maximum

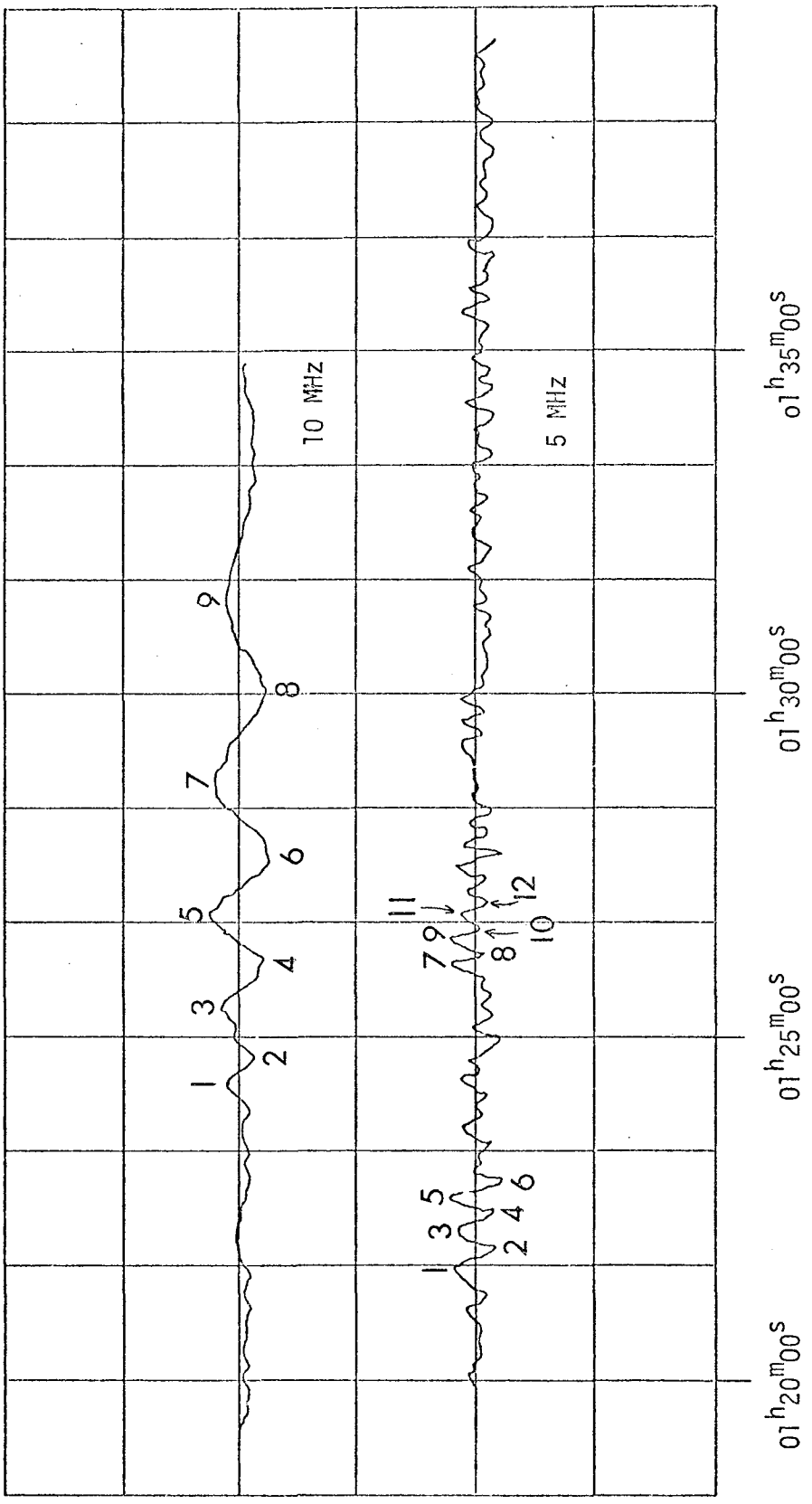

Figure 3. Doppler waveform of ionospheric disturbance produced by the May 16, 1968 Tokachi-Oki earthquake.

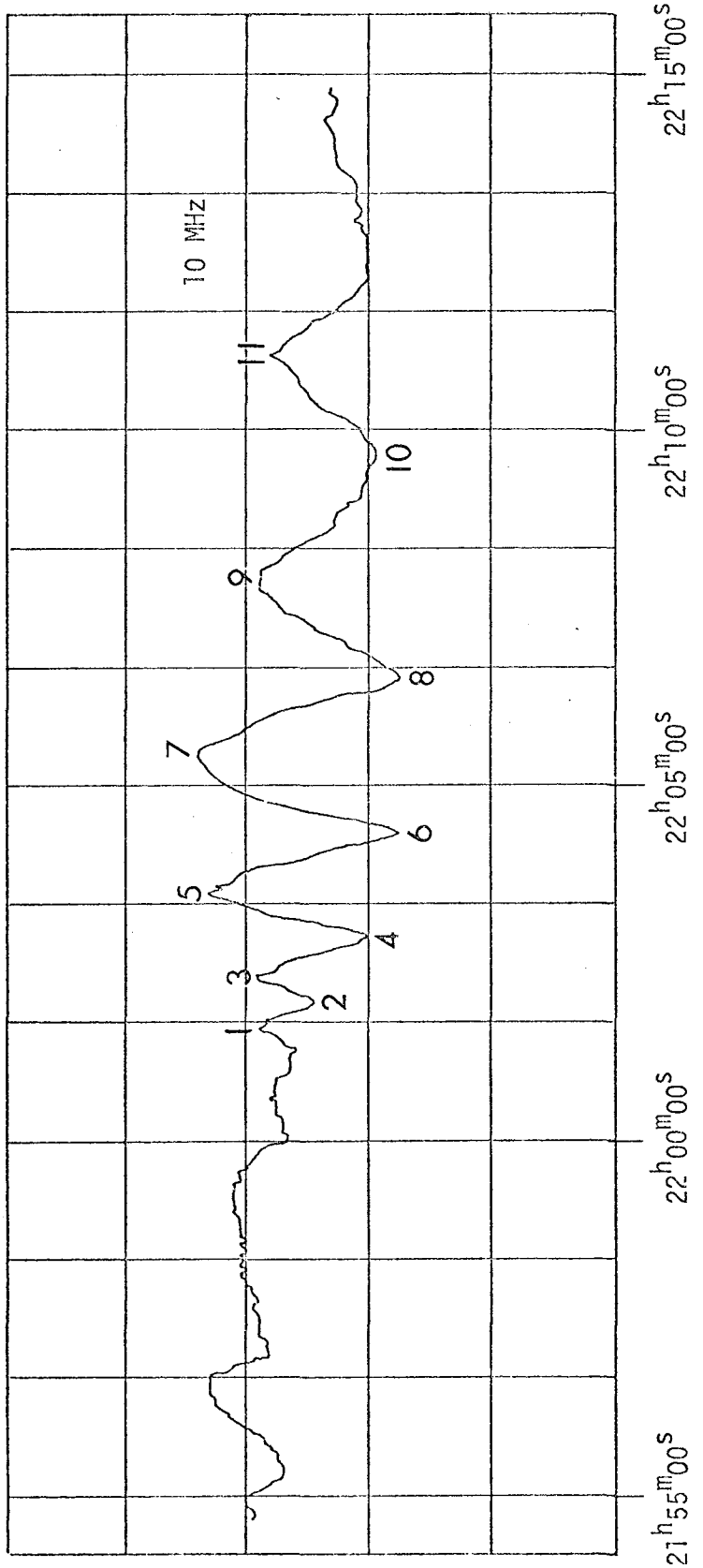

Figure 4. Doppler waveform of ionospheric disturbance produced by the August 11, 1969 Kurile Island earthquake.

Table 2 Period of Peaks and Troughs in Velocity

Year	Frequency	Feature	Character	Period
1968	10 MHz	1	P (peak)	48 sec
		2	T (trough)	68 sec
		3	P	80 sec
		4	T	90 sec
		5	P	93 sec
		6	T	110 sec
		7	P	135 sec
		8	T	170 sec
		9	P	190 sec
1969	10 MHz	1	P	46 sec
		2	T	48 sec
		3	P	52 sec
		4	T	70 sec
		5	P	95 sec
		6	T	110 sec
		7	P	130 sec
		8	T	150 sec
		9	P	170 sec
		10	T	188 sec
		11	P	220 sec
1968	5 MHz	1	P	40 sec
		2	T	38 sec
		3	P	35 sec
		4	T	30 sec
		5	P	28 sec
		6	T	28 sec
		7	P	20 sec
		8	T	20 sec
		9	P	22 sec
		10	T	20 sec
		11	P	20 sec
		12	T	20 sec

upward and downward movement of the ground, the zero-crossings of the waveforms were found by means of the bisector between successive peaks and troughs, then the peak and trough method was applied at these points. The periods found are listed in Table 3. When these periods are plotted as functions of displacement, they show that: (a) the waveforms are well-dispersed; (b) only inverse dispersion is present; and (c) periods less than or equal to about 50 seconds are absent.

The amplitudes of the peaks and troughs were measured from a reference line determined by the set of line segments passing through the mid-points of the upward and downward excursions. Fig. 5 shows the ratios of these amplitudes normalized relative to the largest amplitude. The ratios for successive peaks and troughs are plotted at unit horizontal intervals, with the peaks plotted above and the troughs below the horizontal axis. The feature numbers are used for reference purpose and are indicated at the bottom of the figure. For the 1968 case, the same maximum amplitude occurred at features 5, 6, and 7; hence the ratios were plotted starting with feature 6 located on the vertical axis. Since features 6 and 7 in the 1969 case had the same amplitude and feature 8 was slightly smaller, the ratios for feature 7 were plotted on the vertical axis.

The amplitude ratio plots for 1968 and 1969 indicate that the oscillations both built up at the same rate and again decayed at the same rate. In addition, the maximum appears to occur at the same time if measured in terms of the number of oscillations that have occurred since the beginning of the wave train. Thus it appears that the 1969 disturbance differs from the 1968 disturbance only in scale (it is about three times larger) and perhaps the exact period of the individual oscillatory components but not in the range of the periods. Thus, the R-infrasonic waves for the 1969 case were stronger and of slightly different periods, but were generated and propagated in an essentially similar manner.

Abe (1972) has generated synthetic Rayleigh waves from a source model which has a double-couple pure dip-slip with a dip angle of 45° located at various depths. His results show very distinct Rayleigh spectra for sources at different depths. He points out that "...Rayleigh waves can be used as a good diagnostic element for estimating the source depth." If this is indeed the case, then they could be very useful for the prediction of tsunami generation. We shall pursue this idea further. Since these

Table 3 Period of Peaks and Troughs in Displacement

Year	Frequency	Feature	Character	Period
1968	10 MHz	1	P (peak)	43 sec
		2	T (trough)	52 sec
		3	P	67 sec
		4	T	80 sec
		5	P	94 sec
		6	T	105 sec
		7	P	120 sec
		8	T	145 sec
		9	P	170 sec
		10	T	210 sec
1969	10 MHz	1	P	42 sec
		2	T	42 sec
		3	P	47 sec
		4	T	65 sec
		5	P	81 sec
		6	T	100 sec
		7	P	120 sec
		8	T	135 sec
		9	P	157 sec
		10	T	175 sec
		11	P	200 sec

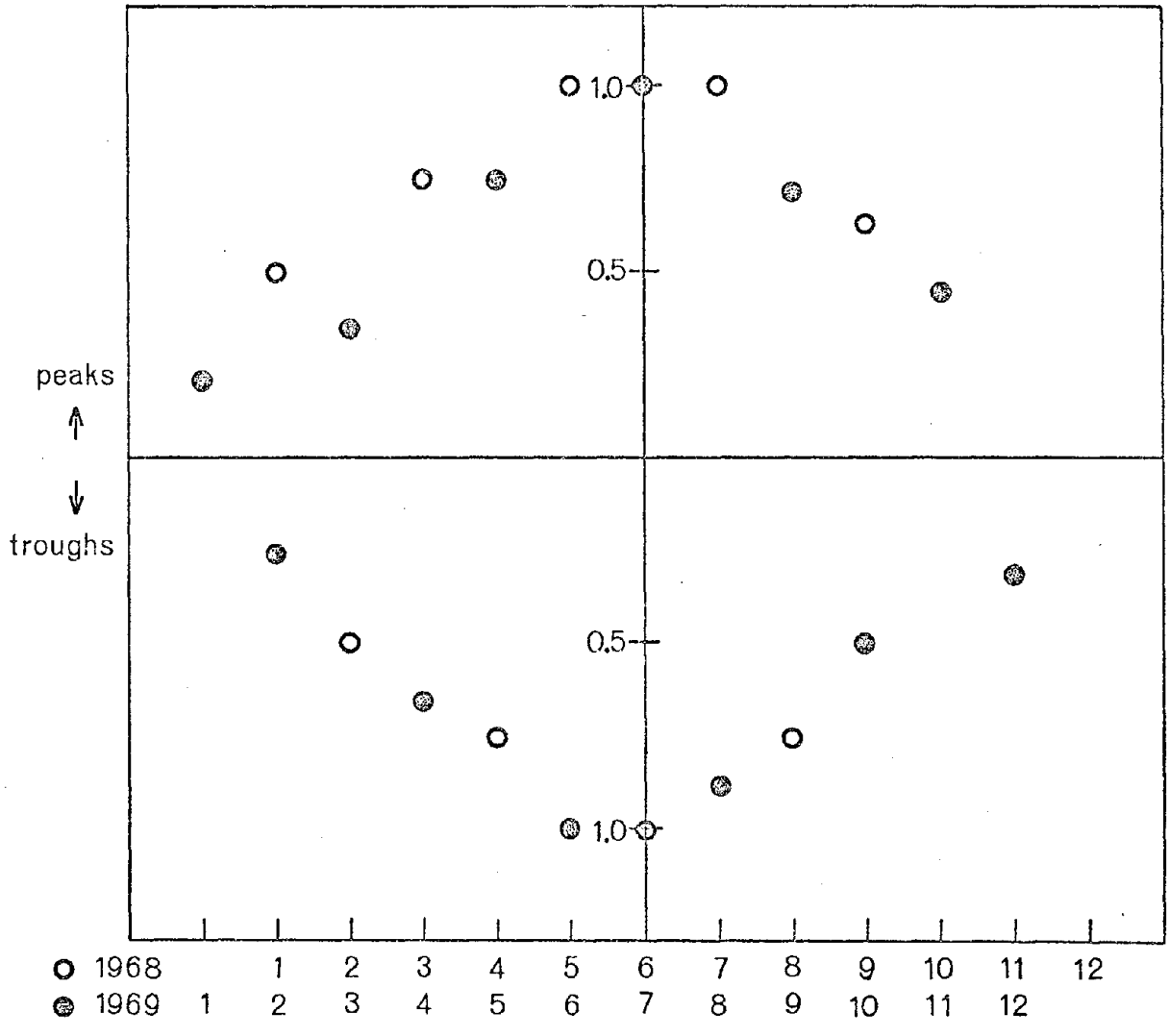

Figure 5. Comparison of increase and decrease of the relative amplitude of peaks and troughs in the 1968 and the 1969 waveforms. Base amplitude located on the vertical axis. Numbers below allow a correspondence between points shown and featured in Figures 3 and 4.

are only two samples, we are not positive as to whether all large shallow-focus earthquakes produce essentially the same type of recordable ionospheric disturbance.

While it would be of great interest to determine the anisotropy of the response of the ionosphere to R-infrasonic waves, there have been only very small disturbances even for very large magnitude earthquakes from the direction of the south-west Pacific Ocean basin. Whether this is due to the type of earthquake sources or whether this lack of data is due to the numerous atolls and relatively shallow ocean depths of the propagation medium is not known at this time. Nevertheless, there is a marked lack of Doppler records of ionospheric disturbances due to earthquakes generated in that area.

III. PROPAGATION PATHS FOR R-INFRASONIC WAVES

Since a part of the energy from an earthquake propagates on the outer surface layer of the solid earth as Rayleigh waves which then cause disturbances which propagate to ionospheric heights as infrasonic waves, propagation paths and delay times for the infrasonic waves to travel from the ground up to the radio reflection height for a Doppler system must be determined in order to trace the wave components back to the source. For our purpose it is most convenient to carry out a ray analysis of infrasonic waves in the earth's atmosphere.

The ray-tracing program attempts to find the path in the atmosphere along which a group of small amplitude infrasonic waves will propagate with a group velocity. This requires one to find a bundle of rays in order to determine the shape of the wave front. To find such paths, the ray-tracing techniques developed for internal gravity waves (but not limited to them) by Cowling, et al., (1970, 1971), Jones (1969), and Yeh and Liu (1974), will be used. In general, the program is essentially the same as that used by Cowling with modifications in the input and output, calculation of the group velocity and certain initial parameters, and vertical variation in the atmospheric parameters. The program uses the complete dispersion relationship for acoustic-gravity waves.

A. The Model Atmosphere and its Parameters

We assume a flat earth surface geometry with atmospheric parameters varying only in the vertical direction and that the air is inviscid and non-dissipative throughout the atmospheric region of interest. Thus it implicitly assumes that the rarefied air at heights of several hundred kilometers can be treated the same as air at low levels and that there is no ionosphere or geomagnetic field. Only two atmospheric parameters appear directly in the program: the speed of sound and the ratio of the specific heats, γ. The pressure, temperature and density of the atmosphere are entered into the program through the speed of sound, the acoustic cut-off frequency and the Brunt frequency. The integration interval is taken to be 10 km, from 0 to 400 km, and the acceleration of gravity, g, is taken to be height dependent.

Presently, we have two sets of the speed of sound distributions; one is for the summer during the period of maximum solar activity and the

other is for a minimum in solar activity. The first case was calculated by Huang using the 15°N annual model in the 1962 Standard Atmosphere for heights less than 120.0 km and the summer model for an exospheric temperature of 1000° K in the 1966 Supplement for heights greater than 120.0 km. These values were found from the expression in the 1962 Standard Atmosphere, assuming $\gamma = 1.4$ (there is only a small change if γ were allowed to vary with height) and that the molecular weight decreases above 120.0 km as indicated by the summer model. These values are appropriate for the amount of solar radiation that impinged on the atmosphere around August 1969, which was near the solar activity maximum. For the latter case, for solar activity minimum, the expression and procedures used were the same. The height variation of γ was determined by linearly extrapolating the values shown in Midgley and Liemohn (1966).

B. Basic Definitions and Equations for Acoustic-Gravity Waves

The most important physical quantities and the corresponding mathematical expressions that appear in the ray-tracing program are collected for reference. For additional details, see Cowling, et al., (1970) and the references cited in it.

1. Acoustic cut-off frequency, f_a, sets the lower limit on the frequency scale for atmospheric acoustic waves; i.e., acoustic type waves cannot propagate if their frequencies were less than that for f_a. The angular frequency for a plane wave or exponential-like solution in a planar isothermal atmosphere is given by

$$\omega_a = 2\pi f_a = \frac{\gamma g}{2c} \qquad (1)$$

where γ = ratio of specific heats, g = acceleration of gravity, and c = speed of sound.

2. Brunt frequency, f_g, is similar to f_a, except that it applies to internal gravity waves and sets an upper limit to the allowed frequencies, i.e. propagation of buoyancy oscillations is not possible for frequencies greater than f_g. The exponential-like solution in an isothermal atmosphere gives this expression:

$$\omega_g = 2\pi f_g = \frac{\sqrt{\gamma - 1}}{c} g \qquad (2)$$

where the symbols are the same as in (1) above.

3. Dispersion relationships. If the acoustic cut-off and Brunt frequencies were both zero, then propagation of the atmospheric wave would not be dispersive and the angular frequency, ω, would be a linear function of the wave number vector, $\underline{k}$. However, frequencies of plane waves in a planar isothermal atmosphere have the relationship

$$\omega^4 - \omega^2 c^2 (k_x^2 + k_z^2) + \omega_g^2 c^2 k_x^2 - \omega_a^2 \omega^2 = 0 \qquad (3)$$

where k_x and k_z are the x (or horizontal) and z (or vertical) components, respectively, of the wave vector, and ω_a and ω_g are given in 1 and 2 above. Without loss in generality, the propagation is assumed to be two-dimensional. Highly localized pressure of displacement perturbations will tend to disperse or spread out into nearly sinusoidal waves with slowly changing frequency and wavelength in accordance with equation (3).

The phase velocity of a harmonic component depends on the wavelength of the waves. Moreover, it depends on ω_a and ω_g and both k_x and k_z rather than just $|\underline{k}|$. Therefore, it is difficult to completely show the functional relationship of (3) graphically. Thus one dimension or variable is usually suppressed (see the figures on pages 55 and 59 in George (1968) and page 49 in Cowling, et al., 1970).

4. Group velocity, V_g, is defined (Lighthill, 1965) as

$$\underline{V}_g = \nabla_k \omega \qquad (4)$$

where ∇_k is the gradient operator with respect to $\underline{k}$. Applying this to the dispersion relationship of (3), we find that

$$V_{gx} = \frac{\omega c^2 k_x (\omega^2 - \omega_g^2)}{\omega^4 - \omega_g^2 k_x^2 c^2} \qquad (5)$$

and

$$V_{gz} = \frac{\omega^3 c^2 k_z}{\omega^4 - \omega_g^2 c^2 k_x^2} \quad . \qquad (6)$$

Since usually $\omega_a > \omega_g$, we identify the following two branches:

a) Infrasonic branch: $\omega > \omega_a > \omega_g$
$\omega^2 - \omega_g^2 > 0$
$\omega^4 - \omega_g^2 c^2 k_x^2 > 0$
V_{gx} has the same sign as k_x
V_{gz} has the same sign as k_z

b) Internal gravity branch: $\omega < \omega_g < \omega_a$
$\omega^2 - \omega_g^2 > 0$

$$\omega^4 - \omega_g c^2 k_x^2 > 0$$

V_{gx} has the same sign as k_x

V_{gz} has the opposite sign from k_z.

The magnitude of the group velocity is given, as usual, by the sum of the square of its components, $|\overline{V}_g|^2 = V_{gx}^2 + V_{gz}^2$ and the ray-path is the path in the atmosphere traced out by $\overline{V}_g$. The slope of the ray-path with respect to the ground is V_{gx}/V_{gz}.

The group velocity is normal to the ω-contours in k-space, as shown in Fig. 4.1 on page 49 in Cowling, et al., (1970). Such diagrams represent one possible way of studying the characteristics of rays. These ω-contours will be ellipses in the case of infrasonic waves (Georges, 1967).

The above equations have been derived under the assumption that the planar atmosphere is motionless except for the waves. However, if a wind is blowing in the horizontal direction, the frequency of the waves may be Doppler shifted. If Ω is the angular frequency in a reference frame moving with the atmosphere, then this Doppler shifted angular frequency is given by

$$\omega = \Omega - \underline{k} \cdot \underline{v} \qquad (7)$$

where $\underline{k}$ is the real part of the wave vector and $\underline{v}$ is the horizontal velocity of the atmosphere, i.e., the horizontal wind velocity.

Equation (7) is used to transform from the moving frame to the ground or laboratory frame. The equations (1) to (6) are applicable in the moving frame since the atmosphere is stationary (at rest) with respect to it. Observations and initial specification of the wave motion are made relative to the ground frame. Thus, the following relationships are important in making the transformations:

$$k_x = \frac{\Omega}{V_p} \quad \text{in ground frame}$$
$$= \frac{\Omega}{V_p} \quad \text{in rest frame} \qquad (8)$$

where V_p is the phase velocity (as measured in the reference frames mentioned) and

$$\underline{V}_g \text{ (in ground frame)} = \underline{V}_g \text{ (in moving frame)} + \underline{V} \; . \qquad (9)$$

This shows that atmospheric waves may be carried along or retarded by horizontal winds.

5. Interpretations of ω and k_x: According to the derivations leading to the dispersion equation, ω and k_x are the angular frequency and horizontal wave number of a plane sinusoidal wave. However, we can never observe a perfect sinusoidal wave since we can observe only groups of waves, or equivalently, a finite wave train. If the medium is dispersive, the wave train will spread out as it propagates and the frequencies of the oscillations in the wave train will gradually vary along the wave train. If the medium is inhomogeneous, then ω will vary as the wave train travels through the inhomogeneity. Similar remarks apply to the wave vector, k. Therefore, the relationship between $(\omega,\underline{k})$ and features of the waveforms must be understood before the ray-tracing results can be used in interpreting observations.

The horizontal wave number, k_x, cannot vary because the model atmosphere is assumed to be homogeneous in the horizontal direction. Thus k_x must remain fixed at the initial value specified at the onset of a ray-tracing run, regardless of the stage of calculation of a ray. k_z, on the other hand, will vary with height during the different stages of the ray calculation.

The angular frequency, ω, is invariant along the path defined by the group velocity in an inhomogeneous and dispersive medium (Lighthill, 1965) and should remain constant along the rays in the atmosphere. Since the wave train is dispersive, we see that ω is the angular frequency (a sort of average angular frequency) of the narrow band of harmonic components that interfere to produce the sub-group of oscillations in the wave train with the same angular frequency. That is, ω should be interpreted as the angular frequency of a harmonic component in the sense prescribed by the application of the method of stationary phase in the homogeneous case. Since k_x is invariant along a ray, it can also be interpreted in this sense.

C. Determination of Ray-Paths

1. Ray-Path Calculation

For the purpose of ray calculations the dispersion relationship of equation (3) is solved for k_z in the form

$$k_z^2 = \left(\frac{\omega^2 - \omega_a}{c^2} \right) + k_x \left(\frac{\omega_b^2}{\omega^2} - 1 \right) \quad . \qquad (10)$$

Moreover, we define the following quantities:

$\lambda_z = \frac{2\pi}{k_z}$ = wavelength in the vertical direction

h_o = initial height above the ground

x = distance in the horizontal direction from initial position of the wave

t = time

and Θ = angle between $\underline{k}$ and the vertical direction.

The following procedure for calculating the ray for given ω, k_x, h_o, and the initial direction of the phase propagation is used in the ray-tracing program.

a) Find the values of k_x at h_o from the dispersion equation, subject to the modifications introduced by the wind.

b) If k_z is real, then calculate U_x, U_z, and $\lambda_z' = 0.10\,\lambda_z = 0.10\frac{2\pi}{k_z}$. The thickness of the equivalent isothermal layer at this height is λ_z' or 10 km, whichever is smaller.

c) If the thickness is Δh, then the time required to traverse the path in the current layer is $\Delta t = \Delta h / U_z$, where the vertical distance traversed is Δh and the horizontal distance traversed is $\Delta x = U_x \Delta t$.

d) After adding Δh, Δt, and Δx to running sums, replace h_o by $h_o + \Delta h$ and repeat the steps (a) to (d) until the top of the atmosphere is reached or the situation in (e), below, occurs.

e) If k_z is imaginary, divide the current Δh in half, step upwards by $0.5\Delta h$ and repeat steps (a) to (d). This is continued until a height is reached where $k_z \simeq 0.0$ and this is called the reflection height, h_r.

f) Since reflection has occurred at h_r, the program now begins to

trace downward, repeating the sequence (a) to (d) with h_r replaced by $h_r - \Delta h$ initially, then $h_r - \Delta h$ replaced by $(h_r - \Delta h) - \Delta h_{(new)}$, etc., until k_z again becomes 0.0, or the ray reaches the ground, or the ray reaches as close to the ground as possible.

Thus, the rays either continue to the top of the atmosphere or reflect at some intermediate height. If winds are included, rays may be trapped (Cowling, et al., 1970).

The initial step, Δh, either upwards or downwards is controlled by the direction of phase propagation specified at the onset (the phase and energy propagate in the same direction only for infrasonic waves). The program remembers the direction so that it can step in the correct direction after a reflection. Moreover, since λ_z is large for the lower frequency internal gravity waves, it is necessary to divide the interval, Δh, by 10 to keep the steps reasonable. The program interpolates between the layers of the model atmosphere when necessary.

Finally, the reflected rays may not be symmetrical because the steps just before reaching h_r are not necessarily the same as that just after reaching h_r. This is a result essentially because k_z at the point before h_r may be slightly different from k_z at h_r. The computer program and its instructions for the ray calculation are given in Appendix 2.

2. Program Modifications

For the internal gravity waves, the minimum information required at the outset is ω, k_x, h_0, and the direction of phase propagation. If a wind model is to be included, one must also specify the launch time, and the initial azimuth relative to north of the waves. The program can also be changed to accept other sets of initial data, such as ω and the horizontal trace velocity, and let the program compute k_x.

For the infrasonic waves, the program is set up to accept ω, h_0, Θ and the direction of phase propagation. Then k_x and k_z are found from the dispersion equation and the relationship $k_x = k_z(\tan \Theta)$. The range of angles for Θ (3° to 7°) has been chosen to agree as closely as possible with the situation for atmospheric waves launched by Rayleigh waves. In the determination of this angle, k_x is assumed to be the same as the phase constant of the Rayleigh waves at the ground - air interface. On the other hand, we could have specified ω and the Rayleigh phase velocity and allowed

the program to compute k_x and Θ. Finally, since λ_z for these waves is much smaller than that for the internal gravity waves, the factor of 10 in $\lambda_z/10$ has been removed. This has the effect of increasing the steps from 1 km to 10 km, so that the ray-tracing calculation would not be too time-consuming.

D. Results

Figures 6a, 6b, and 6c show ray-paths and travel times for atmospheric acoustic or infrasonic waves in a windless atmosphere. The waves are assumed to be launched from a ground level source and the curves are parameterized in terms of Θ_k, the angle between $\underline{k}$ and the vertical. The set of curves in each figure is for waves with the same period and the travel time along the ray is again indicated by short horizontal bars. To generate these rays, Θ_k rather than k_x or the horizontal trace velocity, was read into the program along with ω (or period). The insert shows the ralationship between Θ_k and both the apparent horizontal velocity (V_h) and the initial angle (Θ_r) between the group velocity and the vertical. Therefore, to apply these results to different ground sources, one only has to match the "launch" angle, k_x, or the horizontal trace velocity, V_h (it is usually difficult to find the initial Θ_r because this requires a superposition of waves).

An interesting result of these calculations is the progressive change in the ray path as the waves change from nearly pure acoustic (Fig. 6a) to long-period infrasonic (Fig. 6c). The latter waves not only take longer to propagate but also travel upward at a steeper angle. However, again we need to pursue ray-tracing in a windy atmosphere before we can reach firm conclusions and check the ray information for periods greater than 30 seconds.

For the vertically propagating infrasounds generated by the seismic Rayleigh waves from some large earthquakes, we assume the phase velocity of the Rayleigh waves is equal to the initial horizontal velocity of the wave. Thus we can find the appropriate ray by setting V_h equal to the phase velocity for the given period and find the proper Θ_k. It is therefore possible to determine the travel time and the horizontal distance traversed by the infrasound from the launch point at the ground to the ionospheric heights.

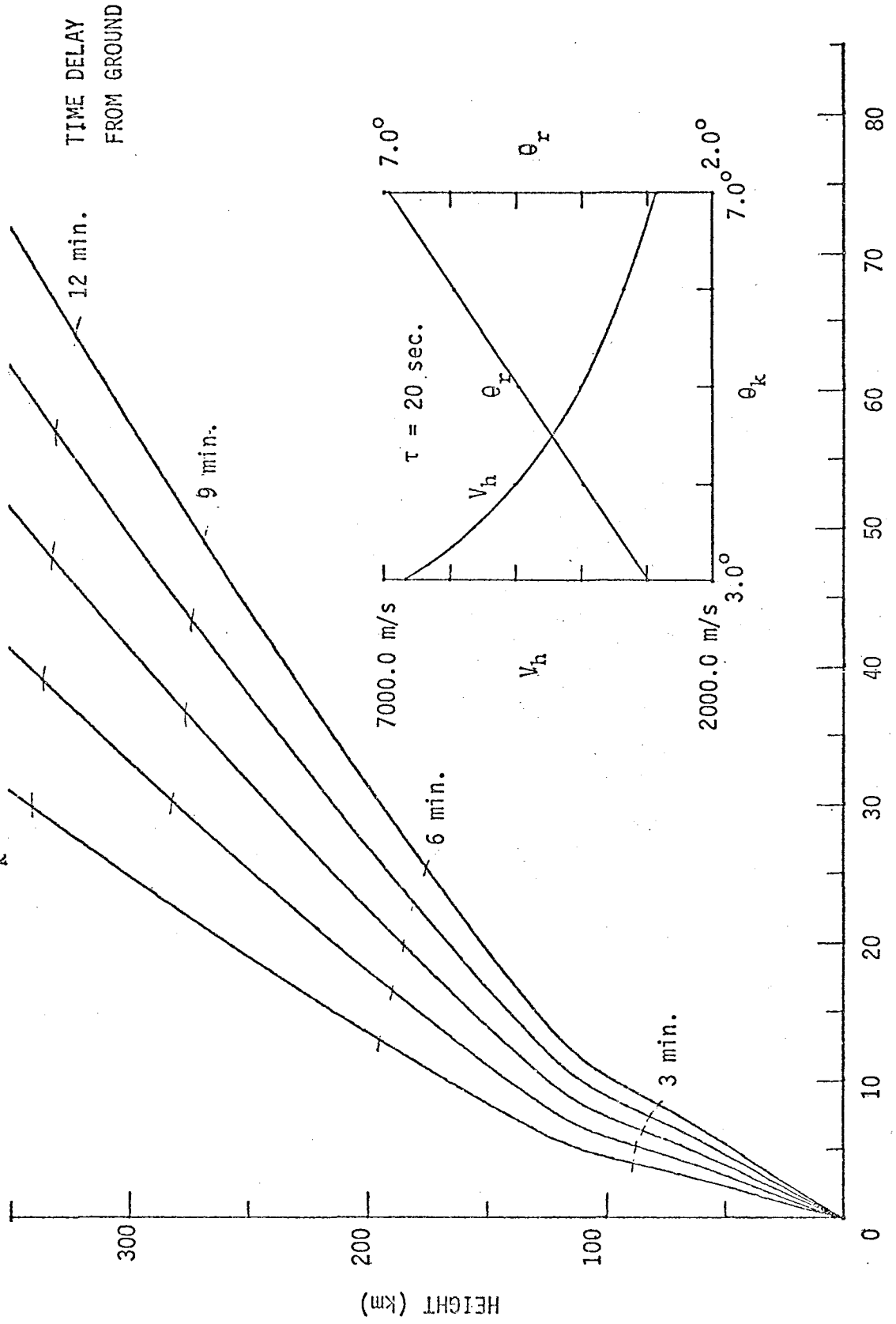

Figure 6a. Ray-paths for infrasonic waves from ground level sources for waves of period, τ = 20 sec.

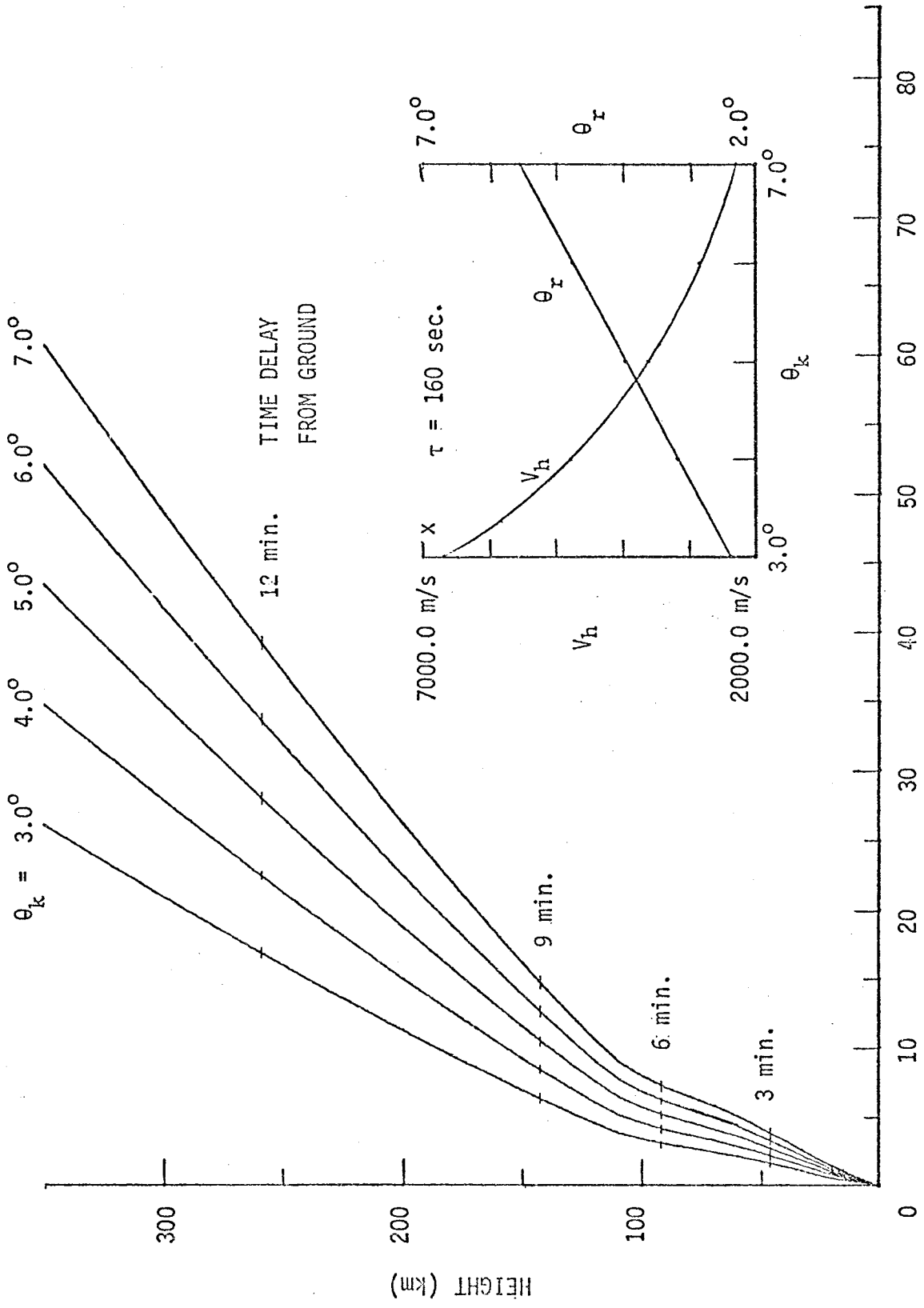

Figure 6b. Ray-paths for infrasonic waves from ground level sources for waves of period, τ = 160 sec.

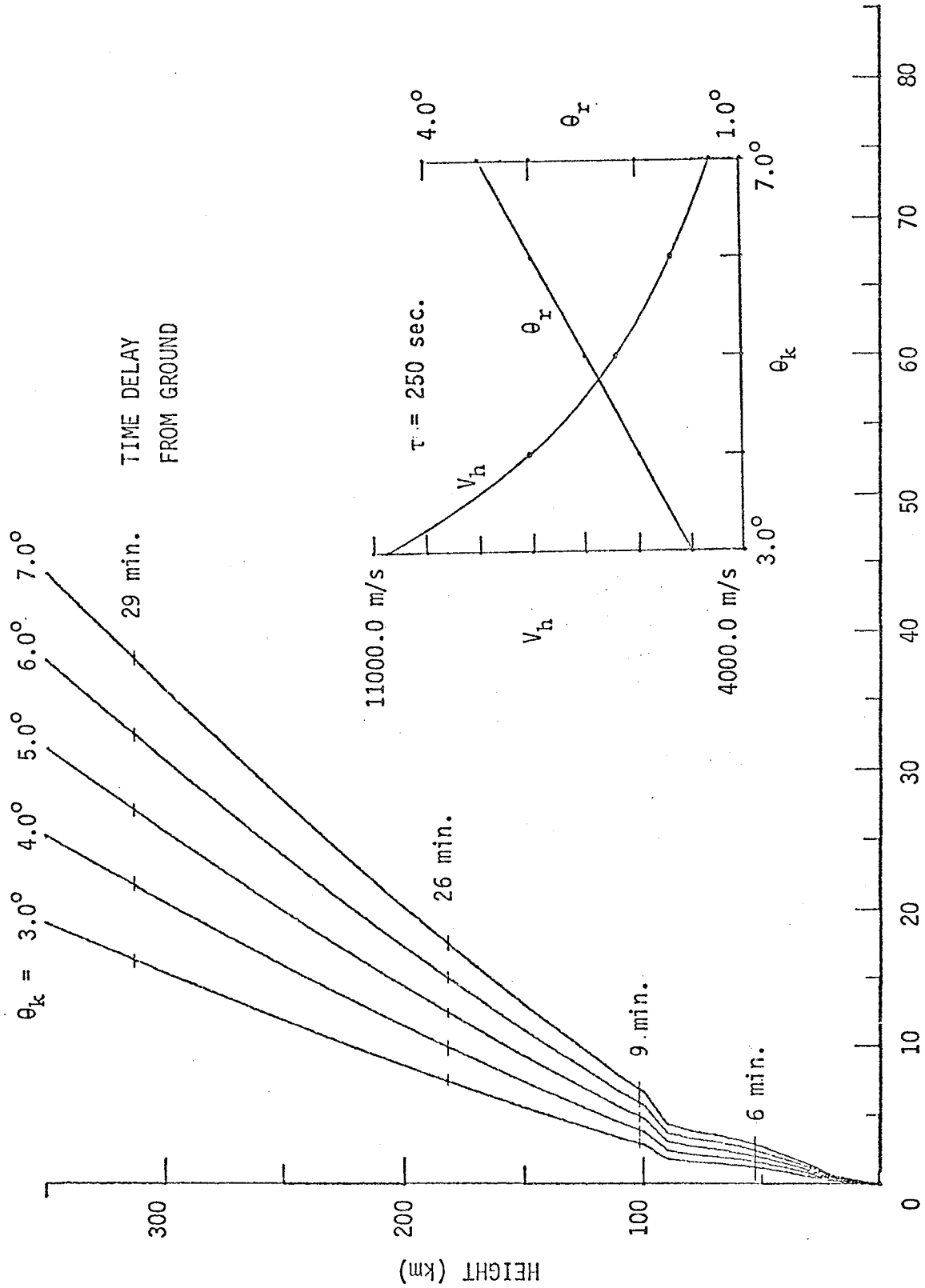

Figure 6c. Ray-paths for infrasonic waves from ground level sources for waves of period, τ = 250 sec.

Another set of curves presenting the ray paths and travel time for different period waves has been plotted in Figs. 7a and 7b. In these curves, the phase velocity for each Rayleigh wave is taken in accordance with the dispersion curve given by Ben-Menahem and Toksoz (1962) or with the results given by Dorman (1969) (see Fig. 21). Thus there is a slightly different Θ_k for the ray paths corresponding to the different periods.

The greatest deviations among the ray paths and delay curves for the different periods occur in the atmosphere below about 125 km where there is also the greatest variation in the temperature/sound speed. At greater heights these curves have essentially the same rate of change for all periods.

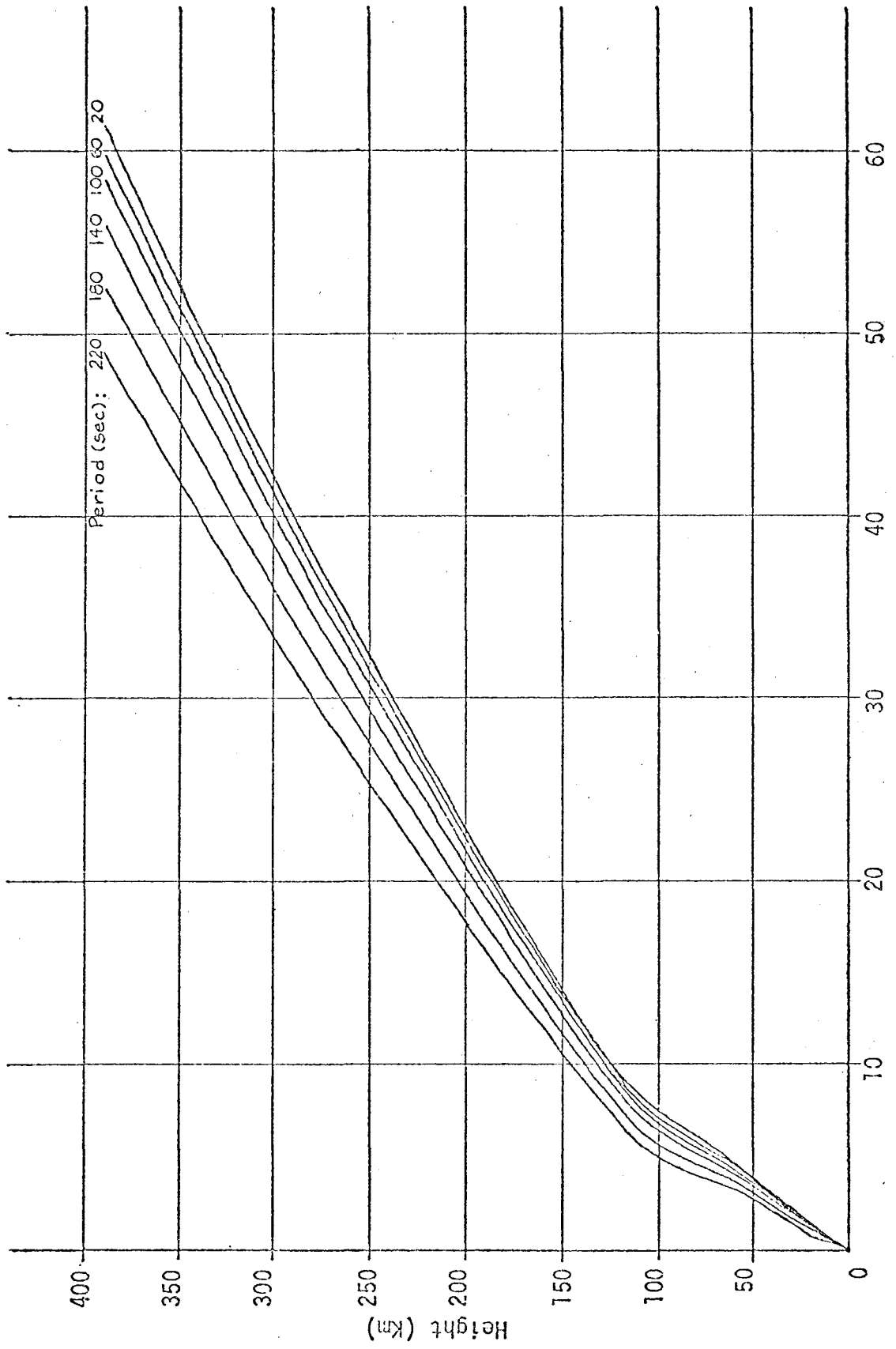

Figure 7a. Ray-paths for infrasonic waves parameterized in terms of periods.

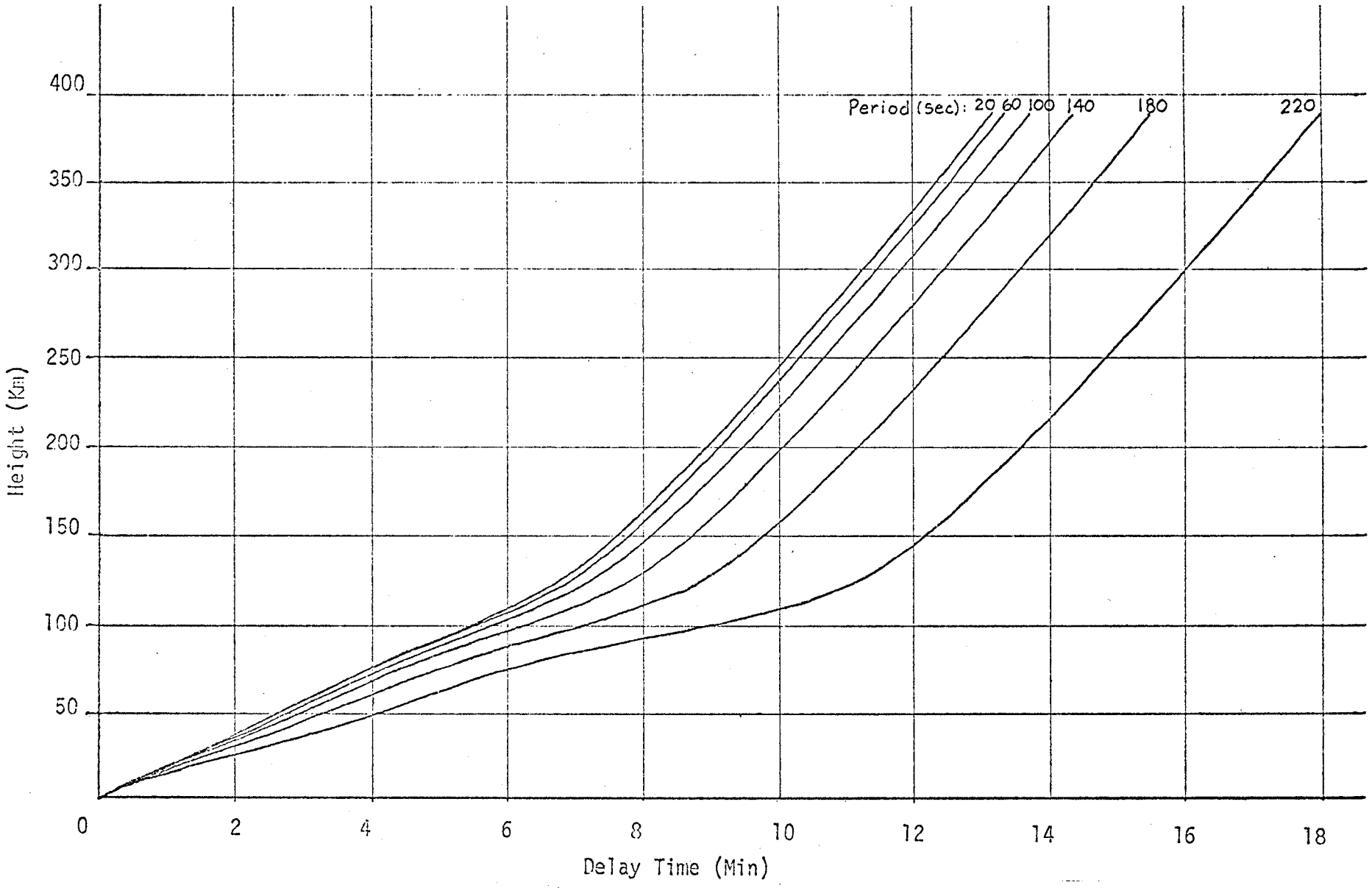

Figure 7b. Travel time along ray-paths as a function of height and period.

IV. THE GROUP VELOCITY OF OCEANIC RAYLEIGH WAVES

Before one can accept the calculations for the infrasonic ray paths and delay times in the earth's atmosphere, it is essential that they be verified and their accuracy established. This can be done by determining the group velocity of the Rayleigh waves and comparing the results with those measured by seismographs. We have made a reasonably thorough literature search of group velocity dispersion data for the Pacific basin and the findings are summarized in Section A. The analysis procedure and the results of the group velocity determined from the Doppler data are presented in Section B and the discussions of the results are given in Section C.

A. Empirical Group Velocity Dispersion Curve

A short description of the literature search for information on the group velocity of seismic Rayleigh waves along paths crossing the Pacific basin is given. The search was confined to the Bulletin of the Seismological Society of America and the Journal of Geophysical Research while other journals were checked only if the particular article was referred to many times. No extensive analysis of the information found was attempted but a set of composite dispersion curves will be presented in this section.

In general the search was confined to papers that contained recent observations made after Oliver's (1962) summary, studies of seismic waves from earthquakes around the Pacific basin, and reported observations from stations in the Pacific basin. Unfortunately there were only a few papers that satisfied these criteria. Relevant observations were reported in Abe (1972), Brune (1969), Dorman (1969), Ewing and Press (1954), Hamada (1971), Dziewonski (1970), Dziewonski and Landisman (1970), Jacob and Hamada (1972), Gupta and Santos (1973), Kanamori (1970), Kausel, et al., (1974), Kuo, et al., (1962), Saito and Takeuchi (1966), Santo (1963), Santo and Bath (1963), and Toksoz and Anderson (1966).

In addition, according to the literature citations, there appears to be very significant research work on Rayleigh wave dispersion being carried out by researchers in Japan. But the papers and articles were not available to us.

Figure 8 summarizes the significant information obtained from the study and shows several sets of recent measurements of the long period

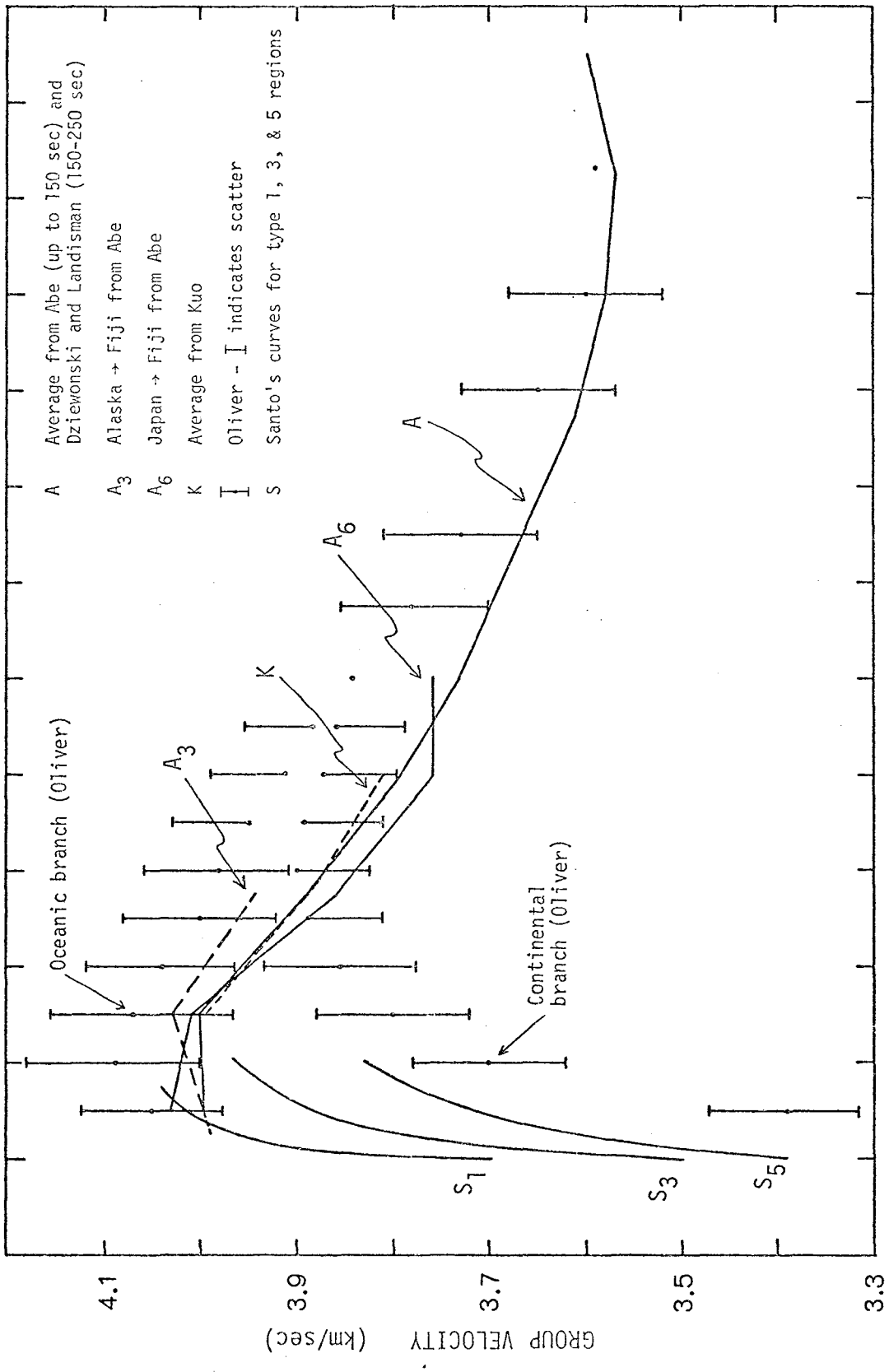

Figure 8. Summary of group velocity of oceanic Rayleigh waves from seismological work.

Rayleigh wave group velocities in the Pacific basin and the average curve obtained by Oliver (1962). Not all the values in a given set of measurements were plotted, but only enough to show the general shape of the dispersion curve. Table 4 gives the symbol notation for the different curves, the particular path over which the Rayleigh waves propagated, and the references for which the curves were obtained. There are also several short period (less than 40 seconds) Rayleigh oceanic curves from Santos (1963) for reference.

Table 4 Quantities Plotted in Figure 8

Symbol	Quantity, reference, and path
A	Period < 150 seconds: representative curve obtained by taking average of values from Abe (1972).
	Period > 150 seconds: representative values from Dziewonski and Landisman (1970).
A_3	Values for Alaska to Fiji as a typical oceanic path from Abe (1972).
A_6	Values for Japan to Fiji as a typical oceanic path from Abe (1972).
K	Average values of typical oceanic path in Pacific from Kuo (1962).
↕	Early standard values for oceanic paths with error bars from Oliver (1962).
	(A continental branch is also included for reference.)

Several general observations that can be made about these oceanic Rayleigh wave group velocities have been reported in the research journals:

1. There is no one dispersion curve that applies throughout the Pacific basin.
2. The deviations in the dispersion curves are inversely proportional to the period and the measurements tend to converge at about 160 to 180 seconds.
3. The peaks of the group velocity waves occur at periods of about 45 seconds.
4. The lowest group velocity occurs at periods of about 220 seconds at the long period range.

The variability of the Rayleigh wave group velocities appears to be due to the depth of penetration of the components of the guided wave into

the underlying surface. If the wave components penetrate to between 1/2 to 1 wavelength, then the wave propagation characteristics are largely determined by the velocity properties of the structure within this depth. Thus the behavior of the waves of periods shorter than ≈40 seconds is determined by the crustal structure. The behavior of the waves of periods greater than 180 seconds is determined by the structure of the upper mantle, which is fairly homogeneous laterally, and should show little or no variability. Many of the average values in Fig. 8 are for very long paths, up to several earth circumferences and much of the variation due to the crustal structure has been averaged out. Therefore, the velocity observations for periods less than 80 seconds do not provide a good measure if the paths were very long. Thus direct path measurements are always preferred over those made over long paths. The intermediate periods, between 80 to 180 seconds, may or may not be anisotropic.

An impressive work is that of Santo (1963) on the sectioning of the Pacific basin according to Rayleigh wave group velocities. The results are shown in Figs. 2(a) and 2(b) of Appendix 3 which were taken from Saito and Takeuchi (1966). The sectioning was made directly in terms of group velocities rather than other geophysical quantities such as shear velocities and heat flow as in Brune (1969). It is particularly valuable because it is empirical and not theoretical. A single dispersion curve applies to all points of a given region and different curves apply to different types of regions. The types of regions range from typical deep water basin ("0") and typical oceanic structure ("1") to typical continental structure ("7"). The structure is very complex for regions west of the andesite line and less complex but variable in the South Pacific regions. Most of the northern Pacific region is of the deep water basin type, except for the continental type along the Hawaiian Island chain.

The number of regions as well as the shape of the regions will vary with the range of periods under consideration. One would expect that as longer period waves are considered, the number of regions will become less, the size of the region will become broader and more regular, and there may only be one region for periods greater than 180 seconds.

A possible way of summarizing the anisotropy and the dispersion properties of the Rayleigh wave group velocities in the Pacific basin might be to construct maps such as Santo's showing isodispersive areas. There would be probably 2 to 4 maps for each of the 2 to 4 ranges of periods, such as

0 - 60 seconds, 60 - 120 seconds, 120 - 180 seconds, and 180 - 280 seconds. If such maps can be constructed, one can determine, reasonably accurately, the time of arrival of the different frequency components if the epicenter and the observation points are known.

However, if one is limited to the use of a single dispersion curve, the best compromise appears to be one synthesized by the average of Kuo's and Abe's data between 20 and 100 seconds, the average of Abe's and Dziewonski and Landisman's data between 120 and 150 seconds, and Dziewonski and Landisman's data for periods beyond 150 seconds. Such a curve, shown in Fig. 8, lies in the middle of the scatter and would probably be in serious error only toward the short period end. It is of some interest to see that Santo's curve ("O") shows a high velocity of about 4.15 km/sec near the peak of the curve at 40 seconds.

B. Dispersion Curves from Doppler Data

We have assumed that the Rayleigh waves and the R-infrasonic waves are well-dispersed and, according to the method of stationary phase, the group velocity is the distance traveled divided by the travel time (Ewing and Press, 1954). The records analyzed were the waveforms recorded by the HF Doppler array after the 1968 Hachinohe and the 1969 Kurile Island earthquakes. The procedure is:

1. Find the period of the R-infrasonic waves from the data by the peak and trough method.
2. Note the arrival time of the peaks and troughs and hence, the arrival times of the waves.
3. Find the time taken by the R-infrasonic waves of a given period to reach the appropriate radio reflection height from a set of ray paths, which are parameterized in terms of wave periods.
4. Find the distance away from the sub-ionospheric point at which the R-infrasonic waves were launched from the ray paths.
5. Determine the times the R-infrasonic waves of the given periods were launched by subtracting atmospheric travel time from the ionospheric arrival time.
6. Determine the launch-point by starting at the sub-ionospheric point and back-tracking along the great circle seismic path by the amount found in (4) above.

7. Calculate the group velocity by dividing the path length between the epicenter and launch point by the time interval between the occurrence of the earthquake and the launching of the R-infrasonic waves.

The initial calculations were carried out by Huang, et al., (1973), for periods greater than about 50 seconds and the results were displayed in the usual manner on a dispersogram. The values agreed reasonably well with the values inferred from seismograms, for example, the dispersion curve compiled by Oliver (1962). However, the curves were systematically lower by about 0.1 to 0.2 km/sec at long periods of about 150 to 200 seconds. At shorter periods of about 40 to 50 seconds, the calculated values were slightly higher. While the short period portion of the curve may be explained in terms of the properties of the crustal structure, the difference in the two curves for the very long period portion of the curve appeared strange since one would have expected greater agreement and less deviation.

The group velocity dispersion curves were re-calculated from the 1968 and 1969 Dopplergrams. A new set of supposedly more accurate ray paths were generated. The calculations were also extended to include the shorter and longer period waves in the 10 MHz waveforms and the shorter period waves in the 1968 5 MHz waveforms. The Dopplergrams which are proportional to velocity were converted to corresponding peaks and troughs in the displacement. The details of this work and the results are presented below.

Figures 9 and 10 show the arrival times of the maxima and minima in the 1969 and the 1968 waveforms as functions of the extrema according to the peak and trough method. Similar plots for the extrema in displacements are shown in Figs. 11(a) and 11(b). In these plots, smooth best-fit curves are drawn through the points rather than connecting them with straight line segments because (1) of the slight but real change in period near the beginning of the 5 MHz curve, and (2) of the increased reading error and uncertainty near the end of the 10 MHz curve (the period of the last trough in the 1969 waveform could not be determined and the position of the previous peak is somewhat uncertain). The curves thus obtained appear to give better representation of the period variation. The periods shown in Table 2 (see page 10) were then determined by constructing the tangent at each point and evaluating the slope. Figure 12 plots the period as a function of the event number. The curves show the general consistency

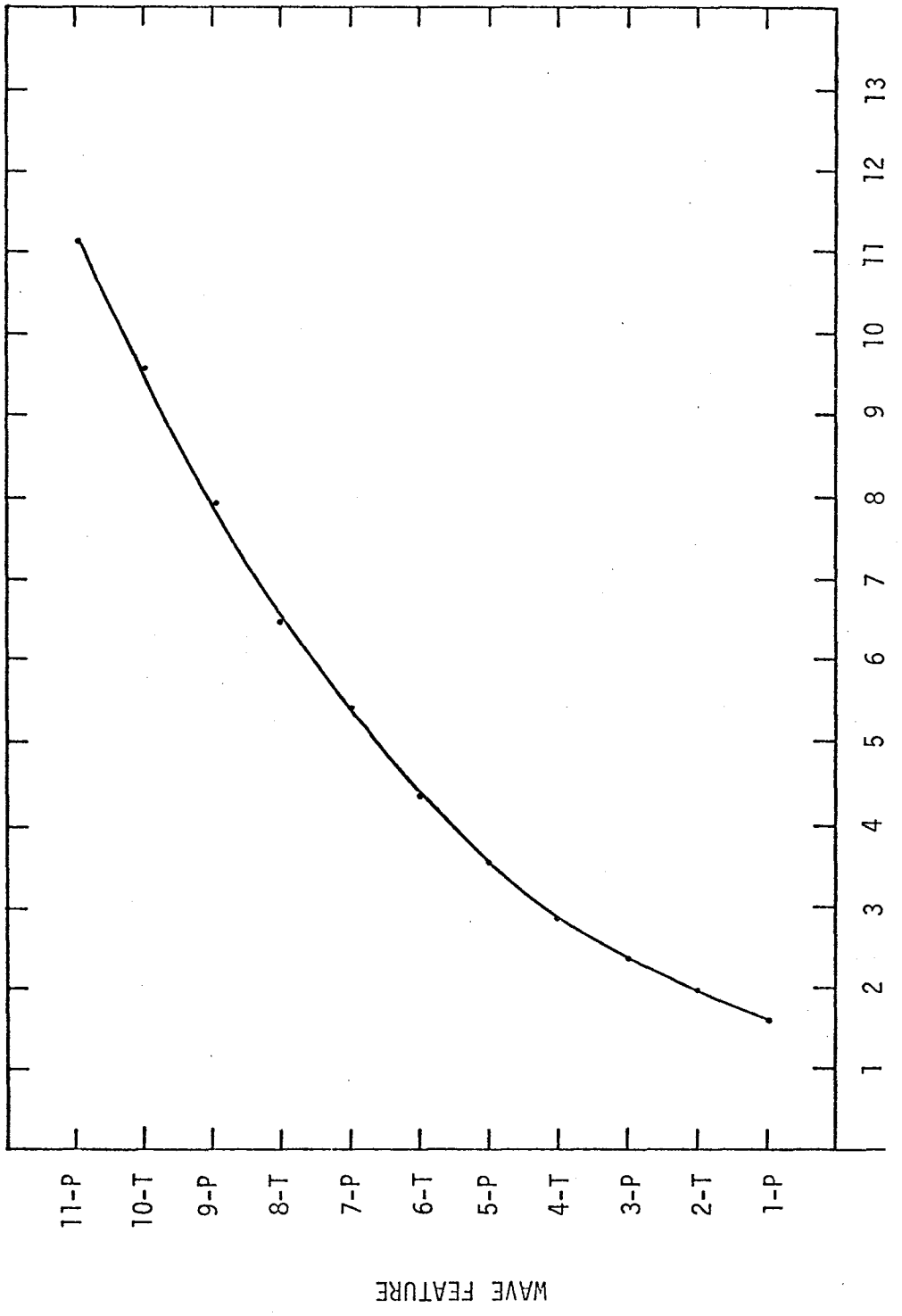

Figure 9. Phase of oscillations vs. arrival time of phase of the 1969 10 MHz event. "N-P" and "N-T" refer to the nth peak or nth trough, respectively. Slope of curve over one cycle is the period.

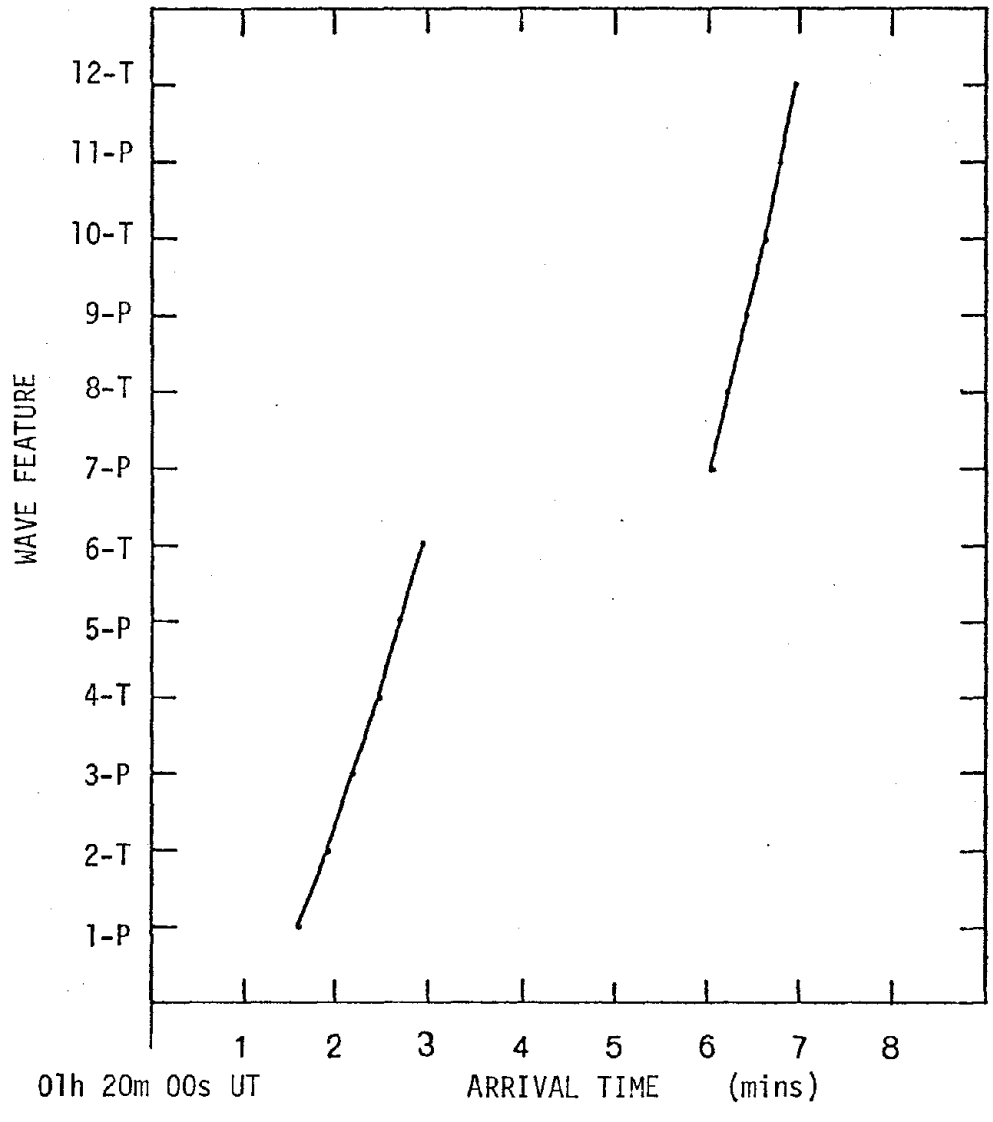

Figure 10a. Same as Figure 9, except for the 1968 5 MHz event.

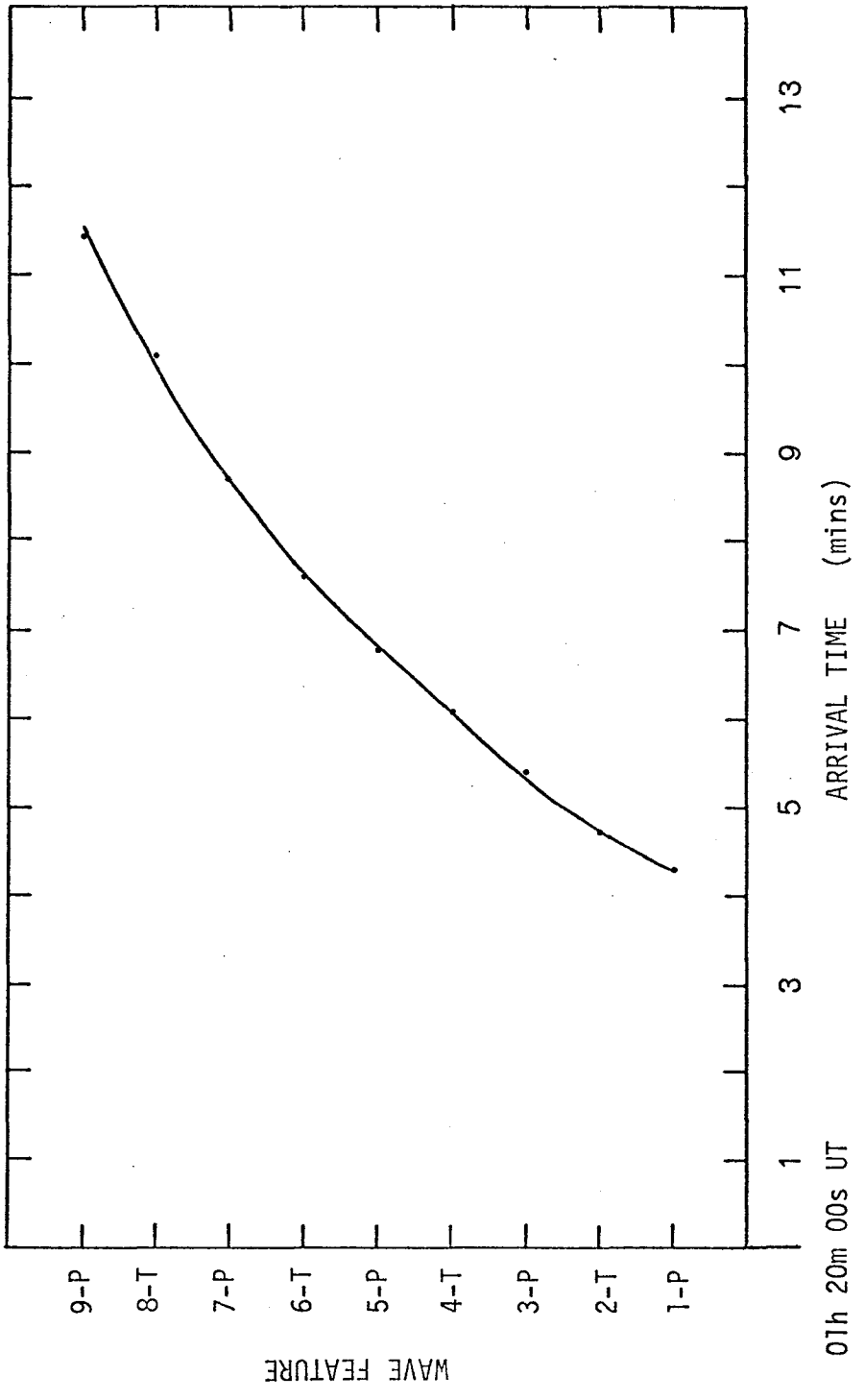

Figure 10b. Same as Figure 9, except for the 1968 10 MHz event.

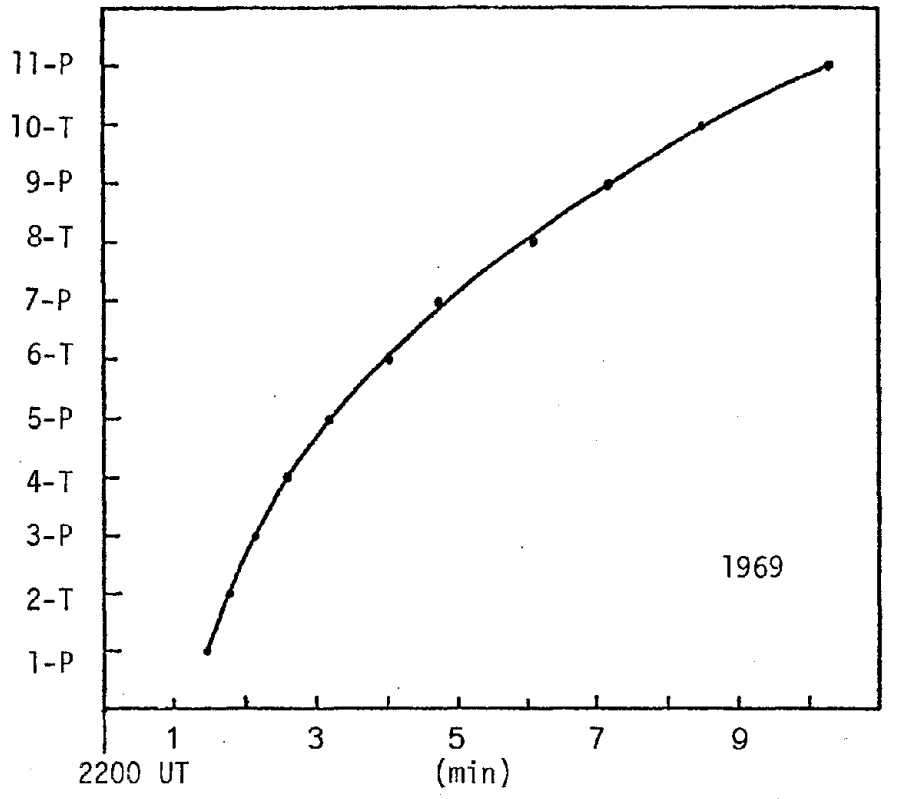

Figure 11a. Same as Figure 9 except peaks and troughs refer to displacement.

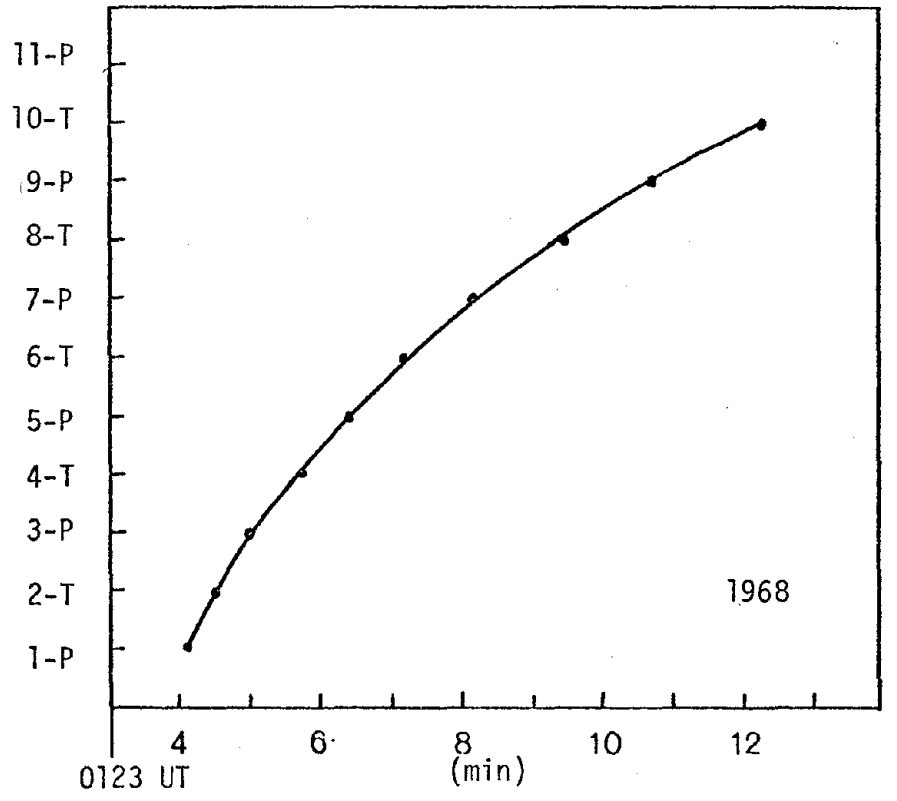

Figure 11b. Same as Figure 10b except peaks and troughs refer to displacement.

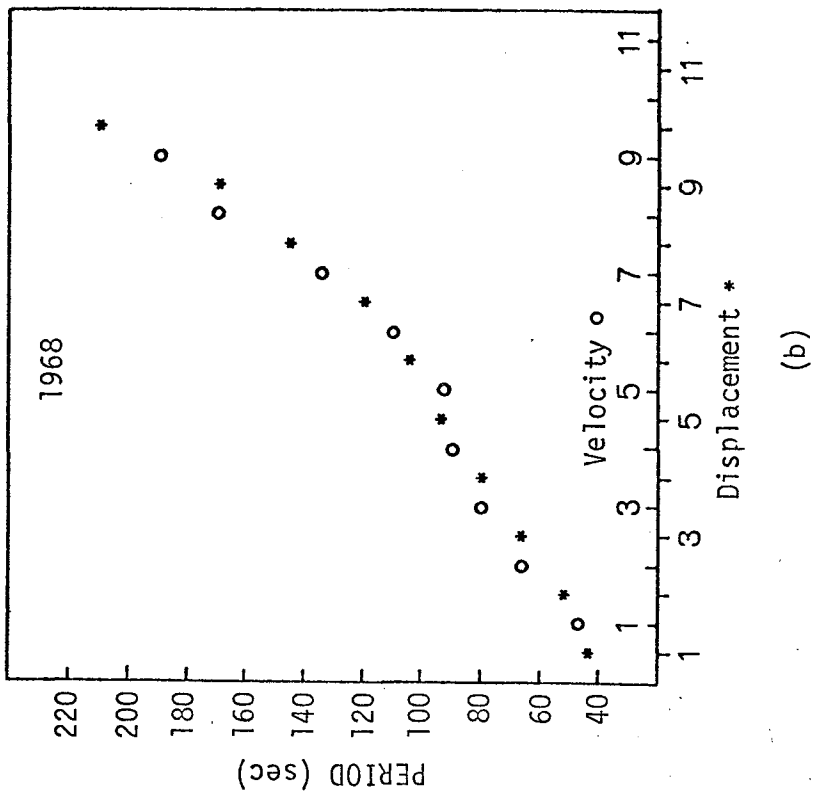

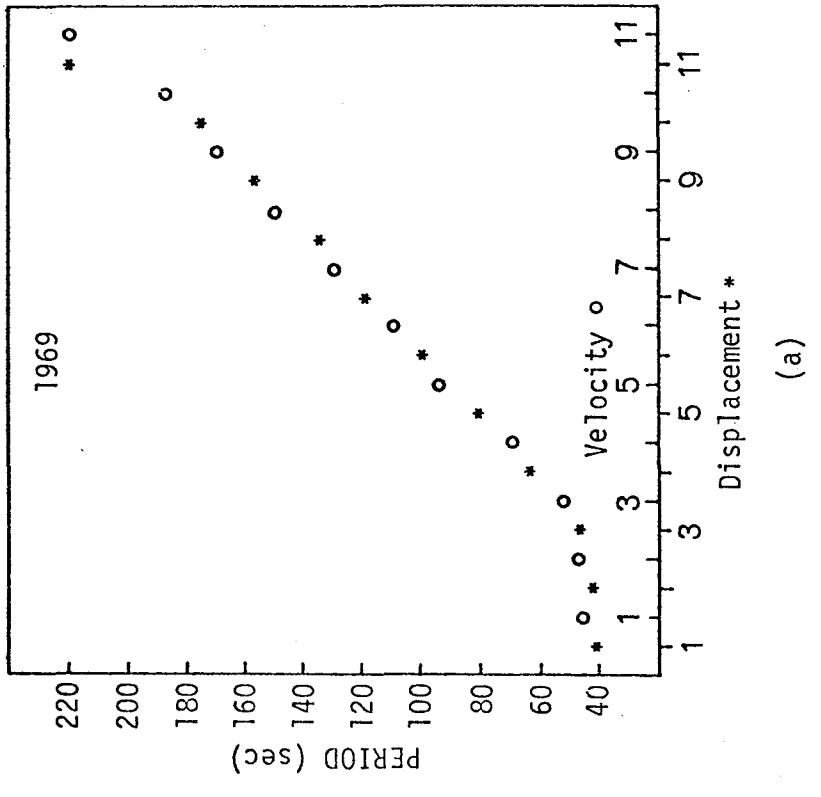

Figure 12. Period of peaks and troughs vs. event number.

of the periods determined from the velocity and the displacement. The general shape of the curves indicates that the waveforms belong to the inverse dispersion branch. (The periods for the 10 MHz waveforms generally differed by about 5 - 10 seconds from the periods determined by Furumoto (1970) and Huang, et al., (1973)).

Since the 5 MHz record was not of the same quality throughout the time interval for the disturbance, only two packets that could be clearly read were chosen. The first packet shows normal dispersion, i.e., a drift toward shorter periods, while the second was essentially of constant period.

The travel time in the atmosphere and the horizontal trace distance of the R-infrasonic waves as functions of the periods for the ionospheric event are respectively shown in Figs. 13 and 14. These curves were determined directly from the ray path and travel time curves in Figs. 7(a) and 7(b) by reading the values given by the radio reflection height for each event. The final values represent converged values found by decreasing the thickness of the layer toward 1 km and determining the limiting value (see Figs. 15a to 15d).

The origin time for the 1968 and 1969 earthquakes were reported in the "Preliminary Determination of Epicenters" at $00^h48^m55^s$UT and $21^h27^m-^s$UT, respectively. The location of the epicenters were (40.8°N, 143.2°E) and (44°N, 149°E) for the Hachinohe (magnitude 7.5) and Kurile (magnitude 7.9) earthquakes, respectively. The distance from the epicenter to the sub-ionospheric point (21°N, 157°W) for the 10 MHz signal for the Manoa station (WWVH was located at Kihei, Maui at that time) is 5975 km and 5615 km, respectively.

Subtracting the travel time of the infrasonic waves in the atmosphere from the observation time of the Doppler signal (Figs. 3 and 4) gives the launch point. Dividing the distance between the launch point and the epicenter by the difference in time between the origin time and the launch time gives the Rayleigh wave group velocity. These calculations are carried out for each period observed in the 1968 and 1969 events in the Doppler data and the results are plotted in Figs. 16 and 17, respectively. These group velocities are thus inferred from the peaks and troughs in the velocity. The process is repeated by considering the peaks and troughs in the displacement and the results are also plotted in Figs. 16 and 17. The dispersion curves determined from the displacements show at the very long

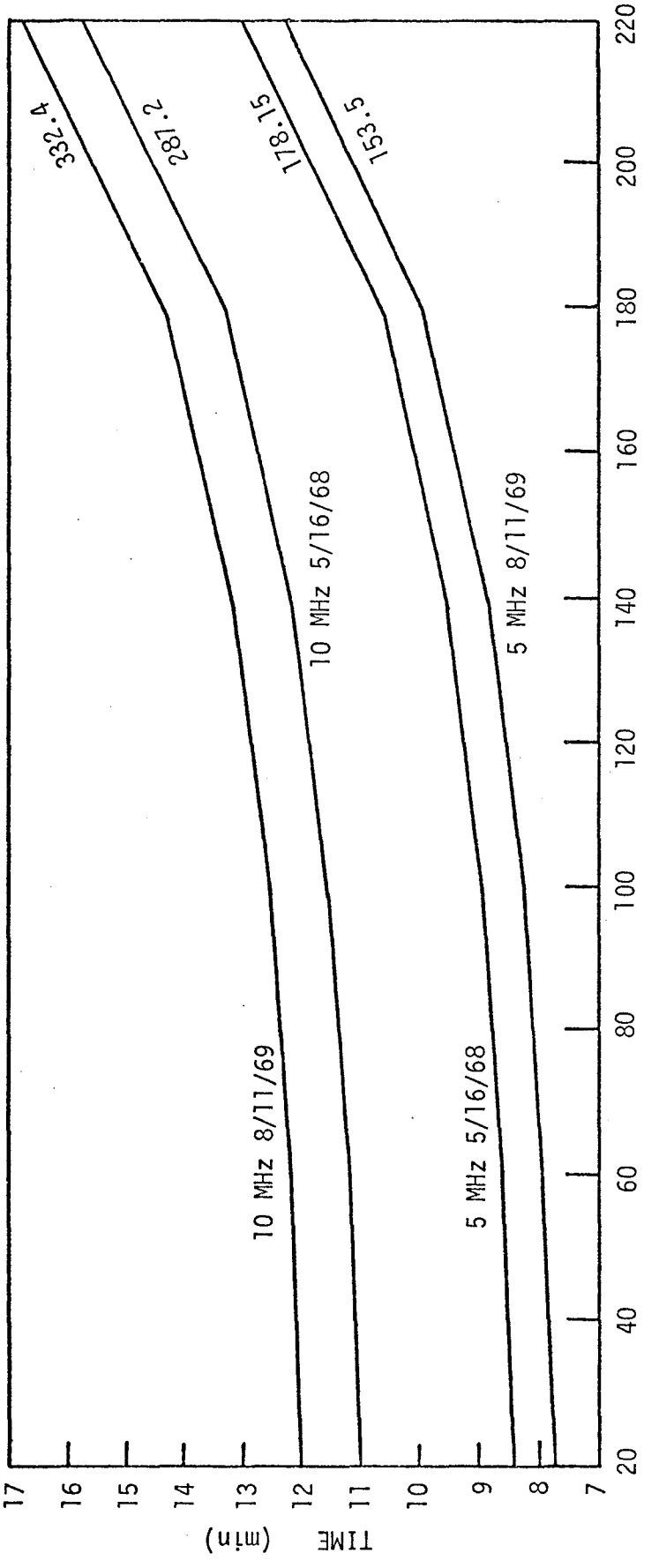

Figure 13. Travel time for R-infrasonic waves as a function of period for the four ionospheric events.

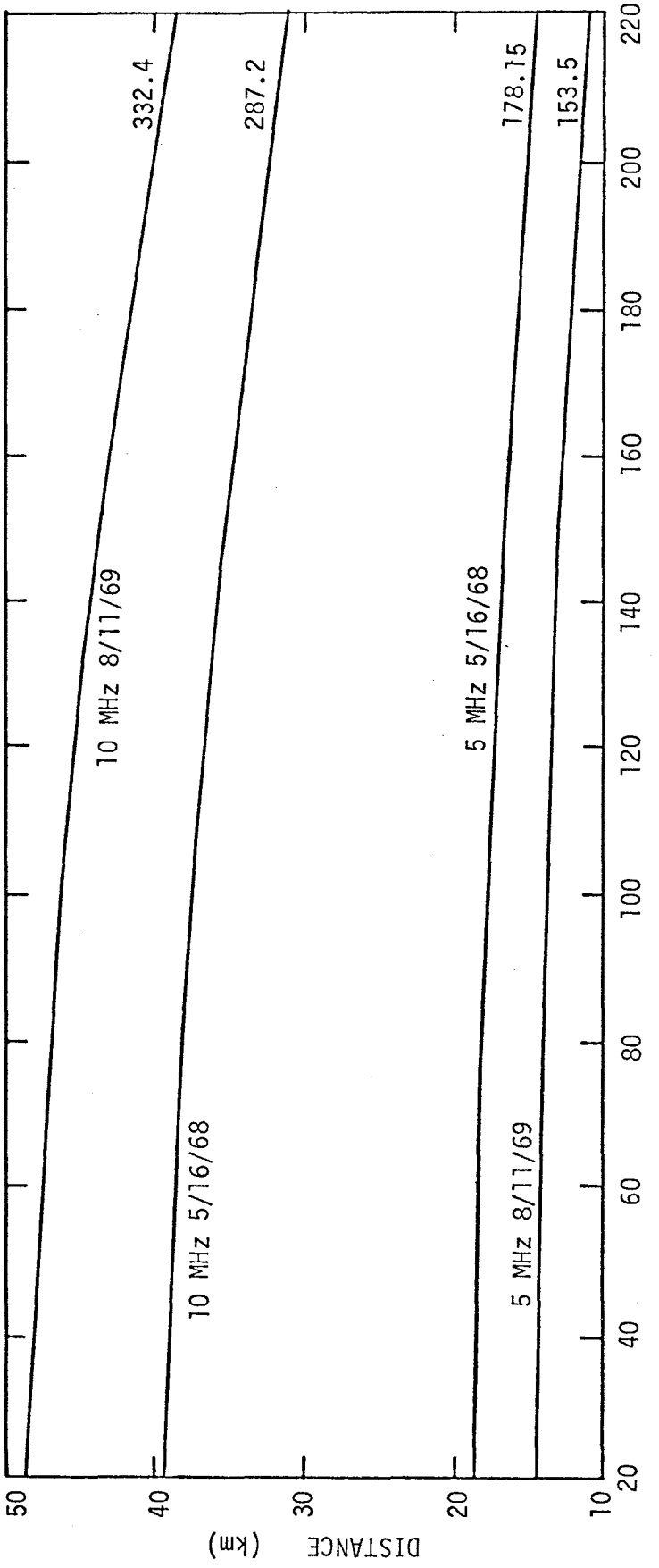

Figure 14. Horizontal displacement of rays as a function of period for the four ionospheric events.

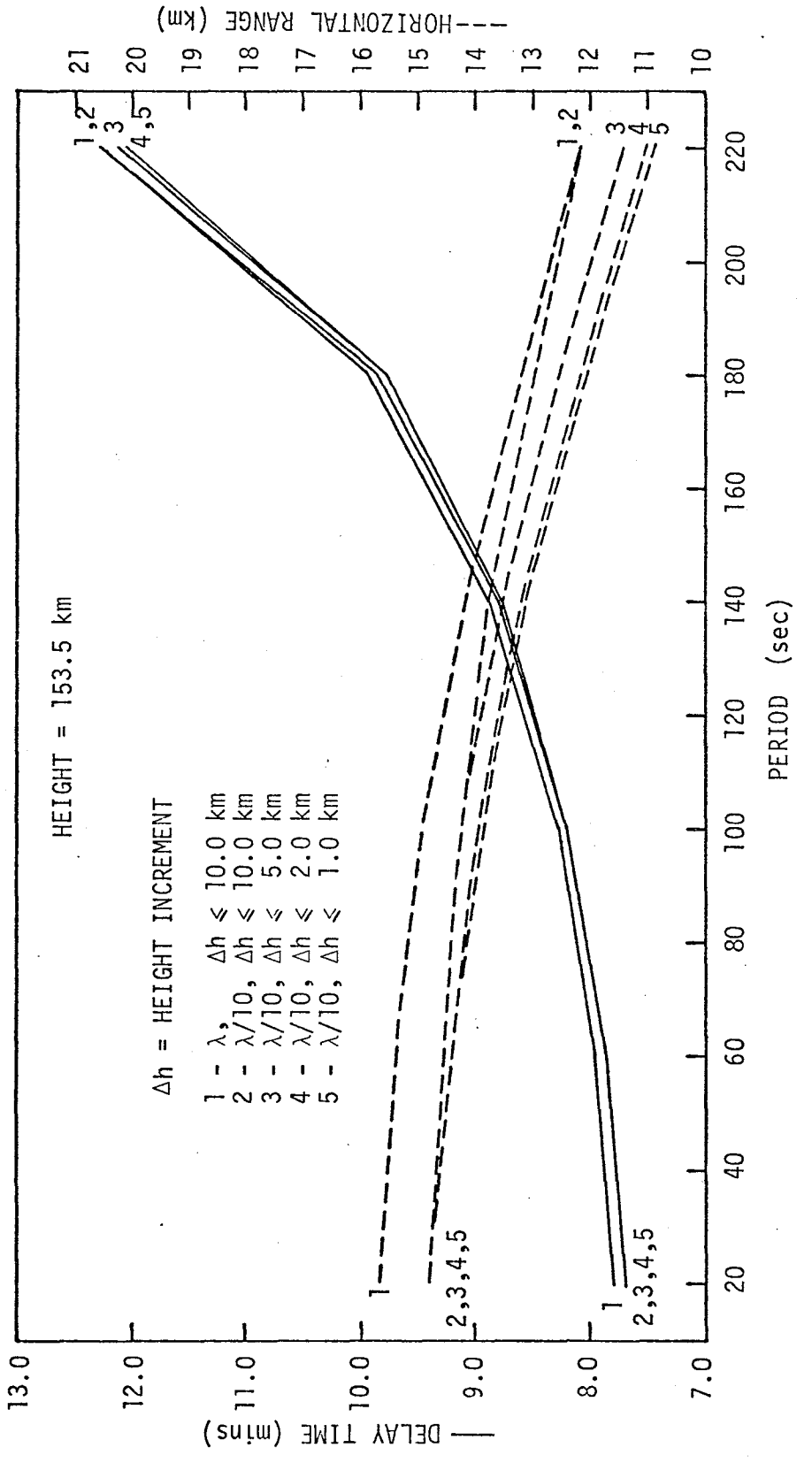

Figure 15a. Limiting values of travel time and horizontal displacement, as atmospheric layer thickness decreases. Separated according to radio reflection height.

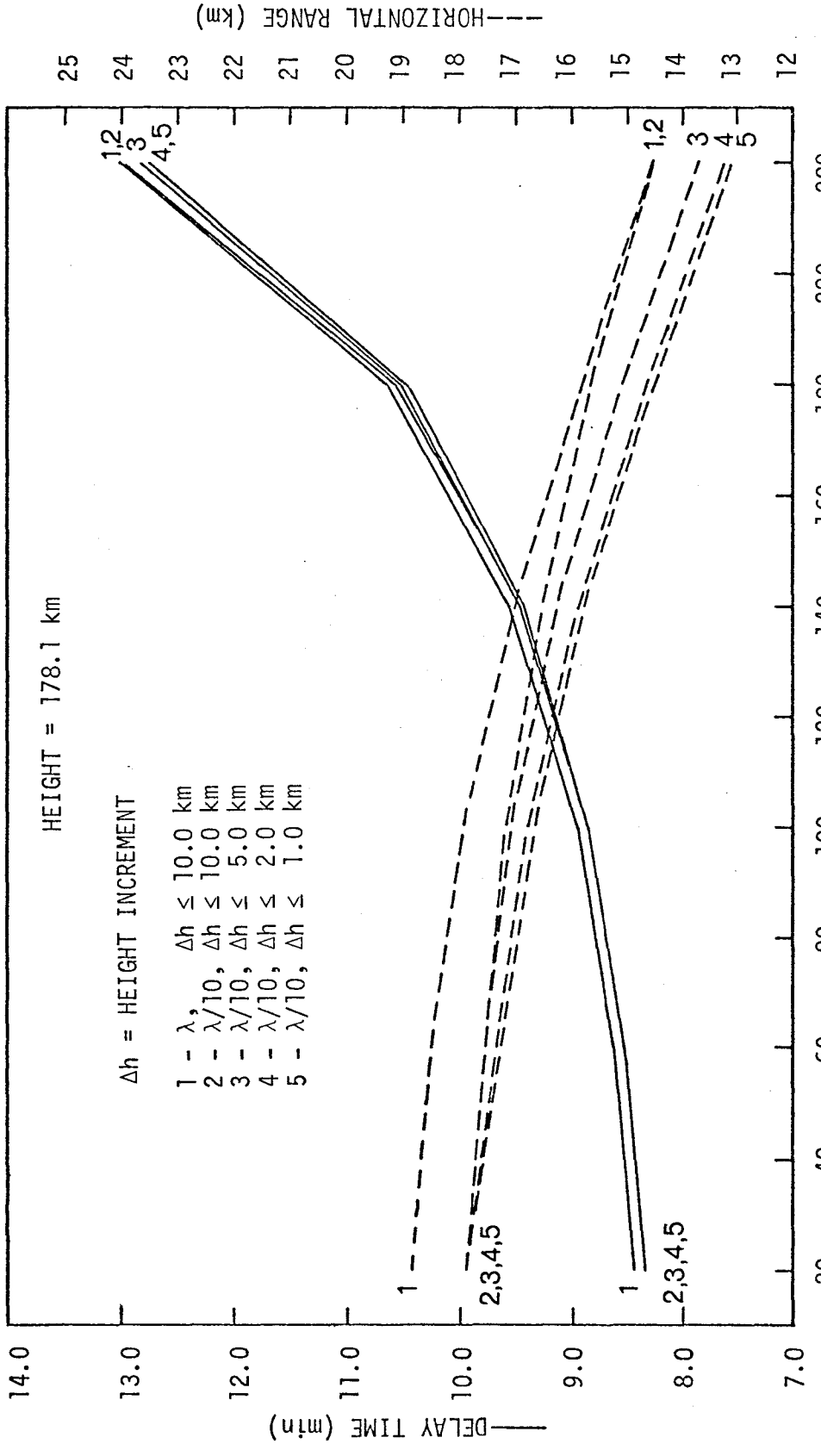

Figure 15b. Limiting values of travel time and horizontal displacement, as atmospheric layer thickness decreases. Separated according to radio reflection height.

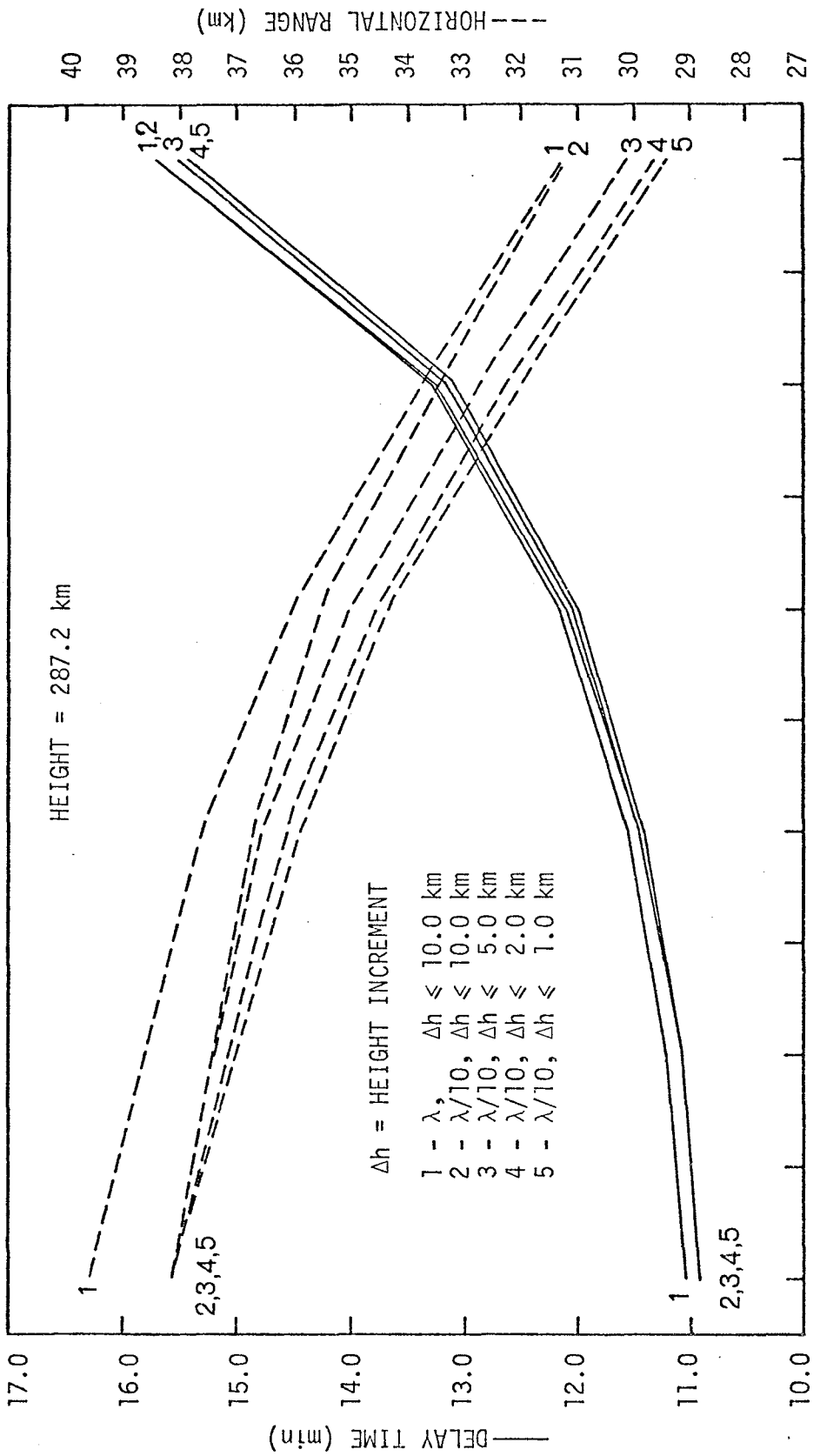

Figure 15c. Limiting values of travel time and horizontal displacement, as atmospheric layer thickness decreases. Separated according to radio reflection height.

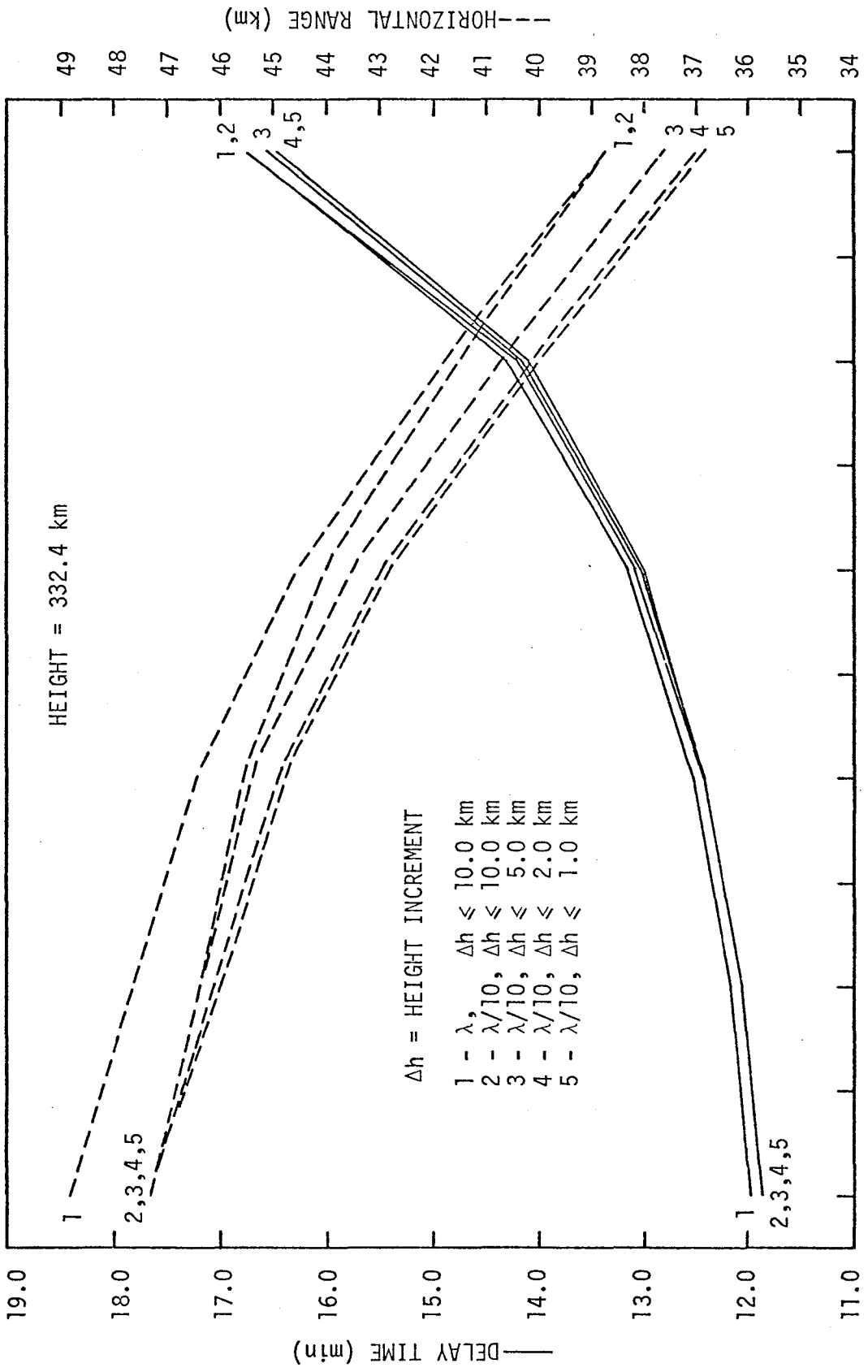

Figure 15d. Limiting values of travel time and horizontal displacement, as atmospheric layer thickness decreases. Separated according to radio reflection height.

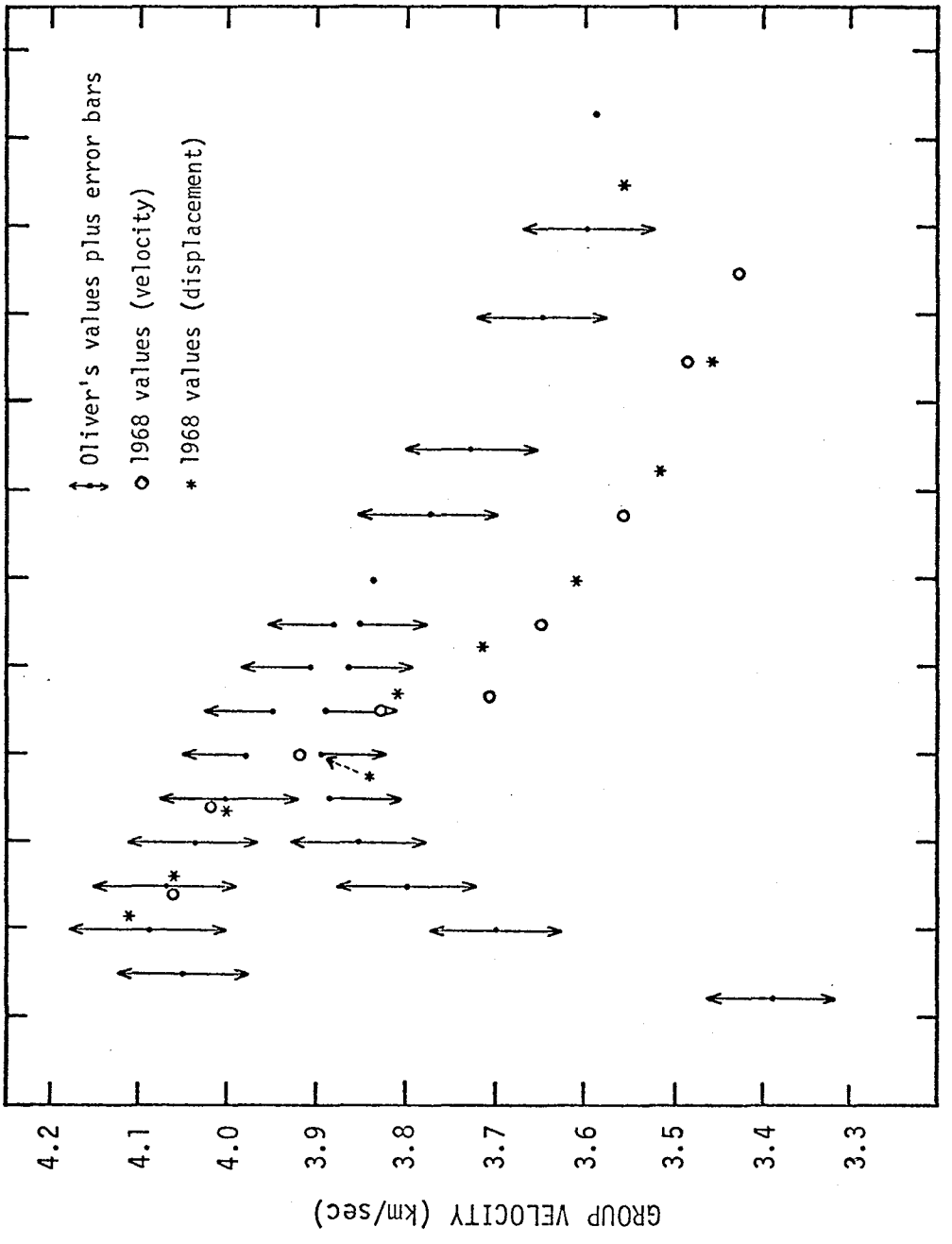

Figure 16. Values of group velocity from the 1968 Dopplergram. Values inferred from the velocity waveform shown separately from those inferred from displacement.

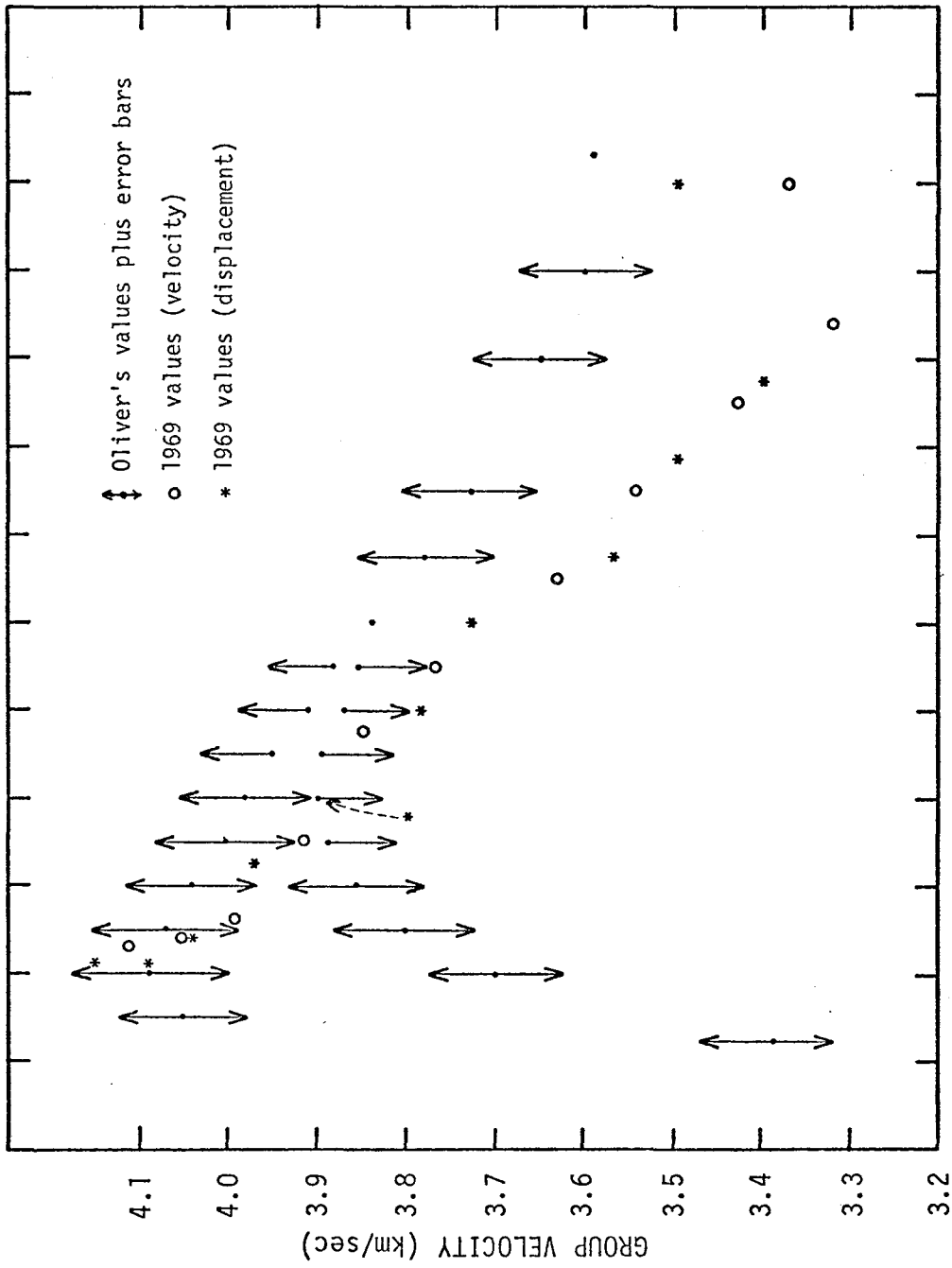

Figure 17. Values of group velocity from the 1969 Dopplergram. Values inferred from the velocity waveform shown separately from those inferred from displacement.

periods, less deviations from Oliver's curve than that determined from the velocity.

In Fig. 19, the above results are compared with several sets of group velocities presented in Fig. 8. The vertical scale has been expanded to avoid congestion. In addition, we have included the averages of Yoshii's studies of earthquakes in the Kurile Islands and Japan and measured at Kipapa, Hawaii (1975). Generally it is difficult to find measurements inferred from R_1 for earthquakes in the Japan - Kurile area and observing stations either in Hawaii or on a path passing through the Hawaiian Islands.

C. Discussion of Results

Figures 16 to 18 show that the group velocity curves determined from the Dopplergrams are within about 5% of the values reported for comparable paths and for average oceanic paths determined from seismograms. The agreement is good for periods less than about 100 seconds and fair for longer periods. The agreement is excellent over periods less than 40 seconds and agrees with Santo's assignment of group velocity regions in the Hawaiian Island chain. The values for periods from 50 to 100 seconds lie above the R_1 curve reported by Yoshii (1975) for R_1 paths measured along oceanic paths. On the other hand, the values determined for the 100 to 200 second periods fall noticeably below the values reported for oceanic and averaged-out paths.

There appears to be a break in the 1968 and 1969 Dopplergram-determined values at a period of about 100 seconds. This is shown by drawing a smooth, best-fit curve through the values. The curve is parallel to the seismogram-determined curves and suggests a delay at the source in the time at which the long period waves were emitted.

There are several possible sources of error in our method for determining the group velocity:

1. Uncertainty in the geographic location of the earthquake.
2. Uncertainty in the time of occurrence of the earthquake.
3. Error in the arrival time.
4. Error in the path of the R-infrasonic waves.
5. Error in the travel time of the R-infrasonic waves.
6. Error in the radio reflection height.

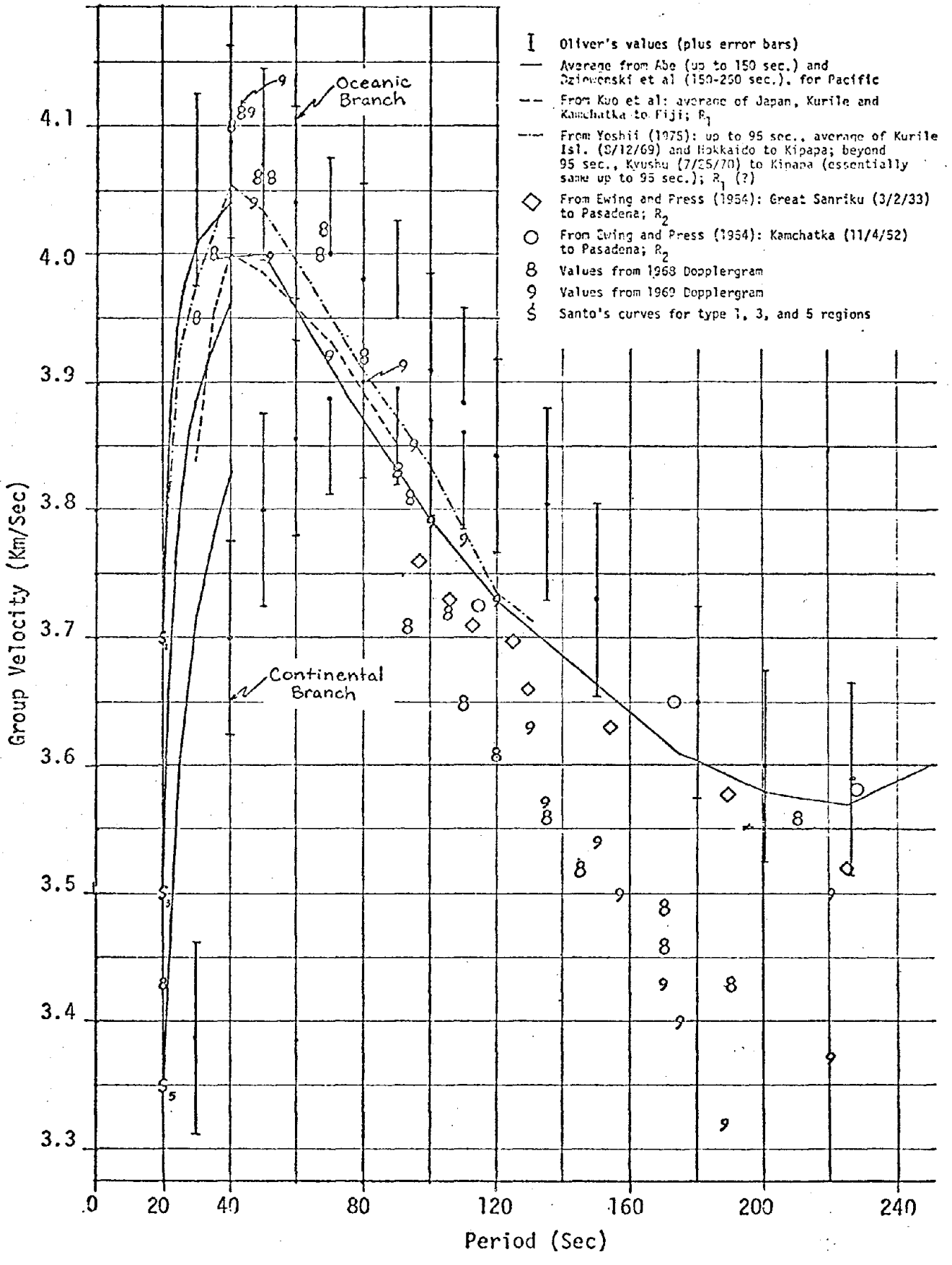

Figure 18. Measurements of group velocity, as determined from the 1968 and the 1969 Dopplergram and seismograms.

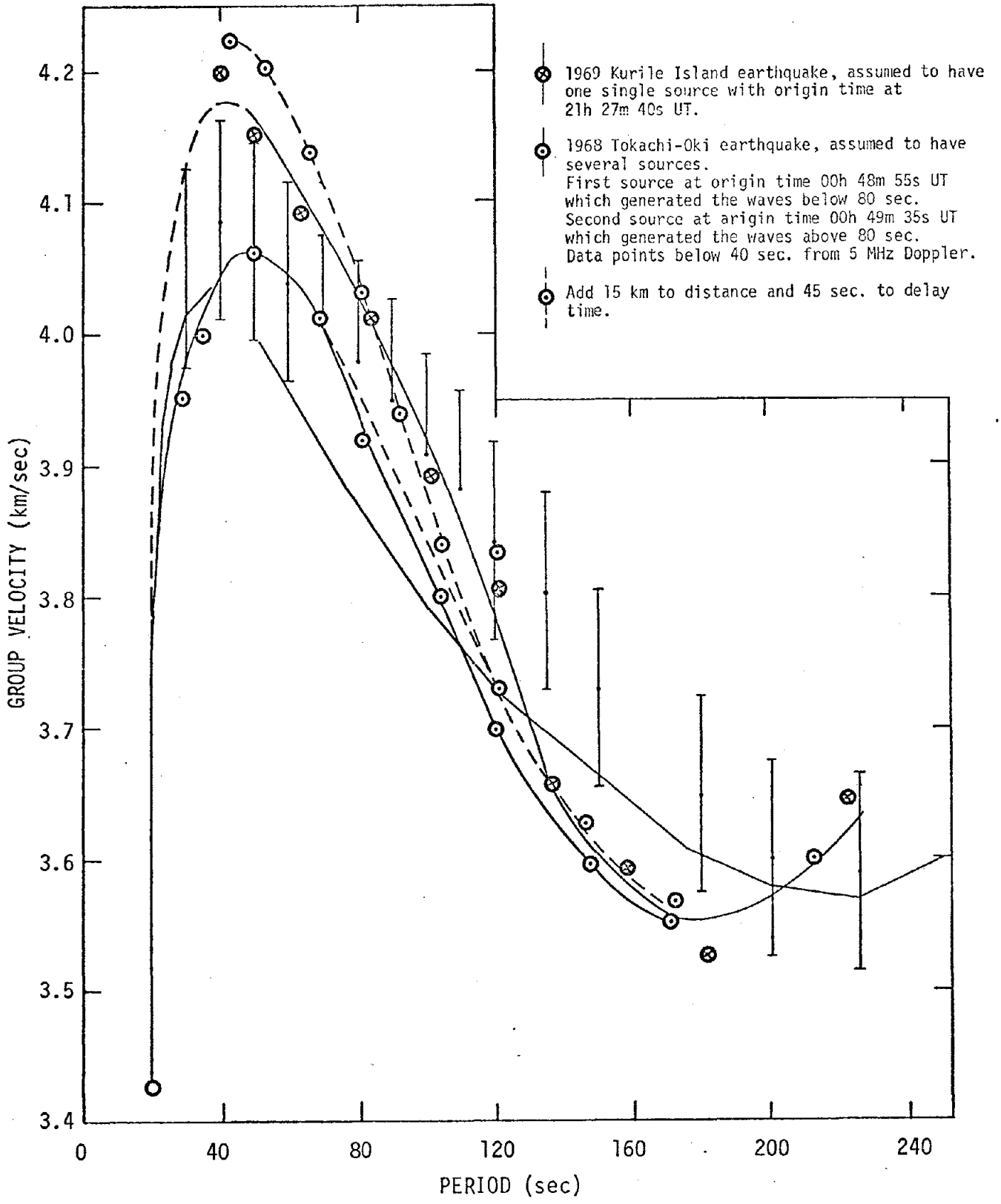

Figure 19. Rayleigh wave group velocity dispersion curves from the 1968 and 1969 Dopplergrams with the correction of 40 seconds in the origin time.

7. Error in the period of the waves.

In addition there are possible errors in applying the correct model to the different types of earthquakes such as those with long ruptures which develop at finite speeds and those with the sinking or rising of approximately elliptic regions.

Due to lack of sufficient data, it is not possible to discuss all of these sources of error and their effect on the calculation of the group velocity. There are no independent data which could be used to indicate whether there is an error in the ray path and travel times (items 4 and 5, above). In fact, when all details are carefully evaluated, this study would give an indication of the correctness of the theory used in calculating the ray paths and travel times. A very complex calculation is used to determine the reflection height (6) from the distribution of the electron density which depends on the season, the solar activity, and the time of day. While it is complex, the physics and theory are relatively well understood and the reflection height reasonably accurately determined (see Appendices 4 and 5). Thus we shall discuss the sources of error due to 1, 2, 3, and 7 in greater detail below.

In studying great earthquakes in the Japan - Kurile Islands area, Abe (1973) recalculated epicentral data for the 1969 earthquake from data provided by the U. S. Coast and Geodetic Survey and also in the Seismological Bulletins of the Japan Meteorlogical Agency. He found slightly different geographic coordinates for the epicenter (43.18°N, 147.48°E) instead of the usual position given (43.1°N, 147.7°E) and an origin time of $21^h27^m40^sUT$, a correction of 40 seconds from the initially listed time of $21^h27^m-^sUT$. While the change in geographic coordinates has almost no effect on the group velocity calculations, the 40 seconds later time of occurrence increases the group velocities by about 0.1 km/sec.

Fukao and Furumoto (1975) studied the Hachinohe earthquake of 1968 using long period seismograms of the World Wide Seismological Stations Network (WWSSN). They show that this earthquake was formed of multiple-shock activities with the largest two shocks generated at 57 km and 93 km WSW of the initial hypocenter at 32 and 45 seconds after the initial break, respectively.

The group velocities were re-calculated with the 40 seconds delay for the above two cases and replotted in Fig. 19. Over almost the entire

range of periods from 40 to 220 seconds, the new curve does not deviate more than about 1.5% from the generally accepted curve. However, there appears to be a jump discontinuity at about 100 seconds period as pointed out earlier. The curves in the lower period range, from 40 to 80 seconds, fall above the average curve and deviate considerably to approximately 4.2 km/sec at 40 seconds. While this is within the error bar indicated by Oliver (1962), it is on the extreme high side. According to Santo's classification of the Pacific basin and the corresponding dispersion curve for Rayleigh waves of periods below 40 seconds (see Fig. 8), aside from the Hawaiian chain, the northern Pacific ocean is of the deep ocean type with group velocities of about 4.15 km/sec at 40 seconds. A relatively smooth curve can be drawn through the points if we assume that the apparent discontinuity in the curves near 100 seconds period is in error and draw an average curve through these points.

The two curves for 1968 and 1969 as constructed give a large difference of about 0.1 km/sec, which does not appear to be normal for waves from two sources separated by about 450 km and propagating to Hawaii. Another possibility then, is that the curve is a composite made up of the shorter period wave components (40 - 80 seconds) generated by the early event and the longer period components generated by the second event about 40 seconds later.

In calculating the group velocity from the Dopplergram, the arrival time could be read fairly well on the front half of the waveforms before the peak in the envelope, which contains the short and medium periods less than 100 - 120 seconds. However, the arrival time could not be read as well on the back half which contains the longer periods. The upward and downward excursions in the front half are nearly sinusoidal with well-defined maxima and minima. On the other hand, the upward excursions in the back half have sharp rises and gradual declines and vice versa for the downward excursions. This has made it difficult to locate the "peaks" and "troughs". An error of 10 to 20 seconds may be possible and this could lead to an error of about 1% in the calculated group velocity.

An error in the arrival time could lead to an even larger error in the group velocity because of the way the periods are determined. As shown in Figs. 9 to 12, a change in the arrival time will alter the shape of the curve in the figures and thereby alter the slope of the tangent to the curve. The period is related to the value of the slope and could

ultimately affect the value of the group velocity calculated since the error in period will lead to errors in both the atmospheric travel time and the horizontal displacement. However, no attempt was made to estimate the magnitude of the error.

There are two other sources of error in finding the periods: (1) in determining the curves which give the best representation of the data on arrival time vs. phase and (2) in determining the tangent to this curve. Large errors can be introduced by connecting consecutive points and forming derivatives from neighboring points, unless the figure contains a large number of closely spaced points, i.e., the waveform contains many sinusoid-like oscillations with only slightly different periods. A better method would be to find the curve which best fits the given points and find the tangent to the curve. This latter method was used to determine the periods in Figs. 9 to 12. It is quite easy and quick but it can introduce an error of 10 - 20 seconds in the period, especially at the ends of the curve. Lau (1974) computed the periods using the Hilbert transform and analytic signal method. This latter method tends to give periods representative of the curvature of the waveform near the peak or the trough. The largest difference in the period in the two methods was about 20 seconds.

As previously noted, an error in period will result in an error in the atmospheric travel time and horizontal displacement. The error in the travel time from ground level to the ionosphere could be quite significant at the long periods where a 20 second error in the period could result in an error in the travel-time by as much as 1.5 minutes. A careful FFT calculation should be carried out to determine the period of the waves with possibly greater accuracy.

Ben-Menahem (1961) has shown that the phase of the harmonic components of a Rayleigh wave train will be retarded by the amount

$$X = \frac{b\omega}{2V_f}\left(1 - \frac{V_f}{V_p}\cos\Theta\right) \qquad (11)$$

if the ground ruptures of length b along a line, at a speed V_f, and at an angle Θ between the rupture line and the direction of the observer. ω is the angular frequency and V_p is the phase velocity of the Rayleigh wave component. Press and Ben-Menahem (1961) then showed that one will observe a group velocity:

$$U' = \frac{X}{t} = \frac{U}{1 + \frac{b}{2X}\left(\frac{U}{V_p} - \cos\Theta\right)} \qquad (12)$$

where X is the distance traveled, t is the travel time, and U is the usual group velocity, i.e., $U = \frac{d\omega}{d\underline{k}}$, where $\underline{k}$ is the wave vector. Thus the observed group velocity U' will not be the same as the mathematically defined velocity U because of the influence of b and V_f.

Solving equation (12) for U, we have

$$U = \frac{U'\left(1 - \frac{b}{2X}\cos\Theta\right)}{\left(1 - \frac{b}{2X}\frac{U'}{V_f}\right)} \quad . \qquad (13)$$

From Abe (1973) we assume the parameters

	b (km)	V_f (km/sec)	Θ (°) estimated
1968	100	3.8	40
1969	400	3.8	50

Table 5 shows the calculated results of the finiteness factor correction to the group velocity for some of the longer period waves. The increase from U' to U is less than 0.02 km/sec and 0.05 km/sec for the 1968 and 1969 events, respectively. Since b = 400 km, used for the 1969 event, is about two times as large as the area reported by Abe (1973), we can say that the finiteness factor introduces an error in the group velocity of less than 1%.

With the new information on the origin time of the 1968 and 1969 earthquakes, the group velocity dispersion curves calculated from the Dopplergrams is within about 2% or less of the values inferred from seismograms. Possibly 1% of the error could be due to an uncertainty in the travel time which comes from the proper choice of the occurrence time, the arrival time of the various periods, the travel time of the R-infrasonic waves, and the determination of the reflection height of the radio wave. The other 1% of the error could be due to an uncertainty in the period of the harmonic component recorded on the Dopplergram. This affects the ray path and travel time of the R-infrasonic waves, especially at the long periods. The finiteness factor due to b and V_f is evidently too small to account for any sizable portion of the error.

Table 5 Finiteness Factor Correction

1969 Kurile Islands earthquake:

V_f = 3.8 km/sec
b ≃ 400 km
Θ ≃ 50°
x = 5615 km

Feature #	Period	U' (km/sec)	U (km/sec)
5	95 sec	3.85	3.91
6	110 sec	3.77	3.82
7	130 sec	3.63	3.68
8	150 sec	3.54	3.58
9	170 sec	3.43	3.46
10	188 sec	3.32	3.35
11	220 sec	3.37	3.40

1968 Tokachi-Oki earthake:

V_f = 3.8 km/sec
b ≃ 100 km
Θ ≃ 40°
x = 5975 km

Feature #	Period	U' (km/sec)	U (km/sec)
5	93 sec	3.71	3.72
6	110 sec	3.65	3.67
7	135 sec	3.56	3.56
8	170 sec	3.49	3.49
9	190 sec	3.43	3.49

V. DETERMINATION OF THE INITIAL PHASES OF RAYLEIGH WAVES

According to the theories of Iida (1970), Ben-Menahem, et al. (1972), and others, a large dip-slip type earthquake in the ocean could generate long period Rayleigh waves and long period water waves simultaneously while a strike-slip type will generate neither Rayleigh nor water waves. Moreover, the generation of long period Rayleigh waves would imply that the source of the earthquake is of large areal dimensions and involves huge amounts of energy. The sudden change in the gravitational potential energy due to the sudden displacement of the ocean floor would transfer this energy into kinetic wave energy of the water waves. Thus the mere observation of the long period Rayleigh waves should signal the possibility of strong long period water waves, which could travel to great distances, if the earthquake occurred in relatively shallow waters. It has been implicitly assumed in our study that the initial phase would give us another measure of the earthquake source and improve the predictability of whether a tsunami has been generated.

This chapter is concerned with a method of determining from the Dopplergram the initial phase of the ground motion of an earthquake. Furumoto (1970) first proposed the method and applied it to the 1969 Kurile Island earthquake. The method was subsequently modified by Najita and Lau (1974) and it was applied to the 1968 Tokachi-Oki as well as the 1969 Kurile Island earthquake. In Section A, the steps in the method will be presented. In Section B, the method will be applied to the 1968 and 1969 earthquakes and in Section C, a discussion of the results will be presented.

A. The Concept and Method

We assume that an earthquake with strong vertical motion has generated large amplitude long period Rayleigh waves, and that these waves have generated R-infrasonic waves in the lower atmosphere which then propagated to the upper atmosphere and produced oscillatory ionospheric motions. These motions are then detected by the HF Doppler method and a Dopplergram of the oscillations is produced in the manner schematically presented in Fig. 1. The procedure for determining the initial phase of the Rayleigh waves from the Dopplergram follows:

1. Convert the Dopplergram from one representing variations in the vertical velocity of the reflecting layer to one representing the variation in the height of the layer.

2. Determine the arrival time of the peaks and troughs in the converted record.
3. From the information in Step 2 and the properties of the R-infrasonic waves, calculate the arrival time and the location (relative to the sub-ionospheric point) of the corresponding peaks and troughs in the Rayleigh wave train.
4. From the results in Step 3 and the phase velocity of Rayleigh waves at the appropriate periods, determine the initial phase of the harmonic components that produced the peaks and troughs.

The procedure described above is an adaptation of a general method of determining source mechanism devised by Brune, et al., (1960). Brune's method attempts to use the phase information available in records of well dispersed wave trains to find the initial phase of the harmonic components if the phase velocity dispersion curve is known. The method has also been used to determine the phase velocity dispersion curve if the initial phase is known as in the case of a known source in a laboratory experiment. The method has been used in a number of different situations (e.g. Brune and Dorman, 1963; Nafe and Brune, 1960; Gregersen, 1970; and Weidner, 1974).

Brune's method starts with the disturbance written as a Fourier integral (in a one-dimensional format):

$$U(x,t) = \frac{1}{2\pi} \int_0^\infty A(k) \cos(\omega t - kx + \phi)\, dk \qquad (14)$$

where $U(x,t)$ is a component of the disturbance at position x and time t, k is the wave-number, ω is the angular frequency, $A(k)$ is the amplitude of a harmonic component and $\phi(k)$ is the initial phase. If we expand the cosine term we have:

$$U(x,t) = \frac{1}{2\pi} \int_0^\infty A(k) \cos\phi \cos(\omega t - kx)\, dk - \frac{1}{2\pi} \int_0^\infty A(k) \sin\phi \sin(\omega t - kx)\, dk \,. \qquad (15)$$

The stationary phase approximation (see e.g. Jeffreys and Jeffreys, 1966; Murray, 1973) can be applied to each integral separately and the results recombined to obtain:

$$U(x,t) \simeq \left[\frac{1}{2\pi t |\omega''|_0} \right]^{1/2} A(k_0) \cos(\omega_0 t - k_0 x + \phi(k_0) \pm \pi/4) \qquad (16)$$

where $\omega'' = \frac{d^2\omega}{dk^2}$, the subscript "o" denotes the solution $k = k_0$ to the equation for the group velocity, $x/t = V_g(k)$. The phase shift, $\pi/4$,

introduced by the approximation is positive for normal dispersion, $\frac{dV_g}{dP} > 0$, where P = period, and negative for inverse dispersion. The phase term in equation (16) implies that the harmonic component of period $P_o = \frac{2\pi}{\omega_o}$, which produced a peak or trough at time t_o, arrived at $t_o - \frac{P_o}{8}$ for inverse dispersion. This shows how one can relate the extrema in the observed wave form to the corresponding extrema in the harmonic component. There is an additional phase advance of $\pi/4$ for the components due to the mechanism of wave-emission for seismic sources (Brune, 1961).

While both Furumoto (1970) and Najita and Lau (1974) carried out Step 4 graphically, they differed in the criteria used to find the initial phase on the graph.

The graphical method consists of the following steps:

1. Plot a periodic wave of the appropriate period, such as a sawtooth wave, as a function of distance to represent the harmonic component that produced the first peak or trough in the observed wave train.
2. Plot periodic waves of the appropriate periods for the harmonic components that produced the succeeding peaks and troughs below the first wave. However, delay them relative to the first wave by a distance = (phase velocity) x (difference in arrival time relative to the first peak or trough).

3a. (Furumoto) Trace back along the periodic waves toward the source and find the position where the phase of the waves are identical. This phase is then the required initial phase.

3b. (Najita and Lau) Calculate the distance the point of the initial phase of the different periodic waves had traveled during the time between the occurrence of the earthquake and the arrival of the first peak or trough at the launch point, then trace forward on the periodic waves by this distance and read the initial phase for the harmonic components for the given periods (see Appendix 7).

Furumoto arrived at an initial phase of $\pi/4$ before a trough (for all periods, because this is built into his criterion) and concluded that the initial motion was downward at a dip angle of 45°. Interestingly enough, Najita and Lau also arrived at the same initial phase for all periods. These agreements were arrived at in spite of the fact that both Furumoto and Najita and Lau did not include all of the necessary phase shifts or

even the same phase shifts.

Our present procedure for calculating the initial phase of the ground motion of earthquakes follows the steps outlined earlier. However, the following modifications are made: 1) the peaks and troughs in displacement are used; 2) the revised calculations of the ray paths and travel times of the R-infrasonic waves are used; and 3) the $\pi/4$ phase shift from the stationary phase approximation is included.

The peaks and troughs in the displacements and the corresponding periods are listed in Table 3 (see page 12). The phase velocity at the different periods was determined from the graph of Fig. 20, which is a reproduction from Dorman (1969). The basic travel time is the number of seconds between the time of occurrence of the earthquakes and the time the R-infrasonic waves were launched. This is obtained from the work on group velocity and corrected for the $\pi/4$ phase shift from the stationary phase approximation by adding P/8. The distance the point of initial phase traveled is found by multiplying the corrected travel time and the phase velocity. The distance this point is ahead or behind the peak or trough at the launch point is found by subtracting the distance from the epicenter to the launch point. The residual (i.e. excess distance) is then expressed in units of wavelength by dividing it by the product of phase velocity and period. Thus, the point of initial phase is found to be ahead of or behind the corresponding peak or trough by an integral number of wavelengths plus a portion of a wavelength, and the latter, the fractional part, is the initial phase given essentially in fractions of a cycle. For convenience in representing the results on a graph, the calculated values are adjusted so that they give the phase relative to the nearest peak, as shown schematically in Fig. 21. The phase is read with respect to the peak since $\phi = 0$ corresponds to a peak for the cosine function. As shown in the diagram, a positive (negative) phase corresponds to a point in the first cycle ahead of (behind) a peak.

These first estimate values of initial phase are plotted in Figs. 22(a) and 22(b) to provide a more direct visual representation of the initial phase. The peaks and troughs at the launch points have been shifted laterally so that they coincide at the vertical reference line.

Ben-Menahem and Toksoz (1962, 1963) point out that the initial phase is made up of three parts:

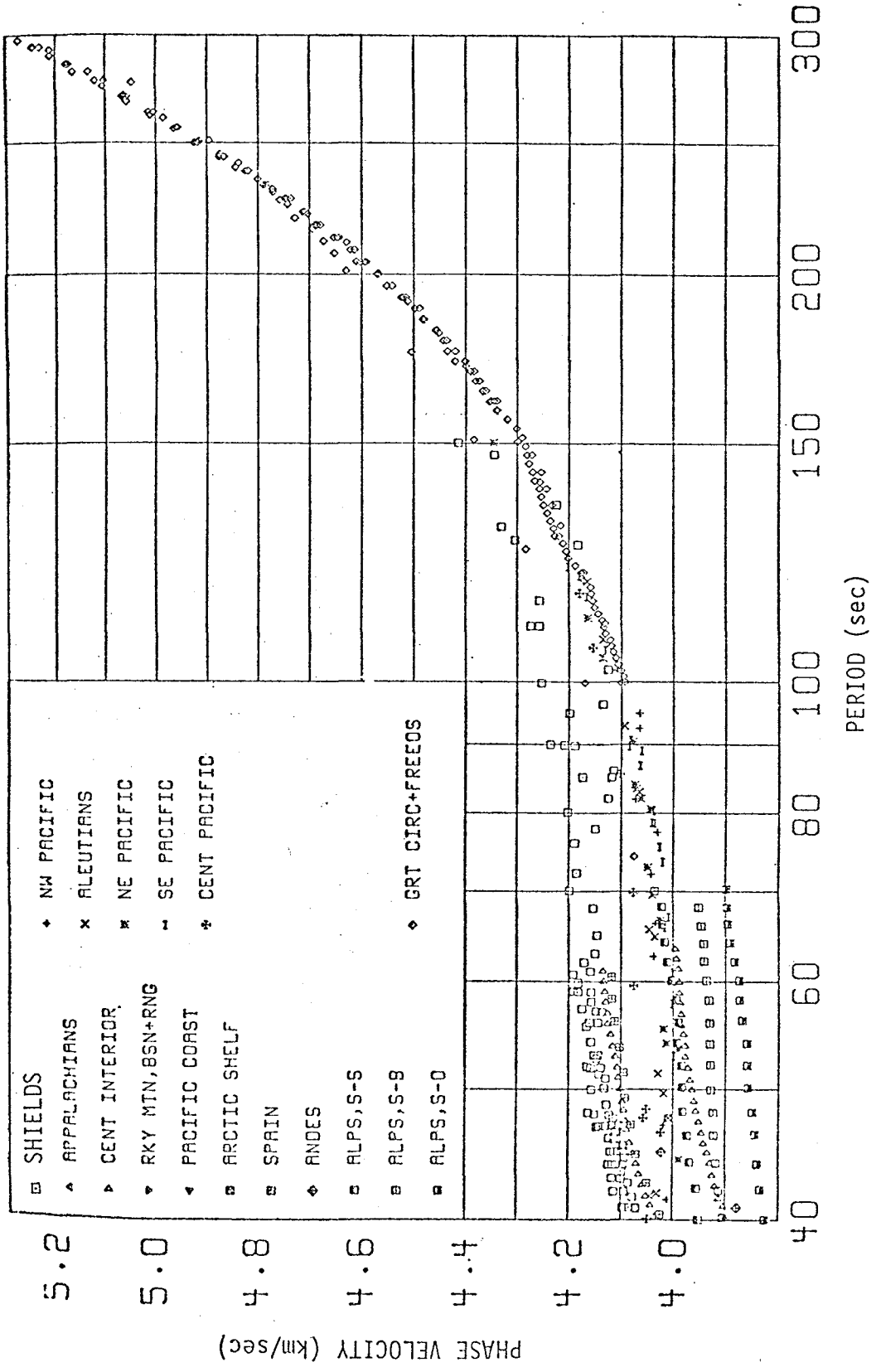

Figure 20. Summary of phase velocity of oceanic Rayleigh waves (from Dorman, 1969, p. 259).

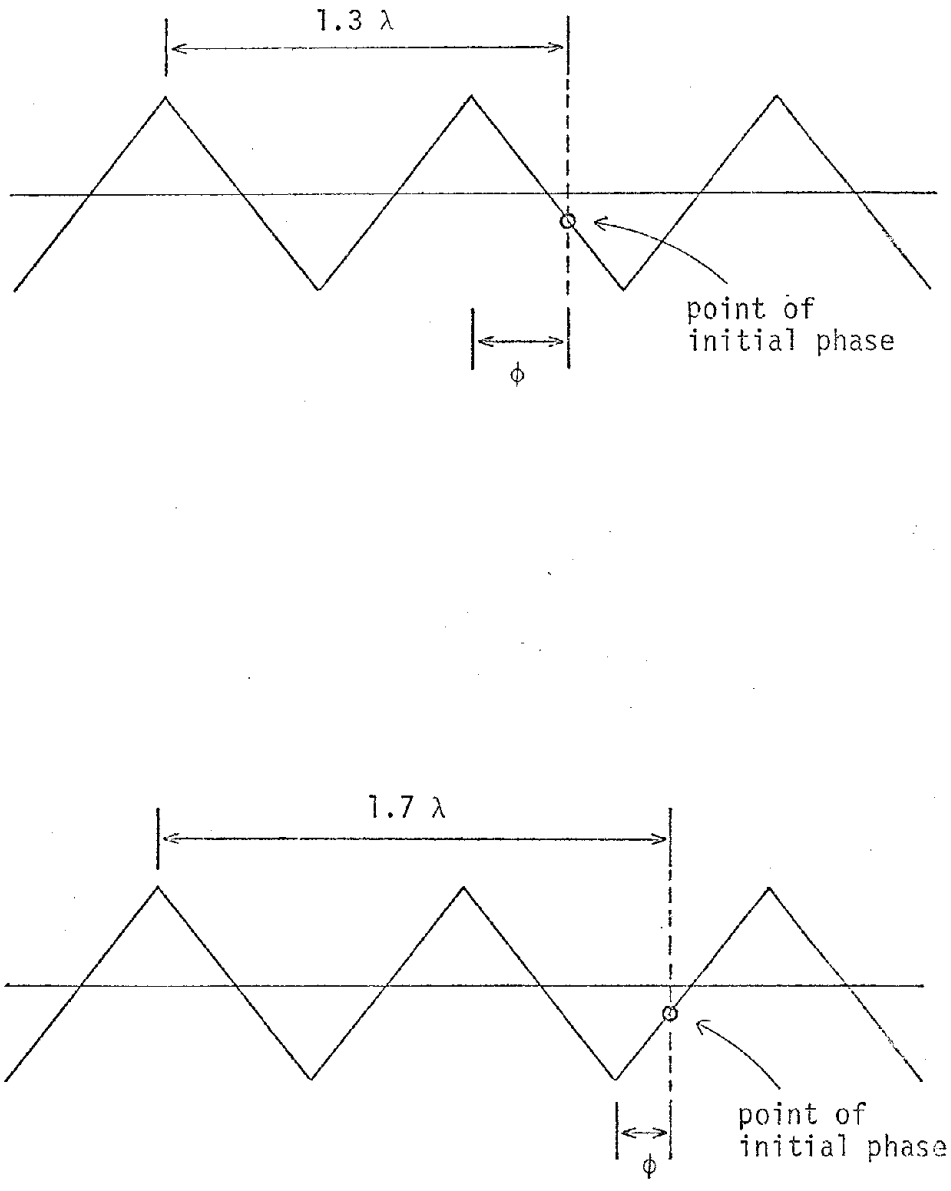

Figure 21. Diagram showing how the initial phase, ϕ, is defined.

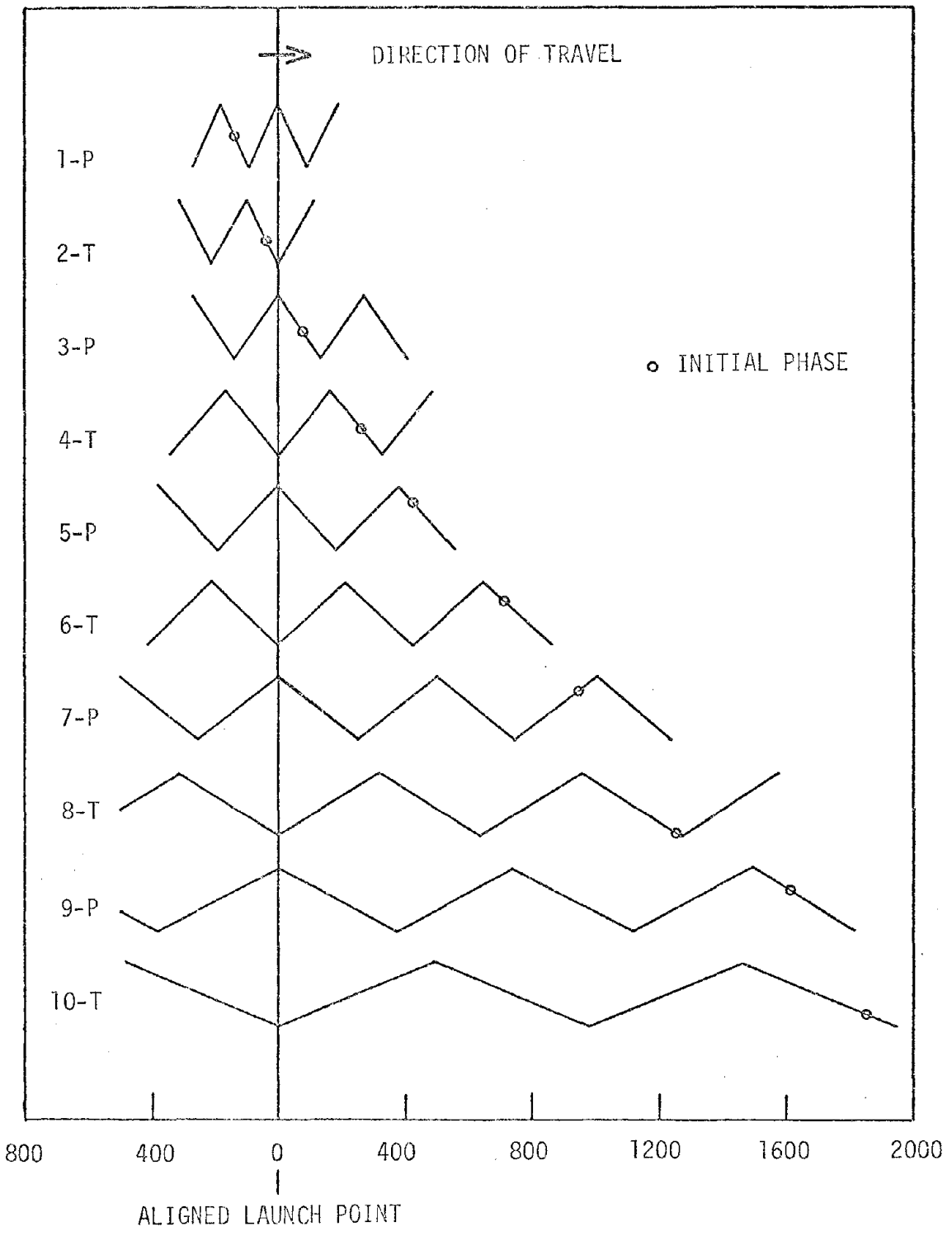

Figure 22a. Determination of the initial phase of the ground motion at the epicenter for the 1968 earthquake. The initial phase is shown on the period waves of the appropriate period. The peaks and troughs at the launch points have been shifted horizontally until they coincide at the vertical line.

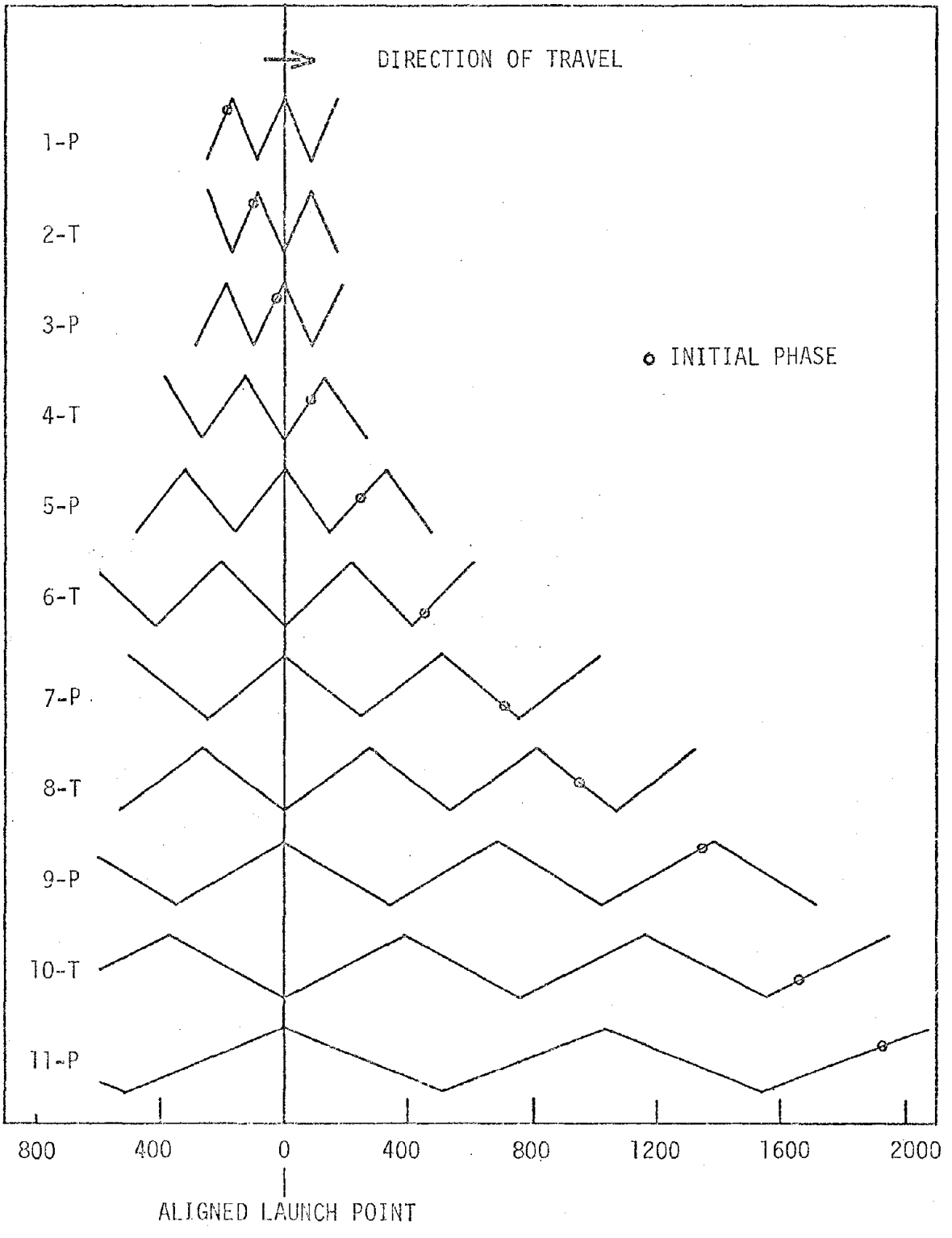

Figure 22b. Determination of the initial phase of the ground motion at the epicenter for the 1969 earthquake. The initial phase is shown on the period waves of the appropriate period. The peaks and troughs at the lauch points have been shifted horizontally until they coincide at the vertical line.

$$\phi = \phi_s + \phi_t - \phi_f \qquad (17)$$

where ϕ_s = phase due to the spatial distribution of the stress;

ϕ_t = phase due to the function describing the temporal response of the disturbance, i.e., essentially the rise time function;

ϕ_f = phase due to the finiteness of the faulting, i.e., a finite rupture developing at a finite speed.

To examine the intrinsic behavior of the disturbance, we estimate the finiteness phase ϕ_f and remove it from ϕ and obtain

$$\phi' = \phi + \phi_f = \phi_s + \phi_t \quad . \qquad (18)$$

The finiteness phase is:

$$\phi_f = \frac{b\omega}{2V_f}\left(1 - \frac{V_f}{V_p}\cos\Theta\right) \qquad (19)$$

where b is the overall rip length, V_f is the rip velocity, and Θ is the angle between the direction of the rip and the direction of the observation station.

B. Application and Discussion of Results

The source parameter values used in estimating the finiteness phase angle for the 1968 and 1969 earthquakes were taken from Abe (1973) and are given below:

Event	Overall rip length, b (km)	Rip velocity, V_f (km/sec)	Orientation angle, Θ (°)	Finiteness phase angle, ϕ_f
1968	100	3.8	40	0.52 to 0.15
1969	200	3.8	50	1.53 to 0.38

and the ϕ_f for the periods corresponding to the peaks and troughs in the displacement were calculated. Moreover, $\phi - \phi_f = \phi_s + \phi_t$ was calculated, where ϕ is the initial phase determined by the graphical calculation. The tabulation of the calculations and the graphical determination of each initial phase for the 1968 and 1969 earthquakes are shown in Appendix 7. The plots of the initial phase, ϕ, and the corrected initial phase, $\phi - \phi_f$, as functions of period are plotted in Figs. 23 and 24, respectively.

Because of the lack of detailed information, one can expect on the initial phases for the different types of earthquakes, the interpretation and assessment of the results shown in Figs. 23 and 24 will not be obvious. In particular, we cannot at this time determine whether the

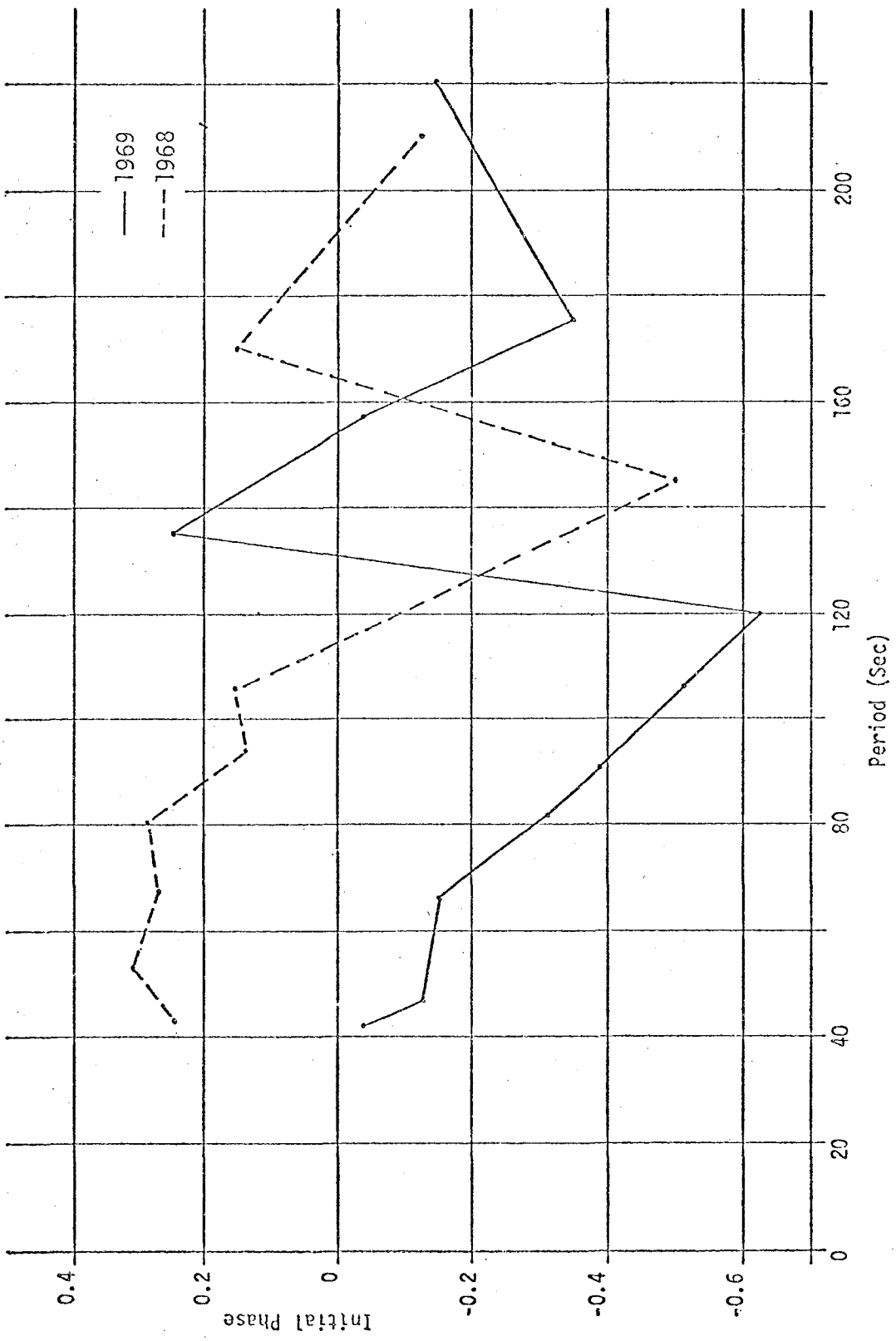

Figure 23. The initial phase of the ground motion at epicenter, as calculated from the 1968 and the 1969 Dopplergrams.

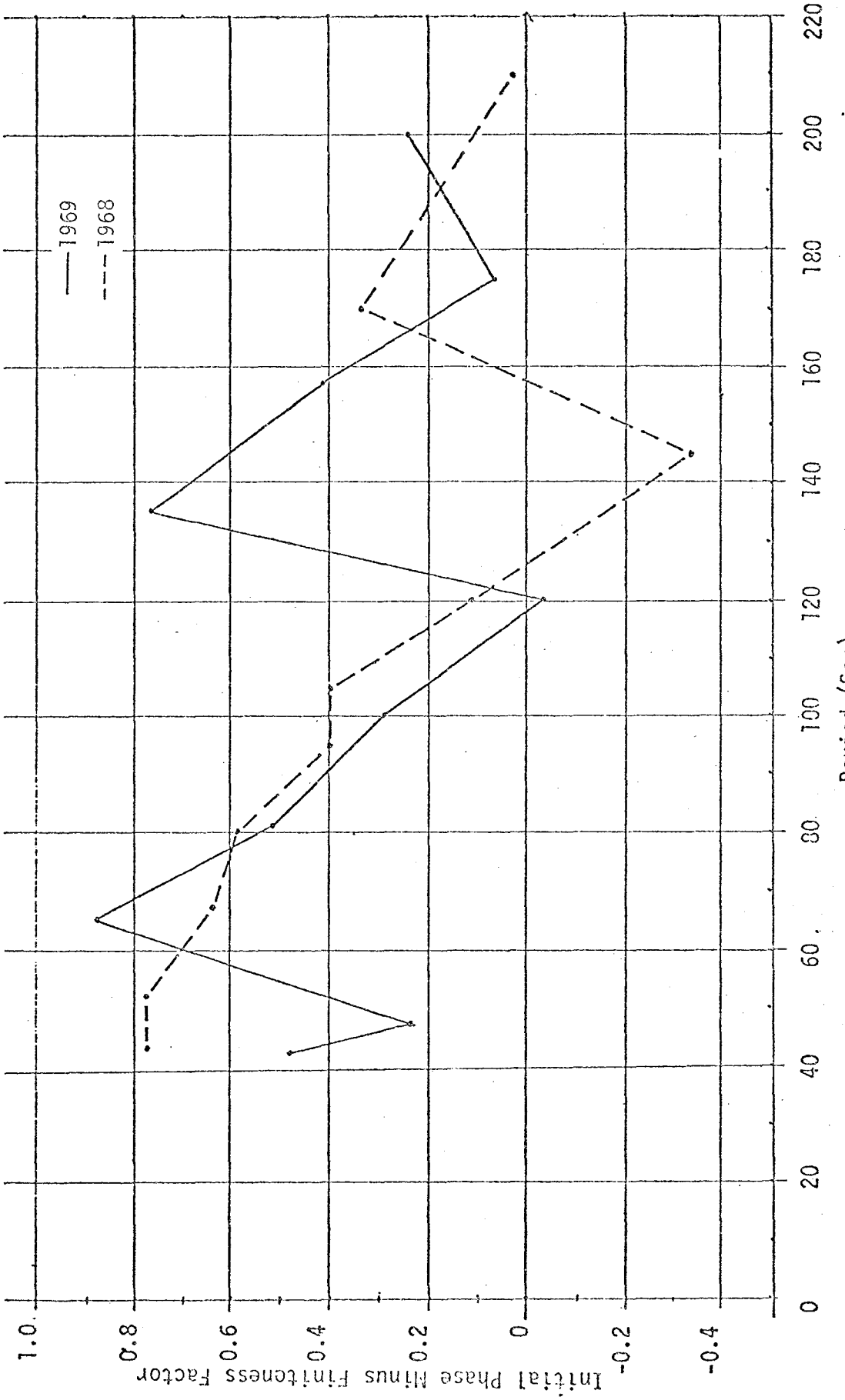

Figure 24. Initial phase from Figure 23 with finiteness factor removed. Values equal the sum of spatial and temporal phase factors.

calculated distribution of initial phase for the 1968 and 1969 earthquakes is reasonable. Therefore, we shall first discuss the initial phase obtained for other large earthquakes around the Pacific basin by other researchers. While this should possibly provide some reference for comparison and evaluation of our results, it is not necessarily representative.

Brune, et al. (1960b), examined records of surface waves from the large Chilean earthquake of May 22, 1960, and calculated the initial phase as seen at three stations with different azimuths. The Rayleigh modes used were R_2, R_3, and R_4. The initial phases in units of 2π turned out, in general, to be constant over the range of periods from 200 to 500 seconds at the three stations and had a magnitude of either 1.0 or 0.5. Ben-Menahem and Toksoz (1962), on the other hand, calculated the initial phase for the large Mongolian earthquake of December, 1957, from records of long period surface waves made at Pasadena. They used the Rayleigh modes R_3 and R_4 which resulted in values of ϕ varying between -1.0 to -0.5 for periods from 100 to 200 seconds, then increasing more or less linearly toward +0.5 as the period increased beyond 400 seconds.

Ben-Menahem and Toksoz (1963) calculated the initial phase of the large Kamchatka earthquake of November 4, 1952. Again they used the long period surface waves made at Pasadena. The initial phases inferred from the R_2 and G_2 modes had a more or less constant value of -0.5 cycles over the range of periods from 80 to 120 seconds, but increased toward -0.25 as the period increased further to about 500 seconds. Ben-Menahem, et al., (1972) also found the initial phase of the Alaskan earthquake of 1964 during the course of studying the source mechanism of this very large seismic disturbance. The procedure was essentially the same as their previous analyses. While no figures were presented, a table giving the initial phase as a function of period was included. Generally, ϕ varied and decreased from +0.25 to +0.6 as the period decreased from 300 to 200 seconds at some stations and varied in the opposite direction for others.

In view of the above results, the initial phase in Fig. 23 appears reasonable except for the sharp jump around a period of 140 seconds. That is, the values for the 1968 and the 1969 events are of the same order of magnitude as the values obtained by other researchers for other earthquakes. The sharp jump is the only "discontinuous" type of variation

that occurs over the range of periods measured and the curves vary smoothly. Also the data points that correspond to the jumps for both cases come from those peaks and troughs in displacement that occur where the waveform is changing from a series of sinusoidal-like oscillations to longer strung-out oscillations. However, no attempt was made to determine whether or not such changes would lead to large errors in some of the derived quantities such as travel time, which could contribute to the sharp jumps.

The curves for $\phi - \phi_f$ vs. period, plotted for the 1968 and 1969 earthquakes in Fig. 24, appear to be very close but this may be just an accident for several reasons. First, the magnitude, ϕ_f, is proportional to the rip length b, so will change rapidly with this parameter and the value of this parameter could be as large as 200 km (Kanamori, 1971, 1973b). Second, ϕ_f also depends on V_f. However V_f does not vary as rapidly as with b and it may be as low as 3.0 km/sec (Kanamori, 1971, 1973b). Therefore, the 1968 curve could lie as much as 0.3 above the 1969 curve. Furthermore, if the long period waves for the 1968 earthquake were generated by a very strong second event 40 seconds after the initial break, the above analysis would have to be modified.

In summary, the initial phases inferred from the 1968 and 1969 Dopplergrams are very tentative and require further study. While the initial phases from the two Dopplergrams seem to agree fairly well with each other, we cannot tell, at this time, whether or not this should be so. Generally, it is not possible to draw firm conclusions concerning the source mechanism for the 1968 and the 1969 earthqakes from the initial phase without further information on the relationship between initial phase and source mechanism. In particular, there does not seem to be any obvious relationship between initial phase and dip angle, or the initial phase and dip-slip and/or strike-slip components, Hence it is not possible at the present time to use Iida's results on earthquakes and tsunamis (see Furumoto, 1970) to infer whether or not the 1968 and 1969 earthquakes were tsunamigenic because we have not been able to determine every parameter accurately enough to determine the initial phase.

Ben-Menahem (personal communication, 1976) suggests that one should Fourier-analyze the Dopplergram to determine the periods and the position of the peak. He suggests that the asymptotic expansion and Ewing's peak-and-trough method would not be accurate enough for the determination of the initial phase. This aspect will be carefully studied.

REFERENCES

Abe, K., 1972, Group velocities of oceanic Rayleigh and love waves, Phys. Earth Planet. Int., 6, 391.

Abe, K., 1973, Tsunami and mechanism of great earthquakes, Phys. Earth and Planet. Int., 7, 143.

Ben-Menahem, A., 1961, Raidation of seismic waves from finite moving source, Bull. Seism. Soc. Am., 41(3), 401.

Ben-Menahem, A., et al., 1972, Source mechanism of the Alaskan earthquake of 1964 from amplitude of free oscillations and surface waves, Phys. Earth Planet. Int., 5, 1.

Ben-Menahem, A. and M.N. Toksoz, 1962, Source mechanism from spectra of long period seismic surface wave 1. The Mongolian earthquake of Dec. 4, 1957, J. Geophys. Res., 67(5), 1943.

Ben-Menahem, A. and M.N. Toksoz, 1963, Source mechanism from spectra of long period seismic waves 2. The Kamchatka earthquake of Nov. 4, 1952, J. Geophys. Res., 68(18), 5207.

Brune, J.N. et al., 1960, A simplified method for the analysis and synthesis of dispersed wave train, J. Geophys. Res., 65, 287.

Brune, J.N. et al., 1960b, Long period surface waves from the Chilean earthquake of May 22, 1960, recorded on linear strain seismographs, J. Geophys. Res., 66(9), 2895.

Brune, J.N., 1961, The polar phase shift of surface waves on a sphere, Bull. Seism. Soc. Am., 51(2), 247.

Brune, J.N., 1969, Surface waves and crustal structure, The Earth's Crust and Upper Mantle, Am. Geophys. Un. Geophys. Monogram 18, P. Hart (ed).

Brune, J.N. and J. Dorman, 1963, Seismic waves and earth structure in the Canadian shield, Bull. Seism. Soc. Am., 53, 167.

Cha, M.Y., 1974, Ray-tracing for atmospheric acoustic and atmospheric gravity waves, Radioscience Internal Rept., 1974-2.

Cha, M.Y., 1975, Measurements of the phase and group velocity of Rayleigh waves in the Pacific basin, Radioscience Internal Rept., 1975-1.

Cowling, D.H. et al., 1970, A study of traveling disturbances in the ionosphere, Ionospheric Radio Laboratory Tech. Rept. 38, University of Illinois.

Cowling, D.H. et al., 1971, Group rays of internal gravity waves in a wind-stratified atmosphere, J. Geophys. Res., 76, 213.

Dorman, J., 1969, Seismic surface wave data on the upper mantle, from The Earth's Crust and Upper Mantle, Geophys. Monogram 13, (Am. Geophys. Un., P. Hart (ed)).

Dziewonski, A., 1970, On regional differences in dispersion of mantle Rayleigh waves, Geophys. J. R. Astro. Soc., 22, 289.

Dziewonski, A. and M. Landisman, 1970, Great circle Rayleigh and love wave dispersion from 100 to 900 seconds, Geophys. J. R. Astron. Soc., 19, 37.

Ewing, M. and F. Press, 1954, An investigation of mantle Rayleigh waves, Bull. Seism. Soc. Am., 44, 127.

Ewing, M. and F. Press, 1954, Mantle Rayleigh waves from the Kamchatka earthquake of Nov. 4, 1952, Bull. Seism. Soc. Am., 44(3), 471.

Fukao, Y. and M. Furumoto, 1975, Foreshocks and multiple shocks of large earthquakes, Phys. Earth Planet. Int., 10, 355.

Furumoto, A., 1970, Ionospheric recording of Rayleigh waves for estimating source mechanisms, Tsunamis of the Pacific Ocean, Proceedings of the International Symposium of Tsunamis and Tsunami Research, W.M. Adams (ed), East-West Center Press, 119.

George, T.M., 1968, HF Doppler studies of traveling ionospheric disturbances, J. Atmos. Terr. Phys., 30, 735.

Gregersen, S., 1970, Surface wave dispersion and crust structure in Greenland, Geophys. J., 22, 29.

Gupta, H.K. and T. Santo, 1973, World-wide investigation of the mantle Rayleigh wave group velocities, Bull. Seism. Soc. Am., 63, 271.

Hamada, K., 1971, Mantle wave analysis by a phase-equalization-and sum method for the Montana LASA long period data, Bull. Seism. Soc. Am., 61, 875-892.

Huang, Y.N., 1973, Dynamic response of the ionosphere to geomagnetic sudden commencements, Ph. D. dissertation, University of Hawaii.

Huang, Y.N. et al., 1973, A study of the construction of the Rayleigh seismic wave dispersion curve at long periods by using HF Doppler frequency shift records, Radioscience Internal Rept., 1973-1.

Iida, K., 1970, Generation of tsunamis and the focal mechanism of earthquakes, Tsunamis of the Pacific Ocean, Proceedings of the International symposium on Tsunamis and Tsunami Research, W.M. Adams (ed), East-West Center Press, 3-18, 1970.

Jacob, K.H. and K. Hamada, 1972, The upper mantle beneath Aleutian island arc from pure-path Rayleigh wave dispersion data, Bull. Seism. Soc. Am., 62, 143.

Jeffreys, H. and B. Jeffreys, 1966, Methods of Mathematic Physics, 3rd ed., Cambridge University Press, England.

Jones, W.L., 1969, Ray-tracing for internal gravity waves, J. Geophys. Res., 74, 2028.

Kanamori, H., 1970, Velocity and Q of mantle waves, Phys. Earth Planet. Int., 2, 259.

Kanamori, H., 1971, Focal mechanism of the Tokachi-Oki earthquake of May 16, 1968: contortion of the lithosphere at a junction of two trenches, Tectonophys., 12, 1.

Kanamori, H., 1973b, Long period ground motion in the epicentral area of major earthquakes, Tectonophys., 21, 341.

Kausel, E. et al., 1974, Variations of Rayleigh wave phase velocity across the Pacific Ocean, Science, 186, 139.

Kuo, J. et al., 1962, Rayleigh wave dispersion in the Pacific Ocean for period range 20 to 140 seconds, Bull. Seismo. Soc. Am., 52(3), 333.

Lau, C.K., 1974, Hilbert transform method of determining the period of Rayleigh-acoustic wave generated ionospheric Doppler recording, Honors Thesis, Dept. of Elec. Eng., University of Hawaii.

Lighthill, M.J., 1965, Group velocity, J. Ins. Math. Appl., 1, 1-28.

Midgley, J.E. and H.B. Liemohn, 1966, Gravity waves in a realistic atmosphere, J. Geophys. Res., 71, 3729.

Murray, J.D., 1973, Asymptotic analysis, Clarendon Press, Oxford.

Nafe, J. and J.N. Brune, 1960, Observation of phase velocity for Rayleigh waves in the period range 100-400 seconds, Bull. Seims. Am., 50, 427.

Najita, K. and C.K. Lau, 1974, A report on suggested modification to Dr. A.S. Furumoto's method of determining the initial phase of the source of an earthquake, Radioscience Internal Rept., 1974-1.

Oliver, J., 1962, A summary of observed seismic surface wave dispersion, Bull. Seism. Soc. Am., 44, 127.

Press, F. and A. Ben-Menahem, 1961, Experimental determination of V_f and b, J. Geophys. Res., 66, 3471.

Saito, M. and H. Takeuchi, 1966, Surface waves across the Pacific, Bull. Seism. Soc. Am., 56, 1067.

Santo, T., 1963, Division of the Pacific area into seven regions in each of which Rayleigh waves have the same group velocities, Bull. Earth Res. Ins. (Tokyo), 41, 719.

Santo, T. and M. Bath, 1963, Crustal structure of Pacific Ocean area from dispersion of Rayleigh waves, Bull. Seism. Soc. Am., 53, 151.

Toksoz, M. and D.L. Anderson, 1966, Phase velocities of long period surface waves and structure of the upper mantle, J. Geophys. Res., 71, 1649.

Weaver, P.F. et al., 1970, Acoustic coupling into the ionosphere from seismic waves of the earthquake at Kurile Islands on August 11, 1969, Nature, 226, 1239.

Weidner, D., 1974, Rayleigh wave phase velocities in the Atlantic Ocean, Geophys. J., 36, 105.

Yeh, K.C. and C.H. Liu, 1974, Acoustic-gravity waves in the upper atmosphere, Reo. Geophys. Space Phys., 12, 193.

Yoshii, T., 1975, Regionality of group velocities of Rayleigh waves in the Pacific and thickening of the plate, Earth and Planet. Letts., 25, 305.

Yuen, P.C. et al., 1969, Continuous traveling coupling between seismic waves and the ionosphere evident in May 1968 Japan earthquake data, J. Geophys. Res., 74(9), 225.

APPENDIX 1

REFRACTION OF DISPERSED WAVETRAINS AT THE BOUNDARY BETWEEN TWO DISSIMILAR MEDIA

The main kinematic properties of the coupling between Rayleigh waves and the concomitant atmospheric waves can be found by applying the argument of Jeffreys and Jeffreys (1966; see also Officer 1958) to a planar boundary between the atmosphere and the ground. In the diagram below, medium 1 is the ground, S and O are the source and point of observation, respectively and distances along the ground (denoted by l) are measured from A. Also shown are 1) the path of waves from S to O; 2) distances, α_1 and α_2, from S to the boundary B, and from B to O; and 3) the normal and angles of refraction in each medium. After expressing the

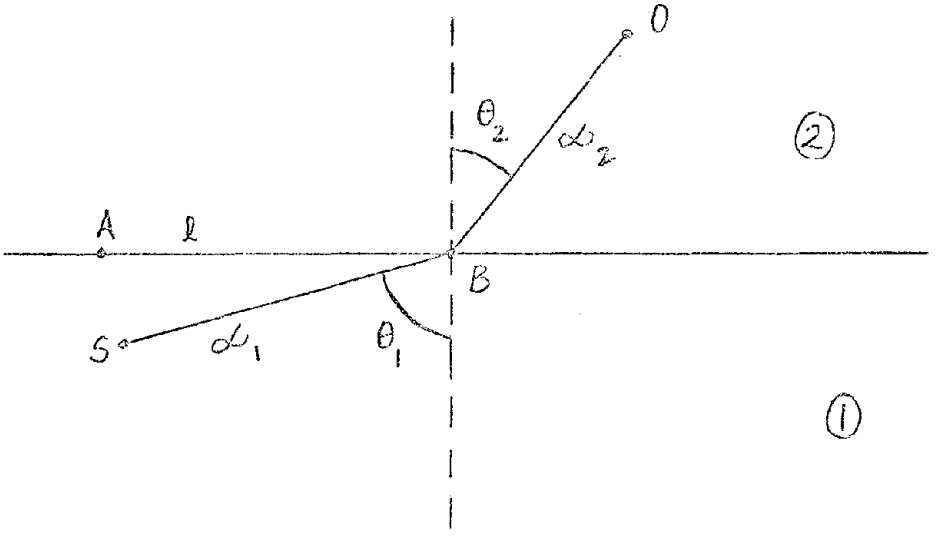

disturbance at O as a superposition of harmonic components from S with phase, $\exp(i(wt - k_1\alpha_1 - k_2\alpha_2))$, where k_1 and k_2 are the appropriate wave numbers and w is the angular frequency, the method of stationary phase is applied in order to determine the asymptotic form for large t; only now one seeks stationary values with respect to w (the variable of integration) and ℓ. The latter must be included because the components may cross the boundary at different points (i.e., different ℓ's). The conditions for stationary

values are then

$$k_1 \frac{d\alpha_1}{dl} + k_2 \frac{d\alpha_2}{dl} = 0$$

$$t - \alpha_1 \frac{dk_1}{dw} - \alpha_2 \frac{dk_2}{dw} = 0.$$

In terms of the phase and group velocity, V and U, respectively, these equations have the form

$$\frac{1}{V_1} \frac{d\alpha_1}{dl} = \frac{1}{V_2} \frac{d\alpha_2}{dl} \qquad (1)$$

$$\frac{\alpha_1}{U_1} + \frac{\alpha_2}{U_2} = t \qquad (2)$$

The derivatives may be expressed in terms of the angle of refraction, θ_1 and θ_2 (note that a displacement, dl, increases one of the paths and decreases the other); so that (1) becomes

$$\frac{\sin \theta_1}{V_1} = \frac{\sin \theta_2}{V_2} \qquad (3)$$

Thus, waves are refracted according to Snell's law. The second equation, (2), states that travel time from S to O is determined by the group velocity in each medium.

Finally, if we apply (3) to the problem at hand, $\theta_1 = 90^o$, V_1 = phase velocity of Rayleigh waves, V_2 = phase velocity of atmospheric acoustic waves and

$$\sin \theta = \frac{V_2}{V_1} \qquad (4)$$

If the frequency, w, is known, along with V_1, (4) allows the pair (w, k_x) to be replaced by (w, θ).

REFERENCES

Jeffreys, H. and B. Jeffreys, 1966, Method of Mathematical Physics, 3rd ed., Cambridge University Press, England.

Officer, C., 1958, Introduction to the Theory of Sound Transmission, McGraw Hill, N.Y.

APPENDIX 2

RAY-TRACING FOR ATMOSPHERIC ACOUSTIC AND ATMOSPHERIC GRAVITY WAVES

I. INTRODUCTION

Ray-tracing is concerned with the calculation of the path of waves for a given underlying medium (and boundaries), characteristics of the waves and some definition of "path". The end results of the calculations--the "rays"-- are usually analogous to light rays in geometrical optics, but may not be so because of the dependence on the given definition, and also, because the physical situation may not properly be one of geometrical-optics.

Since the waves under consideration are atmospheric acoustic or atmospheric upwards from some initial height, the paths will lie in the atmosphere. They generally extend from some initial height but may extend in other directions depending on the physical conditions. Such path calculations are necessary when studying atmospheric waves, since these waves usually travel for considerable distances vertically and/or horizontally. Thus an analysis of observations of these waves does not usually reveal where they originate or the time at which they were produced. Path calculations can also provide information on an equally important problem, viz., the effect that variations in atmospheric structure along the path will have on the propagation of these waves. For example, they might indicate that the frequency and direction of propagation were altered by strong winds along the path or that the waves were channeled by large thermal gradients. In general, rays provide a causal link between the waves (observed at some position) and the source, from which one may infer useful information.

In view of the importance of path calculations, we have developed a computer program that will calculate the ray-path of acoustic-gravity waves in the terrestrial atmosphere for a given vertical structure of the atmosphere, some initial conditions and certain properties of the waves. The program is fairly general, quite flexible (e.g., it can be run with or without winds) and simple to run. The output contains the spatial coordinates of the ray-path and other useful information such as the travel time along the path.

In the remainder of this section we shall give a brief overview of the program. The sections following then take up various aspects, such as the model atmosphere and the basic methods. The last two sections presents examples of ray-paths and a discussion of their validity.

Because of the length of the program and different initial conditions for the atmospheric acoustic and atmospheric gravity waves in question, we actually developed two programs: one for waves with frequencies above the acoustic cutoff frequency (i.e., the "atmospheric" acoustic or "infrasonic" waves) and one for waves with frequencies below the Brunt frequency (i.e., the "Atmospheric gravity" or "internal gravity" waves). These programs differ in only one phase of the calculations, however, and not in the over-all "logic" of ray-tracing. Hence, they will be referred to collectively as the ray-tracing programs (or RTP) throughout most of the following report. The difference, in turn, is discussed in Section V.

The RTP attempts to find the "path" in the terrestrial atmosphere, along which a group of small amplitude infrasonic or internal gravity waves will propagate. Since the basic entity is a group of waves (rather than a solitary wave or an individual wave in the group), the "path" must be calculated from the group velocity. And it is this "path" that is called a "ray". In this regard, there are two points that should be mentioned: 1) use of the group velocity instead of the phase velocity or the wave velocity (corresponding to an individual wave) will make a difference in such quantities as the travel time along the path; and 2) one needs to find a bundle of rays in order to determine the shape of the wavefront.

To find such paths, the program makes use of ray-tracing techniques developed for internal gravity waves (Cowling, et al., 1970, 1971; Jones, 1969; and Yeh and Liu 1974), except for those parts dealing with the input and output, calculation of the group velocity and certain initial parameters, and the vertical variations in some of the atmospheric parameters.

Finally, we should mention that 1) the RTP uses the complete dispersion relationship for acoustic-gravity waves, rather than any convenient high- or low- frequency approximations; 2) the atmospheric structure may include horizontal winds over a range of heights, since the RTP carries out calculations in the reference frame attached to the wind, then transforms to a reference frame defined by the surface of the earth; and 3) the waves may be started at any height above the ground.

II. THE MODEL ATMOSPHERE AND ATMOSPHERIC PARAMETERS

The RTP assumes that 1) the terrestrial atmosphere is planar; 2) atmospheric parameters vary in the vertical direction; 3) atmospheric parameters do not vary in the horizontal direction; and 4) air is inviscid and non-dissipative from ground level to the top height. It also assumes implicitly that the rarefied air at heights of few hundred km's can be treated the same as air at low levels, and that there is no ionosphere or geomagnetic field. However, there can be horizontal winds over any range of heights between ground level and 400 km, although winds are usually included only at heights greater than about 100 km.

Whether these assumptions are reasonable cannot be answered a priori, since it depends on the problem at hand. For example, the first and third assumptions would be appropriate for situations involving waves that propagate upwards or downwards in a nearly vertical direction. On the other hand, they may not be reasonable for waves that travel for long distances horizontally; especially in the N-S direction because of possible latitudinal variations in atmospheric structure and the curvature of the earth's surface. Another complication is the lateral deflection of rays away from a plane produced by the vertical gradients in wind speed and direction (an example may be found in Cowling et al., 1970). When judging ray-tracing results, one must consider the agreement with observations or priori knowledge, as well as the appropriateness of the above assumptions.

Of the required atmospheric parameters, the speed of sound and the ratio of the specific heats ("γ") are entered directly into the program. In the current RTP, both are given as functions of height at 10.0 km intervals from 0.0 km to 400.0 km. The acceleration of gravity has also been allowed to vary with height over the range from 0.0 km to 400 km.

At present, we have two decks of cards for the speed of sound. One deck was computed earlier by Albert Hwang, using the 15°N annual model in the 1962 Standard Atmosphere for heights <120.0 km and the summer model for an exospheric temperature of 1000°K in the 1966 Supplement for heights ≥120.0 km. These values were found from the expressions in the 1962 Standard Atmosphere, assuming $\gamma = 1.4$ (There is only a small change if γ varies with height.) and that the molecular weight decreases above 120.0 km as indicated in the summer model. The values are appropriate for the amount of solar radiation that impinged on the

atmosphere around August, 1969; and hence, for a period of maximum solar activity. To allow for solar cycle variations, we have also computed values for a minimum in solar activity (Circa August, 1973). The expressions and the procedures used were the same as before. The values are in the second deck of cards and ready to be incorporated into the program whenever necessary. Finally, we determined the height variation of γ by linearly extrapolating the values shown in Midgley and Liemohn (1966). These are on cards in the data section of the RTP.

Although it may seem surprising that one does not input the pressure or temperature or density of the atmosphere, a moments' thought will show that these parameters are really in the program. They are entered through the speed of sound, the acoustic cutoff frequency and the Brunt frequency. Moreover, the form of the expressions for these frequencies used in the program is not of the general form, but of the form appropriate for an exponentially decreasing pressure and density. In other words, given the scale heights associated with the exponential drop-off, the general expressions can be put in the form actually used by means of thermodynamic relationships.

III. BASIC DEFINITIONS AND EQUATIONS, AND SOME NECESSARY COMMENTS

For immediate reference we list the most important physical quantities and corresponding mathematical expressions that appear in the program. For additional details the reader is referred to the document by Cowling, et al., (1970) and the references therein.

A. ACOUSTIC CUTOFF FREQUENCY

The acoustic cutoff frequency (f_a) sets the lower limit on the frequency scale for atmospheric acoustic waves; that is, propagation is not possible for frequencies $< f_a$.

Plane wave or exponential-like solutions for a planar isothermal atmosphere indicate that

$$W_a = 2\pi f_a = \frac{\gamma g}{2c}, \qquad (1)$$

where γ is the ratio of the specific heats, g is the acceleration of gravity and c is the speed of sound.

B. BRUNT FREQUENCY

The Brunt frequency (f_g) sets an upper limit to the allowed frequencies of the internal gravity waves. The same type of wave solutions show that

$$W_g = 2\pi f_g = \frac{\sqrt{\gamma - 1}}{c}\, g, \tag{2}$$

where the symbols on the right are the same as in A above.

C. THE DISPERSION RELATIONSHIP

If there were no cutoff frequencies (i.e., $W_a = W_g = 0$), then propagation of atmospheric waves would not be dispersive and, W, the angular frequency of the component, would be a linear function of $\vec{k}$, the wave number vector. However, analysis of plane-waves in a planar isothermal atmosphere shows that

$$W^4 - W^2C^2(k_x^2 + k_z^2) + W_g^2\, C^2k_x^2 - W_a^2W^2 = 0, \tag{3}$$

where k_x and k_z are the horizontal and vertical components of the wave vectors, respectively, W is the angular frequency of the wave and the other symbols are as given in A and B above. Without loss of generality, the propagation problem is assumed to be two-dimensional.

The phase velocity of a harmonic component depends on the wave-length. An added complication is its dependence on both k_x and k_z (rather than just $|\vec{k}|$) as well as on W_a and W_g. Thus it is difficult to show the relationaship (3) graphically, unless one variable is suppressed (see the figures on pages 55 and 59 in George, 1967 and page 49 in Cowling, et al., 1970). Impulses -- highly localized and/or momentary pressure or displacement perturbations -- will tend to disperse or spread out into nearly sinusoidal waves with slowly changing frequency and wavelength as they propagate to great distances.

D. GROUP VELOCITY

The group velocity, V_g, is generally defined as

$$\vec{V}_g = \nabla_k W, \tag{4}$$

where ∇_k is the gradient operator with respect to $\vec{k}$ (Lighthill, 1965). Using

the dispersion relationship in (3), we then find that

$$W_{gx} = \frac{Wc^2k_x(W^2 - W_g^2)}{W^4 - W_g^2k_x^2c^2} \quad , \tag{5}$$

and

$$V_{gz} = \frac{W^3c^2k_z}{W^4 - W_g^2c^2k_x^2} \quad . \tag{6}$$

Since $W_a > W_g$, we note the following:

$W > W_a > W_g$

infrasonic branch: $W^2 - W_g^2 > 0$

$W^4 - W_g^2c^2k_x^2 > 0$

V_{gx} has same sign as k_x

V_{gz} has same sign as k_z

internal gravity branch: $W_a > W_g > W$

$W^2 - W_g^2 > 0$

V_{gx} has same sign as k_x.

V_{gz} has opposite sign to kz.

Of course,

$$/\vec{V}_g/^2 = V_{gx}^2 + V_{gz}^2 \quad .$$

By definition, the ray-path is the path in the atmosphere traced out by $\vec{V}_g$ and the slpoe of the ray-path with respect to the ground is V_{gx}/V_{gz}.

The group velocity is normal to the W-contours in k-space, as shown in Figure 4.1 on page 49 of Cowling, et al., (1970). Such diagrams represent one possible way of studying the characteristics of rays. Note that the W-contours will be ellipses in the case of infrasonic waves (see George, 1967).

E. WAVE MOTION IN AN ATMOSPHERE WITH WINDS

All the equations mentioned above have been derived under the assumption that the planar atmosphere is stationary. If it is moving -- in particular moving in the horizontal direction, then the waves may be Doppler shifted in frequency. If Ω is the angular frequency in a reference frame fixed to the ground, and W, the angular frequency in a reference frame moving with the atmosphere, then

$$W = \Omega - \vec{K} \cdot \vec{V}, \tag{7}$$

where $\vec{K}$ is the real part of the wave vector and $\vec{V}$ is the horizontal velocity of the atmosphere or the horizontal wind velocity.

Equation (7) is used to transform from the moving frame to the ground (or laboratory) whenever necessary. The point to remember is that equations (1) to (6) apply in the moving frame, since the atmosphere is stationary with respect to it; while observations-- in particular, the initial specification of the wave-motion--are made relative to the ground frame. The following relationships are of some importance in this regard:

$$\begin{aligned} k_x &= \frac{\Omega}{V_p} \text{ in ground frame} \\ &= \frac{W}{V_p} \text{ in rest frame,} \end{aligned} \tag{8}$$

where V_p is the phase velocity (as measured in reference frames mentioned), and

$$\vec{V}_g \text{ (in ground frame)} = \vec{V}_g \text{ (in moving frame)} + \vec{V}. \tag{9}$$

This shows quite clearly that waves may be carried along or retarded by horizontal winds.

F. ADDITIONAL QUANTITIES AND EXPRESSIONS

If the dispersion relationship is solved for k_z, one obtains

$$k_z^2 = \left(\frac{W^2}{C^2} - \frac{W_a^2}{C^2} \right) + k_x^2 \left(\frac{W_b^2}{W^2} - 1 \right) \qquad (10)$$

The RTP actually uses the dispersion relationship in this form.

Other quantities used are:

$\lambda_z = \frac{2}{k_z}$ = wavelength in the vertical direction

h_o = initial height above ground

x = distance in the horizontal direction from initial position of wave

t = time

and

θ = angle between $\vec{k}$ and vertical direction

G. INTERPRETATION OF W AND k_x

According to the derivation leading to the dispersion equation, W and k_x are the angular frequency and horizontal wave number of a plane sinusoidal wave. However, we can never observe a perfect sinusoidal wave--we can only observe groups of waves, or equivalently, a finite waveform. If the medium is also dispersive, then the wavetrain will spread out as it propagates and the "frequency" of the oscillations in the wavetrain will gradually vary along the wavetrain. If the medium is also inhomogeneous, it is not obvious that W will not vary as the wavetrain travels through the inhomogeneity. Similar remarks apply to the wave vector, k. Clearly, if we plan to use ray-tracing results in conjunction with observations, we need to clarify the relationship between W, $\vec{k}$ and the features of the waveforms.

We note that k_x cannot vary because the model atmosphere is homogeneous in

the horizontal direction. Thus, k_x remains fixed at the initial value specified at the onset of a run, regardless of the stage of calculation of a ray. On the other hand, k_z will vary if the height changes during the calculations.

Lighthill (1966) has shown that W is invariant along the path defined by the group velocity even in an inhomogeneous, dispersive medium. Thus, W will be constant along the rays in the atmosphere. If we now combine this with the fact that the wavetrains will be dispersed, we see that W is the angular frequency (actually, a sort of average angular frequency) of the narrow band of harmonic components that interfere to produce the sub-group of oscillations in the wavetrain with the same angular frequency. In other words, W should be interpreted as the angular frequency of a harmonic component in the sense prescribed by the application of the method of stantionary phase in the homogeneous case. Since k_x is invariant along a ray, it can also be interpreted in this sense.

IV. DETERMINATION OF RAYS

A ray path can be determined if W, k_x, h_0 and the initial direction of phase propagation are specified. The problem of specifying k_x will be discussed later. The following procedure is used in the RTP to calculate a ray:

a. Find the values of k_z at h_0 from the dispersion equation, subject to the modification introduced by winds.

b. If k_z is real, calculate U_x, U_z, and $\lambda_z' = 0.10\ \lambda_z = 0.10\ (2/k_z)$. The thickness of the equivalent isothermal layer at this height is λ_z' or 10 km, whichever is smaller.

c. If the thickness is Δ_z, then the time required to traverse the path in the current layer is

$$\Delta t = \frac{\Delta_z}{U_z} , \tag{11}$$

The vertical distance traversed is Δ_z, and the horizontal distance traversed is

$$\Delta x = U_x \Delta t. \tag{12}$$

d. After adding Δ_z, Δt and Δx to the running sums, replace h_o by $h_o + \Delta_z$ and repeat the steps starting at a. above. Continue the sequence a. to d. until the top of the atmosphere is reached or the situation in e. below occurs.

e. If k_z is imaginary, divide the current Δ_z in half, step upwards by $0.5\Delta_z$ and repeat step a. This continues until a height is reached where $k_z \simeq 0.0$. Call this height, h_r.

f. Since reflection has occurred at h_r, the RTP now begins to trace downward, repeating the sequence a. to d. with h_r replaced by $h_r - \Delta_z$ initially, then $(h_r - \Delta_z)$ replaced by $(h_r - \Delta_z)$ - new Δ_z, etc., until k_z again becomes 0.0, or the ray reaches the ground, or the ray reaches as close to ground as possible in terms of Δ_z.

Thus, the rays either continue to the top of the atmosphere, or reflect at some intermediate height. If winds are included, ray may show trapping (as illustrated in Cowling, 1970).

It should be mentioned that the initial steps upwards or downwards by Δ_z is controlled by the direction of phase propagation specified at the onset (phase and energy propagate in the same direction only for infrasonic waves). The RTP "remembers" the direction, so that it can step in the right direction after a reflection. Further since λ_z tends to be large for the lower frequency internal gravity waves, it is necessary to divide it by 10 to keep the steps reasonable. Also, the program interpolates between the layers of the model atmosphere, if necessary. Finally, reflected rays may not be symmetric because the steps just before reaching h_r are not necessarily the same as that just after reaching h_r.

V. PROGRAM MODIFICATIONS

The input to the original RTP was modified to allow more flexibility in specifying the wave characteristics and to avoid a lengthy read-in of the speed of sound and wind data. The output, on the other hand, was changed to display as many wave characteristics as possible in as few lines as possible. The other major changes were 1) allowing rays to start at an arbitrary height above ground; and 2) allowing some variation in the initial wave characteristics, especially, for infrasonic waves.

For the modification in the program mentioned above applied to the internal gravity wave, the minimum information required at the outset is again W, k_x, h_o and the direction of phase propagation. If a wind model is included then the launch time and the initial azimuth of the waves relative to N must also be specified.

Since ray-tracing of this type will be used most likely in connection with observations of TID's, and since the horizontal trace velocity can usually be obtained from such observations, the initial data seems reasonable. However, the program can easily be changed to accept other sets of initial data. For example, one could specify W and the horizontal trace velocity, and let the program compute k_x.

For the infrasonic waves the program has been set up to accept W, h_o, and the direction of phase propagation θ. Then, k_x and k_z are found from the dispersion equation and

$$k_x = k_z \tan \theta.$$

The range of angles (3^0 to 7^0) has been chosen to agree as closely as possible with the situation for atmospheric waves launched by Rayleigh waves. Here, the assumption is that k_x remains constant across the ground-air interface. However, W and the Rayleigh phase velocity could be specified instead, and the program could then compute k_x and θ. Finally, since λ_z for these waves is much less than for internal gravity waves, the factor of 10 in $\lambda_z/10$ has been removed. This has the effect of increasing the steps from 1 km to a reasonable size and reducing the computer time.

VI. RESULTS

The first three figures show ray-paths for internal gravity waves in a windless atmosphere. Phase propagation is downward in all cases. For comparison, the waves were allowed to start above ground level at a height of 125 km in one of the runs. The short horizontal lines along the rays indicate the travel time (in increments of 20 minutes) from the starting height; while the longer horizontal line at the top of some of the rays indicate that a reflection took place at that level and that the energy of the waves then proceeded to move downwards. Finally, the periods and horizontal trace velocities were chosen to fall in the range usually associated with medium scale traveling ionospheric disturbances (George, 1968), mainly because we expect these TID would be of the type that might occur most frequently at our latitude.

The ray-paths support the commonly held view that internal gravity waves in the guise of TID's can transport energy and momentum (from lower levels) to considerable heights in the atmosphere if the period and wavevector happen to be "favorable." However, results such as these are still tentative because of the strong influence thermospheric winds have on these waves (Cowling, et al., 1971; and Yeh, et al., 1972). These winds can for example, draw out rays for a long distance horizontally or "induce" a reflection in the lower thermosphere in waves that would otherwise penetrate to very great heights. Thus, more ray-tracing studies should be made, both with and without winds, in order to learn about the effects produced by thermospheric winds and the most probable ray-paths for waves of a given period and wavevector at times and places when the thermospheric winds had certain spatial and temporal characteristics.

The next three figures are for atmospheric acoustic or infrasonic waves in a windless atmosphere from a ground level source. They are parameterized in terms of θ_k, the angle between $\underline{k}$ and the vertical and the period is the same for all rays in a given figure. The travel time along a ray is indicated again by short horizontal lines. However, the time increments are not uniform. In order to generate these rays, θ_k, rather than k_x on the horizontal trace velocity, was read into the program along with the period or, equivalently, W. However, the insert shows the relationship between θ_k and both apparent horizontal

velocity (V_n) and the initial angle (θ_r) between the group velocity and the vertical for waves of the given period. Hence, in order to apply these results to different ground sources one need only match the "launch" angle, k or the horizontal trace velocity, V_h. Notice that it is usually difficult to find the initial θ_r because this requires a superposition of waves.

One of the more interesting points that these results illustrate is the progressive change in the ray-paths as the waves change from nearly pure acoustic (Fig. 4) to long-period infrasonic (Fig. 6). The latter type not only takes longer to propagate, but also travels upwards at a stepper angle. Our interest in this type of atmospheric wave comes mainly from the discovery that Rayleigh waves from large earthquakes can generate vertically propagating infrasound (Yuen, et al., 1969). Since the phase velocity of Rayleigh waves has been determined, we can find the appropriate ray by setting V_h equal to the phase velocity for the given period, then finding the proper θ_k. In this way, it is possible to determine the travel time, and lateral deflection, of the infrasonic waves that were launched by Rayleigh waves.

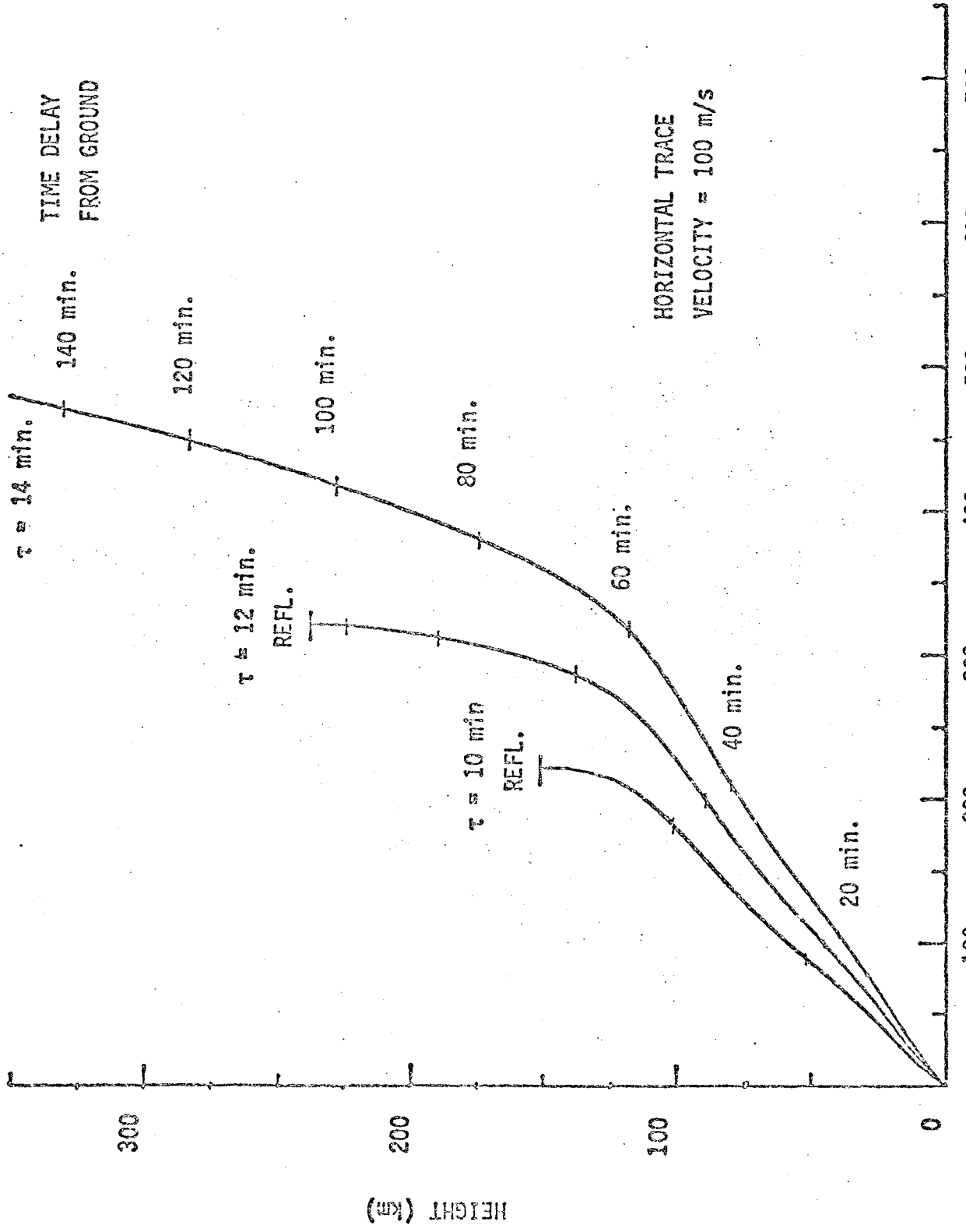

Figure 1. Ray-path for long period internal gravity waves with a horizontal trace velocity of 100 m/s. Horizontal bar indicates height at which waves are reflected. τ is the wave period.

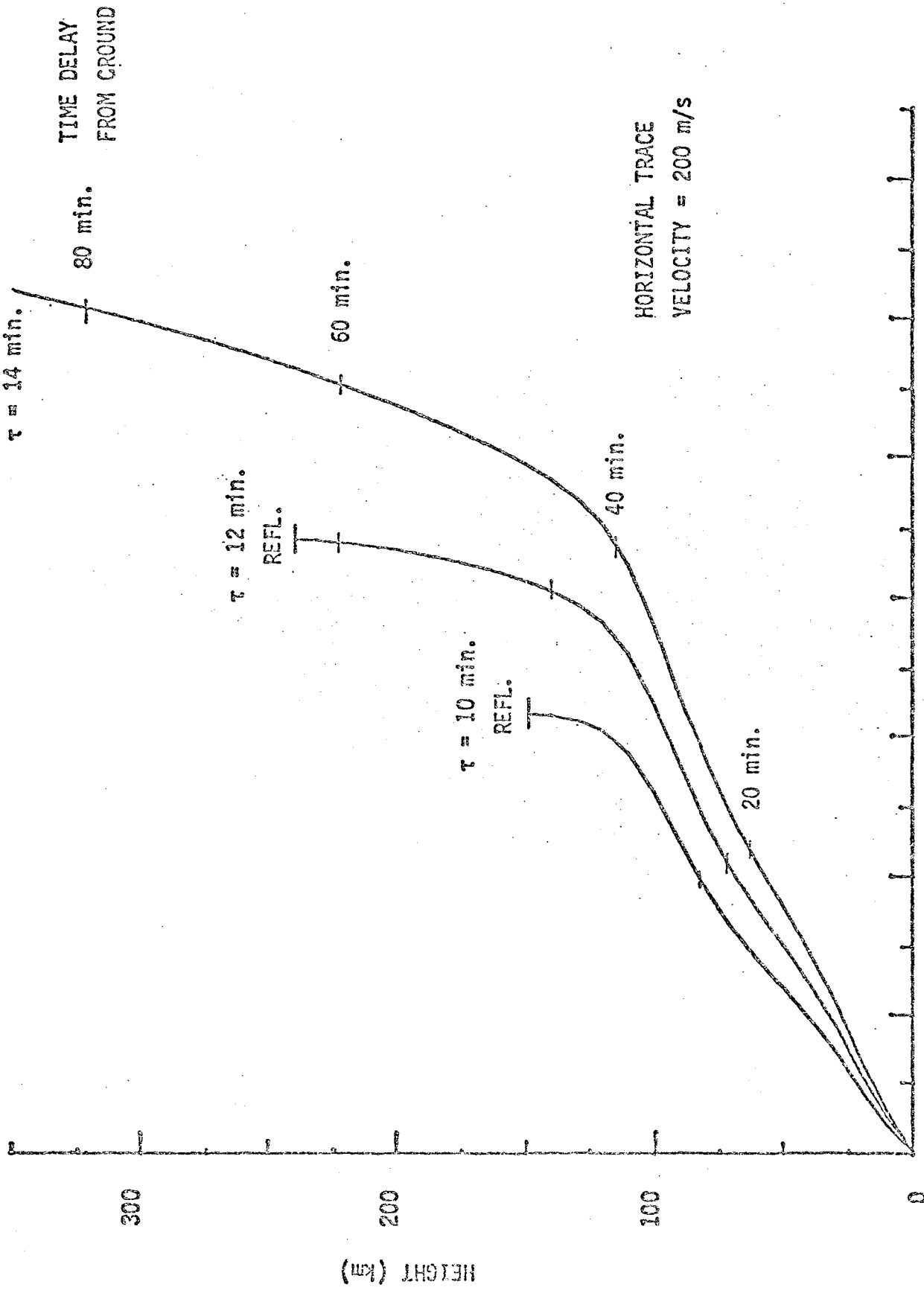

Figure 2. Same as in Figure 1 except for horizontal trace velocity of 200 m/s.

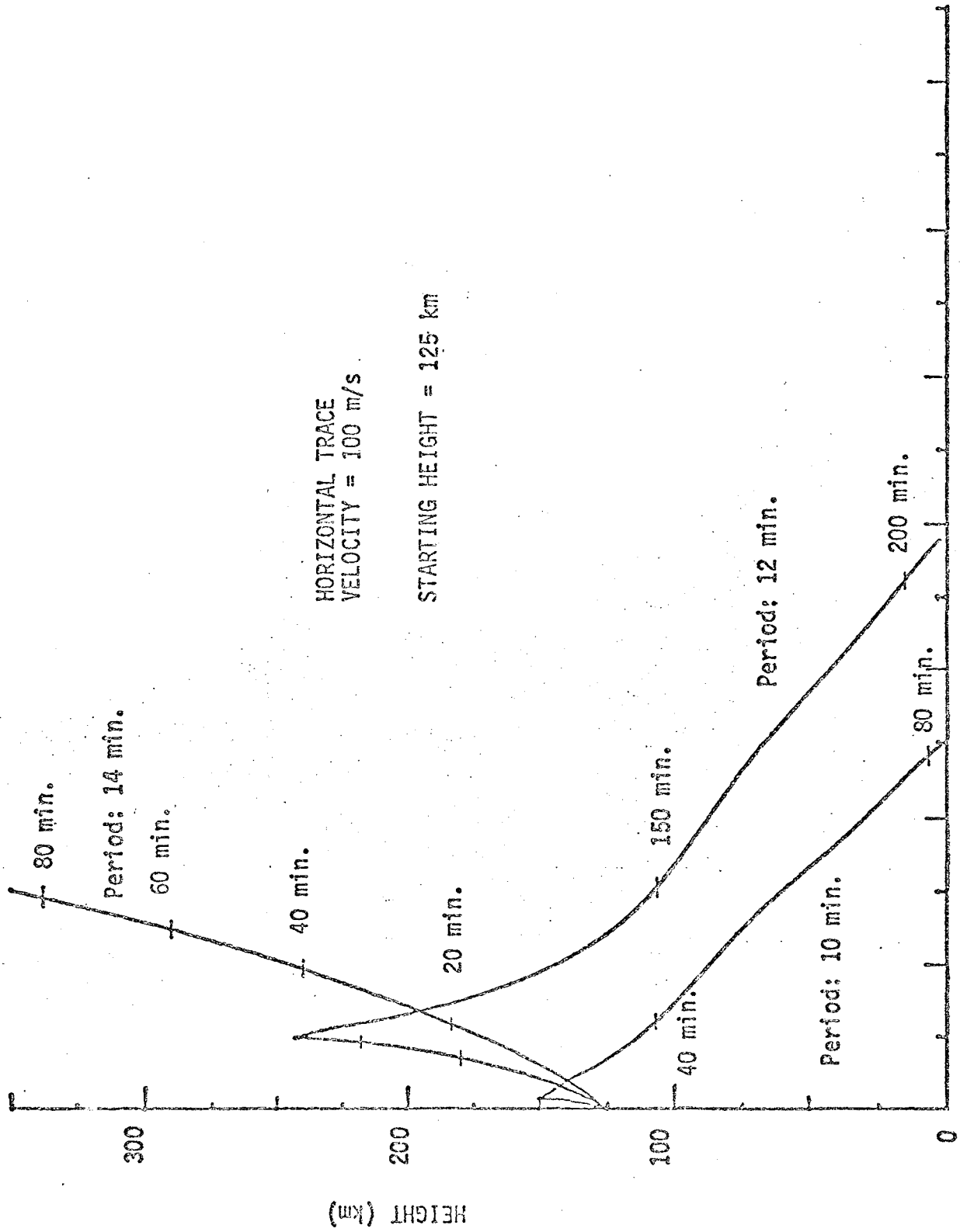

Figure 3. Ray-path for long internal gravity waves which start at a height of 125 km. Otherwise, the rays are the same as in Figure 1.

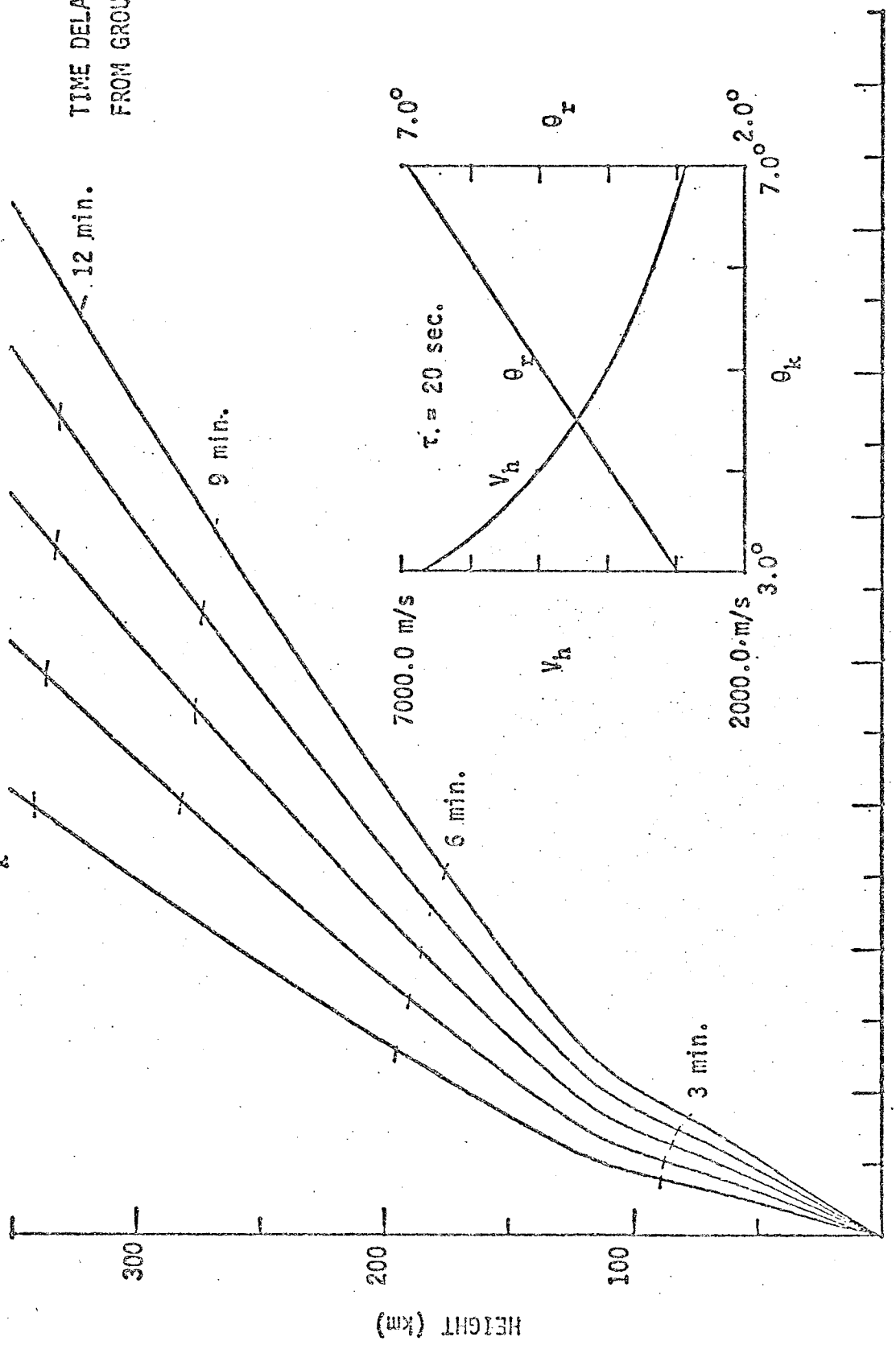

Figure 4. Ray-path for infrasonic waves from ground level source for wave period, τ = 20 sec. Symbols and insert explained in text.

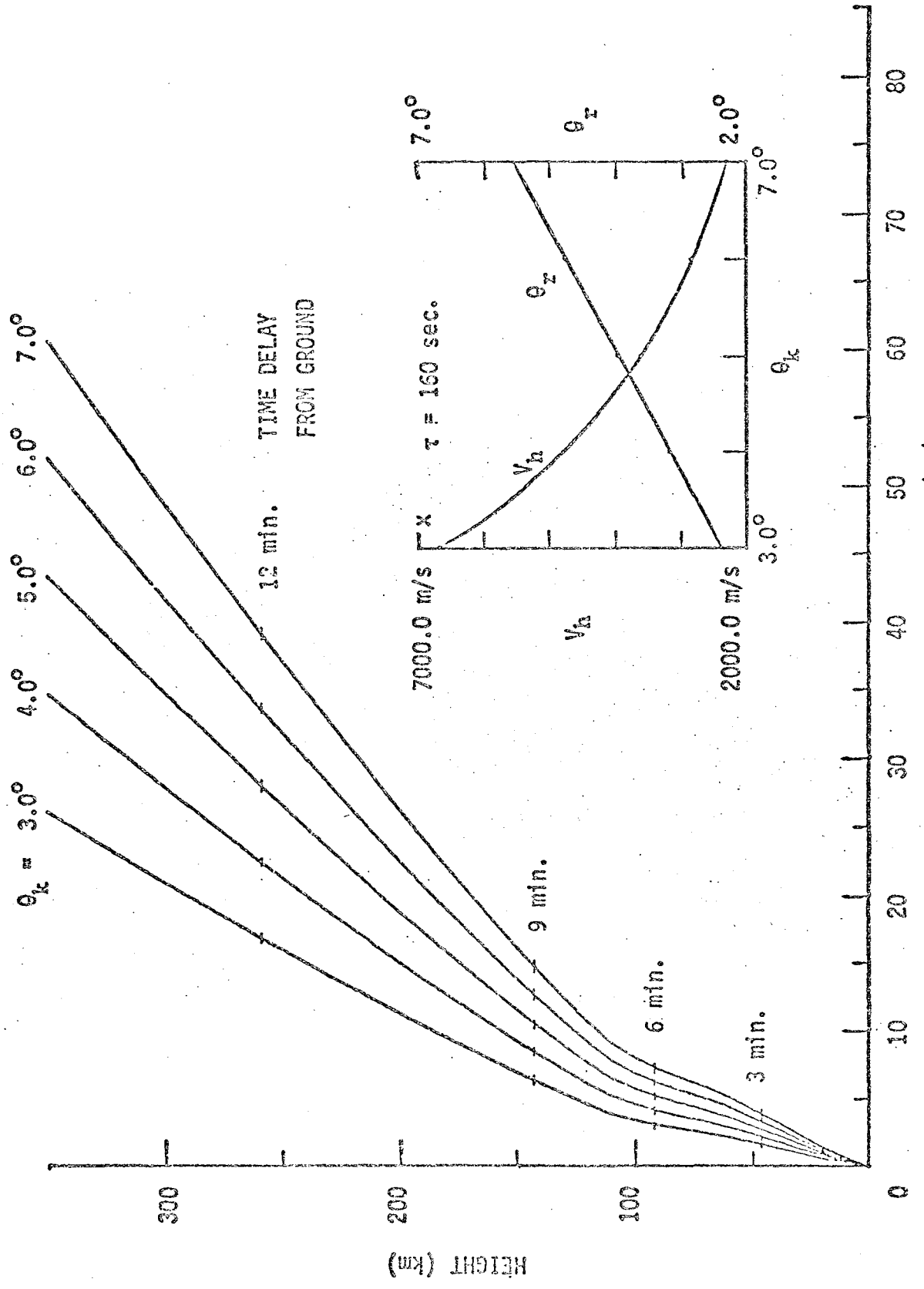

Figure 5. Same as Figure 4 except for wave period, τ = 160 sec.

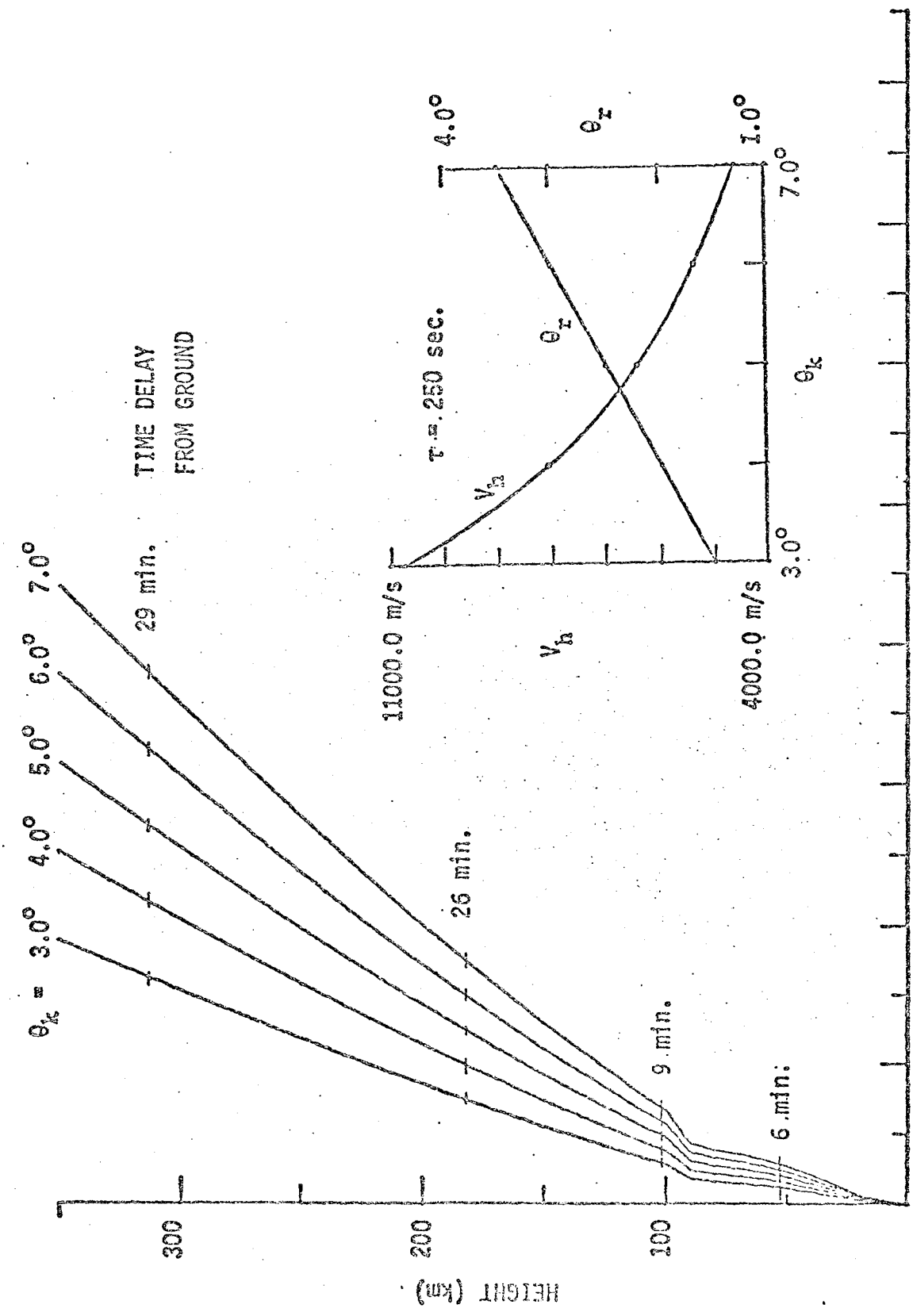

Figure 6. Same as Figure 4 except for wave period, τ = 250 sec.

REFERENCES

Cowling, D.H., et al., 1970, A study of traveling disturbances in the ionosphere, Ionospheric Radio Laboratory Tech. Rept. 38, University of Illinois.

Cowling, D.H., et al., 1971, Group rays of internal gravity waves in a windless stratified atmosphere, J. Geophys. Res., 76, 213.

George, T.M., 1968, HF Doppler studies of traveling ionospheric disturbances, J. Atmos. Terr. Phys., 30, 735.

Jones, W.L., 1969, Ray-tracing for internal gravity waves, J. Geophys. Res., 74(8), 2028.

Lighthill, M.J., 1965, Group velocity, J. Inst. Math. Appl., 1, 1-28.

Midgley, J.E. and H.B. Liemohn, 1966, Gravity waves in a realistic atmosphere, J. Geophys. Res., 71(5), 3729.

Yuen, P.C. et al., 1969, Continuous traveling coupling between seismic waves and the ionospheric evident in May 1968 Japan earthquake data, J. Geophys. Res., 75, 2256.

Yeh, K.C. et al., 1972, Evidence of directional filtering of traveling ionospheric disturbances, Nat. (Phys. Sci.), 235, 131 (Feb. 14).

Yeh, K.C. and C.H. Liu, 1974, Acoustic-gravity waves in the upper atmosphere, Rev. Geophys. Space Phys., 12(2), 193.

APPENDIX 3

MEASUREMENTS OF THE PHASE AND GROUP VELOCITIES OF SEISMIC RAYLEIGH WAVES IN THE PACIFIC BASIN

The following is a short description of the search for data on phase and group velocities of seismic Rayleigh waves along paths crossing the Pacific basin. No extensive analysis of the data found was attempted. The velocity observations found in the literature were plotted and comments are made on the different observations.

In general, the search was confined to papers that

1. contain recent observations after 1962, the year of Oliver's summary;
2. studied seismic waves from earthquakes around the Pacific basin; and
3. reported observations from stations in the Pacific basin.

Unfortunately, there were only a few papers that satisfied these requirements. The others, however, usually contained very useful information. According to the literature citations very important work on Rayleigh wave dispersion has been carried out recently by researchers in Japan but the corresponding papers are not available in Hamilton Library. Finally, the search was confined mainly to journals, such as the Bulletin of the Seismological Society of America and the Journal of Geophysical Research, which seismologists are most likely would publish their results. Other journals were checked only if referred to many times.

I. Empirical dispersion curves for seismic Rayleigh waves

Since Dorman (1969) has already constructed a fairly extensive plot of empirically determined values of the phase velocity, no attempt was made to display the data on phase velocity in the above sources. Measurements of phase velocity have probably been made since 1969 and while Dorman's plot should be updated, this was not done because the phase velocity at long periods appear to be reasonably well behaved.

The dispersion plot in Figure 1 shows several sets of measurements of the Rayleigh group velocity in the Pacific basin, as well as the values from Oliver (1962). Also shown are values we determined from the HF Doppler recordings

of the concomitant Rayleigh-related infrasound. The sets of measurements were identified using the first letter of the first author's name, except for the Dopplergram values (denoted by "o") and Oliver's values (denoted by ---x---). The legend contains the general location of the earthquake and recording station; the type, direction and length of path; and necessary explanatory notes. For additional details, the reader is referred to the paper (or papers) containing the measurement. Finally, just enough values in a given set of measurements were plotted so as to show the general shape of the dispersion curve. These values were then connected with straight lines to indicate the general shape. Thus, there is some distortion (eg., Kuo et al report a value of 4.0 km/sec at 45-50 sec), so that the curve formed by "k" is not flat as indicated), and the original data should be examined if fine details are under consideration.

II. Comments on the Group Velocity

1. Figure 1 suggets the following conclusions:
   a. There is no one dispersion curve (i.e., a single curve) that applies throughout the Pacific basin;
   b. Variability in group dispersion is inversely proportional to period, with "convergence" of measurements starting at about 160-180 sec.;
   c. The largest group velocity occurs at periods of about 45 sec.;

and

   d. The lowest group velocity occurs at a period of about 220 sec (excluding the drop-off near 20 sec).

2. A key to understanding the variability of the group velocity is the depth below the earth's surface to which each Rayleigh wave component penetrates. The rule appears to be that the components penetrate to about 1/2 to 1 wavelength, so that the wave characteristics are largely determined by the velocity structure within this depth.
3. In view of 2, conclusion 1.b is not too difficult to understand.
   a. Behavior of short period Rayleigh waves (period ~40 sec) is determined by the crustal structure, which varies considerably for different regions of the earth's surface.

b. Behavior of long-period waves of ~200 sec is determined by the structure of the upper mantle, which is fairly homogeneous in the lateral direction. Hence, one would expect less variablity. It should be noted, however, that many of the values in Figure 1 are for very long paths (up to several earth circumferences) and that much of the variations would be averaged out. Nevertheless, the rule seems to be applicable, since the crust forms only a small fraction of the controlling upper mantle layer.

4. If Rayleigh waves travel along paths of the order of 1 earth circumference, then much of the variation caused by differences in crustal structure along the path will cancel out. This, along with the points in 3., lead to the following general rules which are useful in interpreting the representative measurements in Figure 1.
   a. Gravity velocity observations provide a good measure at periods $\geq$ 180 sec, regardless of the length of the path.
   b. Very long path ($\geq$ 1 earth circumference) observations do not provide a good measure of group velocity at periods $\leq$ 80 sec.
   c. Direct path measurements are always preferable to long path measurements.
5. Most cases reported in the literature we studied was concerned with paths in the western half of the Pacific basin. Thus the dispersion in group velocity plotted in Figure 1 is strictly applicable to that region of the Pacific basin.
6. If the scatter in the measurements is real and not the results of instrumental and observational uncertainties, then the following statements seem to be valid.
   a. Propagation at short periods ($\leq$ 60 sec) is anisotropic in the western half of the Pacific basin, and different dispersion curves will have to be applied to the events on the location of the epicenter and the recording station.
   b. Propagation at long periods ($\geq$ 180 sec) is fairly isotropic, so that one dispersion curve applies at these periods.
   c. Propagation at intermediate periods (80 sec to 180 sec) may or may not be anisotropic.
7. Perhaps, the most impressive work was that of Santo (1963, and a later paper

referred in Saito and Takeuchi 1966) on the sectioning of the Pacific basin according to Rayleigh group velocity. The result is shown in Figure 2a and 2b (taken from Saito and Takeuchi 1966). The sectioning was made directly in terms of group velocity rather than other geophysical quantities such as shear velocity and heat flow as in Brune (1969). It is a "good" sectioning process because it is empirical and not theoretical (as far as can be determined). Thus it shows what the basin actually looks like from the point-of-view of group velocity measurements, and not what it should look like according to a theoretical model of the crust and upper mantle.

a. A single dispersion curve applies to all points of a given region and the different curves apply to the different types of regions.
b. Types of regions range from typical deep water basin ("0") and typical oceanic structure ("1") to typical continental structure ("7").
c. Note the complexity of the portion west of the andesite line; the structuring between East Island and Baja, California; and the graduation from oceanic to continental type as one approaches the Hawaiian Islands.

Two final points need to be mentioned.

d. It seems that the number of regions, as well as the shape of the regions, will vary with the range of periods under consideration. Generally, there will be less regions, and broader, more or less regular regions, for ranges towards the long period end of the spectrum. Indeed, there may be only one region for periods $\geq$ 180-200 sec.
e. This type of sectioning allows one to "display" the anisotropy present in the dispersion for the given range of periods.

8. Note that the dispersion in group velocity may differ for fairly similar and closely spaced paths such as those for K and A_3.

IV. CONCLUSIONS

Although the measurements in Figure 1 were not analyzed in great detail, there appears to be two rather obvious points concerning the curves as a whole.

1. There are measurements in the 80-180 sec range, but only a few of these are for the direct path. Thus, the latter type of measurements for this period range are needed in order to "complete" the study. In actuality, more measurements are needed in this range than in any other because this is a transition range where behavior changes from that determined by crustal structure to that determined by the upper mantle. In particular, it is not clear from Figure 1 at what period behavior ceases to be anisotropic and becomes isotropic.
2. Measurements are needed for paths crossing the eastern half of the Pacific basin. While this area is mostly oceanic, and hence, somewhat uniform, it seems that the Easter Island ridge introduces variations in the dispersion.

Further, it seems that one possible way of summarizing all the measurements would be to construct maps such as Santo's in Figure 2a, showing isodispersive areas. There would probably be 2-4 maps for 2-4 ranges of periods. For example, there might be maps for the ranges: 0-60 sec; 60-120 sec; 120-180 sec; and 180-280 sec. Clearly given such maps, the location of the epicenter and observing point, one can then accurately determine the time of arrival of various frequency components.

Finally, if one is limited to the use of just one dispersion curve, the best seems to be

1. the average of K and A between 20 and 100 sec;
2. the average of A and D between 120 and 150 sec;

and

3. measurements D for periods beyond 150 sec.

Such a curve lies in the middle of the scatter, and would probably be in serious error only towards the short period end.

NOMENCLATURE FOR FIGURE 1.

Direct · — From Dopplergrams; allowing for varying launch angle and using Huang's periods; Arrival time taken at peak.

Direct K — Kuo et al, 1962; Rayleigh waves from Kuril earthquake recorded at Suva, Fiji; R_1 waves.

Direct P — Pomeroy, 1963; Rayleigh waves from Eniwitok and Bikini blasts recorded at Honolulu; R_1 waves.

S — Santo (from Saito and Takeuchi, 1966); S_0, S_1, S_3, S_5 refers to different regions in Pacific basin. See Saito and Takeuchi, 1966, for divisions of regions; R_1 waves?

Direct A — Abe, 1972; "A" refers to average for Pacific A_3 refers to South Alaska earthquake recorded at Samoa, R_1 waves; A_6 refers to West Japan earthquake recorded at Samoa R_1 waves; 90 percent Oceanic

Direct Ap — Abe and Kanamori (Japan Journal); Equatorial earthquakes recorded in Japan; R_1 waves; Path lies west of the Andesite line; Mostly oceanic.

KA — Kanamori, 1970;
KA_1 refers to Kuril earthquake recorded at Tokyo.
KA_2 refers to Kuril earthquake recorded at Samoa.
Group velocities measured using R_3. R_4. R_5 and R_6 with the following estimated path mixtures:

	Oceanic(%)	Tectonic(%)	Shield(%)
KA_1	66	9	25
KA_2	75	5	20

D — Dziewonski and Landisman, 1970;
Averages for Kuril earthquake recorded at N.E. Australia and Tasmania. Uses R_n, n>2. Path mixture estimate is

68% Oceanic, 14% Tectonic and 18% Shield.

G — Gupta and Santo, 1973; Approximate values for Japan to Alburquerque using R_4. Path mixture not reported.

H — Hamada, 1971;
H_1 refers to Taiwan earthquake recorded by LASA in Montana (path traverses Japan, Kuriles, Aleutian, and Pacific Ocean).
H_2 refers to Mongolia earthquake recorded by LASA in Montana (path traverses Siberia, Arctic, Mid-Canada).
Path mixture not reported.

--x-- Approximate curves of Oceanic (upper) and Continental (lower) branches as given by Oliver's summary taken from his 1962 paper.

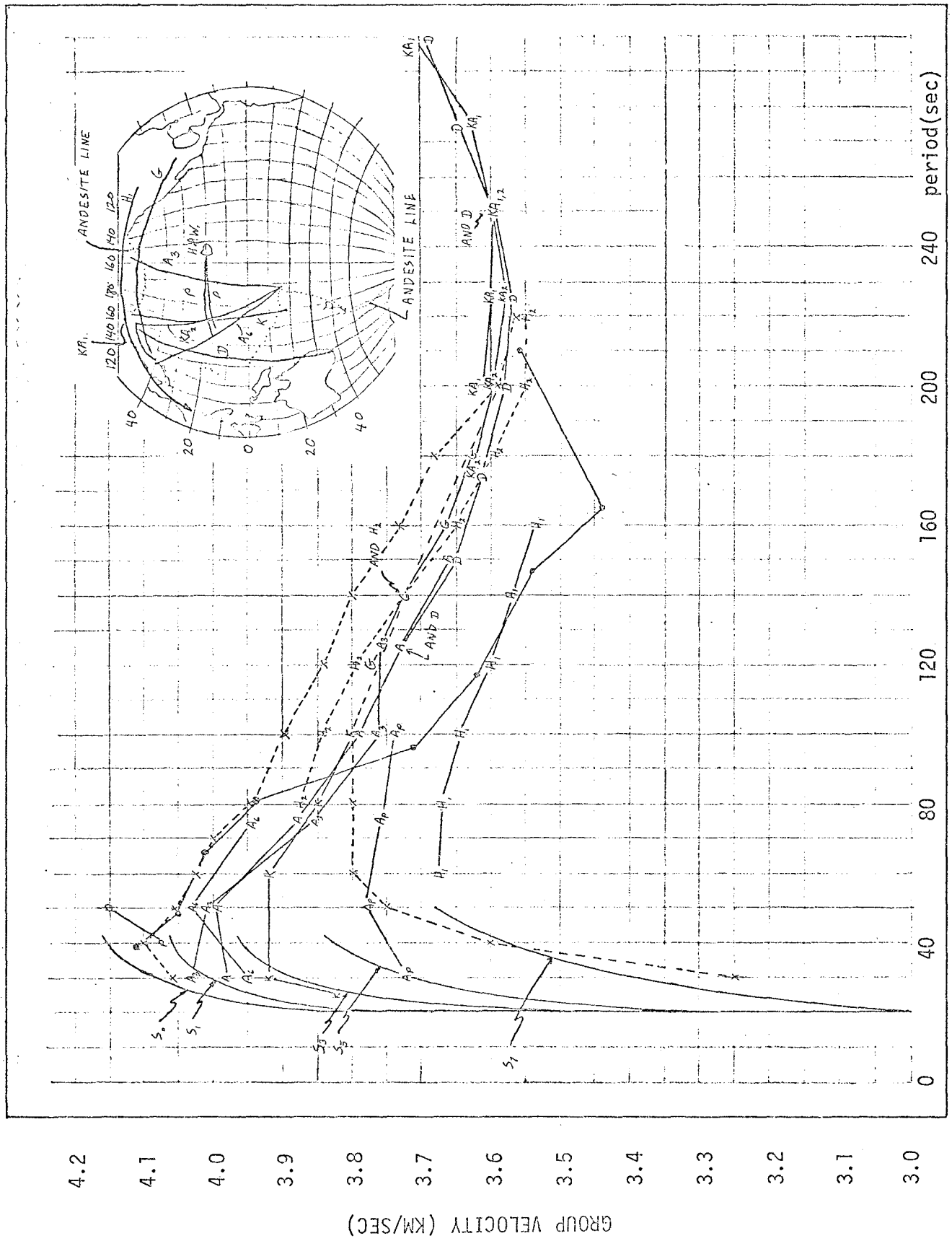

Figure 1. Compilation of Rayleigh wave group velocity curves from seismograph data of the Pacific Ocean.

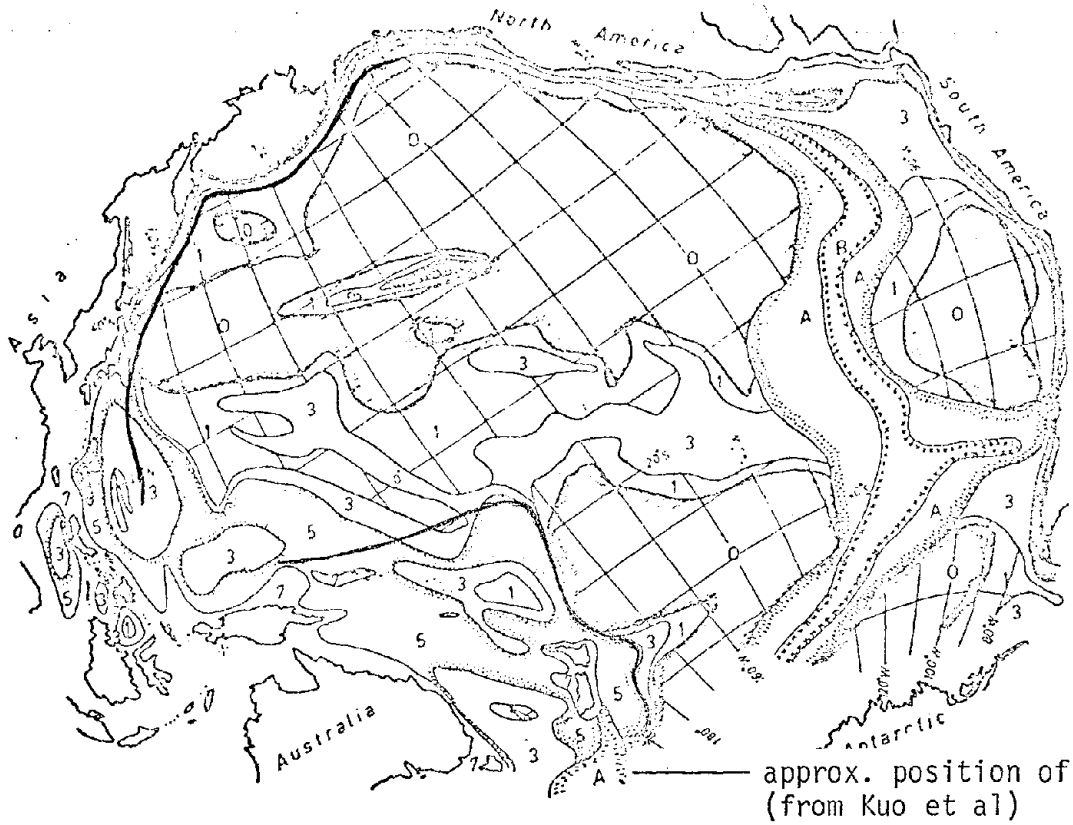

Fig. 2a. Division map of the Pacific (after T.A. Santo, by courtesy of Bull. Earthq. Res., Inst.).

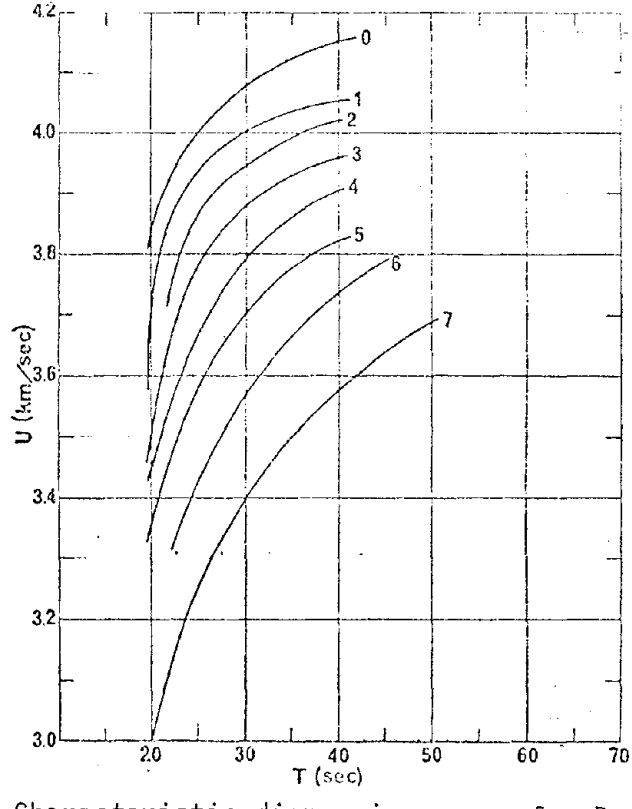

Fig. 2b. Characteristic dispersion curve for Rayleigh wave.

Abe, K., 1972, Group velocities of oceanic Rayleigh and love waves, Phys. Earth Planet. Int., 6, 391.

Brune, J.N., 1969, Surface waves and crustal structure, from "The Earth's Crust and Upper Mantle" (Am. Geophys. Un. Geophys. Monogr. 18, P. Hart (ed).

Dorman, J., 1969, Seismic surface wave data on the upper mantle, from "The Earth's Crust and Upper Mantle (Am. Geophys. Un. Geophy. Monogr. 13, P. Hart (ed).

Dziewonski, A.M., 1970, On regional differences in dispersion of mantle Rayleigh waves, Geophy. J. R. Astro. Soc., 22, 289.

Dziewonski, A. and M. Landisman, 1970, Great circle Rayleigh and love wave dispersion from 100 to 900 seconds, Geophy. J.R. Astro. Soc., 19, 37.

Ewing, M. and F. Press, 1954, An investigation of mantle Rayleigh waves, BSSA 44, 127.

Gupta, H., and T. Santo, 1973, Worldwide investigation of the mantle Rayleigh wave group velocities, BSSA 63(1), 271.

Hamada, K., 1971, Mantle wave analysis by a phase-equalization-and sum method for the Montana LASA long period data, BSSA, 61, 875-892.

Jacob, K.H. and K. Hamada, 1972, The upper mantle beneath Aleutian island arc from pure-path Rayleigh wave dispersion data, RSSA, 62(6), 1439.

Kanamori, H., 1970, Velocity and Q of mantle waves, Phys. Earth Planet. Int., 2, 259.

Kausel, E., et al., 1974, Variations of Rayleigh wave phase velocity across the Pacific ocean, Science, 186, 139.

Kuo, J., et al., 1962, Rayleigh wave dispersion in Pacific ocean for period range 20 to 140 seconds, BSSA, 52(3), 333.

Oliver, J., 1962, A summary of observed seismic surface wave dispersion, BSSA, 52(1), 81.

Pomeroy, P., 1963, Long period seismic waves from large, near surface nuclear explosions, BSSA, 53(1), 109.

Saito, M. and H. Takeuchi, 1966, Surface waves across the Pacific, BSSA, 56(5), 1067.

Santo, T., 1963, Division of the Pacific area into seven regions in each of which Rayleigh waves have the same group velocities, Bull. Earth. Res. Ins. (Tokyo), 41,719.

Santo, T. and M. Bath, 1963, Crustal structure of Pacific ocean area from dispersion of Rayleigh waves, BSSA, 53(1), 151.

Toksoz, N. and D.L. Anderson, 1966, Phase velocities of long period surface waves and structure of the upper mantle, J. Geophy. Res. 71(6), 1649.

APPENDIX 4

A METHOD FOR THE DETERMINATION OF THE IONOSPHERIC ELECTRON DENSITY PROFILE

4.1 Introduction

One of the important problems in the theoretical calculation of Doppler frequency shift caused by SC is the determination of the electron density $N_e(z)$ as a function of height z in the ionosphere when the virtual reflection height h'(f) of vertically incident radio waves is known as a function of frequency at or near the onset of a sudden commencement. The function h'(f) is found from the measured time delay for the return of a pulse of radio waves from the ionosphere. It is given by

$$h'(f) = \int_0^{z_r} \mu'(f, N_e)\, dz \qquad (4.1)$$

where z_r is the height at which the radio waves are reflected, and μ' is the group refractive index defined by

$$\mu' = c/u \qquad (4.2)$$

where c is the velocity of light and u is the group velocity of the radio waves used.

As will be shown in the next section, μ' is a known function of f & N_e and the problem is to solve the integral equation (4.1) to obtain the unknown function $N_e(z)$. When the geomagnetic field is neglected, μ' is (Davies, 1969)

$$\mu' = \frac{1}{\sqrt{1 - \left(\frac{f_N}{f}\right)^2}} = \frac{1}{\mu} \qquad (4.3)$$

where μ is the phase refractive index (normally simply referred to as the refractive index) and f_N the plasma frequency. Equation (4.1) becomes

$$h'(f) = f \int_0^{z_r} \frac{dz}{\sqrt{f^2 - f_N^2}} \tag{4.4}$$

This equation is a form of Abel's integral equation whose analytical solution is given by

$$h(f_v) = \frac{2}{\pi} \int_0^{f_v} \frac{h'(f)}{\sqrt{f_v^2 - f^2}}\, df \tag{4.5}$$

where $h(f_v)$ is the true (or real) height of reflection of a radio wave of frequency f_v (Wright et al., 1957). When the geomagnetic field cannot be neglected, this simplification is not possible and there is no analytical solution of (4.1), and it must be solved numerically. A variety of methods have been proposed for solving this equation (see summary by Thomas, 1957).

The purpose of this chapter is to introduce Budden's method for solving integral equation (4.1), and work out a computer program for this purpose.

4.2 Some useful equations

According to magneto-ionic theory (Ratcliffe, 1959), the refractive index μ of the ionosphere is given by

$$\mu^2 = 1 - \frac{X}{1 - \{Y_T^2/2(1-X)\} \pm \sqrt{\{Y_T^4/4(1-X)^2\} + Y_L^2}} \tag{4.6}$$

where

$$X = (f_N/f)^2 \tag{4.7}$$

$$Y_L = Y \cos\Theta \tag{4.8}$$

$$Y_T = Y \sin\Theta \tag{4.9}$$

$$Y = f_H/f \tag{4.10}$$

f_N = plasma frequency

f_H = gyro-frequency

θ = angle between the direction of wave normal and the external magnetic field B_0.

The plasma frequency f_N and the gyro-frequency for electron f_H are given respectively by Equations (4.11) and (4.12).

$$f_N = \sqrt{\frac{e^2 N}{4\pi^2 \varepsilon_0 m_e}} \tag{4.11}$$

$$f_H = \frac{e\, B_0}{2\pi m_e} \tag{4.12}$$

It can be shown that

$$\mu' = \frac{c}{u} = c\,\frac{\partial K}{\partial \omega} = \frac{\partial}{\partial \omega}\,(\omega\mu) = \frac{\partial}{\partial f}\,(f\mu) \tag{4.13}$$

where K and μ are the propagation constant and the refractive index, respectively. Expressing (4.13) in terms of the variables X and Y, instead of f, we have

$$\mu' = \mu + f\left(\frac{\partial \mu}{\partial X}\right)_Y \frac{dX}{df} + f\left(\frac{\partial u}{\partial Y}\right)_X \frac{dY}{df} \tag{4.14}$$

Substituting

$$f\,\frac{dX}{df} = -2X \tag{4.15}$$

and

$$f\,\frac{dY}{df} = -Y \tag{4.16}$$

into (4.14), we have

$$\mu' = \mu - 2X\left(\frac{\partial \mu}{\partial X}\right)_Y - Y\left(\frac{\partial \mu}{\partial Y}\right)_X$$

or

$$\mu\mu' = \mu^2 - X\left(\frac{\partial\mu}{\partial X}^2\right)_Y - \frac{1}{2}Y\left(\frac{\partial\mu}{\partial Y}^2\right)_X \qquad (4.17)$$

Substituting μ and μ^2 from (4.6 into (4.17), we obtain, after manipulation,

$$\mu' = \mu + \frac{(1-\mu^2)^2}{\mu}\left\{\frac{1}{X} + \frac{Y_T^2}{2(1-X)^2} \pm \frac{2(1-X)^3\ Y_L^2 - X\,Y_T^4}{2X(1-X)^2\ Y_T^4 + 4(1-X)^2 Y_L^2}\right\} \qquad (4.18)$$

where the + and - sign refer to the ordinary and extraordinary waves, respectively (Davies, 1969).

Near the level of reflection, we have $X \simeq 1$, $\mu \gtrsim 0$, and μ' approaches infinity for ordinary wave and the group refractive index can be approximated by (Davies, 1969)

$$\mu' \simeq \varepsilon^{-1/2}\ \csc\Theta\left(1 - \frac{3}{2}\varepsilon\cot^2\Theta\right) \qquad (4.19)$$

where

$$\Theta = 1 - X$$

is a very small quantity.

It can be shown that

$$f_H = \frac{e\,B_0}{2\pi m_e} = 1.536 \times 10^3\ \frac{B_0}{M_e}$$

where M_e is the mass of the electron in atomic mass unit and total magnetic intensity B_0 in gamma. The annual values of B_0 at Honolulu for the year of 1969 was B_0 = 35804 gamma. Using this value of B_0, f_h at 300 km was calculated to be 0.873 MHz.

4.3 Budden's matrix method

In order to integrate (4.1) numerically to obtain the electron density profile Ne(z) from the ionogram, Budden (1955) has worked out a lamination method under the following assumptions:

(i) The virtual height h'(f) is measured for ordinary wave which is reflected at the level where $f = f_N$,

(ii) The effect of electron collision is neglected,

(iii) The frequency is great enough to permit the assumption of a slowly varying ionosphere so that a ray theory can be used, and

(iv) The electron density increases monotonically with respect to height.

Suppose h'(f) is given as a tabulated function at equal interval Δf of the frequency, and the n^{th} observed virtual height is $h'(n\Delta f) = h'_n$, where n is an integer. Instead of using N_e in (4.1), it is more convenient to use plasma frequency f_N defined in (4.11) so that (4.1) may be written as

$$h'(f) = \int_0^{z_r} \mu' (f, f_N)\, dz \tag{4.20}$$

Using f_N as an independent variable, (4.20) may be written as

$$h'(f) = \int_0^{f} \mu' (f, f_N) \frac{dz}{df_N}\, df_N \tag{4.21}$$

The range of integration in (4.21) is divided into discrete intervals Δf, so that for the m^{th} interval

$$(m - 1)\,\Delta f < f_N < m\Delta f$$

where $1 \leq m \leq n$. In each of these intervals, it is assumed that dz/df_N is constant and is given by

$$\frac{dz}{df_N} \simeq \frac{z_m - z_{m-1}}{\Delta f} = \text{constant} \tag{4.22}$$

where

$$z_m = z(m\Delta f).$$

Then, (4.21) may be written as

$$h'(n\Delta f) = \sum_{m=1}^{n} \left\{ \left(\frac{dz}{df_N}\right)_m \int_{(m-1)\Delta f}^{m\Delta f} \mu'(n\Delta f, f_N)\, df_N \right\}$$

$$= \sum_{m=1}^{n} (z_m - z_{m-1}) \left\{ \frac{1}{\Delta f} \int_{(m-1)\Delta f}^{\Delta f} \mu'(n\Delta f, f_N)\, df_N \right\} \tag{4.23}$$

Let

$$\left.\begin{aligned} M_{nm} &= \frac{1}{\Delta f} \int_{(m-1)\Delta f}^{m\Delta f} \mu'(n\Delta f, f_N)\, df_N \qquad \text{for } m \leq n \\ M_{nm} &= 0 \qquad\qquad\qquad\qquad\qquad\qquad\quad \text{for } m > n \end{aligned}\right\} \tag{4.24}$$

then (4.23) becomes

$$h'_n = \sum_{m=1}^{n} M_{nm} (z_m - z_{m-1}) \tag{4.25}$$

In matrix form (4.25) may be written as

$$\begin{bmatrix} h_1' \\ h_2' \\ h_3' \\ \vdots \\ h_n' \end{bmatrix} = \begin{bmatrix} M_{11} & 0 & 0 & \cdots & 0 \\ M_{21} & M_{22} & 0 & & \vdots \\ M_{31} & M_{32} & M_{33} & & \vdots \\ \vdots & \vdots & & & \vdots \\ M_{n1} & M_{n2} & M_{n3} & \cdots & M_{nn} \end{bmatrix} \begin{bmatrix} 1 & 0 & \cdots & 0 \\ -1 & 1 & & \vdots \\ 0 & -1 & & \vdots \\ \vdots & \vdots & & \vdots \\ 0 & & & -1 \end{bmatrix} \begin{bmatrix} z_1 \\ z_2 \\ z_3 \\ \vdots \\ z_n \end{bmatrix}$$

$$= \begin{bmatrix} M_{11} & 0 & 0 & \cdots & 0 \\ M_{21}-M_{22} & M_{22} & 0 & & \vdots \\ M_{31}-M_{32} & M_{32}-M_{33} & M_{43}-M_{44} & & \vdots \\ \vdots & \vdots & \vdots & & \vdots \\ M_{n1}-M_{n2} & M_{n2}-M_{n3} & M_{n3}-M_{n4} & \cdots & M_{nn} \end{bmatrix} \begin{bmatrix} z_1 \\ z_2 \\ z_3 \\ \vdots \\ z_n \end{bmatrix}$$

$$= \begin{bmatrix} A_{11} & 0 & \cdots & 0 \\ A_{21} & A_{22} & \cdots & \\ A_{31} & A_{32} & \cdots & \\ \vdots & & & \\ A_{n1} & A_{n2} & \cdots & A_{nn} \end{bmatrix} \begin{bmatrix} z_1 \\ z_2 \\ z_3 \\ \vdots \\ z_n \end{bmatrix} \tag{4.26}$$

where $A_{nm} = M_{nm} - M_{n,\, m+1}$ (4.27)

Matrix equation (4.26) can be written as

$$\begin{aligned} h_1' &= A_{11}\, z_1 \\ h_2' &= A_{21} z_1 + A_{22} z_2 \\ h_3' &= A_{31} z_1 + A_{32} z_2 + A_{33} z_3 \\ &\vdots \\ h_n' &= A_{n1} z_1 + A_{n2} z_2 + A_{n3} z_3 + \cdots\cdots + A_{nn} z_n \end{aligned} \tag{4.28}$$

By successively solving for the layer heights Zn, we obtain

$$\begin{aligned} z_1 &= \frac{1}{A_{11}}\, h_1' \\ z_2 &= \frac{1}{A_{22}}\, h_2' - \frac{A_{21}}{A_{22}}\, z_1 \\ z_3 &= \frac{1}{A_{33}}\, h_3' - \frac{A_{32}}{A_{33}}\, z_2 - \frac{A_{31}}{A_{33}}\, z_1 \\ &\vdots \\ z_n &= \frac{1}{A_{nn}}\, h_n' - \frac{A_{n,n-1}}{A_{nn}}\, z_{n-1} - \cdots\cdots - \frac{A_{n,1}}{A_{nn}}\, z_1 \end{aligned} \tag{4.29}$$

Equation (4.29) is the required solution in which the A_{nm}'s are independent of the observational data h'(f) and are only dependent on the total magnetic field intensity B_0, and the dip angle I of the observer. Therefore, once the integrals (4.24) and the quantities in (4.27) have been

evaluated for the station, the real height z_n's can be obtained by solving (4.29) using the observed h_n's. This method was invented by Budden and is called Budden's matrix method (Budden, 1955). For brievity of notation, (4.29) will be written as follows:

$$z_1 = C_{11}h_1'$$

$$z_2 = C_{21}h_2' + C_{22}z_1$$

$$z_3 = C_{31}h_3' + C_{32}z_2 + C_{33}z_1 \qquad (4.30)$$

$$z_n = C_{n1}h_n' + C_{n2}z_{n-2} + \ldots\ldots + C_nz_1$$

In an ordinary ionospheric sounder, the minimum probing frequency is usually set at 1.0 MHz. If we chose Δf = 0.1 MHz, then z_1, z_2, ..., z_9 in (4.30), which are the real reflection heights for the probing frequencies of 0.1, 0.2, 0.3, ..., 0.9 MHz, cannot be determined by using (4.30); because the ionospheric sounder cannot give the virtual heights h_1', h_2', ..., h_g'. At the low frequency end, the h'(f) curve for the ordinary wave is almost horizontal and may be considered as the base height of the ionosphere. Hence h'(f) for all f in the range from 0 to 1.0 MHz can be considered to be roughly constant and equal to $z(f_N)$, where f_N = 1.0 MHz for an ordinary ionospheric sounder, i.e., we may set

$$z_1 = z_2 = \ldots\ldots = z_{10} = h_{10}' \equiv h'o$$

If we redefine z_1, z_2, z_3, ..., z_n to mean the real reflection height for the frequency of 1.0, 1.1, 1.2, then (4.30) can be rewritten as

$$z_0 = h_0'$$

$$z_1 = C_{10}h_0' + C_{11}h_1'$$

$$z_2 = C_{20}h_0' + C_{21}h_2' + C_{22}z_1 \tag{4.31}$$

$$z_3 = C_{30}h_0' + C_{31}h_3' + C_{32}z_2 + C_{33}z_1$$

$$\vdots$$

$$z_n = C_{n0}h_0' + C_{n1}h_n' + C_{n2}z_{n-1} + \cdots + C_{nn}z_1$$

where C_{n0} stands for the sum of the elements for frequencies from 0.1 MHz to 1.0 MHz. Since the sum of all C_{nm}'s in each of the equation in (4.30) must be unity, the C_{n0}'s can be obtained by

$$C_{n0} = 1 - \sum_{m=1}^{n} C_{nm} \tag{4.32}$$

4.4 A computer program for the evaluation of the values of C_{nm}

In order to determine C_{nm}, M_{nm} must be determined first. In the determination of M_{nm}, the evaluation of the integral in equation (4.24) can be carried out directly by Simpson's method except for the case when m = n. When m = n, μ' approaches ∞, i.e., (4.24) cannot be evaluated directly. It can be evaluated by the method described below.

Let a new variable ϕ be defined by

$$\sin\phi = f_N/f = f_N/n\Delta f \tag{4.33}$$

then

$$X = \sin^2\phi$$

$$\varepsilon = 1 - X = 1 - \sin^2\phi = \cos^2\phi$$

and

$$df_N = f\cos\phi\, d\phi = n\Delta f \cos\phi\, d\phi$$

Substituting for f_N and df_N in (4.24) we have

$$M_{nm} = n \int_{\sin^{-1}\left(\frac{(m-1)\Delta f}{f}\right)}^{\sin^{-1}\left(\frac{m\Delta f}{f}\right)} \mu'(n\Delta f, m\Delta f)\cos\phi\, d\phi \tag{4.34}$$

When the level of reflection is reached, the group refractive index μ' (see equation 4.9) reduces to $\mu' \simeq \varepsilon^{-1/2} = 1/\cos\phi$

Therefore, (4.34) becomes

$$M_{nm} = n \int_{\sin^{-1}\frac{(n-1)\Delta f}{f}}^{\sin^{-1}\left(\frac{n\Delta f}{f}\right)} d\phi$$

$$= n \left\{\sin^{-1} 1 - \sin^{-1} \frac{(n-1)}{n}\right\} \qquad (4.35)$$

and the integral converges even though μ' approaches infinity as the integration approaches the level of reflection.

The calculations were processed according to the following steps:

(i) By using annual mean values of B_0 = 358049 gamma and I = 48.31° observed at Honolulu Observatory for the year of 1968, f_H at 300 km height is 0.873 MHz and θ = 90 - I = 51.29° over Maui.

(ii) The frequency range was chosen to be from 1.0 MHz to 18 MHz, i.e., n=1 to 171 and Δf was chosen to be 0.1 MHz.

(iii) Equation (4.18) was used to calculate group refractive index μ' by giving f and f_N. To do this, a subroutine subprogram UDASH (F, FN, U) was developed, where U is the returned value of μ'.

(iv) In order to evaluate M_{nm}, the integral in (4.24) was numerically integrated by Simpson's method using 5 ordinates. For $m \neq n$, the expression in (4.34) was directly used for numerical integration. For m = n, the following equation derived from (4.24) was used for numerical integration.

$$M_{nn} = \frac{1}{\Delta f} \int_{(m-1)\Delta f}^{(m-0.25)\Delta f} \mu'(f, f_N)\, df_N$$

$$+ n\left(\sin^{-1} 1 - \sin^{-1} \frac{n - 0.25}{n}\right) \qquad (4.36)$$

A subroutine subprogram INTEG (Y, H, N, A) was provided to perform Simpson's numerical integration. The arguments Y, H, N, and A represent ordinate value, step width, number of ordinates and the returned value of integration.

(v) A_{nm} was calculated by using (4.27), and C_{nm} by using (4.30) and (4.32).

The whole set of computer program for calculation of C_{nm} for Maui station is given in Appendix 4A. Some of the C_{nm}'s calculated are shown in Table 4.1. The left-most column represents the plasma frequency in MHz. C_{nm}'s are arranged in ascending order of m for each n. If m is too large to allow all C_{nm}'s to be arranged in one row, the extra C_{nm}'s are arranged in the following row or rows. The complete set of C_{nm} require more than 24 pages; hence only those with small n are given in Table 4.1. The complete table of C_{nm} as well as their punched cards is filed in the Radioscience Laboratory.

4.5 A computer program for the determination of an electron density profile from an ionogram.

Once the C_{nm}'s are determined, (4.31) can be used to determine the z_n's. However, the real height corresponding to F_2 layer critical frequency foF_2 cannot be determined by this equation; because the virtual height becomes infinity at this frequency. Therefore, some kind of model electron density distribution of the ionosphere should be assumed and used to fit the actually observed virtual heights near foF_2 so that the real height at foF_2 can be determined. Usually, a parabolic distribution of the electron density is assumed for this purpose.

Table 4.1 Some of the calculated C_{nm} 's.

1.0	0.72014	0.27986								
1.1	0.31633	0.24958	0.43409							
1.2	0.17116	0.22959	0.45378	0.14507						
1.3	0.10358	0.21442	0.46825	0.14174	0.06701					
1.4	0.07505	0.20161	0.47949	0.13903	0.06647	0.03834				
1.5	0.05479	0.19115	0.48764	0.13697	0.06611	0.03855	0.02459			
1.6	0.04196	0.18221	0.49408	0.13528	0.06583	0.03873	0.02495	0.01696		
1.7	0.03303	0.17452	0.49913	0.13386	0.06560	0.03891	0.02528	0.01734	0.01232	
1.8	0.02661	0.16752	0.50389	0.13254	0.06531	0.03901	0.02553	0.01765	0.01265	0.00930
1.9	0.02190	0.16158	0.50717	0.13146	0.06516	0.03915	0.02581	0.01796	0.01297	0.00960
	0.00724									
2.0	0.01831	0.15616	0.51015	0.13048	0.06496	0.03927	0.02603	0.01824	0.01325	0.00988
	0.00750	0.00578								
2.1	0.01551	0.15117	0.51299	0.12953	0.06474	0.03933	0.02621	0.01847	0.01350	0.01012
	0.00774	0.00600	0.00470							
2.2	0.01329	0.14659	0.51551	0.12867	0.06455	0.03936	0.02637	0.01867	0.01371	0.01034
	0.00795	0.00620	0.00489	0.00389						
2.3	0.01154	0.14283	0.51649	0.12807	0.06454	0.03951	0.02658	0.01890	0.01396	0.01058
	0.00817	0.00641	0.00503	0.00407	0.00328					
2.4	0.01007	0.13889	0.51871	0.12734	0.06427	0.03950	0.02668	0.01906	0.01413	0.01076
	0.00835	0.00658	0.00525	0.00422	0.00342	0.00278				
2.5	0.00889	0.13576	0.51911	0.12687	0.06429	0.03964	0.02687	0.01927	0.01434	0.01096
	0.00855	0.00677	0.00542	0.00438	0.00357	0.00292	0.00240			
2.6	0.00788	0.13256	0.52036	0.12629	0.06416	0.03967	0.02698	0.01941	0.01450	0.01113
	0.00871	0.00692	0.00557	0.00452	0.00370	0.00304	0.00251	0.00208		
2.7	0.00703	0.12965	0.52155	0.12571	0.06401	0.03969	0.02707	0.01955	0.01465	0.01128
	0.00886	0.00707	0.00571	0.00465	0.00382	0.00316	0.00262	0.00218	0.00182	
2.8	0.00631	0.12676	0.52255	0.12519	0.06388	0.03970	0.02716	0.01967	0.01479	0.01142
	0.00900	0.00721	0.00584	0.00478	0.00394	0.00327	0.00273	0.00228	0.00191	0.00161
2.9	0.00569	0.12417	0.52333	0.12476	0.06376	0.03972	0.02724	0.01978	0.01492	0.01156
	0.00914	0.00733	0.00596	0.00489	0.00405	0.00337	0.00282	0.00237	0.00200	0.00169
	0.00143									
3.0	0.00516	0.12178	0.52388	0.12435	0.06368	0.03975	0.02733	0.01989	0.01504	0.01166
	0.00926	0.00746	0.00608	0.00501	0.00416	0.00347	0.00292	0.00246	0.00209	0.00177
	0.00150	0.00128								
3.1	0.00468	0.11921	0.52559	0.12370	0.06339	0.03967	0.02733	0.01994	0.01512	0.01177
	0.00936	0.00756	0.00618	0.00510	0.00425	0.00356	0.00300	0.00254	0.00216	0.00184
	0.00157	0.00134	0.00114							
3.2	0.00428	0.11719	0.52556	0.12347	0.06338	0.03972	0.02742	0.02005	0.01523	0.01189
	0.00948	0.00767	0.00629	0.00521	0.00435	0.00365	0.00309	0.00262	0.00224	0.00191
	0.00164	0.00141	0.00121	0.00103						
3.3	0.00392	0.11516	0.52599	0.12317	0.06328	0.03972	0.02747	0.02013	0.01533	0.01199
	0.00958	0.00777	0.00639	0.00530	0.00444	0.00374	0.00317	0.00270	0.00231	0.00198
	0.00170	0.00147	0.00126	0.00109	0.00094					
3.4	0.00360	0.11295	0.52754	0.12255	0.06303	0.03963	0.02745	0.02015	0.01538	0.01206
	0.00965	0.00785	0.00646	0.00538	0.00451	0.00381	0.00324	0.00277	0.00237	0.00204
	0.00176	0.00152	0.00132	0.00114	0.00099	0.00085				

Let z_c and q_c represent the real height at frequency foF_2 and the quarter thickness of the assumed parabolic layer, respectively, then the following equation can represent this layer:

$$f^2 = f_c^2 \{ 1 - (\frac{z-z_c}{2q_c})^2 \} \tag{4.37}$$

where f_c denotes the foF_2. The z_c and q_c are determined by fitting this parabolic layer to the last two real heights. Let the frequencies and the corresponding real height be f_{n-1}, f_n and z_{n-1}, z_n, respectively. Since $\Delta f = 0.1$ MHz, we have

$$f_n = f_{n-1} + 0.1 = f_c - 0.1 \tag{4.38}$$

The equation (4.37) can be solved for the height z and written as

$$z = z_c - \frac{2q_c}{f_c} \sqrt{(f_c - f)(f_c + f)} \tag{4.39}$$

Substituting (f_{n-1}, z_{n-1}') and (f_n, z_n') into (4.39) we obtain the real height at the two levels.

$$z_{n-1} = z_c - \frac{2q_c}{f_c} \sqrt{0.2\,(2f_c - 0.2)}$$

$$z_n = z_c - \frac{2q_c}{f_c} \sqrt{0.1\,(2f_c - 0.1)}$$

Solving these two equations simultaneously for the real height at the maximum of the electron density and the quarter thickness of the parabolic layer, we have

$$z_c = z_n + \frac{(z_n - z_{n-1}) \sqrt{0.1\,(2f_c - 0.1)}}{\{\sqrt{0.2\,(2f_c - 0.2)} - \sqrt{0.1\,(2f_c - 0.1)}\}} \tag{4.40}$$

and

$$q_c = \frac{(z_n - z_{n-1})\, f_c}{2\{\sqrt{0.2\,(2f_c - 0.2)} - \sqrt{0.1\,(2f_c - 0.1)}\}} \tag{4.41}$$

The ordinary ionospheric vertical sounder can observe only the bottom side of the ionosphere. The top side ionosphere can be observed by using top side sounder or coherent scattering technique. Since the top-side ionograms are not available, the electron density distribution above the peak electron density was assumed to coincide with that for a Chapman layer given by (4.42)

$$N_e = N_{ec} \exp \{ \frac{1}{2} (1 - Z - e^{-Z}) \} \qquad (4.42)$$

where N_{ec} is the peak electron density corresponding to f_c, and

$$Z = \frac{z - z_c}{H}$$

where H is a scale height and is assumed to be 100 km (Wright, 1960).

Using Equations (4.31), (4.40), (4.41) and (4.42) a computer program has been developed, the detail of which is shown in Appendix 4B. In order to use this program, the procedures given in Appendix 4B must be followed to digitize the ionogram and prepare a set of data cards. In Fig. 4.1, the dashed line gives the h'(f) curve reproduced from the ionogram obtained at Maui on May 14, 1969 at 0915 HST. The full line shows z(f) curve obtained by using computer program given in Appendix 5A. The horizontal axis refers to $\log_{10} f$, where f is in a unit of MHz. Due to group retardation of radio waves in the ionosphere, z(f) is much smaller than h'(f) for a given frequency f. This difference increases as f increases. In Figure 4.2 are shown the monthly mean hourly electron density profiles obtained for March 1968. The number on each curve represents the hour. Each hourly electron density profile is obtained from a composite h'(f) curve which is constructed by taking an average of 5 hourly ionograms obtained during the 5 international quiet days. The diurnal variation of the electron density can be seen clearly

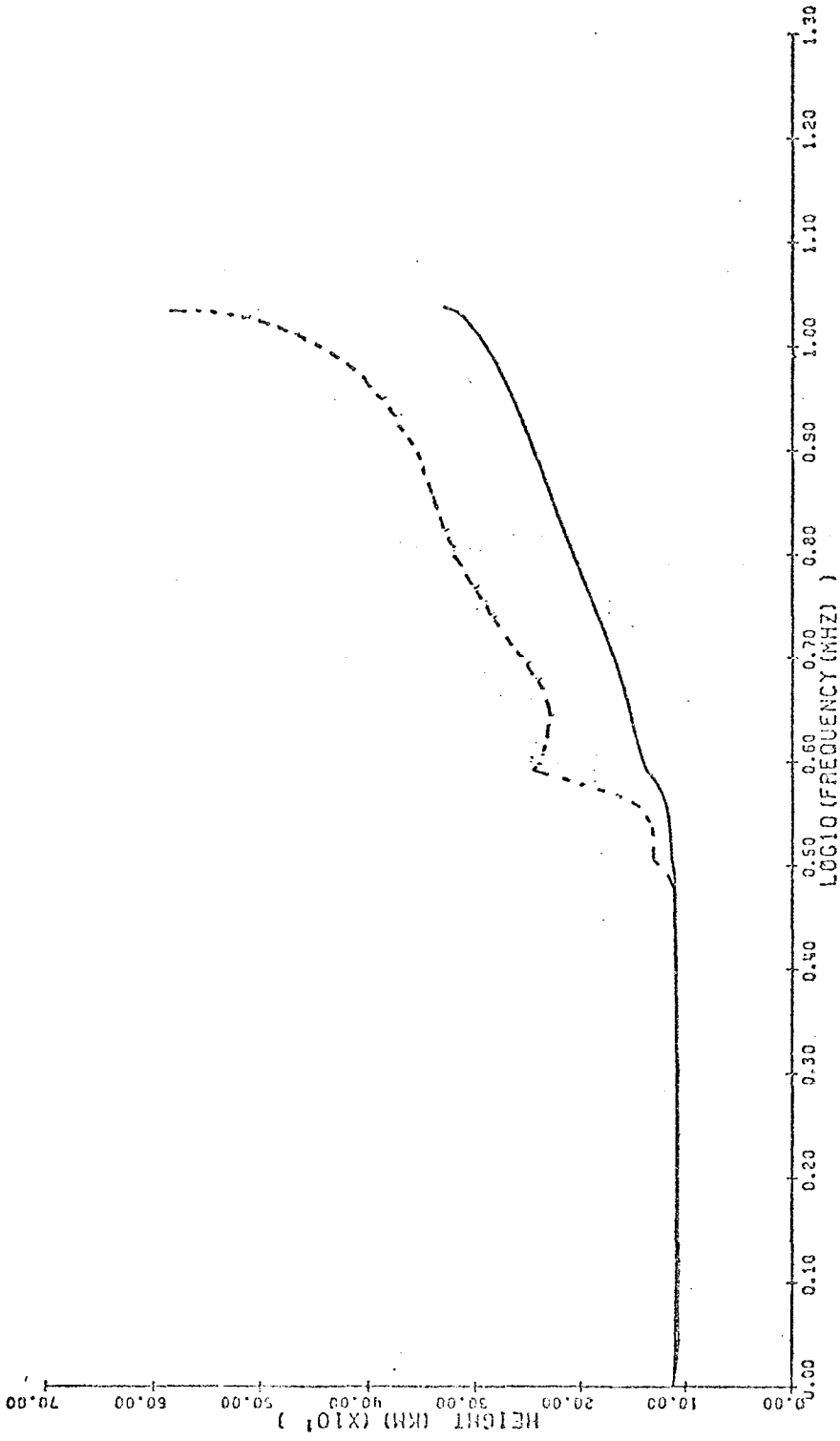

Figure 4.1 Digitized h'(f) curve (upper curve) obtained for the ionogram given in Figure 4.1 and the corresponding electron density profile (lower curve).

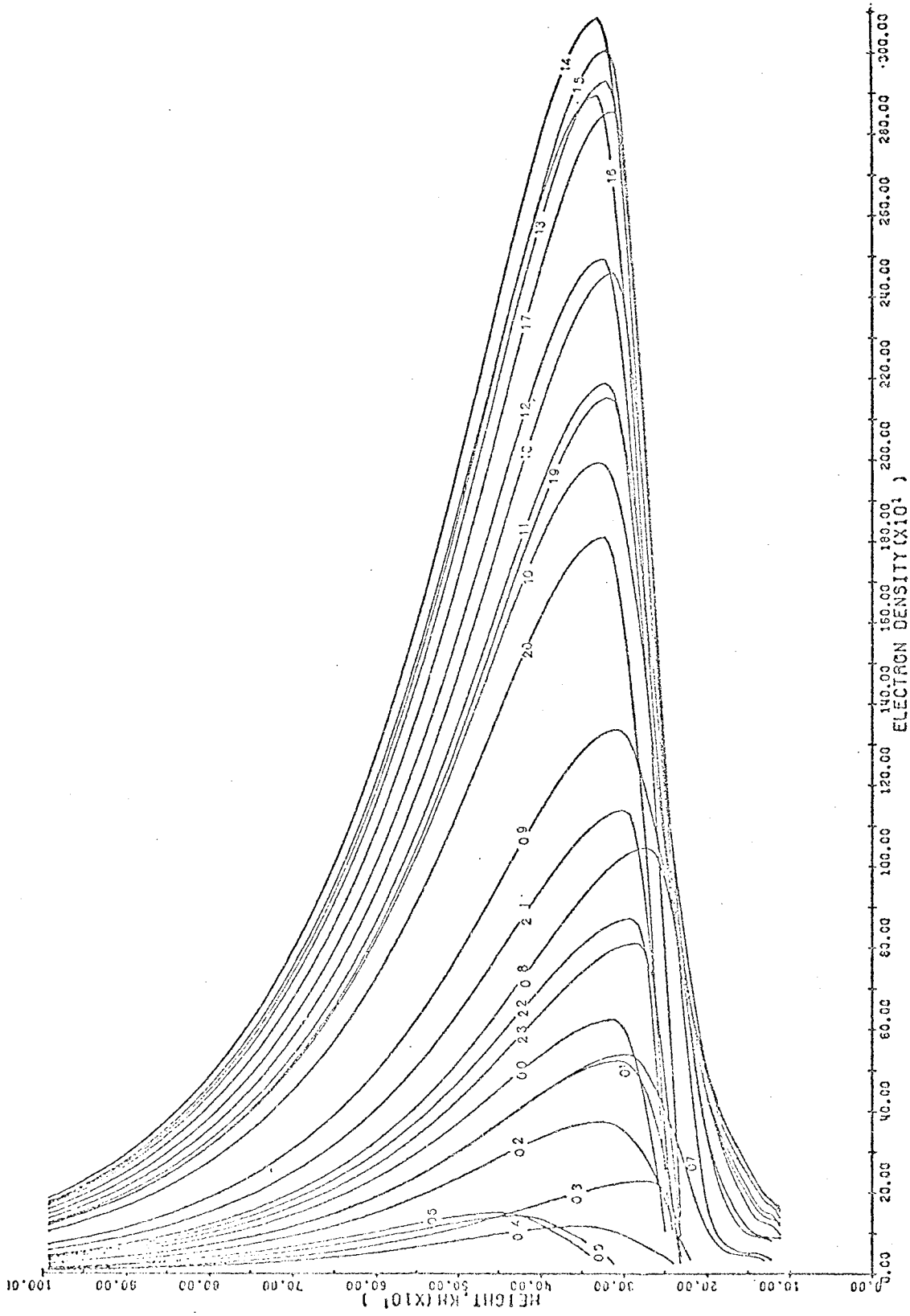

Figure 4.2. The diurnal variation of the electron density profile obtained for the magnetically quiet days of March 1968.

through this figure. Figure 4.3 shows the diurnal variation of the electron density at fixed heights.

While the variation of electron density is similar to a Chapman layer up to above 200 km it becomes quite irregular above 200 km. Some of these electron density profiles will be used in Chapter VII for theoretical calculation of the Doppler frequency shifts caused by a model sudden commencement.

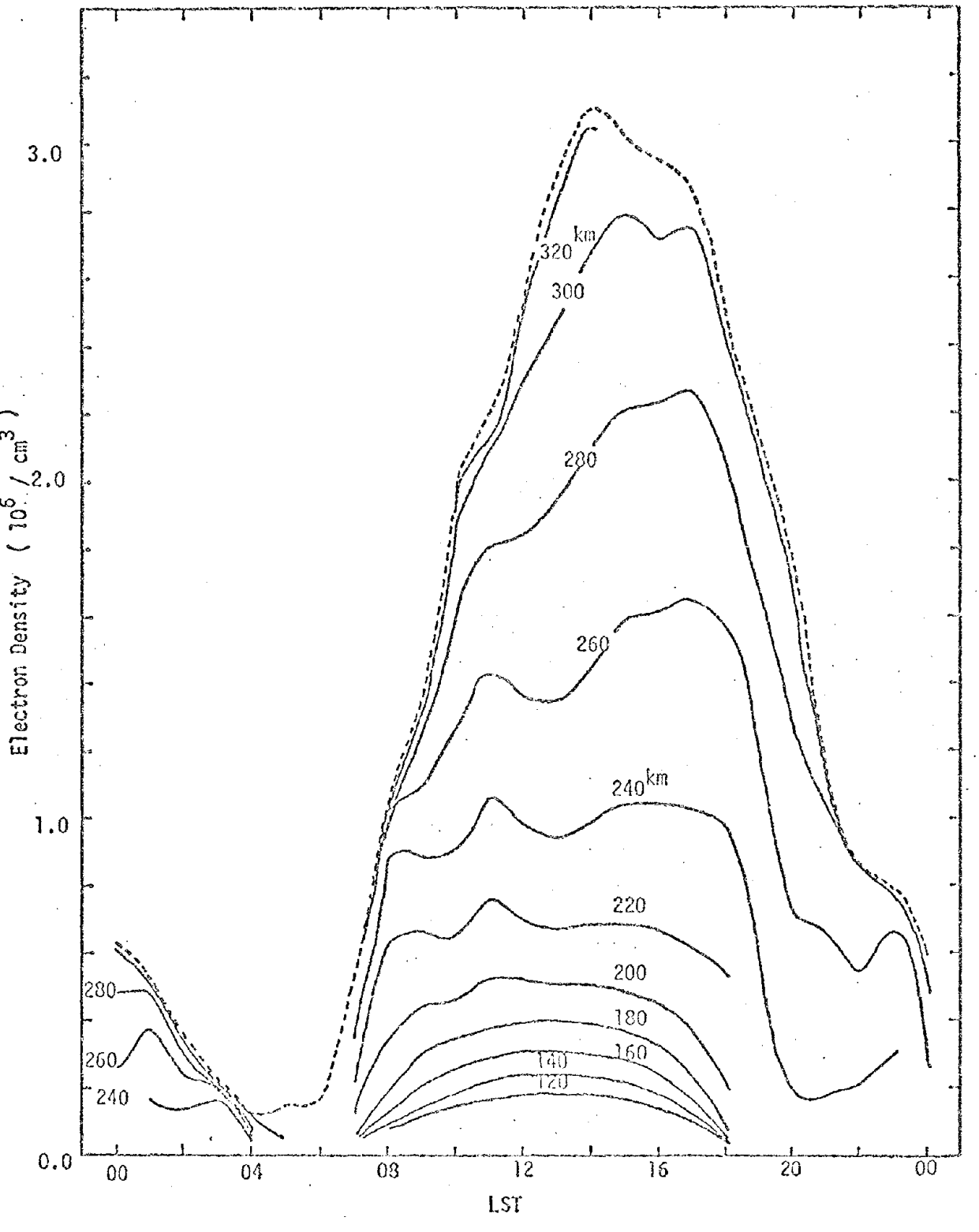

Figure 4.3 The diurnal variation of the electron density at various fixed altitude obtained for the magnetically quiet days of March 1968.

REFERENCES

Budden, K.G., 1955, A Method for Determining the Variation of the Electron Density with Height from Curves of Equivalent Height versus Frequency, Rept. Cambridge Conf. Iono. Phys., (Physical Society, London), 322.

Davies, K., 1969, Ionospheric Radio Waves, (Blaisdell Pub. Co.).

Ratcliffe, J.A., 1959, Magnetoionic Theory, (Cambridge University Press, Cambridge).

Thomas, J.O., 1957, The Distribution of Electrons in the Ionosphere, Proc. IRE, 47, 162.

Wright, J.W., 1960, A Model of the FOregion Above hmaxF_2, J. Geophys. Res., 65, 185

Wright, J.W., et al., 1957, Annuals of the IGY, Vol. III, Part I, (Pergamon Press, Oxford).

APPENDIX 4A

A COMPUTER PROGRAM FOR THE CALCULATION OF C_{NM}.

```
FORTRAN IV G LEVEL  20                  MAIN                    DATE = 73227

            C TO CALCULATE BUDDEN'S C(N,M)
0001            DIMENSION HEIT(170,170),TEMP(170),Y(5)
0002            O=ARSIN(1.0)
0003            DO 10 N=1,170
0004            TEMP(N)=0.0
0005            DO 10 M=1,170
0006         10 HEIT(N,M)=0.0
0007            DO 31 N=1,   25
0008            DO 31 M=1,N
0009            RM=M
0010            RN=N
0011            F=1.0+RN/10.0
0012            IF (M .EQ. N) GO TO 71
0013            DO 70 I=1,5
0014            FN=1.0+(RM-1.0)/10.0+0.025*(I-1)
0015            CALL UDASH(F,FN,U)
0016         70 Y(I)=U
0017            CALL INTEG(Y,0.025,5,A)
0018            HEIT(N,M)=A*10.0
0019            GO TO 31
0020         71 DO 72 I=1,4
0021            FN=1.0+(RM-1.0)/10.0+0.025*(I-1)
0022            CALL UDASH(F,FN,U)
0023         72 Y(I)=U
0024            CALL INTEG(Y,0.025,4,A)
0025            Y(5)=(O-ARSIN((RN-0.25)/RN))*RN
0026            HEIT(N,M)=A*10.0+Y(5)
0027         31 CONTINUE
0028            DO 12 N=2,   25
0029            NN=N-1
0030            DO 12 M=1,NN
0031         12 HEIT(N,M)=HEIT(N,M)-HEIT(N,M+1)
0032            HEIT(1,1)=1./HEIT(1,1)
0033            DO 60 N=2,   25
0034            TEMP(1)=1.0/HEIT(N,N)
0035            NM=N-1
0036            DO 61 M=1,NM
0037         61 TEMP(M+1)=-HEIT(N,N-M)*TEMP(1)
0038            DO 60 M=1,N
0039         60 HEIT(N,M)=TEMP(M)
0040            DO 15 N=1,   25
0041            RESID=0.0
0042            DO 14 K=1,N
0043         14 RESID=RESID+HEIT(N,K)
0044            RESID=1.0-RESID
0045            WRITE (6,20) RESID,(HEIT(N,M),M=1,N)
0046         15 WRITE (7,21) RESID,(HEIT(N,M),M=1,N)
0047         20 FORMAT(10X,10F10.5)
0048         21 FORMAT(11F7.5)
0049            STOP
0050            END
```

```
FORTRAN IV G LEVEL  20                    UDASH                DATE = 73227

0001                SUBROUTINE  UDASH(F,FN,U)
0002                DOUBLE PRECISION    YL,U,A,B,X,FN,YT
0003                X=(FN/F)**2
0004                FN=0.54967/ (3.1416 *2.0)
0005                YL=FN*COS(51.296*3.1416/180.0)/F
0006                YT=FN*SIN(51.296*3.1416/180.0)/F
0007                A=DSQRT(YT**4+4.0*(1.0-X)**2*YL**2)
0008                B=1.0-2.0*X*(1.0-X)/(2.0*(1.0-X)-YT**2*A)
0009                U=(B+(1.-B)**2*(1.0/X+YT**2/(2.0*(1-X)**2)+(2.0*
                   2  (1.0-X)**3*YL**2-X*YT**4)/(2.0*X*(1.0-X)**2*A)))/
                   3  DSQRT(B)
0010                RETURN
0011                END
```

```
FORTRAN IV G LEVEL  20                    INTEG                DATE = 73227

0001                SUBROUTINE INTEG(Y,H,N,A)
                   C THIS PROGRAM GIVES INTEGRATION VALUE A BY GIVING N Y'S
                   C WITH INTERVAL H BY TRAPEZOID RULE
0002                DIMENSION Y(1)
0003                A=Y(1)
0004                M=N-1
0005                DO 10 K=2,M
0006             10 A=A+2.0*Y(K)
0007                A=(A+Y(N))*H/2.0
0008                RETURN
0009                END
```

APPENDIX 4B

A COMPUTER PROGRAM FOR THE CALCULATION OF ELECTRON DENSITY PROFILE

In order to use this computer program, the following procedures should be followed to digitize the ionogram and prepare a set of data cards.

(i) First digitize the virtual height h'(f) of the given ionogram at every 0.1 MHz interval starting from 1.0 MHz and ending at foF2 - 0.1 MHz. In doing so, only ordinary trace of the ionogram must be used; missing parts of the trace must be interpolated; and the trace near the critical frequencies extrapolated. It should be remarked that E_s trace should not be used. Hewlett-Packard Calculator Digitizer Model 9107A was used to digitize these data. Each h_n' was digitized up to 1 km accuracy.

(ii) These h_n' data are key-punched with a FORMAT (20I4). For convenience of programming, the critical frequency foF2 in unit of 0.1 MHz is also key punched at the place next to the last h_n'. Regardless of how may h_n' data we have, some pieces of blank cards should be added so that the total number of data cards becomes nine.

(iii) Finally a data card, which gives the number of ionograms to be analyzed, must be prepared with FORMAT (I5).

(iv) The data set should be read in the following order:

(1) punched output of C_{nm}'s obtained by the computer program given in Appendix 4A,

(2) a card which gives the number of ionograms to be processed, and

(3) digitized h_n' data.

This program can:

(1) Print out the real heights z_0, z_1, z_2, ..., z_n and z_c

(2) Punch out the real heights z_0, z_1, z_2, ..., z_n and z_c with FORMAT (13 f6.1).

(3) Print out a table which shows the electron density in units of 10^3 electrons/cm^3 at every 10 km interval starting from 80 km to 1000 km, and peak electron density N_{ec}, peak height of the ionosphere z_c, minimum height of the ionosphere z_0, and quarter thickness of the

ionosphere q_c. For each ionogram, one column of data will be printed out to give the above mentioned quantities. If 24 monthly hourly mean ionograms are given, the computer will print out a monthly table in two pages. Table 4B-1 given at the end of this Appendix shows an example obtained for March 1968.

(4) Punch out electron density in units of 10^3 electrons/cm^3 at every 10 km interval starting from 80 km to 1000 km with FORMAT (13F6.1) for each given ionogram.

```
FORTRAN IV G LEVEL  20                    MAIN                DATE = 73227

            C THIS PROGRAM GIVES N(Z) PROFILE UP TO FC=18.1MHZ
            C N IN UNIT OF 10**3/CM**3
0001              DIMENSION C(171,170),H(172,24),Z(172),F(171),EM(24),
                 2  ZM(24),ZO(24),QC(24),X(3),Y(3)
0002              DO 10 N=1,170
0003              NN=N+1
0004             10 READ(5,25) (C(M,N), M=1,NN)
0005              READ(5,26) KK
            C KK= NO. OF N(Z) TO BE DETERMINED
0006              DO 9 K=1,KK
0007              9 READ(5,27)  ( H(N,K),N=1,)72)
            C PUT FC IN PLACE OF HC  AFTERWARDS PUT H=0.0
            C FOR EACH N(Z) PROFILE, 9 CARDS SHOULD BE PREPARED
0008              DO 14 K=1,KK
0009              I=1
0010             11 IF (H(I,K) .EQ. 0.0 ) GO TO 12
0011              I=I+1
0012              GO TO 11
0013             12 NN=I-2
            C NN+1= FC-10 IN UNIT OF 0.1 MHZ
0014              Z(1)  =H(1,K)
0015              Z(2)  =C(1,1)*H(1,K)+C(2,1)*H(2,K)
0016              DO 16 N=3,NN
0017              NNN=N-1
0018              T=0.0
0019              DO 15 M=2,NNN
0020             15 T=T+C(M+1,N-1)*Z(N-M+1)
0021             16 Z(N)=T+C(1,N-1)*H(1,K)+C(2,N-1)*H(N,K)
            C TO DETERMINE FC AND HC
0022              NC=NN+1
0023              FC=H(NC,K)/10.0
0024              TEMP=SQRT(0.2*(2.0*FC-0.2))
0025              TEMP=((TEMP-SQRT(0.1*(2.0*FC-0.1)))/FC)*2.0
0026              QC(K)=Z(NN)/TEMP-Z(NN-1)/TEMP
0027              ZC=Z(NN)+2.0*QC(K)*SQRT(0.1*(2.0*FC-0.1))/FC
0028              Z(NC)=ZC
0029              WRITE(6,92) (Z(N),N=1,NC)
0030              WRITE(7,29) (Z(N),N=1,NC)
0031              DO 60 J=1,171
0032              IF (Z(J+1) .GT. Z(J) ) GO TO 61
0033             60 CONTINUE
0034             61 IT=ZC
0035              MAXZ=(IT/10)
0036              IMIN=Z(NN)
0037              IMIN=(IMIN/10)+1
0038              MM=MAXZ-IMIN+1
0039              LL=NN+MM
0040              LN=LL+1
```

```
FORTRAN IV G LEVEL  20                    MAIN                    DATE = 73227

0041                JN=LL-J+1
0042                JM=JN+1
0043                IF ( MM .LT. 0 ) GO TO 39
0044                DO 40 L=1,MM
0045                ZI=(IMIN+L-1)*10
0046                Z(NN+L)=ZI
0047             40 F(JN-MM+L)=FC*SQRT(1.0-((ZI-ZC)/(2.0*QC(K)))**2)
0048                GO TO 38
0049             39 MM=0
0050                LL=NN+1
0051                JN=LL-J
0052                JM=JN+1
0053                IMIN=MAXZ
0054             38 Z(LN)=ZC
0055                JNN=JN-MM
0056                DO 17 I=1,JNN
0057             17 F(I)=1.0+(I+J-2)*0.1
0058                DO 49 I=1,JM
0059             49 Z(I)=Z(I+J-1)
0060                F(JM)=FC
0061                IT=Z(1)+0.05
0062                MINZ=(IT/10)+1
0063                NO=IMIN-MINZ
0064                ZO(K)=H(1,K)
0065                DO 18 I=1,172
0066             18 H(I,K)=0.0
0067                DO 19 I=1,NO
0068                IZ=MINZ+I-8
0069                XI=(MINZ+I-1)*10
0070                DO 43 N=1,JN
0071                IF (Z(N) .GT. XI ) GO TO 44
0072             43 CONTINUE
0073                GO TO 46
0074             44 DO 45 M=1,3
0075                X(M)=Z(N+M-2)
0076             45 Y(M)=F(N+M-2)
0077                CALL ILAG(X,Y,3,XI,YI)
0078             19 H(IZ,K)=1.24E4*YI**2/1000.0
0079                IF (MM .LT. 0 ) GO TO 48
0080             46 DO 47 I=1,MM
0081             47 H(IZ+I,K)=1.24E4*F( JN -MM+I)**2/1000.0
                 C TO DETERMINE N(Z) ABOVE ZC
0082             48 II=100-MAXZ
0083                DO 20 I=1,II
0084                ZZ=(MAXZ+I)*10
0085                ZZ=(ZZ-ZC)/100.0
0086                FM=1.24E4*FC**2
0087             20 H(MAXZ+I-7,K)=FM*EXP((1.0-ZZ-EXP(-ZZ))/2.0)/1000.0
```

```
FORTRAN IV G LEVEL  20                    MAIN                    DATE = 73227

0088                EM(K)=FM/1000.0
0089             14 ZM(K)=ZC
0090                IF (KK .GT. 12 ) GO TO 22
0091                WRITE(6,90)
0092                DO 21 I=1,93
0093                IH=(101-I)*10
0094             21 WRITE(6,26) IH,(H(94-I,K),K=1,KK)
0095                WRITE(6,28) (EM(I),I=1,KK)
0096                WRITE(6,28) (ZM(I),I=1,KK)
0097                WRITE(6,28) (ZO(I),I=1,KK)
0098                WRITE(6,28) (QC(I),I=1,KK)
0099                GO TO 31
0100             22 WRITE(6,90)
0101                DO 23 I=1,93
0102                IH=(101-I)*10
0103             23 WRITE(6,26) IH,(H(94-I,K),K=1,12)
0104                WRITE(6,28) (EM(I),I=1,12)
0105                WRITE(6,28) (ZM(I),I=1,12)
0106                WRITE(6,28) (ZO(I),I=1,12)
0107                WRITE(6,28) (QC(I),I=1,KK)
0108                KT=KK-12
0109                WRITE(6,91)
0110                DO 24 I=1,93
0111                IH=(101-I)*10
0112             24 WRITE(6,26) IH,(H(94-I,K+12),K=1,KT)
0113                WRITE(6,28) (EM(I+12),I=1,KT)
0114                WRITE(6,28) (ZM(I+12),I=1,KT)
0115                WRITE(6,28) (ZO(I+12),I=1,KT)
0116                WRITE(6,28) (QC(I+12),I=1,KT)
0117             31 DO 32 K=1,KK
0118             32 WRITE(7,29) (H(I,K),I=1,93)
0119             25 FORMAT(11F7.5)
0120             26 FORMAT(I5,12F7.1)
0121             27 FORMAT(20F4.0)
0122             28 FORMAT(5X,12F7.1)
0123             29 FORMAT(13F6.1)
0124             90 FORMAT(1H1,3X,'      00      01      02      03      04
                   1   07      08      09      10      11')
0125             91 FORMAT(1H1,3X,'      12      13      14      15      16
                   1   19      20      21      22      23')
0126             92 FORMAT(5X,10F7.1)
0127                STOP
0128                END
```

```
FORTRAN IV G LEVEL  20                    ILAG                    DATE = 73227

0001                SUBROUTINE ILAG(X,Y,N,XI,YI)
                 C LAGRANGE INTERPOLATION POLYNOMIAL
                 C  N= NO. OF DATA POINTS
                 C  Y=F(X)
                 C  YI=F(XI)
0002                DIMENSION X(N),Y(N)
0003                YI=0.0
0004                DO 25 K=1,N
0005                B=1.0
0006                DO 20 J=1,N
0007                IF (J-K) 15,20,15
0008             15 B=B*((XI-X(J))/(X(K)-X(J)))
0009             20 CONTINUE
0010             25 YI=YI+B*Y(K)
0011                RETURN
0012                END
```

TABLE 4B-1 Monthly Table of the Monthly Mean Hourly Electron Density Profile for Geomagnetically Quiet Days in March 1968.

Z \ t	00	01	02	03	04	05	06	07	08	09	10	11
1000	32.7	29.5	24.1	9.9	7.6	13.1	15.7	26.0	44.5	68.5	113.4	119.5
990	34.4	27.9	22.1	10.4	8.0	13.8	16.5	27.4	46.7	72.0	119.2	125.6
980	36.2	29.3	23.3	10.9	8.4	14.5	17.3	28.8	49.1	75.7	125.3	132.0
970	38.0	30.8	24.5	11.4	8.8	15.2	18.2	30.3	51.7	79.6	131.7	138.8
960	40.0	32.4	25.7	12.0	9.3	16.0	19.2	31.8	54.3	83.6	138.4	145.9
950	42.0	34.1	27.0	12.6	9.8	16.8	20.1	33.4	57.1	87.9	145.5	153.3
940	44.2	35.8	28.4	13.3	10.3	17.7	21.2	35.2	60.0	92.4	153.0	161.2
930	45.4	37.6	29.9	14.0	10.8	18.6	22.2	36.9	63.1	97.2	160.8	169.4
920	48.8	39.6	31.4	14.7	11.4	19.5	23.4	38.8	66.3	102.1	169.0	178.1
910	51.3	41.6	33.0	15.4	11.9	20.5	24.6	40.8	69.7	107.3	177.6	187.2
900	53.9	43.7	34.7	16.2	12.5	21.6	25.8	42.9	73.3	112.8	186.7	196.8
890	56.7	46.0	36.4	17.1	13.2	22.7	27.1	45.1	77.0	118.6	196.3	206.8
880	59.6	48.3	38.3	17.9	13.9	23.8	28.5	47.4	81.0	124.7	206.3	217.4
870	62.6	50.8	40.3	18.8	14.6	25.0	29.9	49.8	85.1	131.0	216.8	228.5
860	65.8	53.4	42.3	19.8	15.3	26.3	31.4	52.4	89.5	137.7	227.9	240.2
850	69.2	56.1	44.5	20.8	16.1	27.6	33.0	55.1	94.0	144.8	239.5	252.4
840	72.7	59.0	46.7	21.9	16.9	29.0	34.7	57.9	98.8	152.1	251.7	265.3
830	76.4	62.0	49.1	23.0	17.8	30.5	36.4	60.8	103.9	159.9	264.5	278.8
820	80.3	65.1	51.6	24.2	18.7	32.0	38.2	63.9	109.2	168.1	278.0	293.0
810	84.4	68.4	54.3	25.4	19.6	33.6	40.2	67.2	114.8	176.6	292.2	307.9
800	88.7	71.9	57.0	26.7	20.6	35.3	42.2	70.6	120.6	185.6	307.0	323.6
790	93.2	75.6	59.9	28.1	21.6	37.1	44.2	74.2	126.8	195.1	322.6	340.1
780	97.9	79.4	63.0	29.5	22.7	38.9	46.4	78.0	133.2	205.0	339.0	357.3
770	102.9	83.5	66.1	31.0	23.9	40.9	48.7	82.0	140.0	215.4	356.1	375.4
760	108.1	87.7	69.5	32.6	25.1	42.9	51.1	86.1	147.2	226.3	374.2	394.5
750	113.6	92.1	73.0	34.2	26.4	45.0	53.6	90.5	154.6	237.8	393.1	414.6
740	119.3	96.8	76.7	36.0	27.7	47.2	56.2	95.1	162.5	249.8	412.9	435.4
730	125.3	101.7	80.6	37.8	29.1	49.5	58.9	99.9	170.8	262.5	433.7	457.3
720	131.7	106.8	84.6	39.7	30.5	51.9	61.8	104.9	179.4	275.7	455.5	480.4
710	138.3	112.2	88.9	41.7	32.1	54.5	64.7	110.2	188.5	289.6	478.4	504.5
700	145.3	117.9	93.3	43.8	33.6	57.1	67.8	115.8	198.0	304.2	502.4	529.9
690	152.5	123.8	98.0	46.1	35.3	59.8	71.0	121.6	208.1	319.4	527.5	556.4
680	160.2	130.0	102.9	48.4	37.1	62.6	74.3	127.7	218.6	335.4	553.8	584.2
670	168.2	136.5	108.0	50.8	38.9	65.6	77.7	134.1	229.6	352.2	581.3	613.2
660	176.5	143.3	113.3	53.4	40.8	68.7	81.2	140.8	241.1	369.8	610.0	643.7
650	185.3	150.4	118.9	56.1	42.8	71.8	84.8	147.9	253.2	388.1	640.1	675.5
640	194.4	157.9	124.8	58.9	44.9	75.1	88.6	155.2	265.9	407.3	671.5	708.8
630	204.0	165.7	130.9	61.8	47.0	78.5	92.4	162.9	279.2	427.4	704.4	743.6
620	214.0	173.8	137.2	64.9	49.3	82.0	96.3	170.9	293.1	448.4	738.6	779.9
610	224.5	182.3	143.9	68.1	51.6	85.6	100.3	179.3	307.6	470.4	774.3	817.8
600	235.3	191.2	150.8	71.4	54.0	89.2	104.4	188.1	322.8	493.2	811.5	857.3
590	246.7	200.4	158.0	75.0	56.6	93.0	108.5	197.3	338.7	517.1	850.2	898.4
580	258.5	210.1	165.5	78.6	59.2	96.8	112.8	206.8	355.3	542.0	890.5	941.2
570	270.8	220.1	173.3	82.5	61.9	100.6	116.8	216.8	372.7	567.8	932.3	985.7
560	283.6	230.6	181.3	86.5	64.7	104.5	120.9	227.1	390.8	594.7	975.6	1031.8
550	296.8	241.4	189.7	90.6	67.6	108.5	125.0	237.9	409.7	622.7	1020.4	1079.7
540	310.6	252.7	198.3	95.0	70.5	112.4	129.0	249.1	429.3	651.6	1066.7	1129.2
530	324.8	264.3	207.2	99.5	73.6	116.2	132.8	260.7	449.8	681.6	1114.5	1180.3
520	339.4	276.3	216.4	104.2	76.7	120.0	136.5	272.7	471.1	712.6	1163.7	1233.0
510	354.5	288.8	225.8	109.1	79.8	123.7	139.9	285.1	493.1	744.5	1214.1	1287.2
500	370.1	301.6	235.5	114.1	83.0	127.2	143.0	297.9	516.0	777.4	1265.7	1342.8
490	386.0	314.7	245.3	119.3	86.3	130.6	145.8	311.1	539.7	811.2	1318.4	1399.6
480	402.3	328.1	255.3	124.7	89.5	133.7	148.1	324.7	564.1	845.7	1371.9	1457.6
470	418.8	341.9	265.5	130.3	92.8	136.4	150.0	338.5	589.3	881.0	1426.1	1516.5
460	435.7	355.8	275.7	136.0	96.0	138.8	151.2	352.7	615.2	916.8	1480.6	1576.0
450	452.7	370.0	285.9	141.8	99.2	140.8	151.9	367.1	641.8	953.1	1535.2	1635.8
440	469.7	384.3	296.1	147.6	102.3	142.3	151.3	381.7	669.0	989.7	1589.6	1695.7
430	486.8	398.6	306.2	153.9	105.2	143.1	148.3	396.4	696.7	1026.3	1643.2	1755.2
420	503.7	412.8	316.1	160.0	108.0	143.3	142.6	411.2	724.9	1062.8	1695.6	1813.7
410	520.3	426.9	325.7	166.3	110.6	141.3	134.3	425.9	753.3	1098.8	1746.3	1870.9
400	536.5	440.7	334.8	172.5	113.0	136.5	123.8	440.4	782.0	1134.0	1794.6	1926.0
390	552.0	454.1	343.4	178.8	115.1	128.8	113.1	454.6	810.6	1168.1	1839.8	1978.4
380	566.8	467.0	351.4	185.0	116.8	118.2	101.5	468.5	839.1	1200.6	1881.2	2027.2
370	580.9	479.0	358.4	191.1	118.1	109.2	89.4	481.7	867.1	1231.2	1917.9	2071.7
360	592.8	490.2	364.5	197.0	118.9	98.2	76.5	494.1	894.5	1259.2	1949.1	2110.8
350	603.6	500.1	369.4	202.7	119.2	87.2	63.1	505.5	920.9	1284.1	1973.7	2143.6
340	612.6	508.7	372.9	208.1	118.3	74.7	48.8	515.8	946.0	1305.4	1990.7	2169.0
330	619.3	515.6	374.8	213.1	115.7	61.8	0.0	524.6	969.4	1322.3	1999.2	2185.9
320	623.6	520.6	374.5	217.6	111.4	46.6	0.0	531.6	990.7	1334.2	1993.4	2193.2
310	625.1	523.4	368.1	221.5	105.4	27.3	0.0	536.8	1009.5	1340.4	1953.6	2169.7
300	606.3	523.0	354.5	224.8	97.3	0.0	0.0	539.6	1025.3	1337.3	1877.5	2080.9
290	558.6	510.6	334.9	227.2	88.1	0.0	0.0	539.0	1037.6	1307.7	1760.6	1962.3
280	480.5	483.1	309.4	228.8	78.0	0.0	0.0	524.0	1045.8	1249.9	1623.7	1808.6
270	376.1	437.5	279.7	229.3	67.4	0.0	0.0	492.3	1049.4	1175.5	1452.9	1620.1
260	256.0	370.9	234.5	223.6	56.5	0.0	0.0	452.4	1036.1	1090.8	1265.2	1429.7
250	137.7	285.2	181.9	207.7	45.3	0.0	0.0	405.0	979.9	996.8	1079.8	1239.2
240	0.0	159.9	128.9	165.9	29.3	0.0	0.0	352.7	890.2	892.0	908.6	1064.6
230	0.0	42.9	77.5	96.4	0.0	0.0	0.0	295.3	775.2	781.6	760.9	904.5
220	0.0	0.0	38.8	0.0	0.0	0.0	0.0	226.8	636.5	663.1	637.2	754.4
210	0.0	0.0	0.0	0.0	0.0	0.0	0.0	161.6	489.7	547.6	535.6	627.7
200	0.0	0.0	0.0	0.0	0.0	0.0	0.0	114.1	359.4	447.5	459.2	520.3
190	0.0	0.0	0.0	0.0	0.0	0.0	0.0	81.3	263.3	370.2	394.8	432.7
180	0.0	0.0	0.0	0.0	0.0	0.0	0.0	61.6	197.9	306.7	341.3	368.6
170	0.0	0.0	0.0	0.0	0.0	0.0	0.0	52.1	161.8	252.9	296.3	324.1
160	0.0	0.0	0.0	0.0	0.0	0.0	0.0	49.5	120.7	209.3	254.8	286.2
150	0.0	0.0	0.0	0.0	0.0	0.0	0.0	46.7	101.1	170.0	217.2	251.8
140	0.0	0.0	0.0	0.0	0.0	0.0	0.0	44.4	92.9	140.1	181.4	216.9
130	0.0	0.0	0.0	0.0	0.0	0.0	0.0	35.0	89.3	128.6	157.5	182.6
120	0.0	0.0	0.0	0.0	0.0	0.0	0.0	0.0	82.2	122.0	148.8	169.9
110	0.0	0.0	0.0	0.0	0.0	0.0	0.0	0.0	0.0	97.8	120.9	138.8
100	0.0	0.0	0.0	0.0	0.0	0.0	0.0	0.0	0.0	0.0	0.0	0.0
90	0.0	0.0	0.0	0.0	0.0	0.0	0.0	0.0	0.0	0.0	0.0	0.0
80	0.0	0.0	0.0	0.0	0.0	0.0	0.0	0.0	0.0	0.0	0.0	0.0
TMUF	625.1	523.4	375.1	229.3	119.2	143.3	151.9	540.1	1049.5	1341.2	2000.0	2193.4
2C	310.1	301.5	124.1	270.5	350.1	422.0	446.5	293.7	247.8	305.2	375.1	318.1
2D	240.0	227.0	215.0	224.0	236.0	309.0	331.0	176.0	111.0	107.0	107.0	107.0
QC	29.2	42.5	51.4	33.6	59.0	50.4	53.6	39.7	34.5	48.1	52.8	36.8

Z \ L	12	13	14	15	16	17	18	19	20	21	22	23
1000	136.8	147.6	177.0	164.5	160.3	150.9	128.9	115.5	100.2	55.5	40.7	36.4
990	145.3	156.2	186.0	174.9	170.5	159.6	135.5	121.4	105.4	58.3	42.8	38.1
980	153.4	165.2	196.5	184.8	177.2	166.8	142.5	127.6	110.8	61.3	45.0	40.7
970	161.2	174.7	205.6	194.1	186.2	175.3	149.8	134.1	116.4	64.5	47.3	42.8
960	169.5	184.7	218.1	206.9	195.8	184.3	157.4	141.0	122.4	67.8	49.7	45.0
950	178.2	195.2	227.1	211.2	205.8	193.7	165.5	148.2	128.6	71.2	52.2	47.3
940	187.3	206.2	238.8	222.0	216.3	203.6	174.0	155.8	135.2	74.9	54.9	49.7
930	196.9	217.7	251.0	233.3	227.4	214.0	182.9	163.8	142.1	78.7	57.7	52.2
920	206.9	229.9	263.8	245.3	239.0	225.0	192.2	172.1	149.4	82.7	60.7	54.9
910	217.5	242.7	277.3	257.8	251.3	236.5	202.0	180.9	157.1	87.0	63.8	57.7
900	228.6	256.1	291.5	271.0	264.1	248.6	212.4	190.2	165.1	91.4	67.0	60.7
890	240.3	270.2	306.4	284.8	277.6	261.3	223.2	199.9	173.5	96.1	70.5	63.8
880	252.6	285.0	322.0	299.4	291.8	274.6	234.6	210.1	182.4	101.0	74.1	67.0
870	265.5	300.6	338.4	314.7	306.7	288.7	246.6	220.9	191.7	106.2	77.9	70.5
860	279.0	316.9	355.7	330.7	322.3	303.4	259.2	232.1	201.5	111.6	81.8	74.1
850	293.3	334.1	373.8	347.6	338.8	318.9	272.5	244.0	211.8	117.3	86.0	77.9
840	308.2	352.2	392.9	365.3	356.1	335.2	286.4	256.4	222.6	123.3	90.4	81.9
830	323.9	371.1	412.9	384.0	374.2	352.3	301.0	269.5	233.9	129.6	95.0	86.0
820	340.4	411.0	433.9	403.5	393.3	370.2	316.3	283.2	245.8	136.2	99.9	90.6
810	357.8	431.9	456.0	424.1	413.3	389.1	332.4	297.7	258.3	143.1	105.0	95.0
800	375.9	453.9	479.2	445.6	434.3	408.9	349.3	312.8	271.5	150.4	110.3	99.9
790	395.0	476.9	503.5	468.3	456.4	429.7	367.1	328.7	285.3	158.1	115.9	105.0
780	415.1	501.1	529.1	492.1	479.6	451.5	385.8	345.4	299.7	166.1	121.9	110.3
770	436.1	526.5	555.9	517.0	503.9	474.4	405.3	362.9	314.9	174.6	128.0	115.9
760	458.2	553.1	584.0	543.2	529.4	498.5	425.9	381.3	330.9	183.4	134.6	121.8
750	481.4	581.1	613.5	570.7	556.2	523.7	447.5	400.6	347.6	192.7	141.4	128.0
740	505.7	610.4	644.5	599.5	584.3	550.2	470.1	420.9	365.2	202.5	148.6	134.5
730	531.2	641.1	676.9	629.8	613.8	578.0	493.9	442.2	383.6	212.8	156.1	141.3
720	558.0	673.3	711.0	661.5	644.7	607.1	518.8	464.4	402.9	223.5	164.0	148.5
710	586.0	707.1	746.7	694.8	677.1	637.7	544.9	487.8	423.2	234.8	172.3	156.0
700	615.4	742.5	784.0	729.6	711.1	669.7	572.3	512.3	444.4	246.6	181.0	163.9
690	646.2	779.6	823.2	766.2	746.7	703.3	601.0	538.0	466.6	259.0	190.1	172.1
680	678.4	818.4	864.2	804.4	784.0	738.5	631.1	564.9	489.9	272.0	199.7	180.8
670	712.1	858.9	907.1	844.5	823.0	775.3	662.5	593.0	514.3	285.7	209.7	189.9
660	747.4	901.4	951.9	886.4	863.9	813.9	695.5	622.5	539.8	299.9	220.2	199.4
650	784.3	945.8	998.9	930.2	906.6	854.3	730.0	653.3	566.5	314.9	231.2	209.4
640	822.9	992.2	1047.9	976.0	951.3	896.5	766.1	685.6	594.3	330.5	242.7	219.8
630	863.2	1040.6	1099.0	1023.9	997.9	940.6	803.8	719.3	623.5	346.9	254.7	230.8
620	905.3	1091.1	1152.4	1073.9	1046.6	986.7	843.2	754.4	653.9	364.0	267.4	242.2
610	949.2	1143.7	1208.1	1126.1	1097.5	1034.8	884.4	791.2	685.6	381.9	280.5	254.2
600	994.9	1198.5	1266.1	1180.4	1150.5	1084.9	927.3	829.5	718.6	400.6	294.3	266.7
590	1042.5	1255.5	1326.4	1237.1	1205.7	1137.2	972.0	869.4	753.0	420.1	308.7	279.7
580	1092.0	1314.8	1389.1	1296.0	1263.2	1191.7	1018.6	910.9	788.8	440.4	323.7	293.4
570	1143.5	1376.2	1454.2	1357.2	1323.0	1248.3	1067.0	954.1	826.0	461.6	339.4	307.6
560	1196.8	1439.9	1521.6	1420.8	1385.1	1307.1	1117.4	998.9	864.6	483.6	355.7	322.4
550	1252.1	1505.8	1591.4	1486.6	1449.5	1368.1	1169.6	1045.4	904.6	506.5	372.6	337.9
540	1309.2	1573.8	1663.5	1554.8	1516.2	1431.3	1223.7	1093.5	945.9	530.3	390.2	353.9
530	1368.2	1643.9	1737.8	1625.2	1585.2	1496.7	1279.7	1143.3	988.6	555.0	408.5	370.6
520	1428.9	1716.0	1814.2	1697.7	1656.4	1564.1	1337.5	1194.6	1032.5	580.5	427.5	387.9
510	1491.3	1789.8	1892.6	1772.3	1729.8	1633.6	1397.1	1247.5	1077.7	606.9	447.2	405.9
500	1555.3	1865.4	1972.8	1848.8	1805.0	1705.0	1458.3	1301.7	1124.0	634.1	467.5	424.4
490	1620.6	1942.3	2054.6	1927.1	1881.1	1778.2	1521.0	1357.3	1171.4	662.1	488.4	443.5
480	1687.1	2020.3	2137.6	2006.9	1958.9	1853.0	1585.2	1414.0	1219.6	690.9	509.9	463.3
470	1754.5	2099.2	2221.6	2087.9	2038.8	1929.1	1650.5	1471.6	1268.4	720.3	532.0	483.5
460	1822.5	2178.5	2306.0	2169.7	2119.6	2006.3	1716.9	1530.0	1317.8	750.3	554.6	504.3
450	1890.8	2257.6	2390.5	2252.1	2199.9	2084.2	1783.8	1588.9	1367.4	780.9	577.6	525.5
440	1959.0	2336.2	2474.5	2334.5	2279.1	2162.5	1851.1	1647.9	1416.9	811.8	601.1	547.1
430	2026.4	2413.4	2557.2	2416.2	2359.8	2240.6	1919.4	1706.7	1465.9	842.9	624.8	569.0
420	2092.7	2488.7	2637.9	2496.8	2438.3	2317.9	1985.1	1764.8	1514.1	874.1	648.6	591.1
410	2157.0	2561.0	2715.8	2575.4	2509.9	2393.9	2050.7	1821.7	1561.0	905.2	672.5	613.4
400	2218.7	2629.6	2788.8	2651.1	2583.7	2467.6	2114.5	1876.6	1606.1	935.9	696.3	635.5
390	2277.0	2693.3	2858.9	2723.1	2653.8	2538.7	2175.9	1929.5	1648.7	965.9	719.7	657.5
380	2330.9	2751.0	2921.9	2790.2	2719.2	2605.6	2234.1	1979.0	1688.2	995.0	742.6	679.1
370	2379.4	2801.5	2977.3	2851.2	2778.7	2667.7	2288.2	2024.6	1723.9	1022.7	764.8	700.1
360	2421.3	2843.9	3023.9	2904.9	2831.0	2723.6	2337.1	2065.2	1755.0	1048.8	785.8	720.3
350	2455.7	2875.1	3060.2	2949.9	2874.8	2772.1	2379.8	2100.0	1780.6	1072.7	805.6	739.3
340	2481.1	2895.4	3084.4	2984.6	2908.6	2811.9	2415.3	2127.9	1799.8	1093.9	823.6	757.0
330	2496.3	2902.7	3095.2	3007.7	2931.1	2841.6	2442.1	2147.9	1811.7	1112.1	839.6	772.9
320	2498.5	2899.1	3094.9	3017.4	2940.6	2859.7	2459.2	2158.8	1815.2	1126.5	853.1	786.8
310	2488.7	2885.6	3081.1	2972.7	2958.2	2863.2	2465.2	2150.1	1764.6	1136.7	863.8	798.2
300	2279.4	2453.3	2668.5	2789.7	2721.2	2749.3	2415.9	2055.7	1637.9	1142.1	871.1	806.7
290	2065.9	2229.7	2399.7	2507.3	2469.0	2522.5	2270.2	1902.8	1476.8	1131.7	874.7	812.0
280	1834.8	1936.2	2086.9	2210.4	2231.7	2262.5	2059.5	1690.7	1270.2	1041.7	859.1	813.2
270	1591.7	1623.3	1768.6	1902.4	1938.5	1954.2	1819.6	1450.3	1035.1	882.5	768.7	775.7
260	1352.0	1347.0	1455.5	1558.6	1617.7	1635.6	1549.3	1145.5	714.3	665.5	541.1	676.5
250	1138.7	1113.8	1192.8	1294.5	1369.6	1385.6	1264.0	831.5	385.8	392.1	284.1	498.9
240	961.3	930.7	987.3	1086.3	1038.7	1027.3	906.4	504.0	179.0	183.8	109.7	301.0
230	813.3	786.0	818.8	834.1	827.3	793.8	739.0	144.2	30.5	45.6	0.0	94.6
220	690.9	673.6	689.7	678.9	667.2	597.9	527.3	0.0	0.0	0.0	0.0	0.0
210	589.3	584.8	592.6	565.9	551.3	449.2	340.9	0.0	0.0	0.0	0.0	0.0
200	507.6	506.9	516.6	478.4	457.5	349.3	193.5	0.0	0.0	0.0	0.0	0.0
190	441.5	441.1	452.7	412.9	382.8	275.9	118.2	0.0	0.0	0.0	0.0	0.0
180	381.0	387.1	392.7	353.2	321.9	220.5	82.9	0.0	0.0	0.0	0.0	0.0
170	350.5	343.5	342.6	313.6	271.9	175.6	66.5	0.0	0.0	0.0	0.0	0.0
160	314.1	305.4	303.1	275.9	231.2	142.0	57.5	0.0	0.0	0.0	0.0	0.0
150	276.2	271.0	268.7	242.7	195.8	115.5	54.0	0.0	0.0	0.0	0.0	0.0
140	238.7	234.6	234.4	212.8	164.5	93.4	53.6	0.0	0.0	0.0	0.0	0.0
130	203.4	198.9	202.1	185.9	144.3	92.8	47.7	0.0	0.0	0.0	0.0	0.0
120	172.5	169.9	182.4	166.6	135.4	59.7	37.1	0.0	0.0	0.0	0.0	0.0
110	166.2	156.8	161.2	156.5	127.0	89.3	0.0	0.0	0.0	0.0	0.0	0.0
100	0.0	0.0	0.0	0.0	0.0	0.0	0.0	0.0	0.0	0.0	0.0	0.0
90	0.0	0.0	0.0	0.0	0.0	0.0	0.0	0.0	0.0	0.0	0.0	0.0
80	0.0	0.0	0.0	0.0	0.0	0.0	0.0	0.0	0.0	0.0	0.0	0.0
Rec	2300.3	2982.7	3095.5	3017.7	2940.8	2864.9	2485.2	2140.6	1819.5	1142.8	874.9	813.6
ZC	361.9	329.8	327.8	313.3	318.3	311.4	309.9	314.3	320.8	295.1	286.4	281.0
ZO	102.0	105.0	104.0	105.0	104.0	107.0	115.0	227.0	229.0	227.0	235.0	228.0
QC	35.1	30.7	30.4	33.8	30.9	28.0	35.2	30.7	12.2	25.8	23.9	25.6

APPENDIX 5

RAY TRACING IN THE IONOSPHERE

5.1 Introduction

In order to obtain the Doppler frequency shift Δf, we must first establish the ray path of the radio wave propagating in the ionosphere. A procedure for finding the ray path is called ray tracing. A set of rules which governs the behavior of the wave normal and the ray direction in a uniform magnetoionic medium and enables one to trace a ray path in the ionosphere was summarized by Bremmer (1949). Lawrence and Posakony (1962) worked out a computer program by applying these rules and using an iteration method to avoid the difficulty of calculating the refractive index μ in the next layer, where the wave is going to be refracted, without precisely knowing the direction of the wave normal there.

Based on the principles of Hamilton optics, Hazelgrove (1954) developed a ray tracing method by solving a set of six simultaneous differential equations in terms of the three position coordinates, three variables indicating the direction of wave normal, the phase refractive index, and the partial derivatives of μ with respect to the six variables. Jones (1969) developed a three dimensional ray tracing computer program based on numerical integration of Hazelgrove's equations. Although Hazelgrove's method is suitable for numerical calculation, it does not lend itself easily to physical interpretation (Davies, 1969).

Booker (1939, 1949) has introduced a quantity q as the vertical component of a vector with magnitude equal to the refractive index μ and directed along the wave normal. If we let θ be the angle between

the wave normal and the vertical, then q can be expressed by

$$q = \mu \cos\theta \tag{5.1}$$

By Snell's law, the base of the triangle is always equal to $\sin\theta_I$ as shown in Figure 5.1. Booker's method of ray tracing involves the solution of a quartic in q. By integrating partial derivative of q with respect to height, the ray path can be established.

Besides the above methods, Titheridge's approximate method (1959) and Poeverlein's graphical method (1949) are sometimes used. Although Booker's method is very elegant for ray tracing, no one has reported having developed a computer program based on it. The purpose of the present chapter is to develop a two dimensional ray tracing computer program using Booker's method. This program is essential for the theoretical calculation of Doppler frequency shift.

5.2 Derivation of Booker's quartic

Assume that the ionosphere is constructed by a number of thin discrete layers in each of which the medium is homogeneous. Let a plane wave be indicent on the ionosphere from below and let its wave normal have direction cosines (S_1, S_2, C) so that it makes an angle θ_I with the vertical as shown in Figure 5.2. Then,

$$\begin{aligned} \cos\theta_I &= C \\ \sin^2\theta_I &= S_1^2 + S_2^2 \end{aligned} \tag{5.2}$$

and each field component contains a factor

$$\exp\{-ik(S_1x + S_2y + Cz)\} \tag{5.3}$$

In the n^{th} layer, each field component will contain a factor

$$\exp\{-k(S_1x + S_2y + \mu_n\cos\theta_n z)\} \tag{5.4}$$

and by Snell's law

$$\mu_n\sin\theta_n = \sin\theta_I = \sqrt{S_1^2 + S_2^2} \tag{5.5}$$

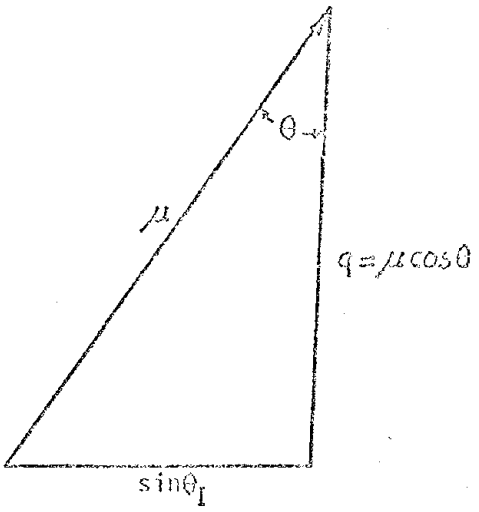

Figure 5.1 A figure showing the relationships among q, μ and θ.

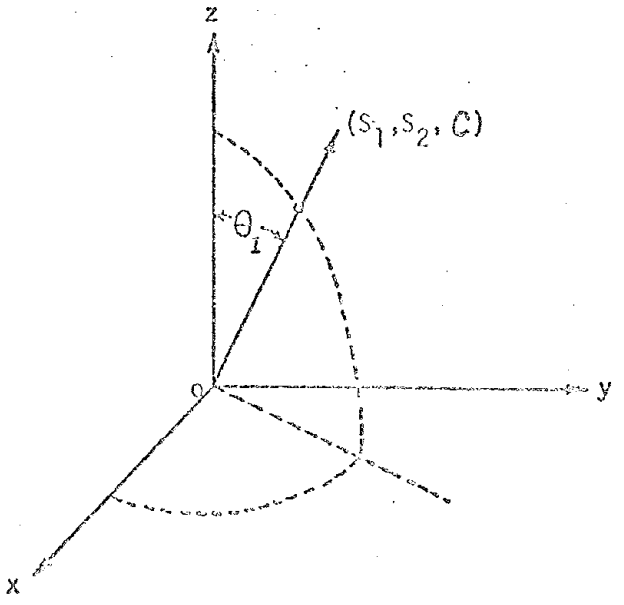

Figure 5.2 A figure showing the direction cosines of a wave normal.

By the definition of q,

$$q = \mu_n \cos\theta_n \tag{5.6}$$

whence with (5.5), we have

$$\mu_n^2 = q^2 + S_1^2 + S_2^2 \tag{5.7}$$

and (5.4) becomes

$$\exp\{-ik(S_1 x + S_2 y + qz)\} \tag{5.8}$$

The direction cosines of the wave normal are from (5.8)

$$S_1/\sqrt{S_1^2 + S_1^2 + q^2}\ ,\quad S_2/\sqrt{S_1^2 + S_2^2 + q^2}\ ,\quad q/\sqrt{S_1^2 + S_2^2 + q^2}\ , \tag{5.9}$$

and

$$\mu_n = \frac{q}{\cos\theta_n} = \sqrt{S_1^2 + S_2^2 + q^2} \tag{5.10}$$

Equations (5.9) and (5.10) show that once the q in the nth layer is found by some means, the refractive index μ as well as the direction of the wave normal can be found. The derivation of Booker's q can be done in the following way.

Consider a plane wave in the nth layer with all field quantities dependent on x, y, z only through the factor (5.8). Then, symbolically, we may write

$$\frac{\partial}{\partial x} \equiv -ikS_1\ ,\quad \frac{\partial}{\partial y} \equiv -ikS_2\ ,\quad \frac{\partial}{\partial z} \equiv -ikq \tag{5.11}$$

The Maxwell's equations in Cartesian coordinate system are

$$\left.\begin{aligned} \frac{\partial E_z}{\partial y} - \frac{\partial E_y}{\partial z} &= -i\mu_0\omega H_x \\ \frac{\partial E_x}{\partial z} - \frac{\partial E_z}{\partial x} &= -i\mu_0\omega H_y \\ \frac{\partial E_y}{\partial x} - \frac{\partial E_x}{\partial y} &= -i\mu_0\omega H_z \end{aligned}\right\} \tag{5.12}$$

and

$$\left.\begin{aligned}
\frac{\partial H_z}{\partial y} - \frac{\partial H_y}{\partial z} &= i\omega D_x = i\omega(\varepsilon_0 E_x + P_x) \\
\frac{\partial H_x}{\partial z} - \frac{\partial H_z}{\partial x} &= i\omega D_y = i\omega(\varepsilon_0 E_y + P_y) \\
\frac{\partial H_y}{\partial x} - \frac{\partial H_x}{\partial y} &= i\omega D_z = i\omega(\varepsilon_0 E_z + P_z)
\end{aligned}\right\} \qquad (5.13)$$

where E, H, and P are electric, magnetic, and polarization field intensities respectively and ω, ε_0, and μ_0 are the angular frequency of the wave, permittivity and permeability of the free space, respectively.

Substituting (5.11) into (5.12) and (5.13), the results can be reduced in the matrix form

$$\begin{bmatrix} 0 & -q & S_2 \\ q & 0 & -S_1 \\ -S_2 & S_1 & 0 \end{bmatrix} \begin{bmatrix} E_x \\ E_y \\ E_z \end{bmatrix} = \frac{\mu_0}{\varepsilon_0} \begin{bmatrix} H_x \\ H_y \\ H_z \end{bmatrix} \qquad (5.14)$$

$$\begin{bmatrix} 0 & -q & S_2 \\ q & 0 & -S_1 \\ -S_2 & S_1 & 0 \end{bmatrix} \begin{bmatrix} H_x \\ H_y \\ H_z \end{bmatrix} = -\sqrt{\frac{\varepsilon_0}{\mu_0}} \begin{bmatrix} E_x \\ E_y \\ E_z \end{bmatrix} - \frac{1}{\sqrt{\varepsilon_0 \mu_0}} \begin{bmatrix} P_x \\ P_y \\ P_z \end{bmatrix} \qquad (5.15)$$

By eliminating H_x, H_y, and H_z between (5.14) and (5.15), we have

$$\begin{bmatrix} 1-q^2-S_2^2 & S_1S_2 & S_1q \\ S_1S_2 & 1-q^2-S_1^2 & S_2q \\ S_1q & S_2q & 1-S_1^2-S_2^2 \end{bmatrix} \begin{bmatrix} E_x \\ E_y \\ E_z \end{bmatrix} + \frac{1}{\varepsilon_0} \begin{bmatrix} P_x \\ P_y \\ P_z \end{bmatrix} = 0$$

The constitutive relation in the magneto-ionic medium can be shown to be (for instance refer to Budden [1961]):

$$\frac{1}{\varepsilon_0}\begin{bmatrix} P_x \\ P_y \\ P_z \end{bmatrix} = -\frac{X}{1-Y^2}\begin{bmatrix} 1-\ell^2Y^2 & -inY-\ell mY^2 & imY-\ell nY^2 \\ inY-\ell mY^2 & 1-m^2Y^2 & -i\ell Y-mnY^2 \\ -imY-\ell nY^2 & i\ell Y-mnY^2 & 1-n^2Y^2 \end{bmatrix}\begin{bmatrix} E_x \\ E_y \\ E_z \end{bmatrix} \tag{5.17}$$

where ℓ, m, n are the direction cosines of the vector $\bar{Y}$ which is defined to be opposite in direction to the earth's magnetic field vector. The matrix multiplying $(E_x, E_y, E_z)^T$ is called the susceptibility matrix of the ionosphere, and will be denoted by [M]. In terms of [M], (5.17) is written as

$$\frac{1}{\varepsilon_0}\begin{bmatrix} P_x \\ P_y \\ P_z \end{bmatrix} = \begin{bmatrix} M_{xx} & M_{xy} & M_{xz} \\ M_{yx} & M_{yy} & M_{yz} \\ M_{zx} & M_{zy} & M_{zz} \end{bmatrix}\begin{bmatrix} E_x \\ E_y \\ E_z \end{bmatrix} \tag{5.18}$$

Eliminate $[P_x, P_y, P_z]^T$ between (5.16) and (5.18), we have

$$\begin{bmatrix} 1-q^2-S_2^2+M_{xx} & S_1S_2+M_{xy} & S_1q+M_{xz} \\ S_1S_2+M_{yx} & 1-q^2-S_1^2+M_{yy} & S_2q+M_{yz} \\ S_1q+M_{zx} & S_2q+M_{zy} & C^2+M_{zz} \end{bmatrix}\begin{bmatrix} E_x \\ E_y \\ E_z \end{bmatrix} = 0 \tag{5.19}$$

For non-trivial solutions, the determinant of the coefficient matrix in (5.19) must be zero. This gives the quartic equation in q

$$F(q) = \alpha q^4 + \beta q^3 + \gamma q^2 + \delta q + \varepsilon = 0 \tag{5.20}$$

where

$$\alpha = (1 - Y^2) + X(n^2Y^2 - 1)$$

$$\beta = 2nXY^2 (S_1\ell + S_2m)$$

$$\gamma = -2(1 - X)(C^2 - X) + 2Y^2(C^2 - X) + XY^2 \{ 1 - C^2n^2 + (S_1\ell + S_2m)^2 \} \quad (5.21)$$

$$\delta = -2C^2nXY^2 (S_1\ell + S_2m)$$

$$\varepsilon = (1-X)(C^2-X)^2 - C^2Y^2(C^2-X) - C^2XY^2(S_1\ell + S_2m)^2$$

In the above derivation of Booker's quartic, the effect of collision has been ignored.

If we consider the two dimensional wave propagation such as in y-z plane, then $S_1 = 0$ and (5.21) reduces to

$$\left.\begin{aligned} \alpha &= (1-Y^2) + X(n^2Y^2-1) \\ \beta &= 2nmSXY^2 \\ \gamma &= -2(1-X)(C^2-X) + 2Y^2(C^2-X) + XY^2(1-C^2n^2 + S^2m^2) \\ \delta &= -2C^2mnSXY^2 \\ \varepsilon &= (1-X)(C^2-X)^2 - C^2Y^2(C^2-X) - m^2S^2C^2XY^2 \end{aligned}\right\} \quad (5.22)$$

where $S = S_2$.

For the n^{th} layer, the electron density N_e and the magnetic field vector $\vec{B}_0$ are known, and, therefore, X, Y, ℓ, m, and n can be calculated. By inserting these quantities, together with S, into (5.22), the coefficients to the quartic equation (5.20) can be calculated for the given layer and q can be determined by solving this equation. There are four solutions two of which represent the upgoing and downcoming ordinary waves, and the other two represent the upgoing and downcoming extraordinary waves.

5.3 Solution of Booker's quartic equation

To find the solution of Booker's quartic equation (5.20), one of the standard methods for solving quartic equations can be used, but it

would be more convenient to assign a series of fixed values of q and solve the equation for X. In terms of X, (5.20) is a cubic equation and can be written as

$$X^3 + AX^2 + BX + \Gamma = 0 \tag{5.23}$$

where

$$\left.\begin{aligned} A &= 2\,(q^2-C^2) - 1 \\ B &= (q^2-C^2)\,\{q^2-C^2+Y^2-2-Y^2(S_1\ell+S_2m+qn)^2\} \\ \Gamma &= (Y^2-1)\,(q^2-C^2)^2 \end{aligned}\right\} \tag{5.24}$$

For a given magnetic field vector $\bar{B}_0$, and an incident angle θ_I, (5.23) can be solved to obtain a q-X curve. Although the curve will be different for different incident angles, they will appear similar to that shown in Figure 5.3. The solid line curves refers to the ordinary wave, and the broken line curves to the extraordinary waves. This set of q-X curves was obtained for the wave frequency twice the gyro frequency, i.e., Y = 1/2, and $\theta_I = 45°$. In Section 5.5, a computer program has been developed to obtain the q-X curves for the radio path with transmitter locating at Maui, and receiver at the University of Hawaii.

5.4 Ray tracing by Booker's equartic

Booker (1939, 1949) has shown that the ray path of the ionospheric radio waves can be obtained by solving following two equations:

$$\frac{dx}{dz} = -\frac{\partial q}{\partial S_1} \tag{5.25a}$$

$$\frac{dy}{dz} = -\frac{\partial q}{\partial S_2} \tag{5.25b}$$

where $-(\partial q/\partial S_1)$ and $-(\partial q/\partial S_2)$ are the increases in horizontal displacement of the wave-packet parallel to the X and Y axes and measured in

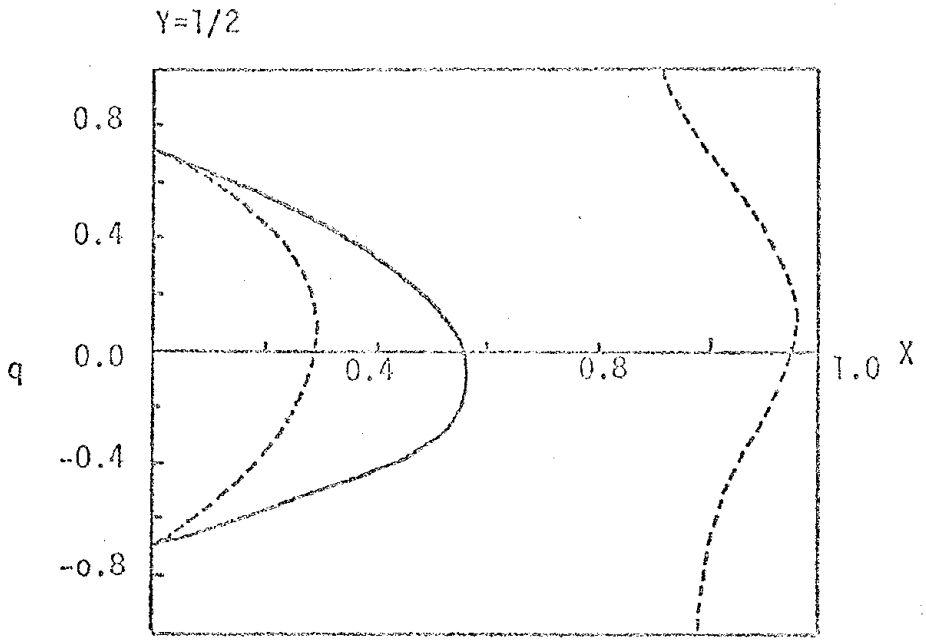

Figure 5.3 Typical q-X curves for Y=1/2 and $\theta_1 = 45^0$

per unit increase of height. In integral form (5.25a) and (5.25b) becomes

$$\chi = - \int_0^z \frac{\partial q}{\partial S_1} \, dz \tag{5.26}$$

$$Y = - \int_0^z \frac{\partial q}{\partial S_2} \, dz \tag{5.27}$$

(5.26) and (5.27) give the horizontal displacements parallel to the x and the y axes of the wave packet in going from height zero to z. The partial derivative $\partial q/\partial S_1$ in (5.25a) can be evaluated by taking the total derivative of (5.23). Let

$$F(S_1, q) = X^3 + AX^2 + BX + \Gamma = 0$$

Then,

$$dF(S_1, q) = \frac{\partial F(S_1, q)}{\partial S_1} \, dS_1 + \frac{\partial F(S_1, q)}{\partial q} \, dq$$

$$= (X^2 \frac{\partial A}{\partial S_1} + X \frac{\partial B}{\partial S_1} + \frac{\partial \Gamma}{\partial S_1}) \, dS_1 + (X^2 \frac{\partial A}{\partial q} + X \frac{\partial B}{\partial q} + \frac{\partial \Gamma}{\partial q}) \, dq$$

$$= 0$$

Thus, we have

$$\frac{\partial q}{\partial S_1} = - (X^2 \frac{\partial A}{\partial S_1} + X \frac{\partial B}{\partial S_1} + \frac{\partial \Gamma}{\partial S_1})/D \tag{5.28}$$

Where,

$$D = X^2 \frac{\partial A}{\partial q} + X \frac{\partial B}{\partial q} + \frac{\partial \Gamma}{\partial q} \tag{5.29}$$

Similarly, we can have

$$\frac{\partial q}{\partial S_2} = - (X^2 \frac{\partial A}{\partial S_2} + X \frac{\partial B}{\partial S_2} + \frac{\partial \Gamma}{\partial S_2})/D \tag{5.30}$$

The partial derivatives of A, B, and Γ in (5.28) and (5.30) can be

obtained by differentiating (5.24). Remembering that $C^2 = 1-S_1^2 - S_2^2$, we have

$$\left.\begin{aligned}
\frac{\partial A}{\partial q} &= 4q \\
\frac{\partial B}{\partial q} &= -2q\{(2-Y^2) + (S_1\ell+S_2m+qn)^2Y^2 + 2(C^2-q^2)\} \\
&\qquad + 2n(S_1\ell+S_2m+qn)Y^2(C^2-q^2) \\
\frac{\partial \Gamma}{\partial q} &= 4q\ (1 - Y^2)\ (C^2 - q^2)
\end{aligned}\right\} \qquad (5.31)$$

$$\left.\begin{aligned}
\frac{\partial A}{\partial S_1} &= 4S_1 \\
\frac{\partial B}{\partial S_1} &= -2S_1\ \{(2-Y^2) + (S_1\ell+S_2m+qn)^2Y^2 + 2(C^2-q^2)\} \\
&\qquad + 2\ell(S_1\ell+S_2m+qn)Y^2(C^2-q^2) \\
\frac{\partial \Gamma}{\partial S_2} &= 4S_1(1 - Y^2)\ (C^2-q^2)
\end{aligned}\right\} \qquad (5.32)$$

$$\left.\begin{aligned}
\frac{\partial A}{\partial S_2} &= 4S_2 \\
\frac{\partial B}{\partial S_2} &= -2S_2\ \{(2-Y^2) + (S_1\ell+S_2m+qn)^2Y^2 + 2(C^2-q^2)\} \\
&\qquad + 2m(S_1\ell+S_2m+qn)^2Y^2\ (C^2-q^2) \\
\frac{\partial \Gamma}{\partial S_2} &= 4S_2\ (1-Y^2)\ (C^2-q^2)
\end{aligned}\right\} \qquad (5.33)$$

It is convenient to think of a wave packet which is incident upon the ionosphere in y-z plane. This means

$$S_1 = 0 \quad \text{and} \quad S_2 \equiv S \qquad (5.34)$$

Although the wave is assumed to be incident in the y-z plane, it will, in general, deviate sideways out of the y-z plane. For this reason, y

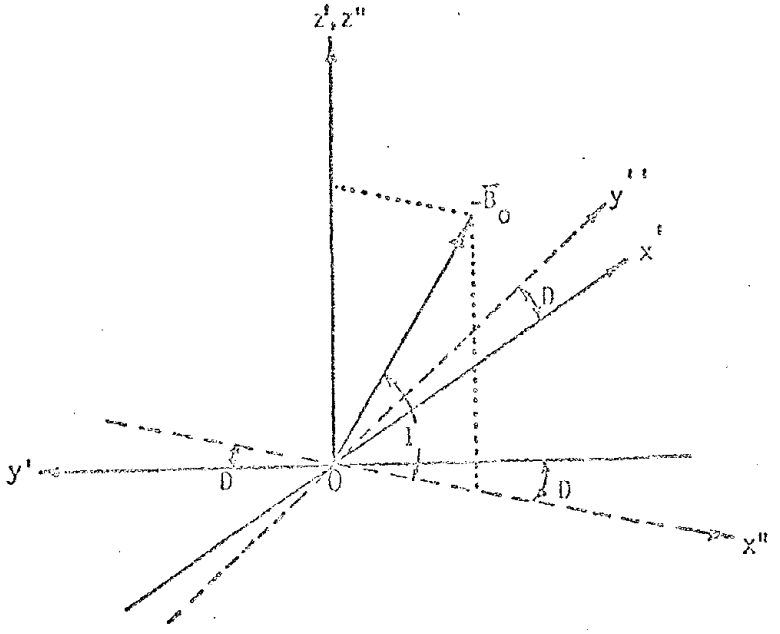

Figure 5.4(a) Relationship between the coordinate systems (x', y', z') and (x'', y'', z'').

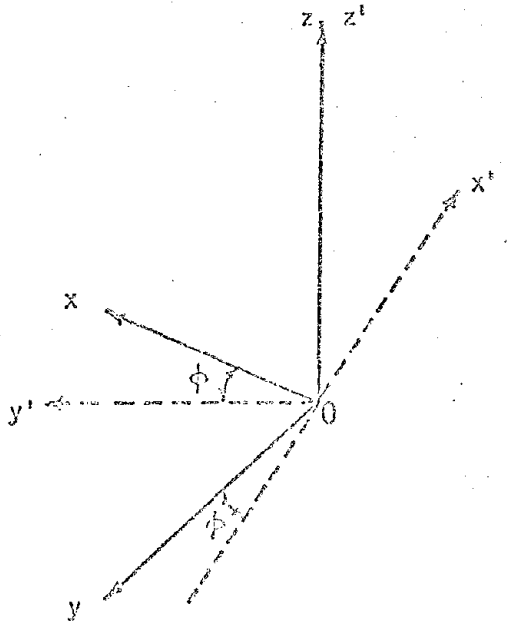

Figure 5.4(b) Relationship between the coordinate systems (x', y', z') and (x, y, z).

is referred to as a horizontal range and x in (5.26) as a lateral deviation. Substituting from (5.34) into (5.31), (5.32) and (5.33), we obtain

$$\left.\begin{aligned}
\frac{\partial A}{\partial q} &= 4q \\
\frac{\partial B}{\partial q} &= -2q\{(2-Y^2) + (Sm+qn)^2Y^2 + 2(C^2-q^2)\} \\
&\quad + 2n\,(Sm + qn)\,Y^2\,(C^2-q^2) \\
\frac{\partial r}{\partial q} &= 4q\,(1-Y^2)\,(C^2-q^2)
\end{aligned}\right\} \qquad (5.35)$$

$$\left.\begin{aligned}
\frac{\partial A}{\partial S_1} &= 0 \\
\frac{\partial B}{\partial S_1} &= 2\ell\,(Sm+qn)\,Y^2(C^2-q^2) \\
\frac{\partial r}{\partial S_1} &= 0
\end{aligned}\right\} \qquad (5.36)$$

$$\left.\begin{aligned}
\frac{\partial A}{\partial S_2} &= 4S \\
\frac{\partial B}{\partial S_2} &= -2S\{(2-Y^2) + (Sm + qn)^2Y^2 + 2(C^2 - q^2)\} \\
&\quad + 2m\,(Sm + qn)\,Y^2(C^2 - q^2) \\
\frac{\partial r}{\partial S_2} &= 0
\end{aligned}\right\} \qquad (5.37)$$

In summary, (5.26), (5.28), (5.29), (5.31), and (5.32) are used for calculating the lateral deviation x; and (5.27), (5.30), (5.29), (5.31), and (5.33) are used for calculating the horizontal range y. q in these equations can be obtained from the q-X curves discussed in Section 5.3.

5.5 A computer program for determining the q-X curves

To obtain the q-X curves for radio path from Maui to the University of Hawaii, the direction cosines (l, m, n) of the vector $\bar{Y}$ must be determined. In Figure 5.4 (a), let the origin O be chosen at the transmitting station on Maui and the two coordinate systems (x', y', z') and (x", y", z") with the x' and y' axes directed in the geographic east and north direction, and the x" and y" axes directed in the geomagnetic south and east directions, respectively. For the radio path, the magnetic dip I and declination angle D are 38.704° and 11.875° E as observed at Honolulu Geomagnetic Observatory, respectively.

From Figure 5.4 (a), the direction cosine of $-\bar{B}_0$ with respect to (x', y', z') coordinate system is given by

$$(-\cos I \sin D, -\cos D \cos I, \sin I) \tag{5.38}$$

Figure 5.4(b) shows the relative orientation between the coordinates systems (x, y, z) and (x', y', z'). The y axis is directed from Maui towards the University of Hawaii on Oahu. The angle ϕ between the y and y' axes is measured to be 15.0°. The direction cosines of the x, y and z axes with respect to the (x', y', z') coordinates are

$$(\sin\phi, \cos\phi, 0), (-\cos\phi, \sin\phi, 0), \text{ and } (0,0,1) \tag{5.39}$$

respectively.

By taking the sums of the products of corresponding elements in (5.38) and (5.39), the direction cosines of $-\bar{B}_0$ with respect

to the (x, y, z) coordinate are calculated to be

$$\ell = -\cos I\,(\sin D \sin\phi + \cos D \cos\phi)$$
$$m = \cos I\,(\sin D \cos\phi - \cos D \sin\phi) \qquad (5.40)$$
$$n = \sin I$$

Substituting the observed values of I, and D and the calculated value of ϕ into (5.40) we finally arrive at the numerical values for the direction cosines of the vector $\bar{Y}$ to be

$$\ell = 0.77900$$
$$m = 0.046624 \qquad (5.41)$$
$$n = 0.62530$$

Using these values for ℓ, m, n in (5.24), we obtain the numerical values for the coefficients A, B, and Γ in the expression of (5.23). Solution to (5.23) will provide the values of X corresponding to the given q, C and f and give the three roots. The root with the intermediate magnetitude corresponds to that for the ordinary wave.

A subroutine subprogram QUART (ANG, FREQ, QUP, QDO, XUP, XDO, NO, XO, QO) was developed for generating Booker's q-X curves for a given incident angle and probing frequency. The meanings of the arguments are as follows:

ANG: Incident angle, θ_I, in radian.

FREQ: Probing frequency, f, in MHz

XO : Returned value of X at the reflection point.

QO : Returned value of q at reflection point.

QUP : Vector of length NO which gives returned values of q for upgoing wave.

XUP : Vector of length NO which gives returned values of X corresponding to q in QUP.

NO : Number of data point on q-X curve corresponding to upgoing wave.

QDO : Vector of length (41-NO) which gives returned values of q for downcoming wave.

XDO : Vector of length (41-NO) which gives returned values of X corresponding to q in QDO.

The total number of data point in q-X curve is chosen to be 41. This number is sufficient to give a detailed numerical q-X curve for the ray tracing discussed in the next section. The values of q and X falling between two of these data points may be calculated by the method of linear interpolation. The values of XO and QO cannot be determined by solving (5.23). They are determined by fitting a parabola to the three data points (X_1, Q_1), (X_2, Q_2) and (X_3, Q_3) closest to the nose of the q-X curve as shown in Figure 5.5. The resulting expressions for Q_0 and X_0 are

$$Q_0 = \frac{(X_1-X_2)\,(Q_3^2 - Q_2^2) - (X_3-X_2)\,(Q_1^2 - Q_2^2)}{2\{(X_1-X_2)\,(Q_3-Q_2) - (X_3-X_2)\,(Q_1 - Q_2)\}} \tag{5.42}$$

$$X_o = X_2 - \frac{(X_1 - X_2)\,(Q_2 - Q_0)^2}{(Q_1 - Q_2)\,(Q_1 + Q_2 - 2Q_0)} \tag{5.43}$$

The subprogram quart was programmed so that the (NO $\pm$ 1) th data point always corresponds to the point of (X_0, Q_0).

The vector lengths NO and (41 - NO) are not fixed numbers but vary for different probing frequencies f and incident angles θ_I. Therefore, in the main program, it is better to give the value of 41 to the dimensions of QUP, QDO, XUP, and XDO. Appendix 5B gives the details of this

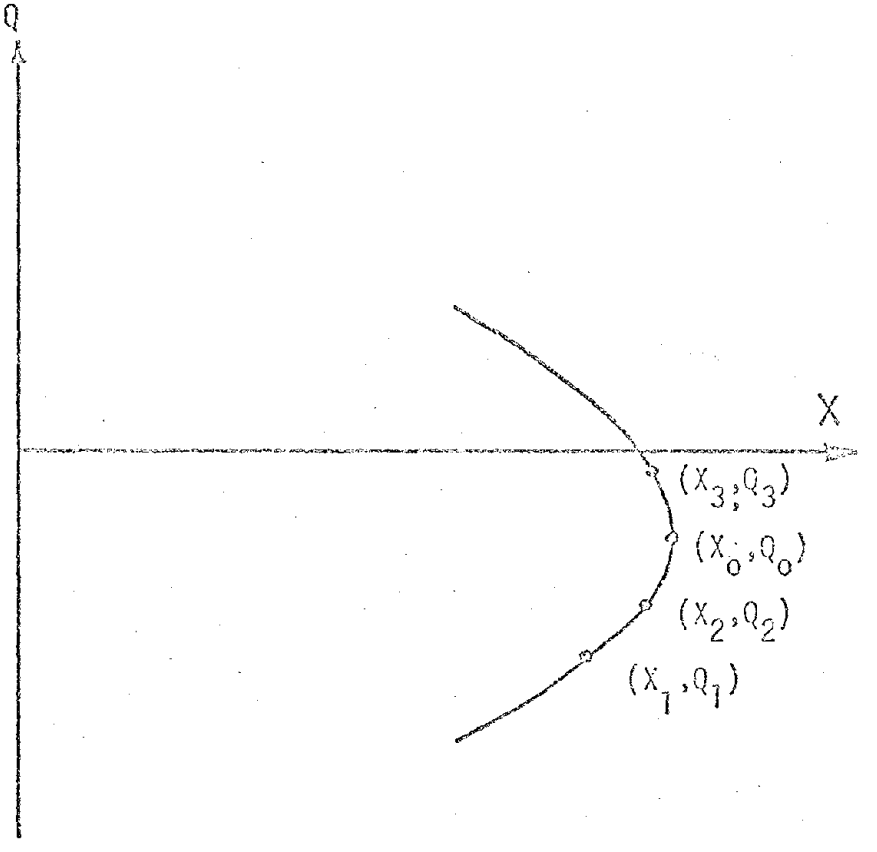

Figure 5.5 A parabola is fitted to the points (X_1,Q_1), (X_2,Q_2), and (X_3,Q_3) to determine the value of X_0 and Q_0.

program.

Appendix 5C gives a program which can plot the q-X curves for incidence angles of 0.1, 0.2, 0.3, 0.4 and 0.5 radian and for frequencies of 5 MHz and 10 MHz. Figure 5.6 (a) is the q-X curves plotted by this program. Since the SUBROUTINE QUART is programmed exclusively for the radio path from WWVH to the University of Hawaii, it cannot be used to obtain q-X curves for another radio path. For that case, m and n in (5.41) should be recalculated for that particular radio path and substitute these newly calculated values of m and n into the right hand side of the equation given in statements 4 and 5. For example, the radio path perpendicular to the WWVH-UH path and directing to the north has direction cosines of

$$\ell = 0.046621$$

$$m = -0.77899$$

$$n = 0.62529 \qquad (5.44)$$

Therefore, by replacing statement (4) in QUART by the following statement

```
Y2 = -0.77899 * Y
```

the program given in Appendix 5C can be used to plot q-X curves corresponding to this newly selected radio path. Figure 5.6 (b) shows the q-X curves for this radio path. For the rest of the studies, the WWVH-UH path will be called as path 1 and the one perpendicular to path 1 as path 2.

It is of interest to note that:

(1) The q-X curves obtained for path 1 and those obtained for path 2 are quite different. For path 1 the curves are quite symmetric

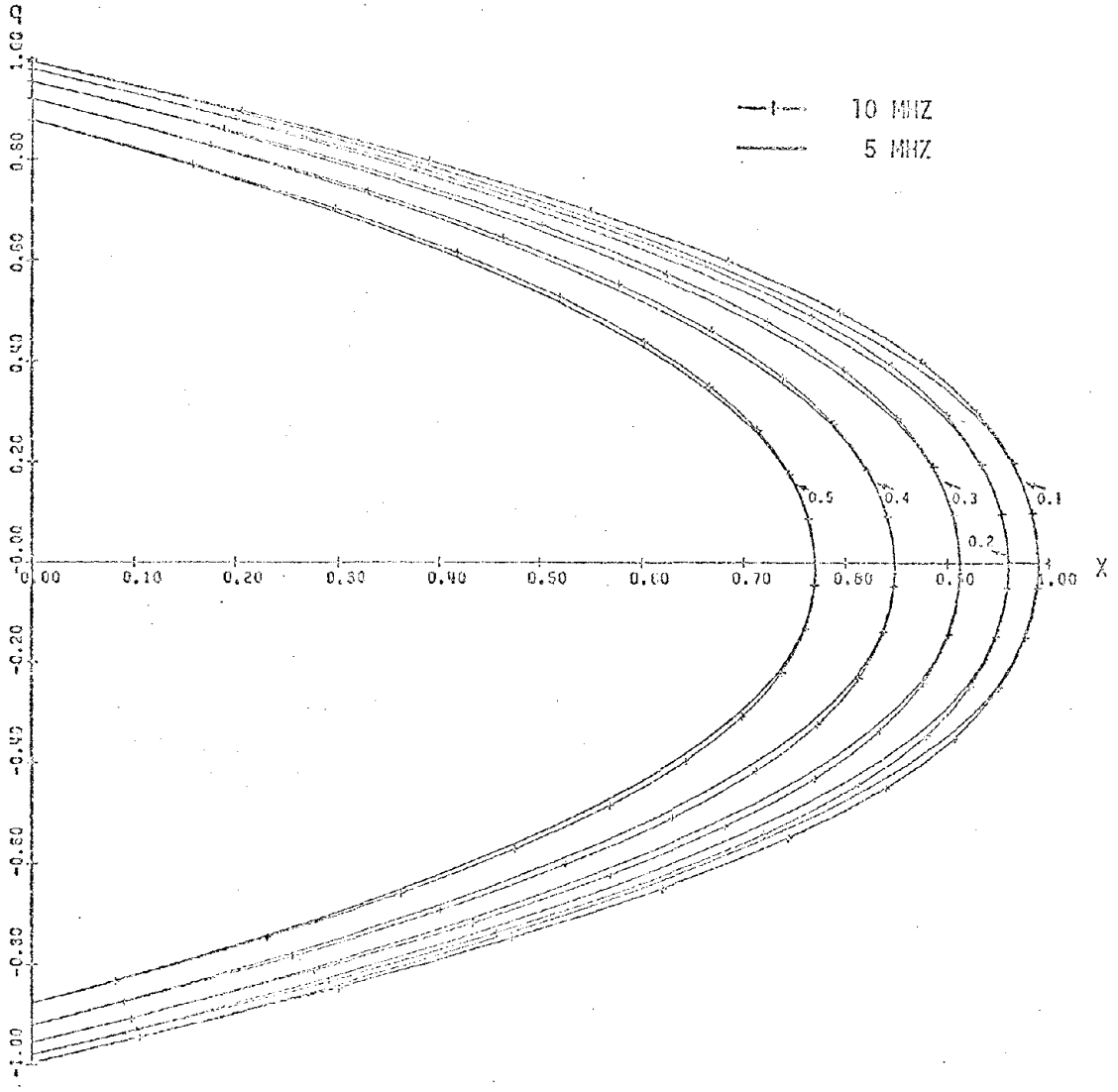

Figure 5.6(a) q-X curves for radio path 1 (WWVH on Maui to UH on Oahu).

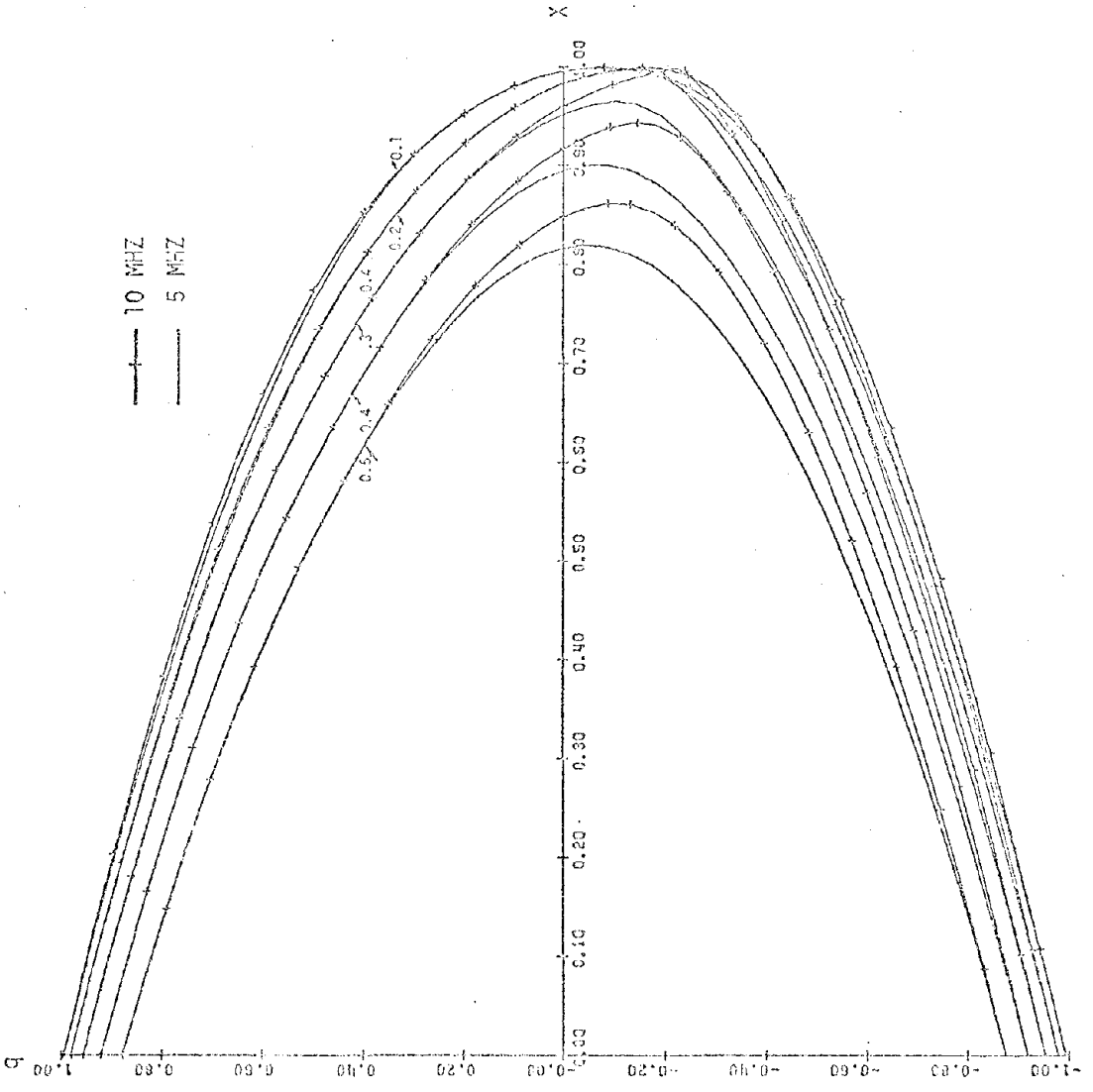

Figure 5.6(b) q-X curves for radio path 2 (perpendicular to path 1)

with respect to the X axis; but for path 2, they are quite asymmetric.

(2) For path 1, the frequency dependence of the q-X curves is quite small. For path 2, the q-X curves obtained for 10 MHz are quite different from those obtained for 5 MHz. The differences are most remarkable near the nose of the q-X curve and the curves corresponding to the downcoming waves. These differences are less for smaller incident angle.

(3) For path 1, (X_0, Q_0)'s for 10 and 5 MHz are almost at the same point; however, for path 2 they are quite different, especially at large incident angles.

(4) For both path 1 and 2, the lengths of the q-X curves corresponding to the upgoing waves are larger than those corresponding to the downcoming waves. This difference will give rise to an asymmetric radio path with respect to the vertical line passing through the center of the ground path between the transmitter and receiver, as will be discussed in the next section.

All of these unexpected characteristics are all due to the effect of geomagnetic field on the ionospheric radio propagation through the factors of ℓ, m, n and Y which are different for different radio paths.

5.6 A computer program for ray tracing

A two dimensional ray tracing computer program was developed based on the equations (5.27), (5.30), and (5.33) and under the assumptions below compatible with the University of Hawaii Doppler system in operation prior to 1971.

(i) The ionosphere is constructed by a number of thin discrete horizontal flat layers of thickness 5 km in each of which the electron density is homogenous as shown in Figure 5.7.

(ii) The lateral deviation given by (5.25) is so small, that this quantity will be ignored. Under this assumption, the ray path becomes two dimensional.

(iii) The horizontal range is so small (only 152 km) that the magnetic field vector $\bar{B}_0$ is assumed to be constant in each discrete layer. This allows us to put ℓ, m, n, and Y to be constants.

In Figure 5.7, z_1, z_2, ... represents the bottom height of the 1st, 2nd, ... layers and x_1, x_2, ..., and q_1, q_2, ... are the values of X and q in those layers, respectively. z_m is chosen to be the bottom height of the layer in which the wave will be reflected. For a given incident angle θ_I, z_m is obtained by comparing the X's for each layer with the NOth value of the returned XUP in subprogram QUART so that X_m is closest but smaller than the NOth value of X in the X-q curve. The X_0 and q_0 values at the reflection point are obtained from the returned output of XO and QO in subprogram QUART. By knowing X_m, and X_{m+1} from the specified ionosphere and XO and QO from the returned output of QUART, the height of reflection can be obtained by using linear interpolation.

$$z_0 = \left(\frac{z_{m+1} - z_m}{x_{m+1} - x_m} \right) (X_0 - X_m) + z_m \qquad (5.45)$$

The value of q_k in the kth layer is determined by linear interpolation of values from the upper and lower sides of the kth layer.

$$q_k = \frac{QUP_u - QUP_\ell}{XUP_u - XUP_\ell} (X_k - XUP_\ell) + QUP_\ell \qquad (5.46)$$

where XUP_u and XUP_ℓ are two returned values of XUP from subprogram QUART which are closest to X_k from upperside and lower side, respectively, and

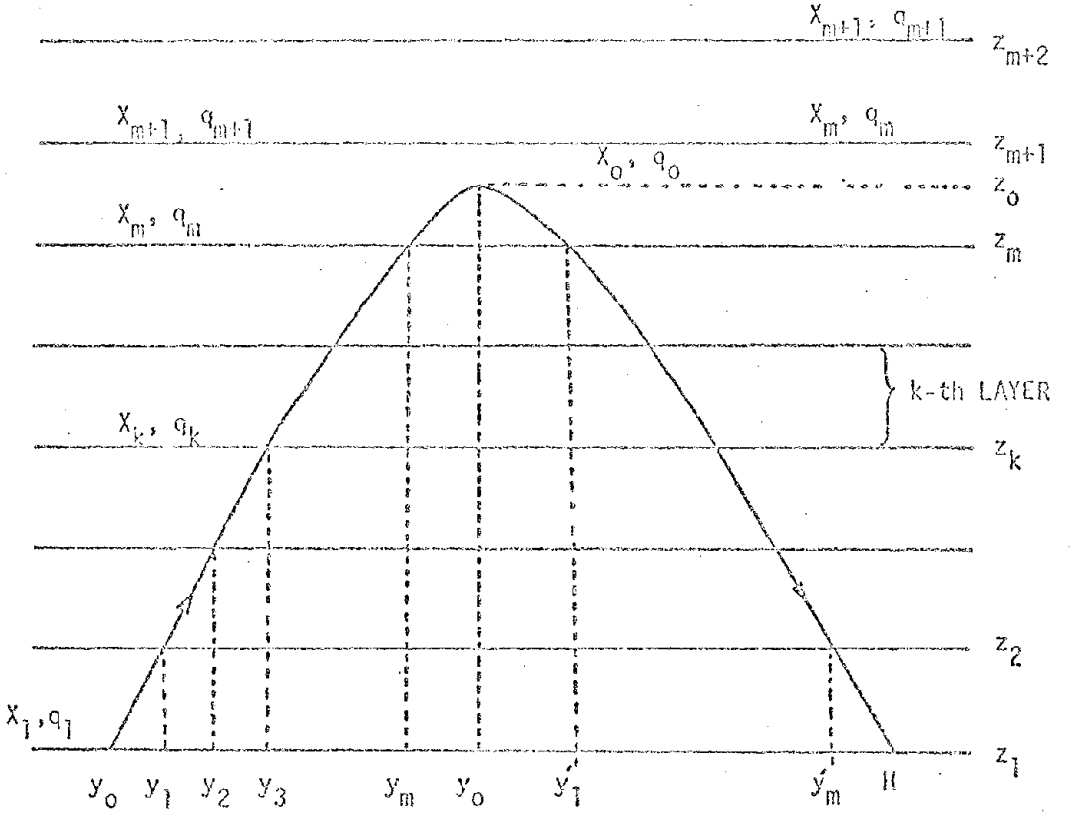

Figure 5.7 For ray tracing, the ionosphere is assumed to be constructed by a number of thin discrete horizontal flat layers in each of which both X and q are constant.

QUP_u and QUP_ℓ are corresponding values of returned q. Since the values of X_k and q_k for each layer and X_0 and q_0 at the reflection point can be obtained from (5.43) and (5.42), respectively, the integrand of (5.27) can be obtained by direct substitutions of these values. For convenience in programming, a subprogram FUNCTION, DX2DH (Y, Y2, Y3, C, S, Q, X), has been developed for this purpose. The symbols of the arguments to DX2DH correspond the following quantities in the equation (5.27)

Y = Absolute value of vector $\bar{Y}$

$Y_2 = mY$

$Y_3 = nY$

$C = \cos\theta_I$

$S = \sin\theta_I$

Q = q

X = X

Since the integrand of (5.27) can be obtained by FUNCTION DX2DH, (5.27) can be integrated to give the horizontal range y.

In order for (5.27) to be numerically integrable throughout the range from 0 to z_0 (i.e., X = 0 to X_0), the values of dy/dz must be continuous throughout this range. Figure 5.8 shows the variation of dy/dz with respect to z by using (5.30), (5.29), and (5.33). The full and dotted lines show the upgoing and downcoming ordinary waves, respectively. Since dy/dz becomes infinite as z approaches the reflecting point z_0, equation (5.27) cannot be integrated numerically over the entire range of integration. To avoid this difficulty, the integration will be performed separately for the range from $0 \leq z \leq Zm$ and from $Zm \leq z < Z_0$. The integrations will be done numerically for the former and analytically for the latter by fitting an analytical function

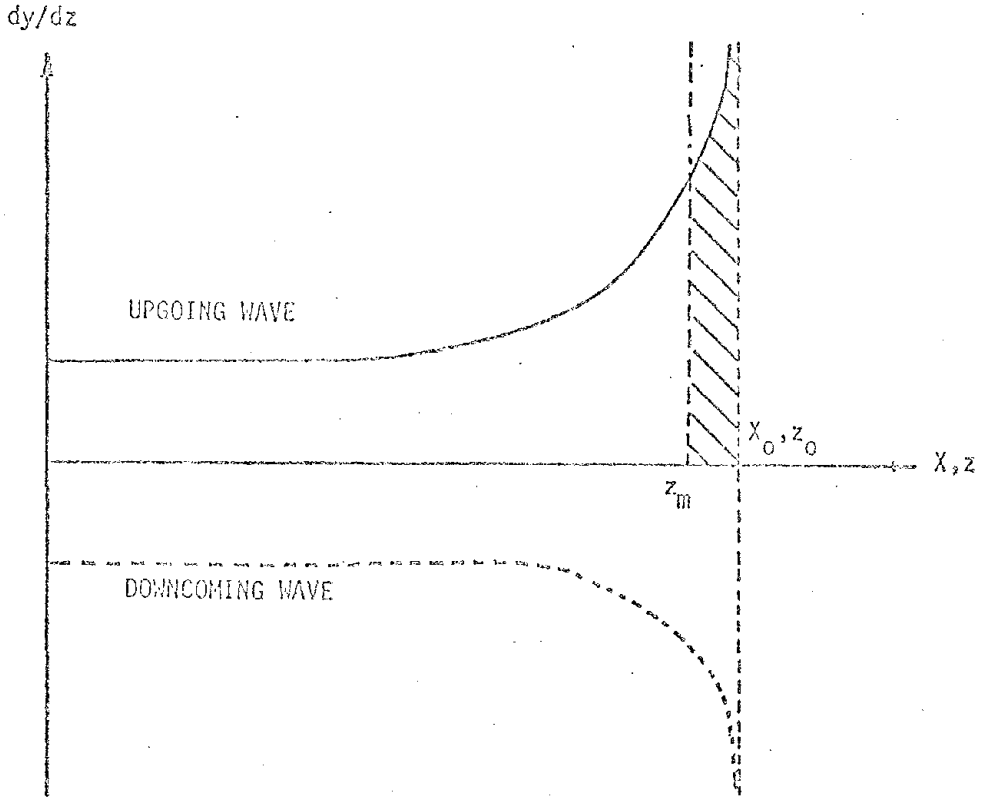

Figure 5.8 Variation of dy/dz with respect to X or z.

to the last data point (corresponding to z_m) and the vertical asymptote at X_0. The analytic function adapted to the curve is

$$\eta = \frac{K}{\sqrt{z_0 - z}} \tag{5.47}$$

where

$$\eta = - \frac{\partial q}{\partial S_2} = \frac{dy}{dz}$$

the height of reflection Z_0 and the parameter K must be determined. If we let η_m be the value of dy/dz at $z = z_m$, then from (5.47) we obtain

$$\eta_m = \frac{K}{\sqrt{z_0 - z_m}}$$

or

$$K = \sqrt{z_0 - z_m} \quad \eta_m \tag{5.48}$$

The horizontal range, Δy_m, corresponding to the hatched part in Figure 5.8 can be obtained by the analytical integration

$$\Delta y_m = \int_{z_m}^{z_0} \frac{K}{\sqrt{z_o - z}} \, dz = -2 K \sqrt{z_0 - z} \Big|_{z_m}^{z_0} = 2 K \sqrt{z_0 - z_m} \tag{5.49}$$

Substituting for K in this result gives

$$\Delta y_m = 2 (z_0 - z_m) \eta_m \tag{5.50}$$

The horizontal range corresponding to the reflection point is then obtained by combining the numerical integration of (5.27) up to $Z=Z_m$ and the result of (5.50). A similar integration can be applied to the downcoming wave to obtain the corresponding horizontal range.

A different incident angle θ_I will result in a different horizontal range. The radio path which is needed in the present study is one which

starts from the transmitter and terminates at the receiver at a fixed position. Therefore, a suitable computer program should be provided for the 'homing' problem. Let D be the horizontal distance between the transmitter and the receiver, θ_I (i) the i^{th} trial of the incident angles, and y(i) the corresponding horizontal range. The first trial angle $\theta_I(1)$ is chosen to be large enough such that the horizontal range y(1) is greater than the horizontal distance D between the transmitter and the receiver. For the assumed value of $\theta_I(1)$, (5.27) and (5.50) are used to calculate y(1). If the difference y(1)-D is greater than preassigned distance D, for example 1 km, a preassigned small angle $\Delta\theta$ is subtracted from $\theta_I(1)$ to give the second trial angle $\theta_I(2) = \theta_I(1) - \Delta\theta$. If this new trial angle $\theta_I(2)$ gives a corresponding horizontal range which is still $y(2) - D > \Delta D$, then $\Delta\theta$ is subtracted again from $\theta_I(2)$ to give a third trial angle $\theta_I(3)$, and so on. This procedure is repeated until a certain value of θ_I, say $\theta_I(j)$, for which the corresponding y(j) satisfies one of the following conditions:

(i) $0 \leq y(j) - D \leq \Delta D$

(ii) $y(j) - D < 0$

If condition (i) is satisfied, then the radio path has homed in on the desired point within the preassigned accuracy ΔD and the process is stopped. If condition (ii) is met, it shows that the incident angle $\theta_I(j)$ is too small and a computer program is provided to bring $\theta_I(j)$ back to $\theta_I(j-1)$, and start a new cycle for which $\Delta\theta$ is halved. If this new cycle still cannot satisfy the condition (i), it will recycle again with the second $\Delta\theta$ halved again. This recycling continues until condition (i) is satisfied.

The complete set of two dimensional ray tracing computer program is given in Appendix 5C. In order to use this program, the procedures given in Appendix 5C must be followed. Table 5C-1 given at the end of Appendix 5C shows the printed output of a ray tracing sample made on the ionogram or electron density profile shown in Figure 4.1. The ray paths obtained are shown in Figure 5.9. The numbers attached to each ray path refer to the sequence of trial. After 12 trials the ray finally homed onto the preassigned range. The number of trials depends on the individual ionograms and the probing frequencies. For ΔD = 1 km, it is usually less than 15. Figure 5.10 shows the ray paths obtained for radio path 1 and 2. It is very interesting to note that: for path 1, the ray path is almost symmetric with respect to the vertical line at the center of the path. However, for path 2, the ray path is quite asymmetric with respect to the centered vertical line, and the horizontal distance of the reflection point deviates from the central point by as much as 11.2 km. For path 1, while the ray is reflected at z_0 = 286.6 km, for path 2 it is reflected at z_0 = 290.4 km. These real reflection heights are lower than the height obtained by determining the reflection height from X = 1 in Figure 4.2, which gives z_0 = 290.5 km. Moreover, due to asymmetry in q-X curve, the ray path for the upgoing wave is much longer than that for downcoming wave. These phenomena are caused by the presence of the geomagnetic field.

Though it is not directly related to the subject of the present study, it is worthwhile to make the following remarks;

(i) A Doppler system with three spaced receivers is sometimes used to determine the phase velocity of the acoustic-gravity waves and travelling ionospheric disturbances (George, 1967,

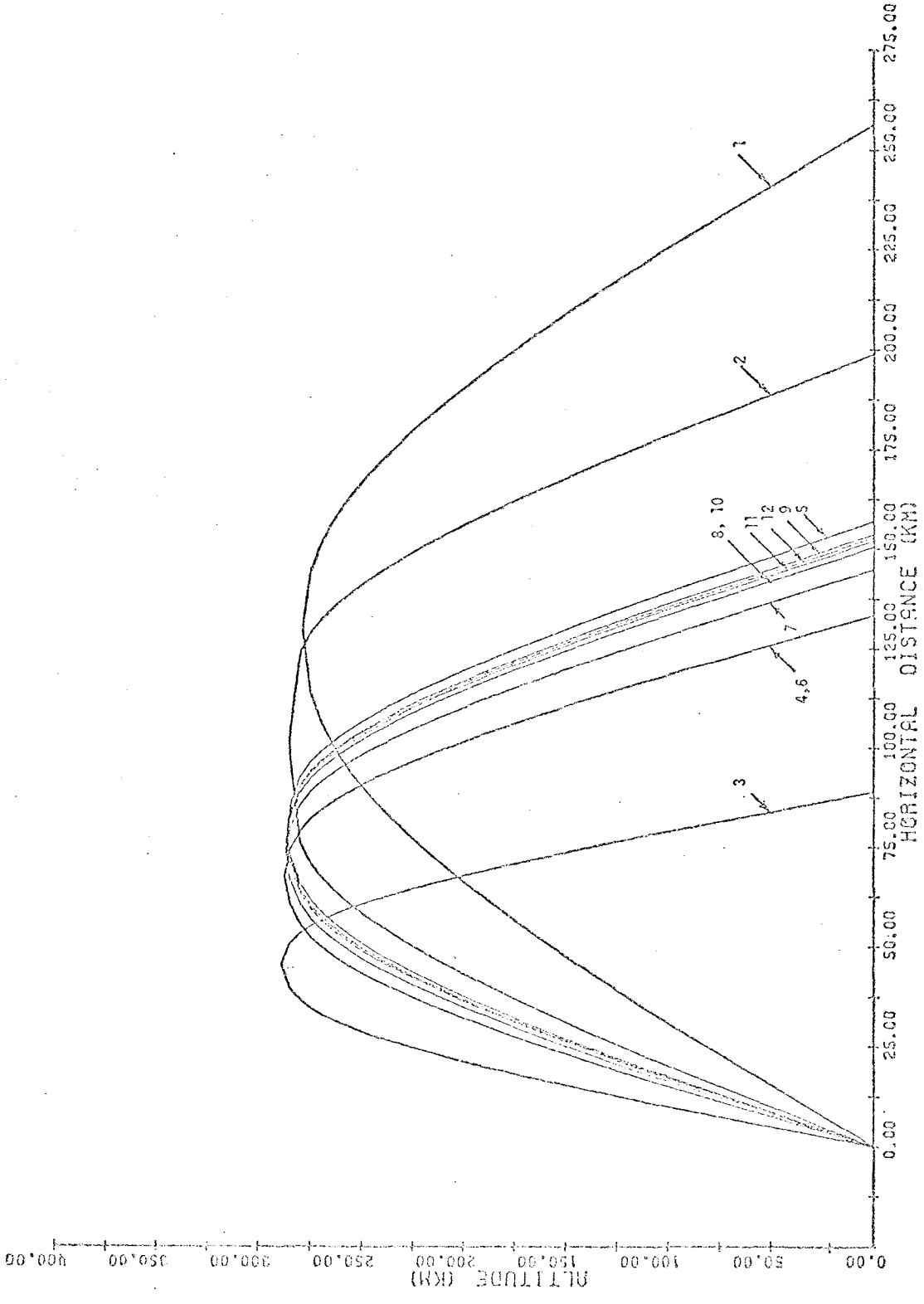

Figure 5.9 Ray tracing made on the electron density profile given in Figure 4.2..

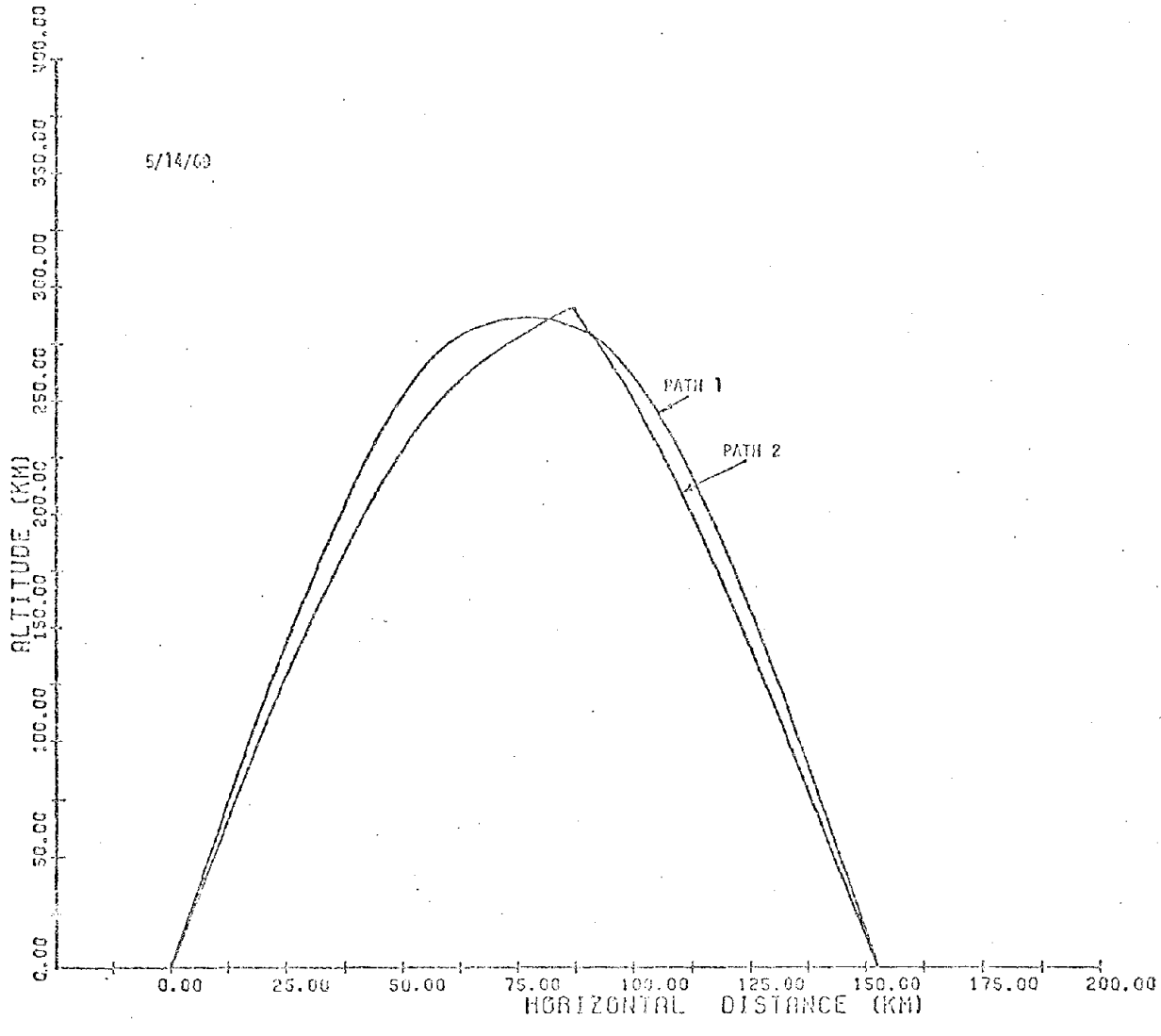

Figure 5.10 Ray paths obtained for radio path 1 and 2.

Jones 1969). For this purpose, the three points used for triangulation are usually chosen at the geometric centers of the radio paths. Since the actual reflection points deviates from the geometric central point by as much as 10% as was discussed in the previous paragraph, it is more accurate to make ray tracings for each radio path to find the actual reflection points rather than merely use the geometric central points for triangulation.

(ii) A construction of dispersion curve for seismic Rayleigh waves at long periods by using Doppler frequency records has been attempted by the author. A preliminary result has revealed that, in order for the dispersion curve obtained by using Doppler record to match the one obtained by Oliver (1962), the travelling time required for the acoustic waves generated by the seismic Rayleigh waves to propagate from the ground level up into the ionospheric reflection height, the ionospheric reflection height should be determined very precisely. This would require a ray tracing to determine a more accurate height of reflection rather than merely using the real height corresponding to $X = 1$.

References

Booker, H.G., 1939, The Propagation of Wave Packets Incident Obliquely on a Stratified Doubly Refracting Ionosphere, Phi. Trans. A., 237, 411.

Booker, H.G., 1949, The Application of the Magnetoionic Theory to Radio Waves Incident Obliquely upon a Horizontally Stratified Ionosphere, J. Geophys. Res., 54, 243.

Bremmer, H., 1949, Terrestrial Radio Waves, (Elsevier Pub. Co., Amsterdam).

Budden, K.G., 1961, Radio Waves in the Ionosphere, (Cambridge University Press, Cambridge).

Davies, K., 1969, Ionospheric Radio Waves, (Blaisdell Publishing Co.).

George, T.M., 1967, Ionospheric Effects of Atmospheric Waves, ESSA Tech. Rep. IER 57-ITSA 54.

Hazelgrove, J., 1954, Ray Theory and a New Method for Ray-tracing, Rept. Conf. on Phys. of the Ionosphere, (Physical Society, London), 355.

Jones, J.F., 1969, Observation of Traveling Ionospheric Disturbances by the Doppler Techniques with Spaced Transmitters, ESSA Tech. Rept. ERL 142-SDL 11.

Lawrence, R.S., and D.J. Posakony, 1962, A Digital Ray-tracing Program for Ionospheric Research, Space Research II (North-Holland Pub. Co., Amsterdam).

Oliver, J., 1962, A Summary of Observed Seismic Surface Wave Dispersion, Bull. Seism. Soc. Am., 52, 81.

Poveverlein, H., 1949, Strahlweze von Radiowellen in der Ionospheren, Z. Angen. Phys., 1, 517.

Tithedridge, J.E., 1959, Ray-path in the Ionosphere, J. Atm. Terr. Phys., 14, 50.

APPENDIX 5A

A SUBROUTINE QUART FOR THE CALCULATION OF Q-X CURVES

```
FORTRAN IV G LEVEL  20                    QUART                    DATE = 73227

0001                  SUBROUTINE QUART(ANG,FREQ,QUP,QDO,XUP,XDO,NO,XO,QO)
                C     THIS PROGRAM GIVES BOOKER'S QUARTIC BY GIVING INCI-
                C     DENCE ANGLE AND PROBING FREQUENCY
                C     STEP WISE=0.05C
0002                  DIMENSION XCOF(4),COF(4),XR(3),XI(3),XUP(1),XDO(1),
                     2   QUP(1),QDO(1),TX(41),TQ(41)
0003                  Y=0.673/FREQ
0004                  Y2=-0.046624*Y
0005                  Y3=0.625297*Y
0006                  C=COS(ANG)
0007                  S=SIN(ANG)
0008                  TEM=0.0
0009                  DO 10 J=1,41
0010                  Q=C-0.05*C*(J-1)
0011                  XCOF(1)=-(1.0-Y**2)*(C**2-Q**2)**2
0012                  XCOF(2)=(C**2-Q**2)*(2.0-Y**2+(S*Y2+Q*Y3)**2
                     2  +C**2-Q**2)
0013                  XCOF(3)=-(1.0+2.*(C**2-Q**2))
0014                  XCOF(4)=1.0
0015                  CALL POLRT(XCOF,COF,3,XR,XI,IER)
0016                  TX(J)=XR(2)
0017               10 TQ(J)=Q
0018                  DO 14 I=1,40
0019                  IF (TX(I+1)-TX(I)) 11,14,14
0020               14 CONTINUE
0021               11 NO=I
                C     TO DETERMINE MAX Q AND X DENOTED BY QO AND XO
0022                  X3= TX(NO-1)
0023                  X2= TX(NO)
0024                  X1= TX(NO+1)
0025                  Q3= TQ(NO-1)
0026                  Q2= TQ(NO)
0027                  Q1= TQ(NO+1)
0028                  T1=((X3-X2)/(X1-X2))*((Q1-Q2)/(Q3-Q2))
0029                  QO=(Q3+Q2-T1*(Q1+Q2))/(2.0*(1.0-T1))
0030                  XO=X2-((Q2-QO)/(Q1-Q2))*((X1-X2)/(Q1+Q2-2.0*QO))*(Q2-QO)
0031                  IF ( TQ(NO)-QO ) 15,15,17
0032               15 NO=NO-1
0033               17 NO1=NO+1
0034                  DO 12 J=1,NO
0035                  XUP(J)=TX(J)
0036               12 QUP(J)=TQ(J)
0037                  DO 16 J=1,NO1
0038                  XDO(J)=TX(NO+J)
0039               16 QDO(J)=TQ(NO+J)
0040                  RETURN
0041                  END
```

APPENDIX 5B

A COMPUTER PROGRAM TO PLOT Q-X CURVES

```
FORTRAN IV G LEVEL  20                  MAIN                DATE = 73234

            C       TO PLOT BUCKER'S QUARTIC
 0001               DIMENSION QUP(41),QDO(41),XUP(41),XDO(41),Q(42),X(42),B(1000)
 0002               CALL PLOTS(B(1),4000)
 0003               CALL PLOT(0.0,0.0,-3)
 0004               DO 9 L=1,2
 0005               IF (L-1) 14,14,15
 0006            14 F=10.0
 0007               GO TO 16
 0008            15 F=5.0
 0009            16 DO 10 I=1,5
 0010               ANG=0.1+  0.1*(I-1)
 0011               CALL QUART(ANG,F,QUP,QDO,XUP,XDO,NO,XO,QO)
 0012               DO 11 J=1,NO
 0013               Q(J)=QUP(J)
 0014            11 X(J)=XUP(J)
 0015               Q(NO+1)=QO
 0016               X(NO+1)=XO
 0017               N=NO+2
 0018               DO 12 J=N,42
 0019               Q(J)=QDO(J-N+1)
 0020            12 X(J)=XDO(J-N+1)
 0021               IF (L-1) 18,18,17
 0022            18 CALL LINE(X,Q,42,1,0,0,0.0,-1.0,0.1,0.2)
 0023               GO TO 19
 0024            17 CALL LINE(X,Q,42,1,2,03,0.0,-1.0,0.1,0.2)
 0025            19 WRITE(6,50) ANG
 0026               WRITE(6,50) (X(K),K=1,42),XO
 0027               WRITE(6,50) (Q(K),K=1,42),QO
 0028            10 CONTINUE
 0029             9 CONTINUE
 0030               CALL AXIS(0.0,5.0,' ',-1,10.0,0.0,0.0,0.1,10.0)
 0031               CALL AXIS(0.0,0.0,' ',1,10.0,90.0,-1.0,0.2,10.0)
 0032               CALL PLOT(0.0,0.0,999)
 0033            50 FORMAT(1X,15F8.4)
 0034               STOP
 0035               END
```


The SUBROUTINE QUART is required and given in Appendix 5A.

APPENDIX 5C

A COMPUTER PROGRAM FOR TWO DIMENSIONAL RAY TRACING IN THE IONOSPHERE

This program consists of a main program, two SUBROUTINE programs, QUART and INTEG2, and a FUNCTION subprogram DX2DH. The SUBROUTINE INTEG2 (Y, H, NO, A) is used for integration of a given numerical function. The meanings of the arguments are as follows:

Y: Input vector of length NO to be integrated

H: Step width of integration

NO: Number of ordinates to be integrated

A: Output vector of length NO which gives the result of integration corresponding to each element of vector Y.

By calling this subprogram, the horizontal range y_k corresponding to k^{th} layer can be obtained.

In using this two dimensional ray tracing computer program, the following steps should be followed:

(1) Prepare a data card with FORMAT (2I4) which supplies the values for

NRAY = Number of ionograms to be ray traced, and

F = Frequency in MHz in this order.

(2) Prepare a data set for electron density profiles of the ionosphere to be ray traced with FORMAT (13F6.1). It is assumed that the punched output of the electron density profiles obtained by using the program given in Appendix 4B should be interpolated to give $N_e(z)$ at every 5 km interval starting from 80 km up to 1000 km.

(3) The data set is read in the order (1) and (2) above.

This program was written for ray tracing of radio path 1. For use at another radio path, m and n should be recalculated for that path and make the changes Y2=m and Y3=n in statements 5 and 6.

The initiating angle of incidence $\theta_I(1)$ was assumed to be 0.4 radian. If the angle other than this is chosen as $\theta_I(1)$, the statement 17 should be changed for this new value. The preassigned error distance ΔD was assumed to be 1 km. If the value other than 1 km is desired, statement 98 should be changed to read

IF (X2D(MD) - DIST - ΔD) 29, 30, 30

where ΔD refers to the new value desired. The distance between WWVH and the University of Hawaii is 152.2 km. If the distance other than this value is desired then statement 3 should be changed.

This program is written to print out the following data for each θ_I in the order.

(i) Horizontal ranges y_0, y_1, y_2, ..., y_m, y_0 for upgoing wave as shown in Figure 5.7.

(ii) Horizontal ranges y_1', y_2', ..., y_m', H for down coming wave as shown in Figure 5.7.

(iii) Height of reflection z_0.

(iv) When the ray homes in on the desired receiving point a dotted line will be printed out to indicate the end of ray tracing for one N(z) profile. If NRAY > 1, it will proceed to produce another ray tracing for the next N(z) profile.

Table 5C-1 shows the printed output of a ray tracing sample made on the electron density profile shown in Fig. 4.1. The required SUBROUTINE QUART is given in Appendix 5A.

```
FORTRAN IV G LEVEL  20                    MAIN                    DATE = 73227

            C     RAY TRACING BY BOOKER'S QUARTIC
0001                DIMENSION       XUP(41),XDO(41),OUP(41),ODO(41),QU(80),X(185)
                   2,QD(80),T1(80),T2(80),XZU(80),XZD(80),XD(64)
0002                DIST=152.2
0003                READ(5,51) NRAY,F
0004                Y=0.873/F
0005                Y2=-0.0466246*Y
0006                Y3=0.625297*Y
0007                DO 70 IK=1,NRAY
0008                READ(5,50) X
0009                DO  8 I=1,64
0010                IF(X(I)) 8,8,9
0011              8 CONTINUE
0012              9 ZO=75.0*I*5.0
0013                N=64
0014                K=I
0015                DO 10 I=K,N
0016             10 X(I-K+1)=(X(I)/12.400)/F**2
0017                A=0.4
0018                DA=0.1
0019                NOTRY=0
0020             31 DO 30 K=1,10
0021                ANG=A-(K-1)*DA
0022                C=COS(ANG)
0023                S=SIN(ANG)
0024                CALL QUART(ANG,F,QUP,QDO,XUP,XDO,NO,XO,QO)
0025                DO 11 I=1,N
0026                IF(X(I)-XO) 11,11,12
0027             11 CONTINUE
0028             12 NN=I-1
0029                DO 14 J=1,N
0030                IF(X(NN-J+1)-XUP(NO) ) 6,6,14
0031             14 CONTINUE
0032              6 NU=NN-J+1
0033                DO 7 I=1,NU
0034                DO 5 J=1,NO
0035                IF (XUP(J)-X(I)) 5,15,16
0036             16 QU(I) =((QUP(J)-QUP(J-1))/(XUP(J)-XUP(J-1)))*(X(I)-
                   2 XUP(J-1)) +QUP(J-1)
0037                GO TO 7
0038             15 QU(I)=QUP(J)
0039                GO TO 7
0040              5 CONTINUE
0041              7 CONTINUE
0042                DO 33 I=1,N
0043                IF (X(NU+I)-XO) 33,34,34
0044             33 CONTINUE
0045             34 DHI=5.0*I
```

```
FORTRAN IV G LEVEL  20                  MAIN                    DATE = 73227

0046              ZI=ZO+(NU-1)*5.0
0047              ZA=(XO-X(NU))*( DHI/(X(NU+I)-X(NU)))+ZI
0048              QQ=QU(NU)
0049              XX=X(NU)
0050              YY= DX2DH(Y,Y2,Y3,C,S,QQ,XX)
0051              X2AU=2.0*(ZA-ZI)*YY
0052              ND=NU
0053              NOD=41-NO
0054              DO 21 I=1,ND
0055              DO 3 J=1,NOD
0056              JJ=42-NO-J
0057              IF(XDO(JJ)-X(I))  3,22,23
0058           23 QD(I)=((QDO(JJ)-QDO(JJ+1))/(XDO(JJ)-XDO(JJ+1)))*
                 2 (X(I)-XDO(JJ+1))+QDO(JJ+1)
0059              GO TO 21
0060           22 QD(I)=QDO(JJ)
0061              GO TO 21
0062            3 CONTINUE
0063           21 CONTINUE
0064              QQ=QD(ND)
0065              XX=X(ND)
0066              YY= DX2DH(Y,Y2,Y3,C,S,QQ,XX)
0067              X2AD=-2.*(ZA-ZI)*YY
0068              DO 60 M=1,ND
0069              T1(M)=QD(M)
0070           60 T2(M)=X(M)
0071              DO 24 M=1,ND
0072              QD(M)=T1(ND-M+1)
0073           24 XD(M) =T2(ND-M+1)
0074              DO 25 I=1,NU
0075              QQ= QU(I)
0076              XX=X(I)
0077           25 T1(I)= DX2DH(Y,Y2,Y3,C,S,QQ,XX)
0078              DO 20 I=1,ND
0079              QQ=QD(I)
0080              XX=XD(I)
0081           20 T2(I)= DX2DH(Y,Y2,Y3,C,S,QQ,XX)
0082              CALL INTEG2(T1, 5.0,NU,X2U)
0083              CALL INTEG2(T2,-5.0,ND,X2D)
0084              X2=ZO*TAN(ANG)
0085              DO 26 I=1,NU
0086           26 X2U(NU-I+2)=X2U(NU-I+1)+X2
0087              X2U(1)=0.0
0088              MU=NU+2
0089              X2U(MU)=X2U(MU-1)+X2AU
0090              TT=X2U(MU)+X2AD
0091              DO 27 I=1,ND
0092           27 X2D(I   )=X2D(I)+TT
```

FORTRAN IV G LEVEL 20 MAIN DATE = 73227

```
              MD=MD+1
              X2D(MD)=X2D(MD-1)+X2
              NOTRY=NOTRY+1
              WRITE(6,53) NOTRY,ANG,K
              WRITE(6,52) (X2U(I),I=1,MU)
              WRITE(6,52) (X2D(I),I=1,MD)
              WRITE(6,57) ZA
              IF(X2D(MD)-DIST) 32,28,28
           28 IF(X2D(MD)-DIST-1.0) 29,30,30
           30 CONTINUE
           32 A=ANG+DA
              DA=DA/2.0
              A=A-DA
              GO TO 31
           29 WRITE(6,58) X2D(MD)
              WRITE(7,54) (X2U(I),I=1,MU)
              WRITE(7,54) (X2D(I),I=1,MD)
              WRITE(7,54) ZA
              WRITE (6,55)
           70 WRITE(6,56)
           50 FORMAT(13F6.1)
           51 FORMAT(I4,F5.1)
           52 FORMAT(4X,10F8.2)
           53 FORMAT(/I4,F12.7,I4)
           54 FORMAT(11F7.2)
           55 FORMAT('.......................................')
           56 FORMAT(1H1)
           57 FORMAT('     REFLECTION HEIGHT= ',F8.3)
           58 FORMAT(' HORIZONTAL RANGE= ',F8.3)
              STOP
              END
```

FORTRAN IV G LEVEL 20 INTEG2 DATE = 73234

```
              SUBROUTINE INTEG2(Y,H,NO,A)
C           Y=VECTOR OF LENGTH NO TO BE INTEGRATED
C             A=VECTOR OF LENGTH NO-1. RESULT OF INTEGRATION
              DIMENSION Y(1),A(1)
              A(1)=0.0
              T=Y(1)
              A(2)=(T+Y(2))*H/2.0
              DO 10 K=3,NO
              M=K-1
              T=Y(1)
              DO 11 L=2,M
              T=T+2.0*Y(L)
           11 A(K   )=(T+Y(K))*H/2.0
           10 CONTINUE
              RETURN
              END
```

FORTRAN IV G LEVEL 20 DX2DH DATE = 73234

```
              FUNCTION   DX2DH(Y,Y2,Y3,C,S,Q,X)
              T=C**2-Q**2
              DX2DH =(4.0*S*X**2+(-2.0*S*(2.0-Y**2+(S*Y2+Q*Y3)**2+
             2  2.0*T)+2.0*Y2*(S*Y2+Q*Y3)*T)*X+4.0*S*(1.0-Y**2)*T)/
             3  (4.0*Q*X**2+(-2.0*Q*(2.-Y**2+(S *Y2+C*Y3)**2+2.*T)+
             4  2.0*Y3*(S *Y2+Q*Y3)*T)*X+4.0*Q*(1.0-Y**2)*T)
              RETURN
              END
```

TABLE 5C-1 Printed Output of the Ray Paths for Two Dimensional Ray tracing Made on the Electron Density Profile Given in Figure 4.1.

```
1   0.4000000   1
     0.0     46.51   48.76   51.05   53.36   55.69   58.02   60.36   62.71   65.09
    67.51    69.95   72.43   74.95   77.50   80.09   82.73   85.41   88.14   90.92
    93.77    96.69   99.70  102.81  106.04  109.42  112.99  116.80  120.93  125.50
   130.68   136.83  144.90  160.90  172.89
   183.70   198.32  206.03  211.99  217.04  221.51  225.57  229.33  232.86  236.20
   239.40   242.48  245.47  248.37  251.20  253.97  256.68  259.34  261.97  264.55
   267.09   269.59  272.07  274.51  276.91  279.29  281.64  283.97  286.30  288.62
   290.92   293.21  295.46  341.97
 REFLECTION HEIGHT=  271.327

2   0.3000000   2
     0.0     34.03   35.67   37.33   39.02   40.70   42.40   44.10   45.81   47.53
    49.28    51.05   52.84   54.66   56.50   58.36   60.25   62.17   64.13   66.11
    68.14    70.22   72.34   74.53   76.79   79.15   81.61   84.20   86.97   89.95
    93.21    96.86  101.08  106.30  113.93  129.47
   143.99   151.16  156.15  160.23  163.77  166.96  169.88  172.60  175.16  177.58
   179.91   182.14  184.31  186.42  188.48  190.49  192.47  194.41  196.32  198.20
   200.05   201.88  203.69  205.48  207.24  208.98  210.70  212.41  214.10  215.79
   217.47   219.15  220.81  222.45  256.48
 REFLECTION HEIGHT=  279.138

3   0.2000000   3
     0.0     22.30   23.37   24.46   25.56   26.66   27.76   28.87   29.99   31.11
    32.25    33.40   34.57   35.75   36.94   38.15   39.38   40.62   41.88   43.17
    44.48    45.81   47.18   48.58   50.03   51.52   53.08   54.71   56.44   58.28
    60.26    62.43   64.85   67.64   71.08   75.90   98.48  101.50
   104.18   124.36  126.84  132.08  134.74  137.07  139.17  141.09  142.89  144.58
   146.18   147.71  149.18  150.61  151.99  153.34  154.66  155.96  157.23  158.48
   159.72   160.93  162.13  163.32  164.49  165.65  166.80  167.93  169.05  170.16
   171.27   172.37  173.47  174.56  175.65  176.72  199.01
 REFLECTION HEIGHT=  285.192

4   0.1000001   4
     0.0     11.04   11.57   12.11   12.65   13.19   13.74   14.29   14.84   15.39
    15.95    16.53   17.10   17.68   18.27   18.87   19.47   20.09   20.71   21.34
    21.99    22.65   23.32   24.01   24.72   25.45   26.21   27.01   27.85   28.74
    29.69    30.73   31.87   33.16   34.68   36.61   39.50   45.44
    50.74    53.33   55.06   56.45   57.64   58.71   59.69   60.60   61.45   62.25
    63.02    63.76   64.47   65.16   65.84   66.49   67.14   67.77   68.39   69.00
    69.61    70.20   70.79   71.37   71.95   72.52   73.08   73.64   74.19   74.74
    75.28    75.83   76.37   76.91   77.44   77.97   89.01
 REFLECTION HEIGHT=  289.125

5   0.1500000   1
     0.0     16.62   17.42   18.23   19.05   19.87   20.69   21.52   22.35   23.19
    24.04    24.89   25.76   26.64   27.53   28.43   29.34   30.26   31.20   32.15
    33.13    34.12   35.13   36.17   37.24   38.35   39.50   40.70   41.97   43.32
    44.77    46.35   48.09   50.08   52.45   55.56   60.88   67.80
    74.22    79.13   82.01   84.23   86.11   87.78   89.29   90.69   92.00   93.23
    94.41    95.53   96.62   97.67   98.69   99.69  100.67  101.62  102.57  103.49
   104.41   105.31  106.20  107.08  107.95  108.82  109.67  110.51  111.34  112.17
   112.99   113.81  114.63  115.44  116.25  117.05  133.67
 REFLECTION HEIGHT=  287.466

6   0.1750000   1
     0.0     19.45   20.38   21.33   22.29   23.25   24.21   25.18   26.15   27.13
    28.12    29.13   30.14   31.17   32.21   33.26   34.33   35.41   36.51   37.63
    38.77    39.93   41.12   42.34   43.59   44.89   46.25   47.66   49.16   50.75
    52.46    54.32   56.39   58.76   61.62   65.49   73.30   79.49
    85.30    92.60   96.19   98.89  101.14  103.13  104.93  106.59  108.13  109.59
   110.98   112.30  113.58  114.82  116.02  117.19  118.34  119.46  120.57  121.66
   122.73   123.79  124.83  125.87  126.89  127.90  128.89  129.88  130.86  131.83
   132.79   133.75  134.70  135.66  136.60  137.53  156.98
 REFLECTION HEIGHT=  286.397
```

```
 7   0.1499999   2
       0.0     16.62    17.42    18.23    19.05    19.87    20.69    21.52    22.35    23.19
     24.04     24.89    25.76    26.64    27.53    28.43    29.34    30.26    31.20    32.15
     33.13     34.12    35.13    36.17    37.24    38.35    39.50    40.70    41.97    43.32
     44.77     46.35    48.09    50.08    52.45    55.57    60.88    67.80
     74.22     79.14    82.01    84.23    86.11    87.78    89.29    90.69    92.00    93.23
     94.41     95.53    96.62    97.67    98.69    99.69   100.67   101.63   102.57   103.50
    104.41    105.31   106.20   107.09   107.96   108.82   109.67   110.51   111.34   112.17
    112.99    113.81   114.63   115.44   116.25   117.05   133.67
  REFLECTION HEIGHT=  287.466

 8   0.1624998   1
       0.0     18.03    18.90    19.78    20.67    21.56    22.45    23.35    24.25    25.16
     26.07     27.01    27.95    28.90    29.86    30.84    31.83    32.83    33.85    34.89
     35.94     37.02    38.12    39.25    40.41    41.61    42.86    44.17    45.55    47.02
     48.60     50.32    52.22    54.40    57.01    60.47    66.76    73.41
     79.66     85.53    88.75    91.20    93.26    95.09    96.74    98.27    99.69   101.04
    102.32    103.55   104.73   105.87   106.98   108.07   109.13   110.17   111.19   112.20
    113.20    114.18   115.14   116.10   117.05   117.98   118.91   119.82   120.72   121.62
    122.51    123.40   124.29   125.17   126.05   126.91   144.95
  REFLECTION HEIGHT=  286.955

 9   0.1687498   1
       0.0     18.74    19.64    20.56    21.48    22.40    23.33    24.26    25.20    26.14
     27.10     28.06    29.04    30.03    31.04    32.05    33.08    34.12    35.18    36.26
     37.35     38.47    39.62    40.79    42.00    43.25    44.55    45.91    47.35    48.88
     50.53     52.32    54.30    56.57    59.30    62.96    69.93    76.38
     82.33     88.77    92.17    94.74    96.90    98.80   100.53   102.12   103.61   105.01
    106.34    107.62   108.84   110.03   111.19   112.32   113.42   114.51   115.57   116.62
    117.65    118.67   119.68   120.67   121.66   122.63   123.59   124.54   125.48   126.41
    127.34    128.26   129.18   130.10   131.01   131.91   150.65
  REFLECTION HEIGHT=  286.672

10   0.1718748   1
       0.0     19.09    20.01    20.94    21.88    22.82    23.77    24.72    25.67    26.64
     27.61     28.60    29.59    30.60    31.62    32.66    33.70    34.77    35.85    36.94
     38.06     39.20    40.37    41.56    42.80    44.07    45.40    46.79    48.25    49.81
     51.49     53.32    55.34    57.66    60.46    64.21    71.58    77.91
     83.77     90.59    94.08    96.71    98.92   100.86   102.62   104.25   105.76   107.19
    108.55    109.85   111.11   112.32   113.50   114.65   115.77   116.88   117.96   119.03
    120.09    121.13   122.15   123.16   124.17   125.16   126.14   127.10   128.06   129.01
    129.96    130.90   131.84   132.77   133.70   134.62   153.71
  REFLECTION HEIGHT=  286.536

11   0.1687497   2
       0.0     18.74    19.64    20.56    21.48    22.40    23.33    24.26    25.20    26.14
     27.10     28.06    29.04    30.03    31.04    32.05    33.08    34.12    35.18    36.26
     37.35     38.47    39.62    40.79    42.00    43.25    44.55    45.91    47.35    48.88
     50.53     52.32    54.30    56.57    59.30    62.96    69.93    76.38
     82.33     88.77    92.17    94.74    96.90    98.80   100.53   102.12   103.61   105.01
    106.34    107.62   108.84   110.03   111.19   112.32   113.42   114.51   115.57   116.62
    117.65    118.67   119.68   120.67   121.66   122.63   123.59   124.54   125.48   126.41
    127.34    128.26   129.18   130.10   131.01   131.91   150.65
  REFLECTION HEIGHT=  286.672

12   0.1703122   1
       0.0     18.92    19.83    20.75    21.68    22.61    23.55    24.49    25.44    26.39
     27.35     28.33    29.32    30.32    31.33    32.35    33.39    34.44    35.51    36.60
     37.71     38.84    39.99    41.18    42.40    43.66    44.97    46.35    47.80    49.35
     51.01     52.82    54.82    57.12    59.88    63.59    70.74    77.09
     83.01     89.66    93.10    95.70    97.89    99.81   101.55   103.16   104.66   106.08
    107.43    108.71   109.95   111.16   112.32   113.46   114.58   115.67   116.75   117.81
    118.85    119.88   120.89   121.90   122.89   123.87   124.84   125.80   126.75   127.69
    128.63    129.56   130.49   131.42   132.34   133.24   152.16
  REFLECTION HEIGHT=  286.599

13   0.1710933   1
       0.0     19.01    19.92    20.85    21.78    22.72    23.66    24.60    25.56    26.51
     27.48     28.46    29.46    30.46    31.48    32.50    33.55    34.61    35.68    36.77
     37.88     39.02    40.18    41.37    42.60    43.87    45.19    46.57    48.03    49.58
     51.25     53.07    55.08    57.39    60.17    63.91    71.15    77.49
     83.39     90.11    93.58    96.20    98.39   100.33   102.08   103.70   105.21   106.63
    107.98    109.28   110.52   111.73   112.90   114.05   115.17   116.27   117.35   118.41
    119.46    120.49   121.51   122.52   123.52   124.51   125.48   126.44   127.40   128.34
    129.28    130.22   131.16   132.09   133.01   133.92   152.93
  REFLECTION HEIGHT=  286.572
HORIZONTAL RANGE=  152.928
```

APPENDIX 6

HILBERT TRANSFORM METHOD OF DETERMINING THE PERIOD OF RAYLEIGH-ACOUSTIC WAVE GENERATED IONOSPHERIC DOPPLER RECORDINGS

I. Introduction

Well-dispersed earthquake generated Rayleigh waves launch acoustic waves into the atmosphere and cause oscillatory disturbances in the ionosphere. These acoustic waves are designated as Rayleigh-acoustic waves throughout this paper. By employing the Doppler sounding technique (Davies, 1969), these oscillatory disturbances at ionospheric height can be recorded. The purpose of this paper is to present a method, which employs the Hilbert transform and the analytic signal representation, for the determination of the period of the oscillatory disturbances recorded. This method is designated as the Hilbert transform method. Besides Rayleigh-acoustic waves, oscillatory disturbances in the ionosphere can be generated by other effects such as the geomagnetic sudden commencement (Davies, 1969). Complication in analysis may arise due to different nature of different disturbances. So we confine our discussion to records representing disturbances caused by Rayleigh-acoustic waves only. Throughout the paper, the term "Doppler record" denotes only those records displaying oscillations caused by Rayleigh-acoustic waves.

The Doppler record has been shown to be a faithful representation of the time rate of change of the displacement of the long-period Rayleigh waves (Yuen et al., 1969) and is equivalent to what an ideal long-period seismometer for measuring vertical component of a disturbance would record. At present, records of long-period Rayleigh waves from seismometers are not very satisfactory. Most of the time they are contaminated by Love waves and the seimometers are unstable due to violent oscillations caused by the strong body waves which arrive before the Rayleigh waves (Furumoto, 1970). On the other hand, ionospheric Doppler recordings do not have such serious drawbacks. So, Doppler records play a unique and important role in representing the long period seismic

Rayleigh waves.

Analysis of Doppler records gives valuable information for earthquake source mechanism investigations and other seismic studies. An example is the experimental tsunami warning system established at the Radioscience Laboratory of the University of Hawaii (Furumoto, 1970; Najita et al., 1974). In the process of analyzing a Doppler record, one essential and significant piece of information needed is the period of the oscillations. Traditionally, the period of the oscillations recorded by seismometers, as well as by Doppler technique, has been determined by the so-called "peak and trough" method (Pekeris, 1948; Ewing and Press, 1954). In this paper, the Hilbert transform method and the "peak and trough" method are compared by applying them to a Doppler record.

Before we go into the details of the Hilbert transform method, we first need to discuss the Doppler record.

II. The Doppler Record

The motion at one point of a dispersive medium due to a disturbance applied earlier at another point may be represented by a superposition of traveling plane waves of different wave number k (Brune et al., 1960)

$$u(x,t) = \frac{1}{2\pi} \int_0^\infty A(k)\cos(\omega t - kx + \phi(k))dk \qquad (1)$$

where $u(x,t)$ is a component of the displacement which is a function of the space coordinate x and the time t. $A(k)$ is an amplitude function, ω the angular frequency, and $\phi(k)$ the initial phase as a function of wave number. Furthermore, Brune (1960) utilized the calculations given by Pekeris (1948) to show that when a wave train, which is generated by the disturbance applied at one point, has become sufficiently dispersed, Equation 1 may be evaluated by the method of stationary phase and shown to be approximately

$$u(x,t) \simeq \left\{\frac{1}{2\pi t\left|\frac{d^2\omega}{dk^2}\right|_0}\right\}^{1/2} A(k_0)\cos(\omega_0 t - k_0 x + \phi(k_0) \pm \frac{\pi}{4}) \qquad (2)$$

provided ω_0 is not too near an extremum of group velocity and the

amplitude does not vary too rapidly as a function of frequency. Equation (2) then indicates that the motion at large x will consist of nearly sinusoidal oscillations whose frequency and amplitude slowly vary with time (essentially because ω_0 and k_0 are functions of (x/t)). Thus at remote points away from the source, the wave-train will be well-dispersed, and oscillation of frequency ω_0 will occur when traveling plane wave components with frequencies equal to and near ω_0 arrive at the point and interfere constructively with one another.

The above results can, and have, been used in the case of Rayleigh waves from large earthquakes (Brune et al., 1960). Since a Doppler record is a faithful representation of well-dispersed Rayleigh waves, they can also be applied to the case of Doppler record. In general, an oscillation recorded by using the Doppler technique at a certain time can be pictured as caused by a Rayleigh wave component $x(t)$,

$$x(t) = A\cos(\omega t+\Phi) \tag{4}$$

where ω is the frequency, A is the amplitude, and Φ is the total phase shift. Actually, the amplitudes of the oscillations recorded are proportional to the particle velocity induced by the Rayleigh-acoustic waves. There is a $\pi/2$ phase difference between the peaks of displacement and the peaks of the Doppler frequency shift (Najita et al., 1974). This $\pi/2$ phase difference could be incorporated into the total phase shift Φ in (4). The ω in (4) is the frequency of the oscillation recorded, where reciprocal of ω gives the period of the oscillation.

III. The Hilbert Transform and The Analytic Signal

The Hilbert transform is frequently encountered in communication theory. The band-pass signals that are of interest in communication are signals that are generated by modulating a carrier signal by a narrow-band low-pass information-bearing signal. And the Hilbert transform provides an easy and elegant way to relate the band-pass modulated signal to the low-pass signal,

especially in single side-band modulation.

The Hilbert transform $\hat{x}(t)$ of a real-valued signal $x(t)$ is defined as (Kuo and Freeny, 1962; Schwarts et al., 1966)

$$\hat{x}(t) = \frac{1}{\pi} P \int_{-\infty}^{\infty} \frac{x(\tau)}{t-\tau} d\tau \tag{5}$$

and the inverse Hilbert transform as

$$x(t) = -\frac{1}{\pi} P \int_{-\infty}^{\infty} \frac{\hat{x}(\tau)}{t-\tau} d\tau \tag{6}$$

Where P denotes the Cauchy principle value of the integral at $\tau=t$. Let us demonstrate equation 5 by finding the Hilbert transform $\hat{x}(t)$ of the function in (4), $x(t) = A\cos(\omega t+\Phi)$. Substitute $\tau=t+\tau'$ in (5):

$$\hat{x}(t) = \frac{1}{\pi} P \int_{-\infty}^{\infty} (x(t+\tau')/-\tau')d\tau' \tag{7a}$$

$$= \frac{1}{\pi} P \int_{-\infty}^{\infty} (x(t+\tau)/-\tau)d\tau \quad . \tag{7b}$$

Then substitute (4) into the equation:

$$\hat{x}(t) = \frac{1}{\pi} P \int_{-\infty}^{\infty} (A\cos(\omega t+\omega\tau+\Phi)/-\tau)d\tau \tag{7c}$$

$$= \frac{A}{\pi} P \int_{-\infty}^{\infty} (\cos(\omega t+\Phi)\cos\omega\tau/-\tau)d\tau \tag{7d}$$

$$- \frac{A}{\pi} P \int_{-\infty}^{\infty} (\sin(\omega t+\Phi)\sin\omega\tau/-\tau)d\tau \quad . \tag{7e}$$

Since $\cos(\omega\tau)/\tau$ is and odd function, the first integral in the above equation is zero, and

$$\hat{x}(t) = \frac{A}{\pi} P \int_{-\infty}^{\infty} (\sin(\omega\tau)/\tau)d\tau \cdot \sin(\omega t+\Phi) \tag{7f}$$

$$= A\sin(\omega t+\Phi) \tag{7g}$$

This result will be helpful in later analysis.

In another approach, $\hat{x}(t)$ may be regarded as the response of a (non-realizable) linear filter to $x(t)$. This Hilbert

transform filter has impulse response $1/\pi t$ and transfer function $-j\mathrm{sgn}(f)$ (Kuo and Freeny, 1962; Schwartz et al., 1966), where $j=\sqrt{-1}$ and sgn(f) is defined as

$$\mathrm{sgn}(f) = \begin{cases} 1 & f>0 \\ 0 & f=0 \\ -1 & f<0 \end{cases} .$$

So, if X(f) is the Fourier transform of x(t), then

$$\hat{X}(f) = -j\mathrm{sgn}(f)\cdot X(f) \tag{8}$$

and

$$\hat{x}(t) = (1/\pi t)*x(t) , \tag{9}$$

where * denotes the convolution.
Other properties of Hilbert transform are discussed in the literatures dealing with communication theory.

Now let us discuss the meaning of the analytic signal. The analytic signal representation of a real waveform was first introduced by Gabor (1946), and is now used widely in communication theory as a means of representing band-pass signals. The analytic signal z(t) of a real waveform x(t) - sometimes referred to as the pre-envelope and the complex signal - is defined as (Kuo and Freeny, 1962; Schwartz et al., 1966)

$$z(t) = x(t)+j\hat{x}(t) , \tag{10}$$

where $\hat{x}(t)$ is the Hilbert transform of x(t) ($\hat{x}(t)$ is sometimes called the quadrature function of x(t) in this case). Equation (10) can be expressed in another form,

$$z(t) = A(t)e^{j\theta} , \tag{11}$$

where

$$A(t) = |z(t)| = (x(t)^2+\hat{x}(t)^2)^{1/2} \tag{12}$$

and

$$\theta = \tan^{-1}(\hat{x}(t)/x(t)). \tag{13}$$

$A(t)$ is the amplitude, θ the instantaneous phase, and the time derivative of θ the instantaneous frequency of the analytic signal $z(t)$ (Schwartz et al., 1966).

IV. The Determination of Period by the Hilbert Transform Method

In section II, we have shown that an oscillation recorded by the Doppler technique is caused by a cosinusoid described by (4): $x(t) = A\cos(\omega t+\Phi)$. From (7g), the Hilbert transform of $A\cos(\omega t+\Phi)$ is $\hat{x}(t) = A\sin(\omega t+\Phi)$. Therefore, the analytic signal representation of $x(t)$ is, from (10)

$$z(t) = A\cos(\omega t+\Phi)+Aj\sin(\omega t+\Phi) \tag{14}$$

From (13) and (14), the instantaneous phase is

$$\theta = \tan^{-1}(\sin(\omega t+\Phi)/\cos(\omega t+\Phi))$$

$$= \tan^{-1}(\tan(\omega t+\Phi))$$

$$\therefore \theta = \omega t+\Phi \quad . \tag{15}$$

Differentiating both sides of (15) with respect to time t, we find that the frequency ω of $x(t)$ is equal to the instantaneous frequency of its analytic signal representation, since Φ is independent of t. That is, finding the frequency ω is the same as finding the instantaneous phase of the analytic signal, and then calculating its time derivative. So, the problem reduces to one of determining the instantaneous phase.

Now, let us transform the analytic signal into the frequency domain,

$$Z(f) = X(f)+j\hat{X}(f) \tag{16}$$

where $Z(f)$ is the Fourier transform of $z(t)$. From (8)

$$\hat{X}(f) = -j\,\mathrm{sgn}(f)\cdot X(f) \ ,$$

so $Z(f) = X(f)+j(-j\text{sgn}(f)\cdot X(f))$

$= X(f)+\text{sgn}(f)X(f)$

$$\therefore Z(f) = \begin{cases} 2X(f) & f>0 \\ X(f) & f=0 \\ 0 & f<0 \end{cases} \qquad (17)$$

Therefore, it follows that the instantaneous phase of the analytic signal representation $z(t)$ of a real signal $x(t)$ can be determined using the following algorithm:

1. Transform $x(t)$ into $X(f)$,
2. Cancel the negative frequency terms and multiply the positive frequency terms by 2. This will give $Z(f)$,
3. Transform $Z(f)$ back into $z(t)$ and plot θ, the instantaneous phase.

V. Practical Consideration

Since Fourier transform is involved in the computation of an analytic signal, a computer is convenient. At present, the most efficient way of doing Fourier transform is by using the Fast Fourier Transform (FFT) routine on a digital computer. Detailed description of writing and using the FFT routine is given by Brigham (1974).

In using a digital computer to calculate the analytic signal representation of a whole Doppler record, it is possible to input the whole Doppler record at one time and display the result by plotting the instantaneous phase as a function of time (i.e., using the same time axis as the Doppler record). Then, by taking the time derivative or the slope of the phase plot, the period at any time can be determined.

Techniques of proper handling a waveform in digital Fourier Transform analysis are discussed in many literatures. Since a continous Doppler record must be sampled discretely

in order to utilize a digital computer, the limitations due to the effect of sampling must be observed: The sampling theorem - a waveform x(t) should be sampled at a frequency of at least twice the largest frequency component of x(t) - must not be violated. Aliasing and leakage must be avoided. Two additional important points in finding the analytic signal are:

1. In the process of finding the analytic signal, the negative frequency terms are truncated. Discontinuity may occur at zero frequency and thus may violate the sampling theorem. So the zero frequency term should be filtered out or kept to a minimum before doing the inverse transform.
2. Since the calculation of the analytic signal of a waveform effectively involves convolution of the waveform with the slowly decaying kernel $1/\pi t$ of the Hilbert transform, the analytic signal representation will be unreliable near the beginning and end of the waveform (White and Cha, 1973).

Two examples of period determination by means of the analytic signal are given below. The first involves a sinusoid of a known period T, as shown in Figure 1. The instantaneous phase plot is given in Figure 2. By taking the time derivative of the phase plot, one can show that the instantaneous frequency found in Figure 2 is exactly equal to the frequency of the sinusoid in (1). The second example involves the 10 MHz. Doppler record obtained from the Radioscience Laboratory of the University of Hawaii at Manoa shortly after the Hachinohe, Japan earthquake of May 16, 1968. The Doppler record is shown in Figure 3 and its instantaneous phase plot is in Figure 4. One can determine the frequency at one time by measuring the slope of the phase plot at the time.

VI. Discussion

Without a digital computer, the determination of period by the Hilbert transform method becomes extremely difficult if not

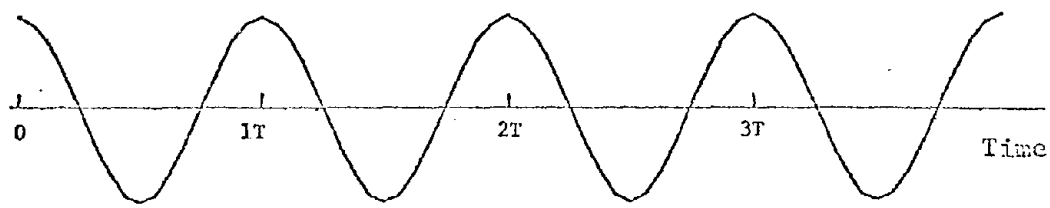

Figure 1. A Sinusoid with a constant Period T.

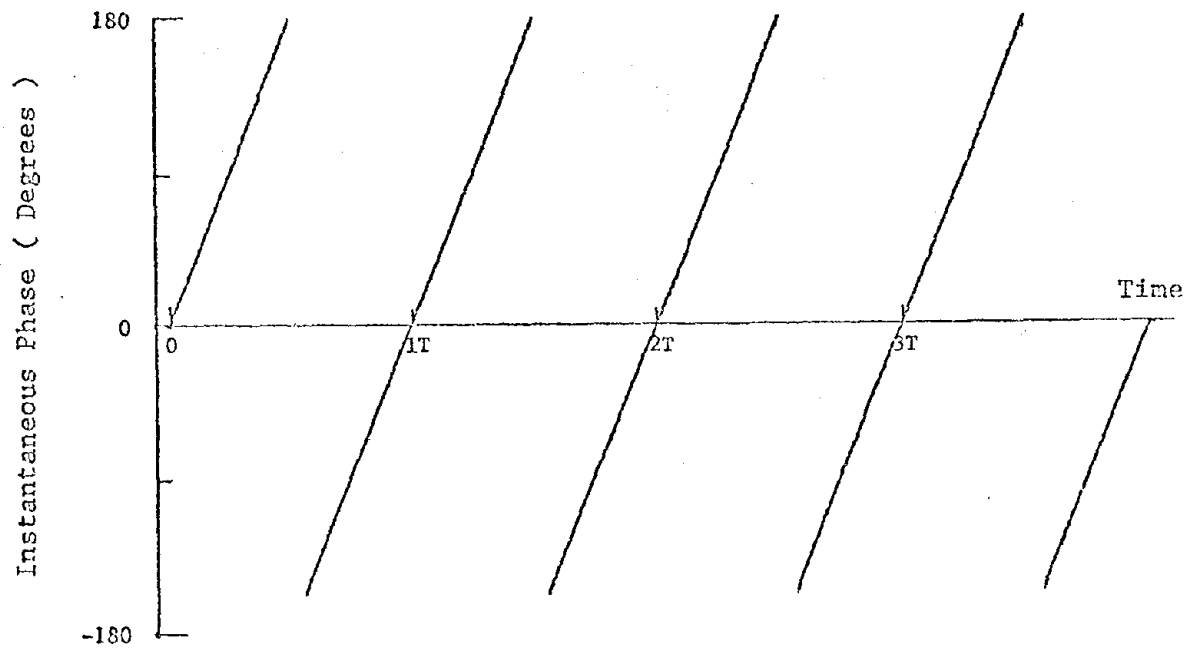

Figure 2. Instantaneous Phase Plot of the Sinusoid with Period T.

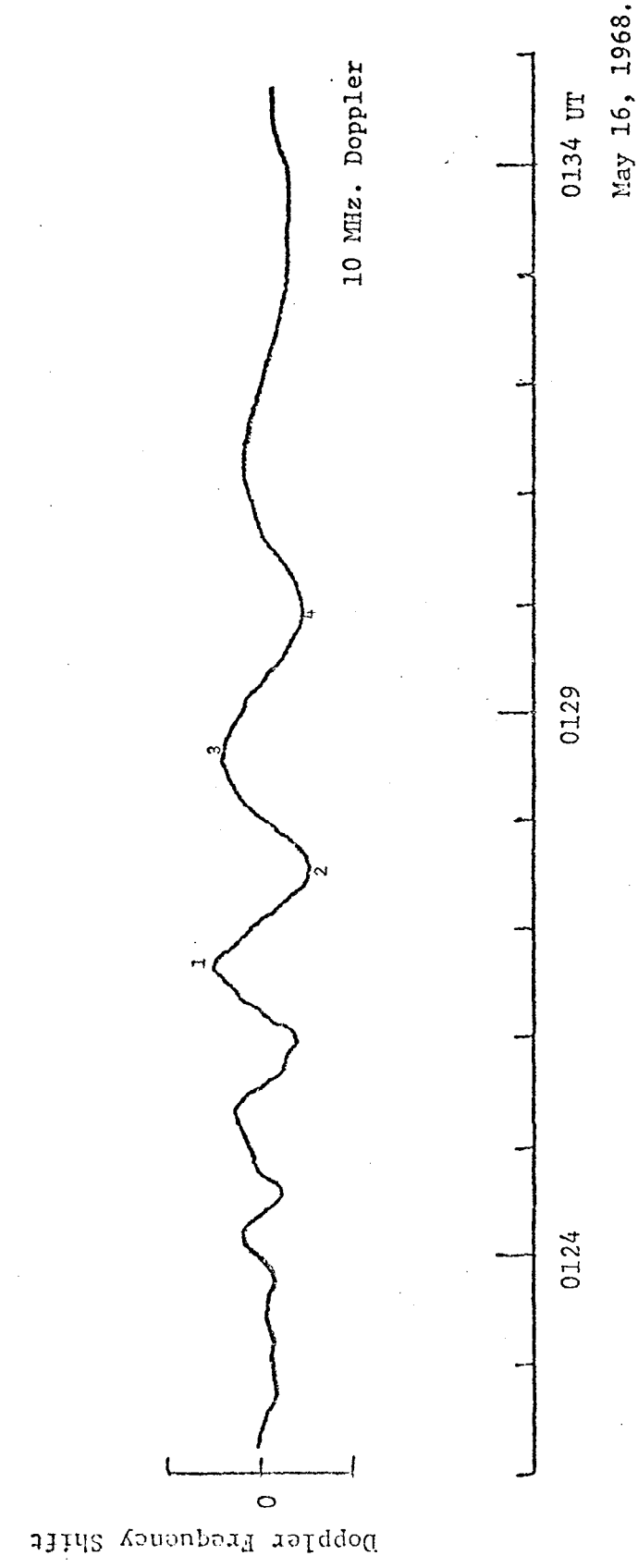

Figure 3. Doppler Shift Record from the Hachinohe, Japan Earthquake.

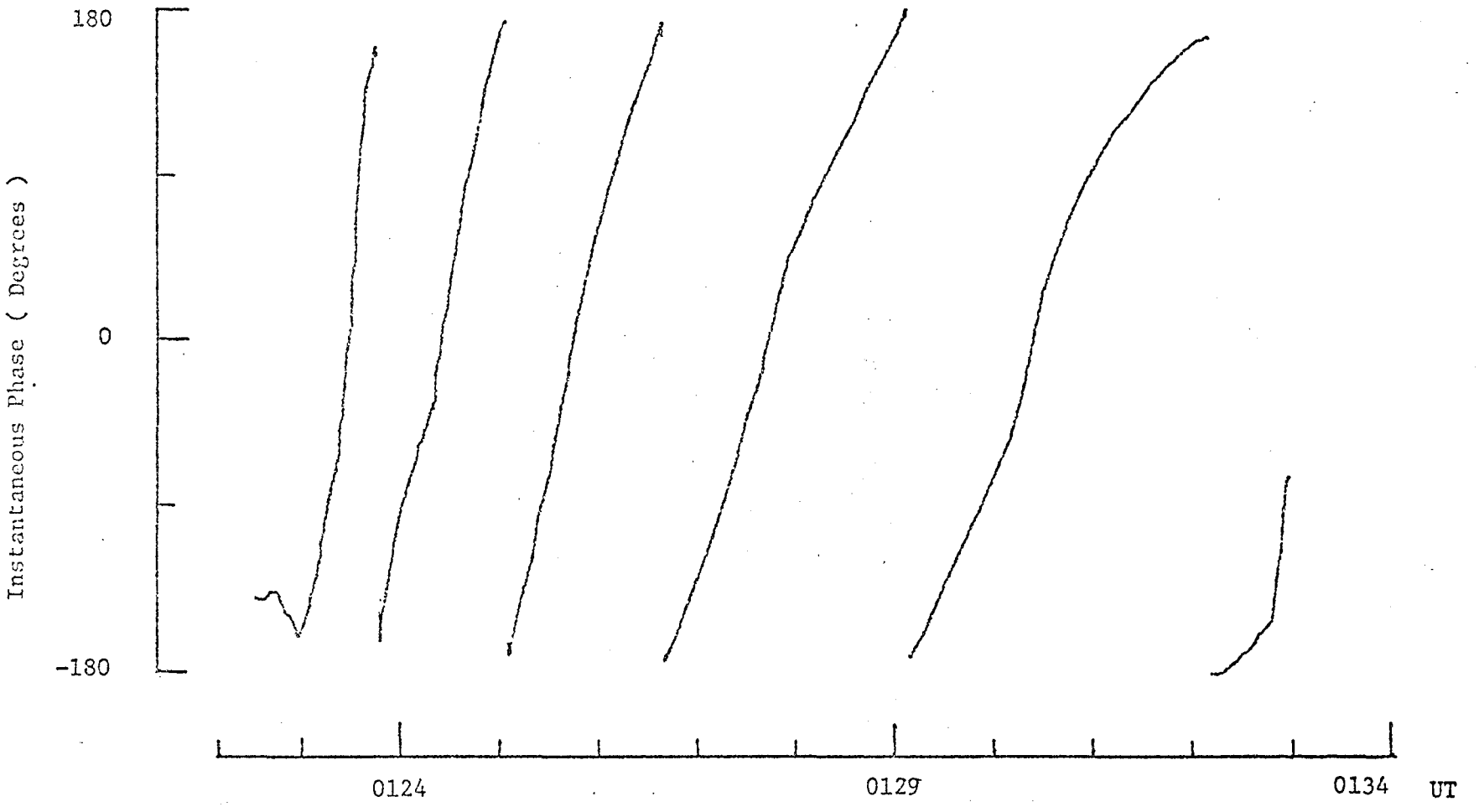

Figure 4. Instantaneous Phase Plot of the 10 MHz. Doppler Record from the Hachinohe, Japan Earthquake.

impossible. Although the analytic signal representation of a waveform was introduced many years ago, the expensiveness and the inefficiency of an early digital computer would certainly have hindered any attempt to use the analytic signal representation in time series analysis. With the introduction of FFT in 1965 and the unprecedented low price and high speed of mini-computers today, the determination of the period of a Doppler record by this method has become feasible. For example, the entire process from digitizing the Doppler record in Figure 3 to plotting the instantaneous phase in Figure 4 takes about 10 minutes using a Hewlett Packard programmable desk calculator system.

Traditionally, the period of the oscillations recorded by seismometers and by Doppler technique has been determined by the so-called "peak and trough" method. A description of this method may be found in Pekeris (1948) and Ewing and Press (1954). Briefly, one reads off the time T_n of the n-th maximum or minimum, and plots T_n against n. Then a smooth and continuous curve is drawn through the plotted points. The period at time T_n is obtained by measuring the slope of the curve at T_n. The crucial step in this method is the fitting of a curve to the plotted points. Since there is no standard way of fitting a curve (a least square fit may not be the best), error may be introduced. Figure 5 shows the curve obtained by applying the "peak and trough" method to the Doppler record in Figure 3. The periods of the labelled peaks and troughs obtained from Figure 4 together with those obtained from Figure 5 are entered into Table 1.

By comparing the two rows of values in Table 1, one can see that they are different for every event. There is no systematic error in going from Event 1 to Event 4: the values of Event 1 and Event 2 obtained by using the Hilbert transform method are smaller than those obtained by using the "peak and trough" method, but the values of Event 3 and Event 4 obtained by using the Hilbert transform method are greater than those obtained by using the "peak and trough" method. The differences between the values obtained from the two methods for Events 1, 2, and 4 are small and can be accounted for by errors introduced when measuring the slope

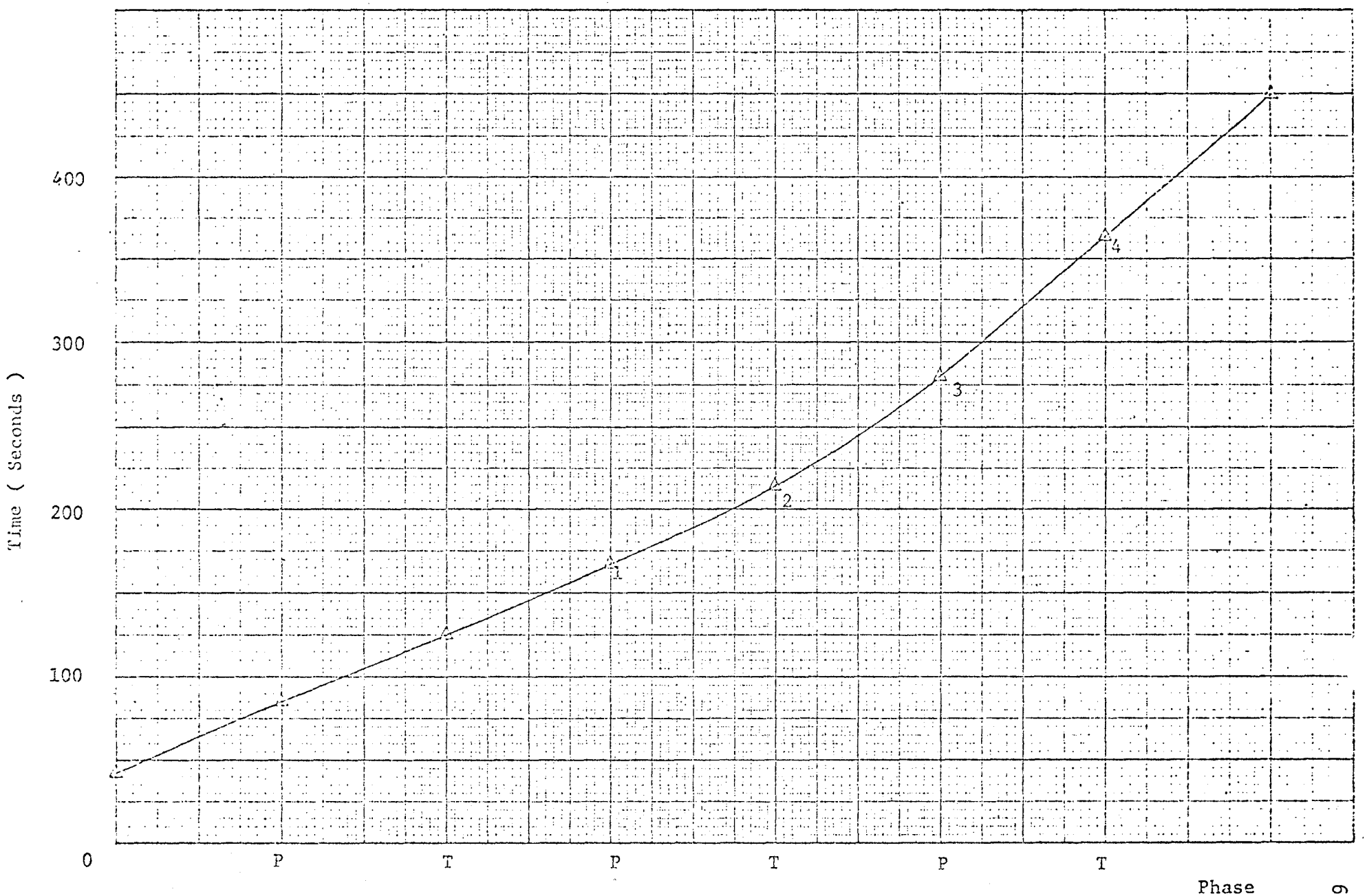

Figure 5. Arrival-time curve of the 10 Mhz. Doppler Record from the Hachinohe, Japan Earthquake.

P = Peak, T = Trough.

Event		1	2	3	4
Period (seconds)	Hilbert Transform Method	80	108	170	173
	Peak and Trough Method	85	114	151	170

Table 1. Periods of labelled events obtained by using two different methods.

of the instantaneous phase plot. But there is a substantial difference between the values for Event 3. One possible explanation for this difference is the error introduced when fitting a curve to the plotted points in the "peak and trough" method as mentioned earlier in this section. Obviously, one advantage of the Hilbert transform method over the "peak and trough" method is that no curve fitting is necessary. But without exhaustive error analysis - which we shall not discuss in this paper due to its complexity - it is difficult and premature to judge which method gives the better result.

References

Brigham, E. O., The Fast Fourier Transform, Prentice-Hall Inc., 1974.

Brune, J. N., J. E. Nafe, and J. E. Oliver, A Simplified Method for Analysis and Synthesis of Dispersed Wave Trains, J. Geophys. Res., 65, 287, 1960.

Davies, K., Ionospheric Radio Waves, Blaisdell Publishing Company, 1969

Ewing, M., and F. Press, An Investigation of Mantle Rayleigh Waves, Bull. Seismol. Soc. Am., 44, 127, 1954.

Furumoto, A. S., Ionospheric Recordings of Rayleigh Waves For Source Mechanisms, Tsunamis in the Pacific Ocean, Proceedings of International Symposium on Tsunami and Tsunami Research, University of Hawaii, East-West Center Press, 1970.

Gabor, D., Theory of Communication, J.I.E.E., 93, 429, 1946.

Kuo, F. F., and S. L. Freeny, Hilbert Transforms and Modulation Theory, Proc. Nat. Electron. Conf., 51, Chicago, 1962.

Najita, K., P. F. Weaver, and P. C. Yuen, A Tsunami Warning System Using an Ionospheric Technique, Proc. IEEE, 62, 563, 1974.

Pekeris, C. L., Theory of Propagation of Explosive Sound in Shallow Water, Geol. Soc. Am. Mem., 27, 1948.

Schwartz, M., W. R. Bennett, and S. Stein, Communication Systems and Techniques, 29, McGraw-Hill, 1966.

White, O. R., and M. Y. Cha, Appendix to Analysis of the 5 Min. Oscillatory Photospheric Motion, Solar Physics, 31, 42, 1973.

Yuen, P. C., P. F. Weaver, and R. K. Suzuki, Continuous, Traveling Coupling between Seismic Waves and the Ionosphere Evident in May 1968 Japan Earthquake Data, J. Geophys. Res., 74, 2256, 1969.

APPENDIX 7
METHOD OF DETERMINING THE INITIAL PHASE OF THE SOURCE OF AN EARTHQUAKE FROM THE DOPPLER RECORDS

Introduction

Rayleigh waves from large earthquakes generate acoustic waves up into the atmosphere and cause delayed oscillations in the ionosphere. These oscillations were confirmed experimentally (Yuen et al., 1969) by employing the Doppler technique.

Doppler records obtained after the Kurile Island Earthquake on August 11, 1969, had been investigated in detail and a method was suggested by Dr. A. S. Furumoto (1970) relating data obtained from the Doppler record to the initial phase of the source.

In this report, a few modifications on the process of locating the initial phase of the source of an earthquake are discussed. Examples are given to illustrate the modifications.

Outline of Furumoto's Method

The details pertaining to Furumoto's method will not be reproduced here. The reader is referred to Furumoto's paper (1970) for a complete picture of the method. However, an outline of his method is given below for the purpose of comparison. The outline is divided into seven steps for easy identification:

1. Identify and label peaks and troughs on the Doppler record. For example, a trough that appeared first on the Doppler record is labelled as Event 1.
2. Find out the time of arrival of each event and determine the period associated with each event using the Peak and Trough method (Ewing and Press, 1954). The time of arrival of an event is the arrival time of the Rayleigh-acoustic waves at the ionospheric reflector.
3. From the data given by Ben-Menahem and Toksoz (1962), determine the phase velocity that corresponds to each event.
4. Tabulate the period, character, phase velocity and the time lag of each event. The time lag of an event is the difference in time between the event and Event 1.
5. Estimate the location where the Rayleigh-acoustic refraction from the ground took place. This location is called the launching point for the Rayleigh-acoustic wave. Also, find out the epicentral distance -

distance between the epicenter of an earthquake and the sub-ionospheric point.

6. Construct wave trains of all the events at the time when Event 1 reached the launching point. At that time, other events were behind Event 1 at a distance equal to the product of phase velocity and time lag. The wave trains are constructed from the launching point back towards the epicenter until a distance is found where the phases from all the trains are in agreement. This is the initial phase of the wave components.
7. When a wave leaves a source, there is an advance of $\pi/4$ in phase for normal branch of dispersion ($dV/dT > 0$, V = group velocity, T = period) (Brune et al., 1961). Hence, the initial phase of the source is $\pi/4$ behind the initial phase of the wave components.

Modifications

A. Estimation of travel time required and horizontal distance elapsed for the Rayleigh-acoustic wave to refract from the launching point up to the ionospheric reflector.

Ray tracing on the Rayleigh-acoustic wave was done by the staff of the Radioscience Laboratory using an IBM 360 computer. Phase velocities were used in the calculation. The results are displayed in Figure 1 and Figure 2. Figure 1 shows the delay time as a function of height and period. Figure 2 shows the horizontal range elapsed as a function of height and period. For a fixed height, a curve showing the relationship between the period and the horizontal range can be constructed using data from Figure 1 and Figure 2 respectively. For example, Figure 3 shows the delay time for different periods of Rayleigh-acoustic wave to reach an altitude of 300 kilometers, and Figure 4 shows the horizontal distance elapsed for that altitude. The curve showing the delay time as a function of period is used to correct the time lag in Step 4 of Furumoto's method, and the curve showing the horizontal range elapsed is used to determine the accurate location of the launching point in Step 5.

B. Location of the initial phase on a wave train plot.

A different approach is introduced here for locating the initial phase on a wave train. In the wave train plot in Step 6, the abscissa represents the straight line path on the earth's surface passing through the epicenter and the launching point. Since the wave train is plotted in a triangular

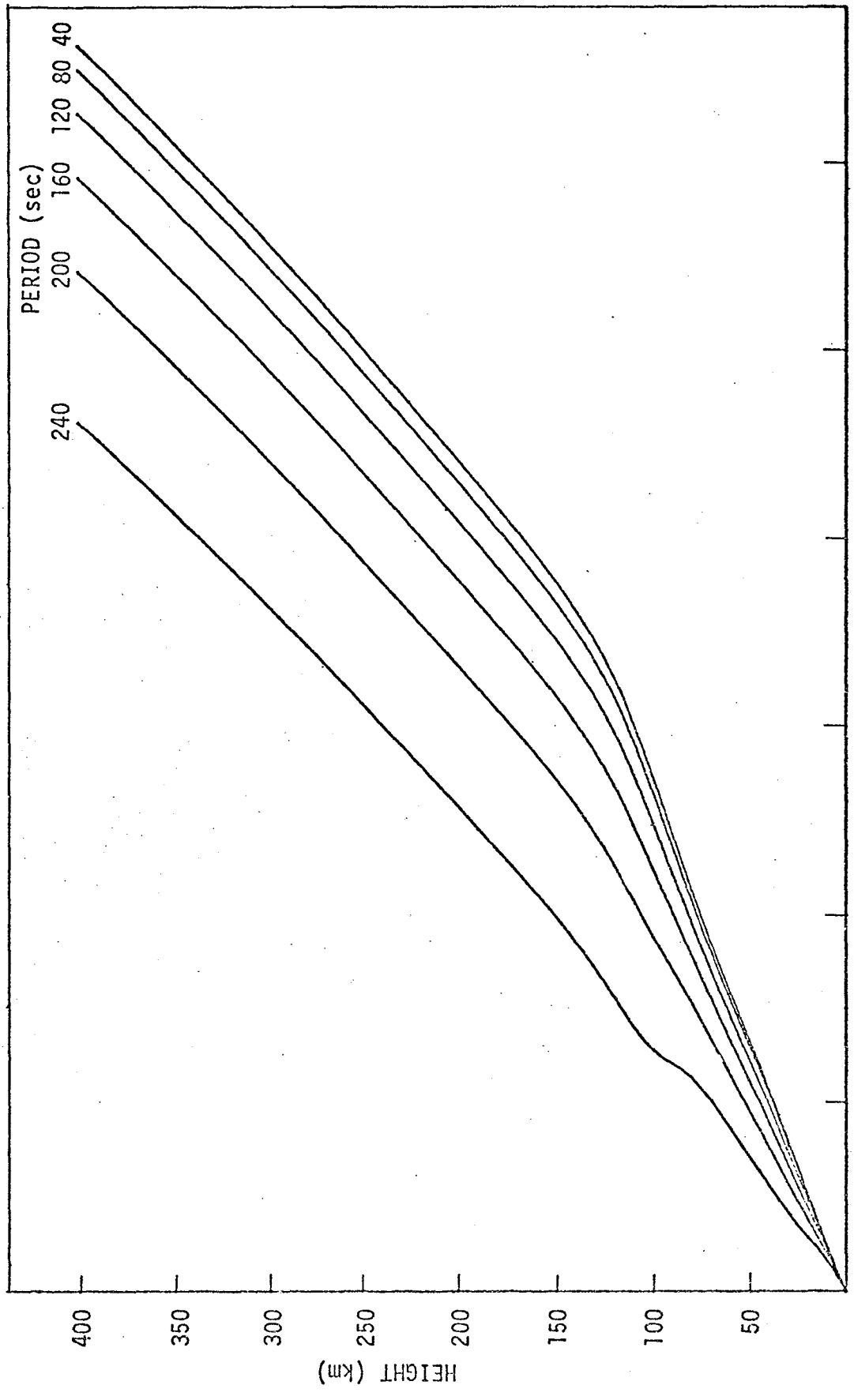

Figure 1. Travel time along ray-paths as a function of height and period.

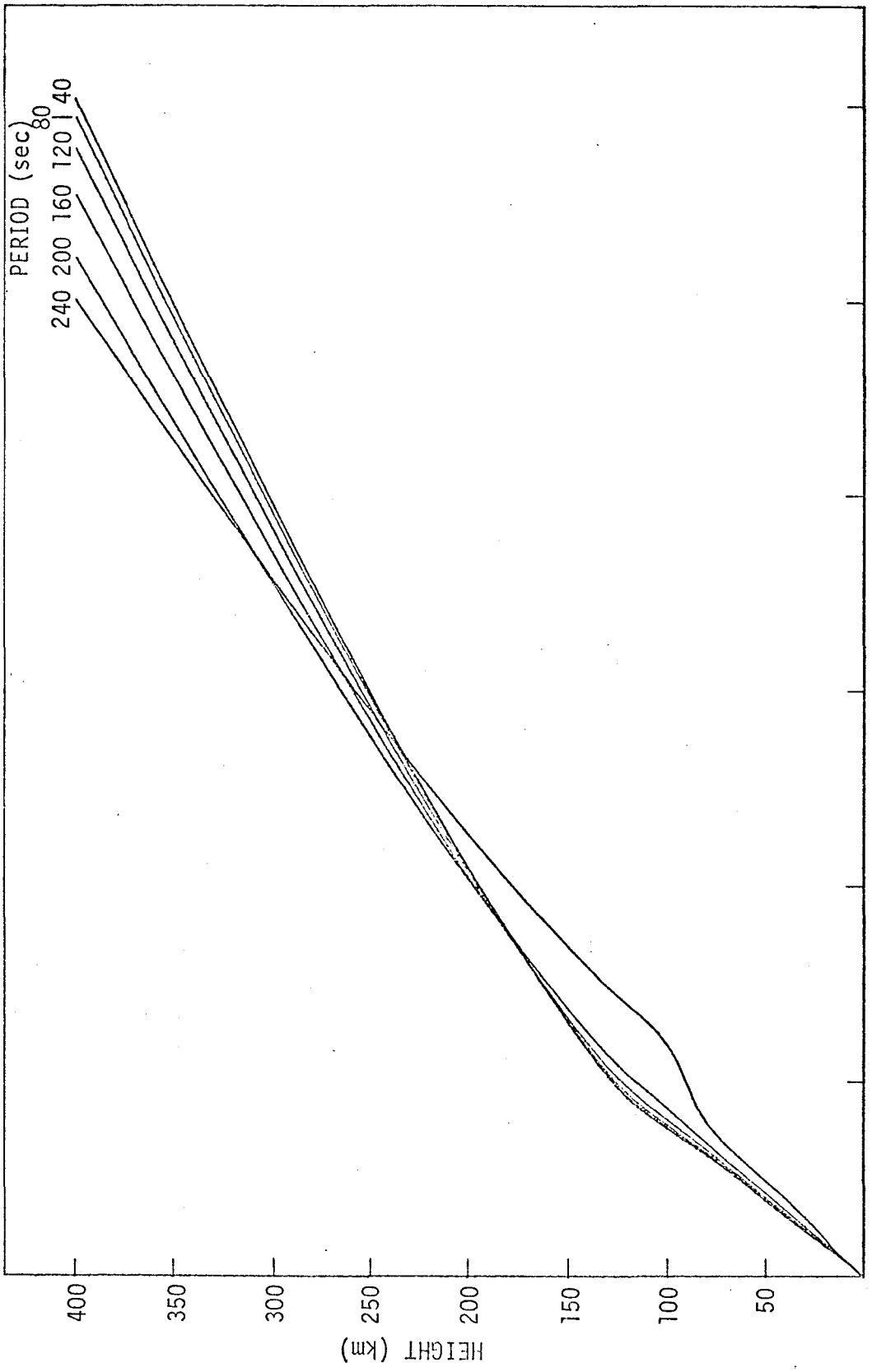

Figure 2. Ray-paths for infrasonic waves parameterized in terms of periods.

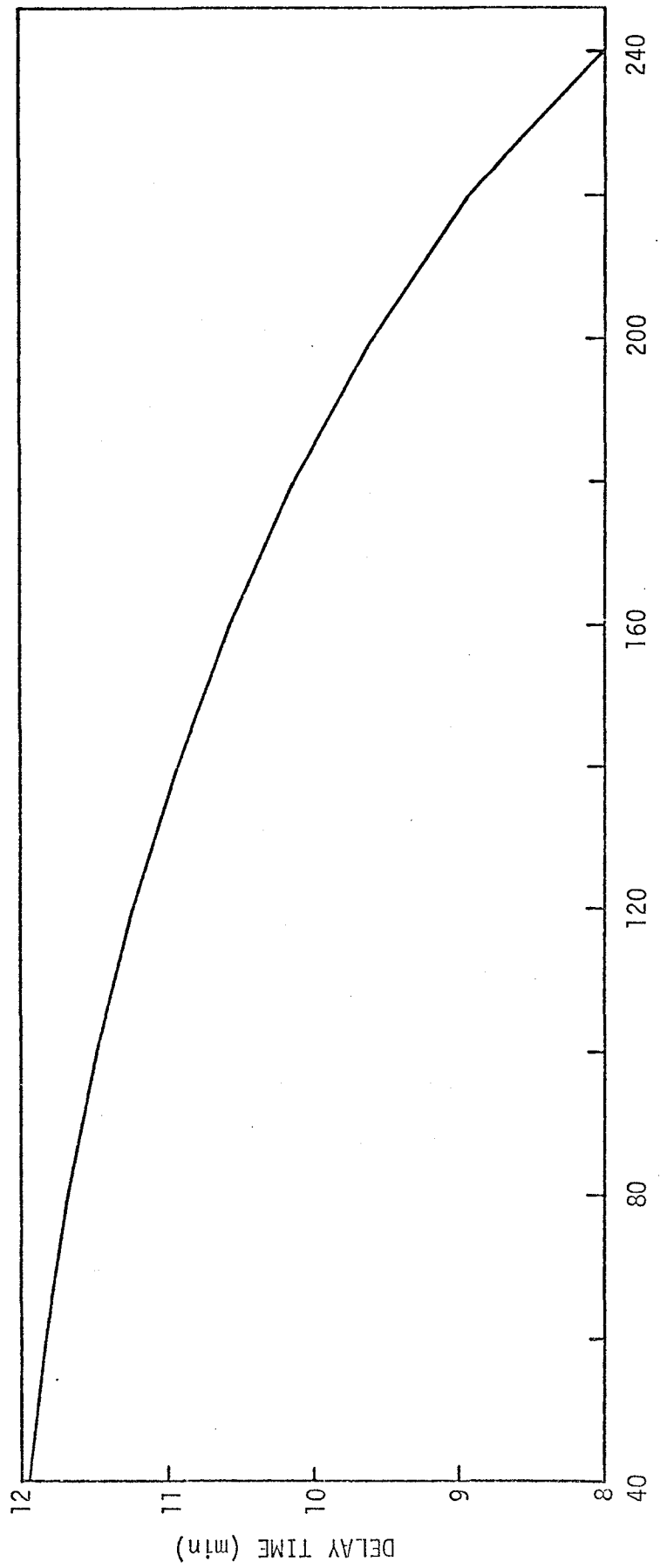

Figure 3. Delay time as a function of period.

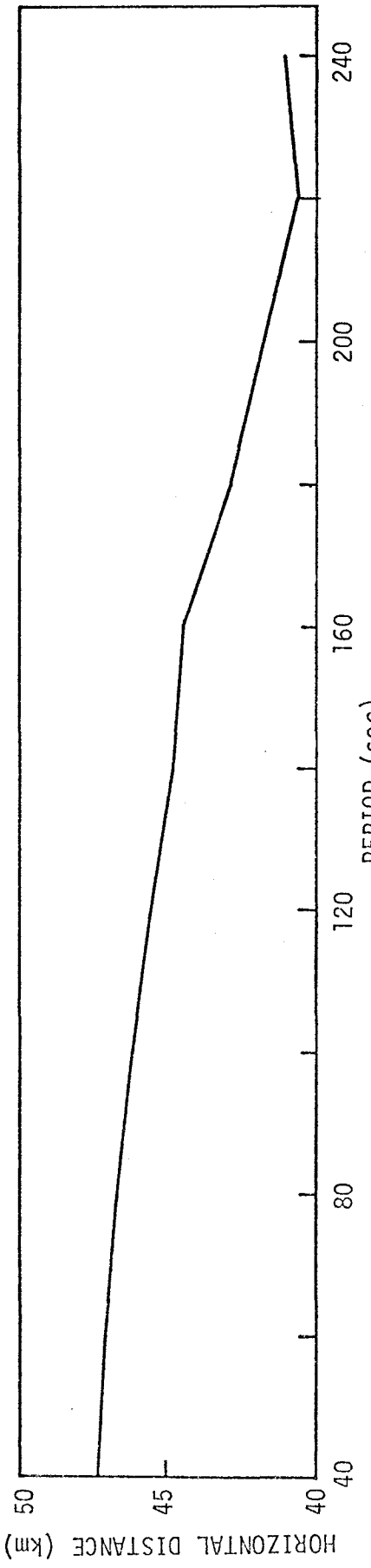

Figure 4. Horizontal displacement as a function of period.

wave pattern with constant amplitude, the ordinate has no meaning except in identifying the pase at a certain location. So, the wave train plot represents the phase variation with respect to distance of a component of the Rayleigh wave packet at a certain instant of time.

When an earthquake occurred, assume it occurred at time t_o, a Rayleigh wave packet was generated from the epicenter. This wave packet can be Fourier analyzed showing an infinite number of wave components with different periods but have the same initial phase. Since the medium is dispersive, they have different phase velocities. The phase velocity V_p of a wave component with certain period can be estimated readily from Figure 2 given in Dorman (1969) or from data given by Ben-Menahem and Toksoz (1962), it is therefore possible to calculate the distance d the initial phase has travelled in a certain period of time t by the simple equation

$$d = V_p t.$$

Since all the wave trains are plotted at the time when Event 1 reached the launching point, let this time be t_1, therefore $t = t_1 - t_o$, and the distance d of the initial phase from the epicenter can be determined:

$$d = V_p(t_1 - t_o).$$

Once the location of the epicenter is known, this distance can be located on the wave train plot to give the initial phase.

C. Initial phase of the source.

A Doppler record shows the Doppler frequency shift with respect to time. In order to apply the $\pi/4$ phase shift mentioned in Step 7, the Doppler record must be translated into a displacement curve. In translating the Doppler record into a displacement curve, there is an advance of $\pi/2$ in phase as shown in Figure 5. Together with the $\pi/4$ advance in phase when a wave leaves a source, the total change in phase is $\pi/4$ when relating the Doppler record to the source. Hence, the initial phase of the source is $\pi/4$ in advance of the initial phase obtained from a wave train plot.

Examples

The August 11, 1969 Kurile Earthquake was used by Dr. Furumoto to illustrate his method. So data from the same earthquake are used here to illustrate the suggested modifications.

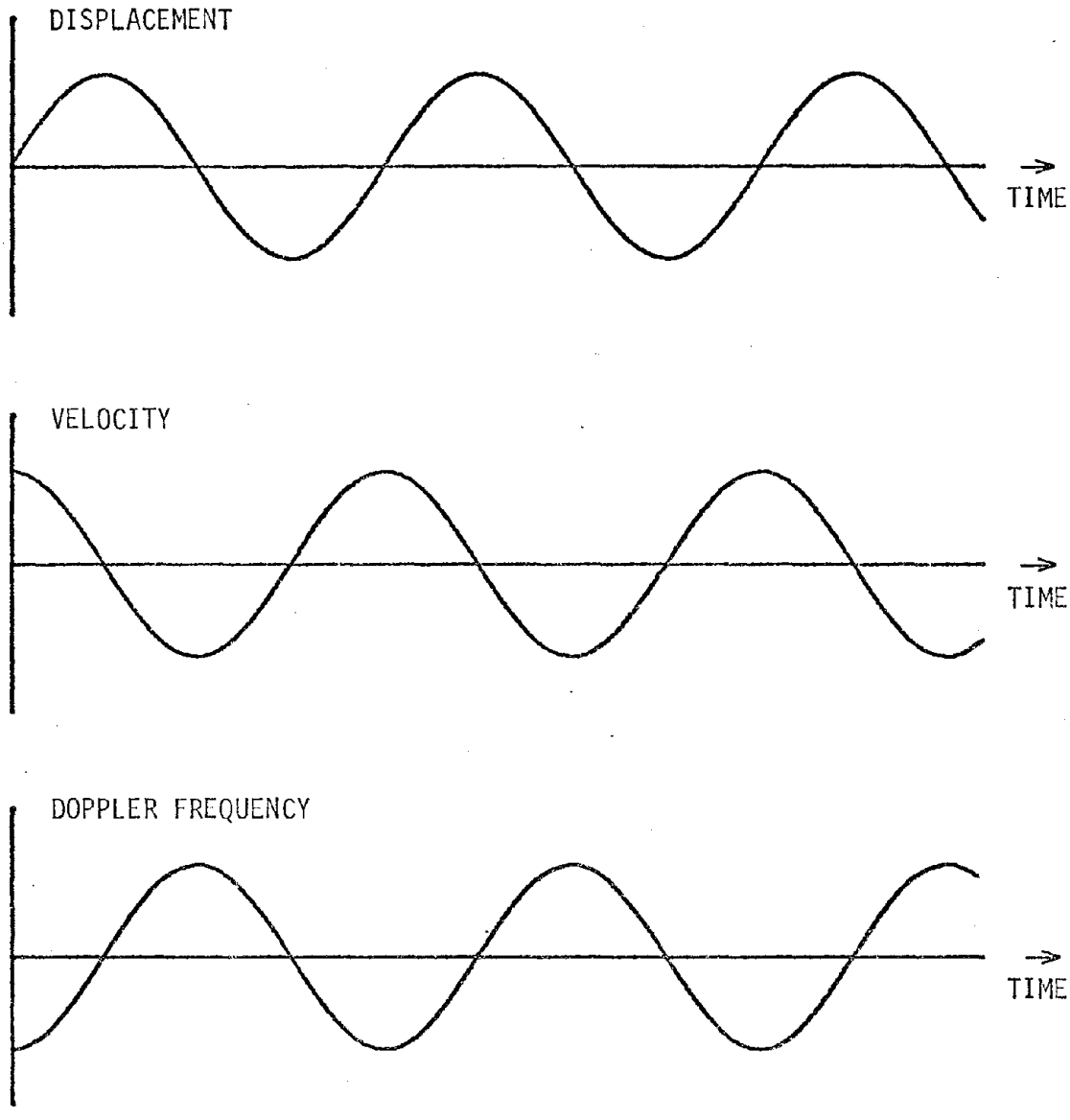

Figure 5. Phase difference between the displacement curve and the Doppler record.

The August 11, 1969 Kurile Earthquake was used by Dr. Furumoto to illustrate his method. So data from the same earthquake are used here to illustrate the suggested modifications.

The 10 MHz Doppler record obtained shortly after the Kurile Earthquake is shown in Figure 6. One can notice that the long period peaks and troughs are labelled. Table 1 shows all the data needed for constructing the wave trains and for locating the initial phase on each wave train. Values in column A through D of Table 1 are obtained directly from Table 1 found in Furumoto's paper (1970). In column E, values of the delay time are obtained from Figure 3. In column F, values of the horizontal distance elapsed are obtained from Figure 4. Time of arrival in column G is obtained directly from the Doppler record shown in Figure 6. Column H shows the time when the acoustic wave was launched. In column I, the distance compensation represents the distance of an event from the launching point of Event 1. Column J gives the wave length and column K the distance of initial phase from the epicenter of an event. Figure 7 is the wave train plot based on data from Table 1. In constructing the wave train plot, the epicenter is used as the reference point. The launching point for Event 1 is located by measuring the distance of the launching point from the epicenter. Triangular wave train is then constructed starting from the launching point. The location of the initial phase is then determined by measuring the distance between the initial phase and the epicenter. The above procedure is repeated for other events. The arrows in Figure 7 indicate the locations of the initial phase. All events except event 2 show good agreement in initial phase.

Another example is given here. Figure 8 shows the 10 MHz Doppler records from the Hachinohe, Japan Earthquake of May 16, 1968 with the peaks and troughs labelled. Table 2 gives all the data needed for the wave train plot. The plot is shown in Figure 9. Again, all the events show an astoundingly good agreement in initial phase.

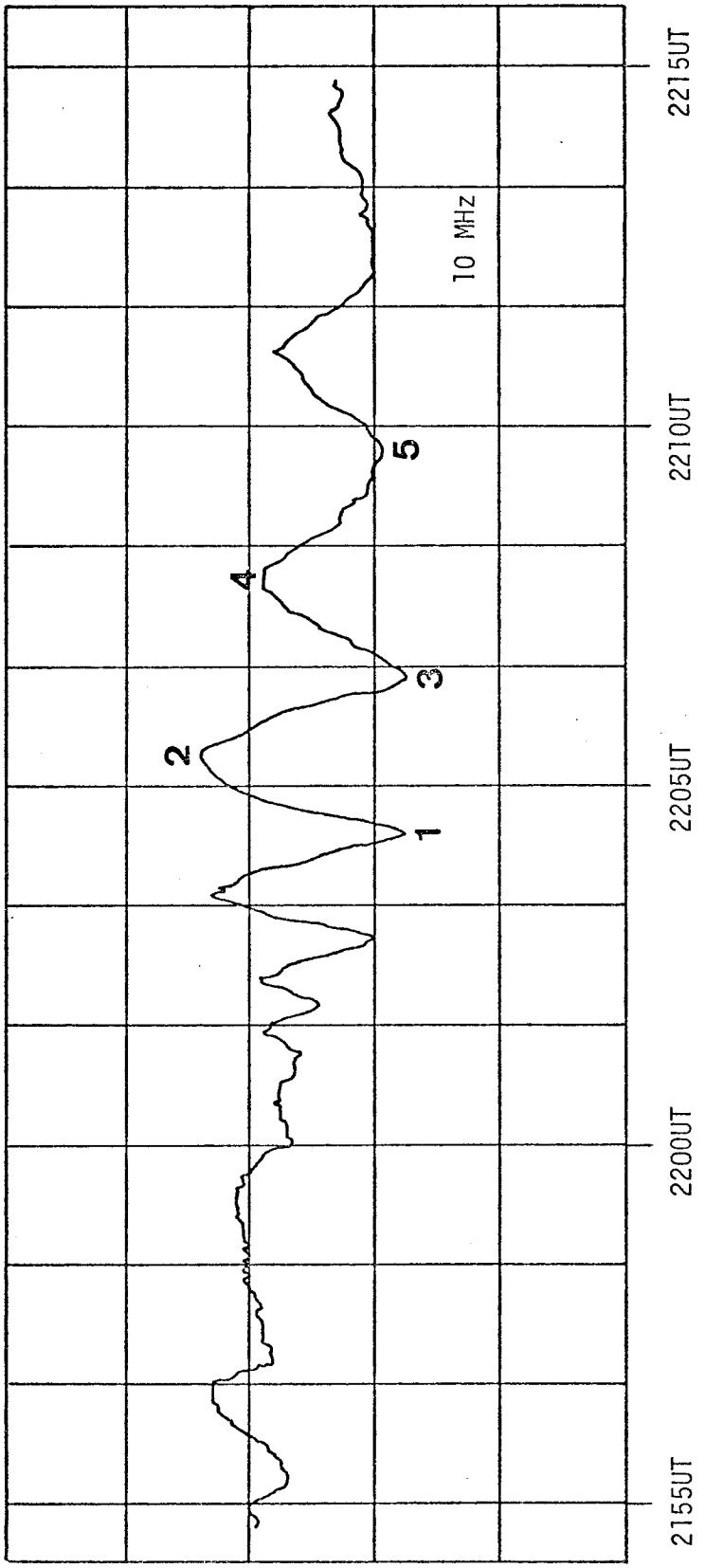

Figure 6. Doppler shift record from the Kurile Earthquake, August 11, 1969.

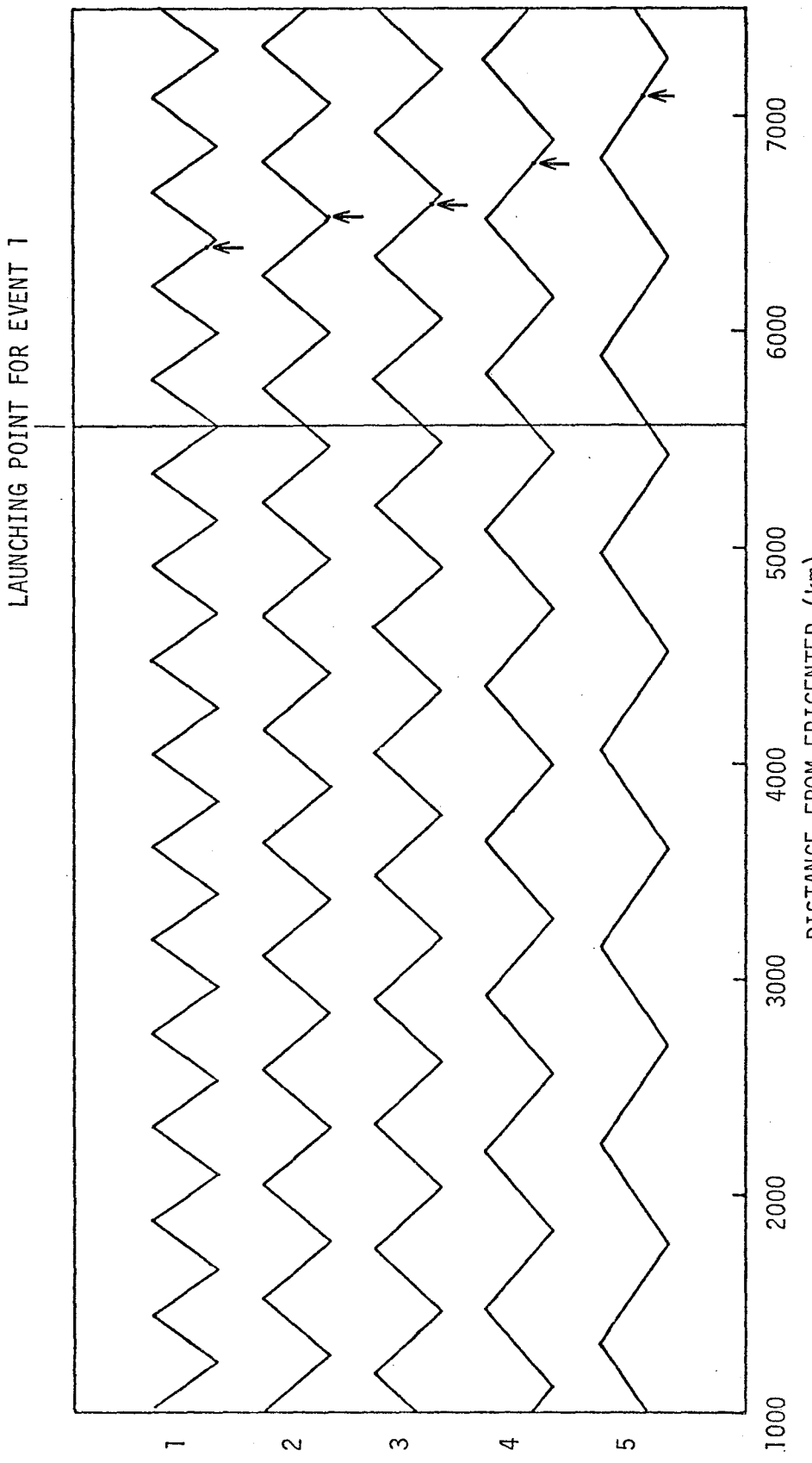

Figure 7. Wave trains from the Kurile Earthquake, August 11, 1969. The arrows indicate the locations of initial phase.

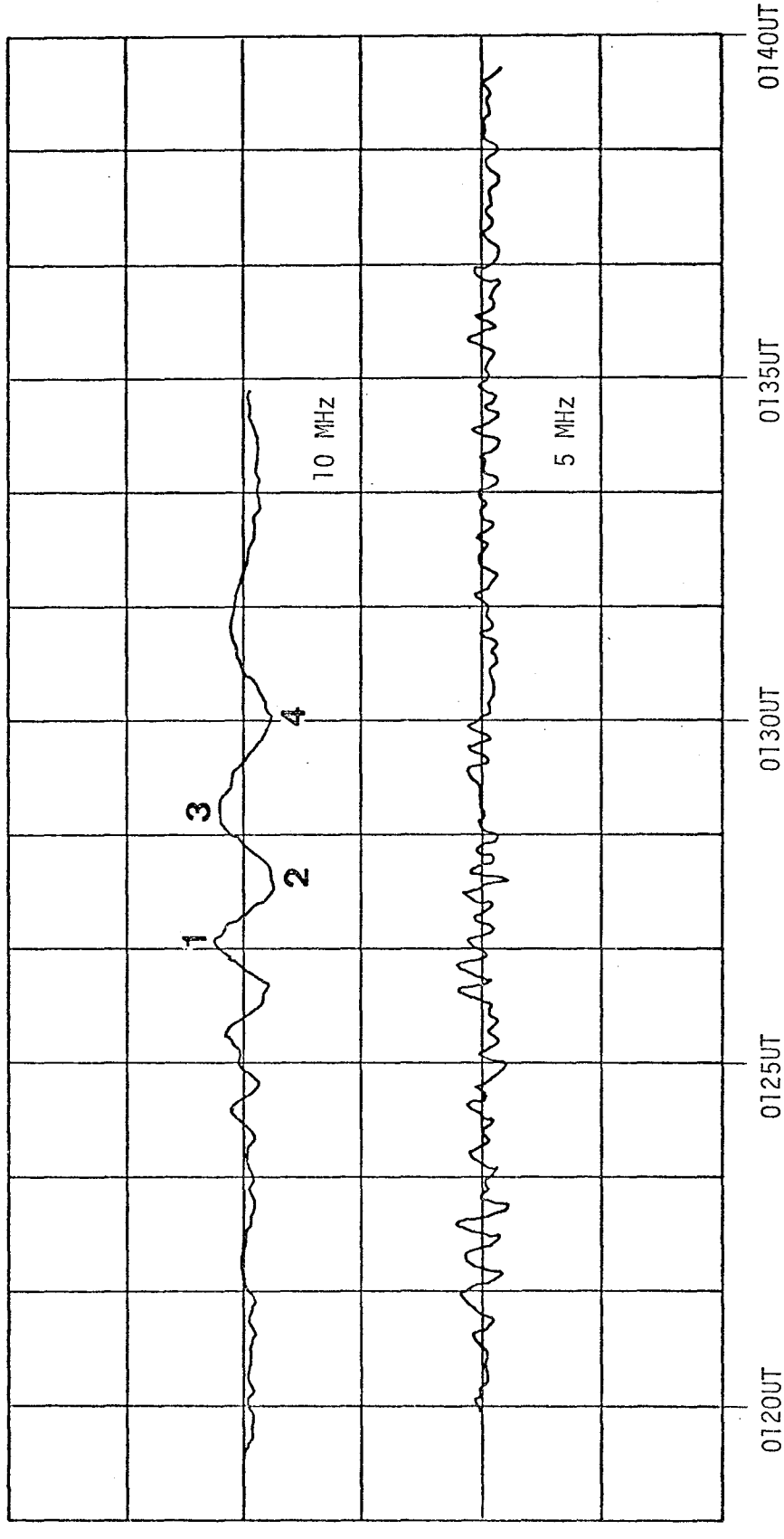

Figure 8. Doppler shift record from the Hachinohe, Japan Earthquake, May 16, 1968.

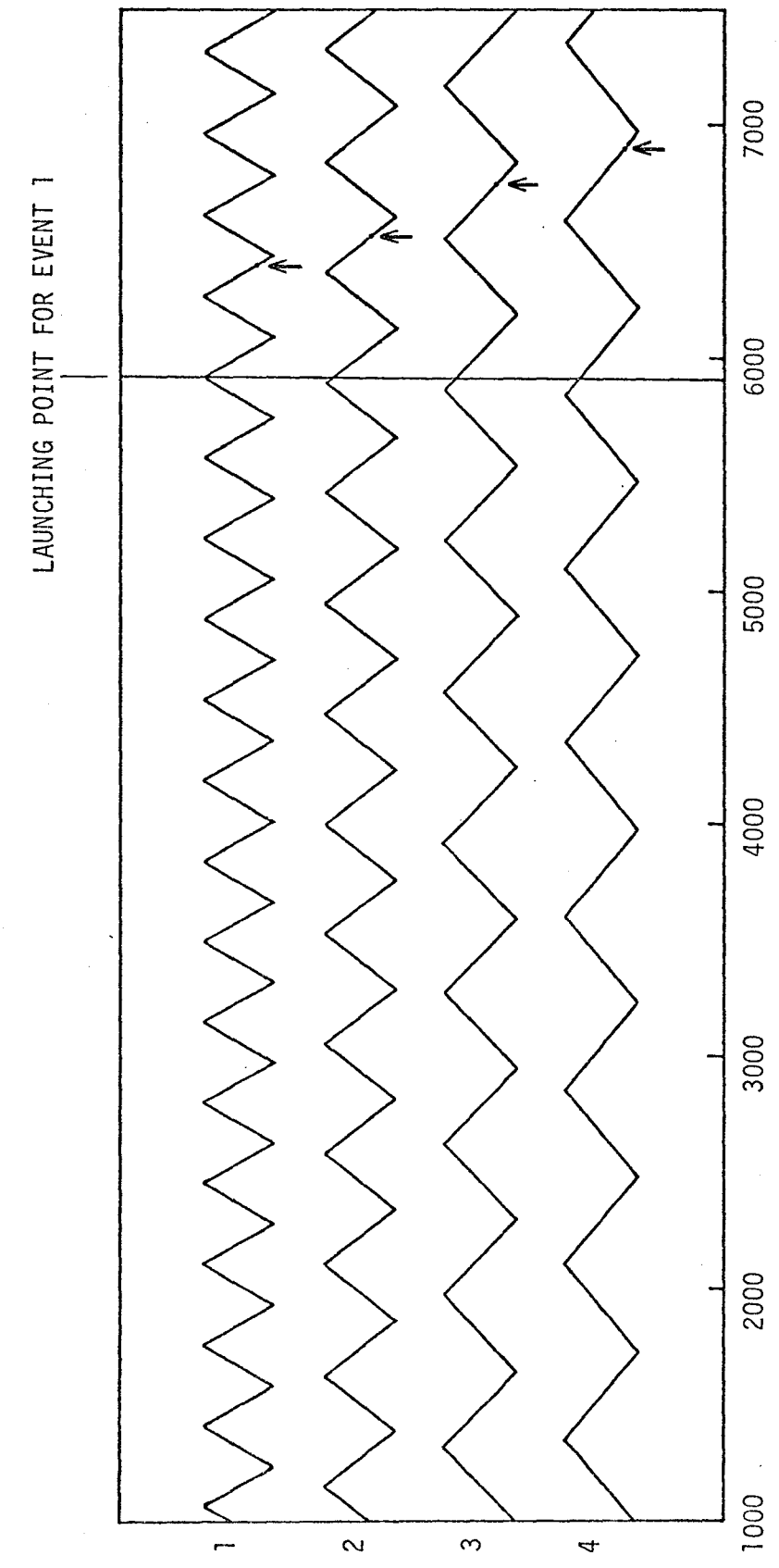

Figure 9. Wave trains from Hachinohe, Japan, Earthquake, May 16, 1968. The arrows indicate the locations of initial phase.

A	B	C	D	E	F	G	H	I	J	K
Event	Period (sec.)	Character	Phase Vel. (km/sec.)	Delay Time (min.)	Horizontal Distance (km)	Time of Arrival (UT)	Time Acoustic Wave Was Launched (UT)	Distance Compensation (km)	Wavelength (km)	Distance of Initial Phase
1	105	Trough	4.116	11.44	46.0	22:04:20	21:52:54	0	432.18	6396.26
2	125	Peak	4.205	11.18	45.3	22:05:30	21:54:19	356.73	525.63	6534.57
3	135	Trough	4.249	11.02	45.0	22:06:30	21:55:29	657.60	573.62	6602.94
4	165	Peak	4.365	10.47	44.0	22:08:00	21:57:32	1211.47	720.23	6783.21
5	200	Trough	4.566	9.60	41.7	22:09:40	22:09:40	1959.08	913.20	7095.56

Table 1. Data for constructing the wave trains of Rayleigh wave components from Kurile Earthquake, August 11, 1969.
Note: Time earthquake occurred 2127 UT.
Distance between epicenter and sub-ionospheric point: 5615 km.
H = G - E, I + D(H - 21:52:54) - (46.0 - F), J = BD, K = (21:52:54 - 21:27:00)D

A	B	C	D	E	F	G	H	I	J	K
Event	Period (sec.)	Character	Phase Vel. (km/sec.)	Delay Time (min.)	Horizontal Distance (km)	Time of Arrival (UT)	Time Acoustic Wave Was Launched (UT)	Distance Compensation (km)	Wavelength (km)	Distance of Initial Phase (km)
1	85	Peak	4.08	11.63	46.6	01:26:48	01:15:10	0	346.80	6405.60
2	114	Trough	4.16	11.32	45.7	01:27:33	01:16:14	263.80	474.24	6531.20
3	151	Peak	4.30	10.75	44.6	01:28:40	01:17:55	706.65	649.30	6751.00
4	170	Trough	4.40	10.36	43.6	01:30:05	01:19:43	1199.07	748.00	6908.00

Table 2. Data for constructing the wave trains of Rayleigh wave components from Hachinohe, Japan Earthquake, May 16, 1968.
Note: Time earthquake occurred: 0049 UT
Distance between epicenter and sub-ionospheric point: 5975 km.

REFERENCES

Ben-Mehahem, A., and M.N. Toksoz, Source-mechanism from spectra of long period seismic surface waves, J. Geophys. Res., 67, 1943, 1962.

Brune, J. et al., The polar shift of surface waves on a sphere, Bull. Am. Seism. Soc., 51(2), 247(1961).

Dorman, J. seismic surface wave data on the upper mantle, Geophys. Monog., 13, Am. Geophys. Union, 1969.

Ewing, M. and F. Press, An investigation of mantle Rayleigh waves, Bull. Seismol. Soc. Am., 44, 127, 1954.

Furumoto, A.S., Tsunamis in the Pacific Ocean, Proceedings of International Symposium on Tsunami and Tsunami Research, University of Hawaii, 1970.

Yuen, P.C., P.F. Weaver and R.K. Suzuki, Continuous, traveling coupling between seismic waves and the ionospheric evident in May 1968 Japan Earthquake data, J. Geophys. Res., 74, 2256, 1969.

APPENDIX 5B

A COMPUTER PROGRAM TO PLOT Q-X CURVES

```
FORTRAN IV G LEVEL  20                  MAIN                    DATE = 73234

            C       TO PLOT ROOKER'S QUARTIC
0001                DIMENSION QUP(41),QDO(41),XUP(41),XDO(41),Q(42),X(42),B(1000)
0002                CALL PLOTS(B(1),4000)
0003                CALL PLOT(0.0,0.0,-3)
0004                DO 9 L=1,2
0005                IF (L-1) 14,14,15
0006             14 F=10.0
0007                GO TO 16
0008             15 F=5.0
0009             16 DO 10 I=1,5
0010                ANG=0.1+  0.1*(I-1)
0011                CALL QUART(ANG,F,QUP,QDO,XUP,XDO,NO,XO,QO)
0012                DO 11 J=1,NO
0013                Q(J)=QUP(J)
0014             11 X(J)=XUP(J)
0015                Q(NO+1)=QO
0016                X(NO+1)=XO
0017                N=NO+2
0018                DO 12 J=N,42
0019                Q(J)=QDO(J-N+1)
0020             12 X(J)=XDO(J-N+1)
0021                IF (L-1) 18,18,17
0022             18 CALL LINE(X,Q,42,1,0,0,0.0,-1.0,0.1,0.2)
0023                GO TO 19
0024             17 CALL LINE(X,Q,42,1,2,03,0.0,-1.0,0.1,0.2)
0025             19 WRITE(6,50) ANG
0026                WRITE(6,50) (X(K),K=1,42),XO
0027                WRITE(6,50) (Q(K),K=1,42),QO
0028             10 CONTINUE
0029              9 CONTINUE
0030                CALL AXIS(0.0,5.0,' ',-1,10.0,0.0,0.0,0.1,10.0)
0031                CALL AXIS(0.0,0.0,' ',1,10.0,90.0,-1.0,0.2,10.0)
0032                CALL PLOT(0.0,0.0,999)
0033             50 FORMAT(1X,15F8.4)
0034                STOP
0035                END
```


The SUBROUTINE QUART is required and given in Appendix 5A.

APPENDIX 5C

A COMPUTER PROGRAM FOR TWO DIMENSIONAL RAY TRACING IN THE IONOSPHERE

This program consists of a main program, two SUBROUTINE programs, QUART and INTEG2, and a FUNCTION subprogram DX2DH. The SUBROUTINE INTEG2 (Y, H, NO, A) is used for integration of a given numerical function. The meanings of the arguments are as follows:

Y: Input vector of length NO to be integrated

H: Step width of integration

NO: Number of ordinates to be integrated

A: Output vector of length NO which gives the result of integration corresponding to each element of vector Y.

By calling this subprogram, the horizontal range y_k corresponding to k^{th} layer can be obtained.

In using this two dimensional ray tracing computer program, the following steps should be followed:

(1) Prepare a data card with FORMAT (2I4) which supplies the values for

NRAY = Number of ionograms to be ray traced, and

F = Frequency in MHz in this order.

(2) Prepare a data set for electron density profiles of the ionosphere to be ray traced with FORMAT (13F6.1). It is assumed that the punched output of the electron density profiles obtained by using the program given in Appendix 4B should be interpolated to give $N_e(z)$ at every 5 km interval starting from 80 km up to 1000 km.

(3) The data set is read in the order (1) and (2) above.

This program was written for ray tracing of radio path 1. For use at another radio path, m and n should be recalculated for that path and make the changes Y2=m and Y3=n in statements 5 and 6.

The initiating angle of incidence $\theta_I(1)$ was assumed to be 0.4 radian. If the angle other than this is chosen as $\theta_I(1)$, the statement 17 should be changed for this new value. The preassigned error distance ΔD was assumed to be 1 km. If the value other than 1 km is desired, statement 98 should be changed to read

IF (X2D(MD) - DIST - ΔD) 29, 30, 30

where ΔD refers to the new value desired. The distance between WWVH and the University of Hawaii is 152.2 km. If the distance other than this value is desired then statement 3 should be changed.

This program is written to print out the following data for each θ_I in the order.

(i) Horizontal ranges y_0, y_1, y_2, ..., y_m, y_0 for upgoing wave as shown in Figure 5.7.

(ii) Horizontal ranges y_1', y_2', ..., y_m', H for down coming wave as shown in Figure 5.7.

(iii) Height of reflection z_0.

(iv) When the ray homes in on the desired receiving point a dotted line will be printed out to indicate the end of ray tracing for one N(z) profile. If NRAY > 1, it will proceed to produce another ray tracing for the next N(z) profile.

Table 5C-1 shows the printed output of a ray tracing sample made on the electron density profile shown in Fig. 4.1. The required SUBROUTINE QUART is given in Appendix 5A.

```
FORTRAN IV G LEVEL  20                    MAIN                    DATE = 73227

            C     RAY TRACING BY BOOKER'S QUARTIC
0001                DIMENSION       XUP(41),XDO(41),OUP(41),ODO(41),QU(80),X(185)
                   2,QD(80),T1(80),Y2(80),X2U(80),X2D(80),XD(64)
0002                DIST=152.2
0003                READ(5,51) NRAY,F
0004                Y=0.873/F
0005                Y2=-0.046624*Y
0006                Y3=0.628297*Y
0007                DO 70 IK=1,NRAY
0008                READ(5,50) X
0009                DO  8 I=1,64
0010                IF(X(I)) 8,6,9
0011              8 CONTINUE
0012              9 ZO=75.0*I*5.0
0013                N=64
0014                K=I
0015                DO 10 I=K,N
0016             10 X(I-K+1)=(X(I)/12.400)/F**2
0017                A=0.4
0018                DA=0.1
0019                NOTRY=0
0020             31 DO 30 K=1,10
0021                ANG=A-(K-1)*DA
0022                C=COS(ANG)
0023                S=SIN(ANG)
0024                CALL QUART(ANG,F,QUP,QDO,XUP,XDO,NO,XO,QO)
0025                DO 11 I=1,N
0026                IF(X(I)-XO) 11,11,12
0027             11 CONTINUE
0028             12 NM=I-1
0029                DO 14 J=1,N
0030                IF(X(NM-J+1)-XUP(NO) ) 6,6,14
0031             14 CONTINUE
0032              6 NU=NM-J+1
0033                DO 7 I=1,NU
0034                DO 5 J=1,NO
0035                IF (XUP(J)-X(I)) 5,15,16
0036             16 QU(I) =((QUP(J)-OUP(J-1))/(XUP(J)-XUP(J-1)))*(X(I)-
                   2 XUP(J-1)) +QUP(J-1)
0037                GO TO 7
0038             15 QU(I)=QUP(J)
0039                GO TO 7
0040              5 CONTINUE
0041              7 CONTINUE
0042                DO 33 I=1,N
0043                IF (X(NU+I)-XO) 33,34,34
0044             33 CONTINUE
0045             34 OHI=5.0*I
```

```
FORTRAN IV G LEVEL  20                  MAIN                    DATE = 73227

0046                ZI=ZO*(NU-1)*5.0
0047                ZA=(XO-X(NU))*( DHI/(X(NU+I)-X(NU)))+ZI
0048                QQ=QU(NU)
0049                XX=X(NU)
0050                YY= DX2DH(Y,Y2,Y3,C,S,QQ,XX)
0051                X2AU=2.0*(ZA-ZI)*YY
0052                ND=NU
0053                NCO=41-NO
0054                DO 21 I=1,ND
0055                DO 3 J=1,NOD
0056                JJ=42-NO-J
0057                IF(XDO(JJ)-X(I))  3,22,23
0058             23 QD(I)=((QDO(JJ)-QDO(JJ+1))/(XDO(JJ)-XDO(JJ+1)))*
                   2 (X(I)-XDO(JJ+1))+QDO(JJ+1)
0059                GO TO 21
0060             22 QD(I)=QDO(JJ)
0061                GO TO 21
0062              3 CONTINUE
0063             21 CONTINUE
0064                QQ=QD(ND)
0065                XX=X(ND)
0066                YY= DX2DH(Y,Y2,Y3,C,S,QQ,XX)
0067                X2AD=-2.*(ZA-ZI)*YY
0068                DO 60 M=1,ND
0069                T1(M)=QD(M)
0070             60 T2(M)=X(M)
0071                DO 24 M=1,ND
0072                QD(M)=T1(ND-M+1)
0073             24 XD(M) =T2(ND-M+1)
0074                DO 25 I=1,NU
0075                QQ= QU(I)
0076                XX=X(I)
0077             25 T1(I)= DX2DH(Y,Y2,Y3,C,S,QQ,XX)
0078                DO 20 I=1,ND
0079                QQ=QD(I)
0080                XX=XD(I)
0081             20 T2(I)= DX2DH(Y,Y2,Y3,C,S,QQ,XX)
0082                CALL INTEG2(T1, 5.0,NU,X2U)
0083                CALL INTEG2(T2,-5.0,ND,X2D)
0084                X2=ZO*TAN(ANG)
0085                DO 26 I=1,NU
0086             26 X2U(NU-I+2)=X2U(NU-I+1)+X2
0087                X2U(1)=0.0
0088                NU=NU+2
0089                X2U(NU)=X2U(NU-1)+X2AU
0090                TT=X2U(NU)+X2AD
0091                DO 27 I=1,ND
0092             27 X2D(I  )=X2D(I)+TT
```

```
FORTRAN IV G LEVEL  20                  MAIN                    DATE = 73227

0093                 MD=MD+1
0094                 X2D(MD)=X2D(MD-1)+X2
0095                 NOTRY=NOTRY+1
0096                 WRITE(6,53) NOTRY,ANG,K
0097                 WRITE(6,52) (X2U(I),I=1,MU)
0098                 WRITE(6,52) (X2D(I),I=1,MD)
0099                 WRITE(6,57) ZA
0100                 IF(X2D(MD)-DIST) 32,28,28
0101              28 IF(X2D(MD)-DIST-1.0) 29,30,30
0102              30 CONTINUE
0103              32 A=ANG+DA
0104                 DA=DA/2.0
0105                 A=A-DA
0106                 GO TO 31
0107              29 WRITE(6,58) X2D(MD)
0108                 WRITE(7,54) (X2U(I),I=1,MU)
0109                 WRITE(7,54) (X2D(I),I=1,MD)
0110                 WRITE(7,54) ZA
0111                 WRITE (6,55)
0112              70 WRITE(6,56)
0113              50 FORMAT(13F6.1)
0114              51 FORMAT(14,F5.1)
0115              52 FORMAT(4X,10F8.2)
0116              53 FORMAT(/14,F12.7,I4)
0117              54 FORMAT(11F7.2)
0118              55 FORMAT('**********************************')
0119              56 FORMAT(1H1)
0120              57 FORMAT('     REFLECTION HEIGHT= ',F8.3)
0121              58 FORMAT(' HORIZONTAL RANGE= ',F8.3)
0122                 STOP
0123                 END
```

```
FORTRAN IV G LEVEL  20                  INTEG2                  DATE = 73234

0001                 SUBROUTINE INTEG2(Y,H,NO,A)
                  C     Y=VECTOR OF LENGTH NO TO BE INTEGRATED
                  C     A=VECTOR OF LENGTH NO-1. RESULT OF INTEGRATION
0002                 DIMENSION Y(1),A(1)
0003                 A(1)=0.0
0004                 T=Y(1)
0005                 A(2)=(T+Y(2))*H/2.0
0006                 DO 10 K=3,NO
0007                 M=K-1
0008                 T=Y(1)
0009                 DO 11 L=2,M
0010                 T=T+2.0*Y(L)
0011              11 A(K  )=(T+Y(K))*H/2.0
0012              10 CONTINUE
0013                 RETURN
0014                 END
```

```
FORTRAN IV G LEVEL  20                  DX2DH                   DATE = 73234

0001                 FUNCTION  DX2DH(Y,Y2,Y3,C,S,Q,X)
0002                 T=C**2-Q**2
0003                 DX2DH =(4.0*S*X**2+(-2.0*S*(2.0-Y**2+(S*Y2+Q*Y3)**2+
                    2   2.0*T)+2.0*Y2*(S*Y2+Q*Y3))*T)*X+4.0*S*(1.0-Y**2)*T)/
                    3   (4.0*Q*X**2+(-2.0*Q*(2.-Y**2+(S *Y2+C*Y3)**2+2.*T)+
                    4   2.0*Y3*(S *Y2+Q*Y3)*T)*X+4.0*Q*(1.0-Y**2)*T)
0004                 RETURN
0005                 END
```

TABLE 5C-1 Printed Output of the Ray Paths for Two Dimensional Ray tracing Made on the Electron Density Profile Given in Figure 4.1.

```
1   0.4000000   1
     0.0    46.51   48.76   51.05   53.36   55.69   58.02   60.36   62.71   65.09
    67.51   69.95   72.43   74.95   77.50   80.09   82.73   85.41   88.14   90.92
    93.77   96.69   99.70  102.81  106.04  109.42  112.99  116.80  120.93  125.50
   130.68  136.83  144.90  160.90  172.89
   183.70  198.32  206.03  211.99  217.04  221.51  225.57  229.33  232.86  236.20
   239.40  242.48  245.47  248.37  251.20  253.97  256.68  259.34  261.97  264.55
   267.09  269.59  272.07  274.51  276.91  279.29  281.64  283.97  286.30  288.62
   290.92  293.21  295.46  341.97
 REFLECTION HEIGHT=  271.327

2   0.3000000   2
     0.0    34.03   35.67   37.33   39.02   40.70   42.40   44.10   45.81   47.53
    49.28   51.05   52.84   54.66   56.50   58.36   60.25   62.17   64.13   66.11
    68.14   70.22   72.34   74.53   76.79   79.15   81.61   84.20   86.97   89.95
    93.21   96.86  101.08  106.30  113.93  129.47
   143.99  151.16  156.15  160.23  163.77  166.96  169.88  172.60  175.16  177.58
   179.91  182.14  184.31  186.42  188.48  190.49  192.47  194.41  196.32  198.20
   200.05  201.88  203.69  205.48  207.24  208.98  210.70  212.41  214.10  215.79
   217.47  219.15  220.81  222.45  256.48
 REFLECTION HEIGHT=  279.138

3   0.2000000   3
     0.0    22.30   23.37   24.46   25.56   26.66   27.76   28.87   29.99   31.11
    32.25   33.40   34.57   35.75   36.94   38.15   39.38   40.62   41.88   43.17
    44.48   45.81   47.18   48.58   50.03   51.52   53.08   54.71   56.44   58.28
    60.26   62.43   64.85   67.64   71.08   75.90   98.48  101.50
   104.18  124.36  126.84  132.08  134.74  137.07  139.17  141.09  142.89  144.58
   146.18  147.71  149.18  150.61  151.99  153.34  154.66  155.96  157.23  158.48
   159.72  160.93  162.13  163.32  164.49  165.65  166.80  167.93  169.05  170.16
   171.27  172.37  173.47  174.56  175.65  176.72  199.01
 REFLECTION HEIGHT=  285.192

4   0.1000001   4
     0.0    11.04   11.57   12.11   12.65   13.19   13.74   14.29   14.84   15.39
    15.96   16.53   17.10   17.68   18.27   18.87   19.47   20.09   20.71   21.34
    21.99   22.65   23.32   24.01   24.72   25.45   26.21   27.01   27.85   28.74
    29.69   30.73   31.87   33.16   34.68   36.61   39.50   45.44
    50.74   53.33   55.06   56.45   57.64   58.71   59.69   60.60   61.45   62.25
    63.02   63.76   64.47   65.16   65.84   66.49   67.14   67.77   68.39   69.00
    69.61   70.20   70.79   71.37   71.95   72.52   73.08   73.64   74.19   74.74
    75.28   75.83   76.37   76.91   77.44   77.97   89.01
 REFLECTION HEIGHT=  289.125

5   0.1500000   1
     0.0    16.62   17.42   18.23   19.05   19.87   20.69   21.52   22.35   23.19
    24.04   24.89   25.76   26.64   27.53   28.43   29.34   30.26   31.20   32.15
    33.13   34.12   35.13   36.17   37.24   38.35   39.50   40.70   41.97   43.32
    44.77   46.35   48.09   50.08   52.45   55.56   60.88   67.80
    74.22   79.13   82.01   84.23   86.11   87.78   89.29   90.69   92.00   93.23
    94.41   95.53   96.62   97.67   98.69   99.69  100.67  101.62  102.57  103.49
   104.41  105.31  106.20  107.08  107.95  108.82  109.67  110.51  111.34  112.17
   112.99  113.81  114.63  115.44  116.25  117.05  133.67
 REFLECTION HEIGHT=  287.466

6   0.1750000   1
     0.0    19.45   20.38   21.33   22.29   23.25   24.21   25.18   26.15   27.13
    28.12   29.13   30.14   31.17   32.21   33.26   34.33   35.41   36.51   37.63
    38.77   39.93   41.12   42.34   43.59   44.89   46.25   47.66   49.16   50.75
    52.46   54.32   56.39   58.76   61.62   65.49   73.30   79.49
    85.30   92.60   96.19   98.89  101.14  103.13  104.93  106.59  108.13  109.59
   110.98  112.30  113.58  114.82  116.02  117.19  118.34  119.46  120.57  121.66
   122.73  123.79  124.83  125.87  126.89  127.90  128.89  129.88  130.86  131.83
   132.79  133.75  134.70  135.66  136.60  137.53  156.98
 REFLECTION HEIGHT=  286.397
```

```
 7   0.1499999   2
       0.0     16.62   17.42   18.23   19.05   19.87   20.69   21.52   22.35   23.19
     24.04     24.89   25.76   26.64   27.53   28.43   29.34   30.26   31.20   32.15
     33.13     34.12   35.13   36.17   37.24   38.35   39.50   40.70   41.97   43.32
     44.77     46.35   48.09   50.08   52.45   55.57   60.88   67.80
     74.22     79.14   82.01   84.23   86.11   87.78   89.29   90.69   92.00   93.23
     94.41     95.53   96.62   97.67   98.69   99.69  100.67  101.63  102.57  103.50
    104.41    105.31  106.20  107.09  107.96  108.82  109.67  110.51  111.34  112.17
    112.99    113.81  114.63  115.44  116.25  117.05  133.67
  REFLECTION HEIGHT=  287.466

 8   0.1624998   1
       0.0     18.03   18.90   19.78   20.67   21.56   22.45   23.35   24.25   25.16
     26.07     27.01   27.95   28.90   29.86   30.84   31.83   32.83   33.85   34.89
     35.94     37.02   38.12   39.25   40.41   41.61   42.86   44.17   45.55   47.02
     48.60     50.32   52.22   54.40   57.01   60.47   66.76   73.41
     79.66     85.53   88.75   91.20   93.26   95.09   96.74   98.27   99.69  101.04
    102.32    103.55  104.73  105.87  106.98  108.07  109.13  110.17  111.19  112.20
    113.20    114.18  115.14  116.10  117.05  117.98  118.91  119.82  120.72  121.62
    122.51    123.40  124.29  125.17  126.05  126.91  144.95
  REFLECTION HEIGHT=  286.955

 9   0.1687498   1
       0.0     18.74   19.64   20.56   21.48   22.40   23.33   24.26   25.20   26.14
     27.10     28.06   29.04   30.03   31.04   32.05   33.08   34.12   35.18   36.26
     37.35     38.47   39.62   40.79   42.00   43.25   44.55   45.91   47.35   48.88
     50.53     52.32   54.30   56.57   59.30   62.96   69.93   76.38
     82.33     88.77   92.17   94.74   96.90   98.80  100.53  102.12  103.61  105.01
    106.34    107.62  108.84  110.03  111.19  112.32  113.42  114.51  115.57  116.62
    117.65    118.67  119.68  120.67  121.66  122.63  123.59  124.54  125.48  126.41
    127.34    128.26  129.18  130.10  131.01  131.91  150.65
  REFLECTION HEIGHT=  286.672

10   0.1718748   1
       0.0     19.09   20.01   20.94   21.88   22.82   23.77   24.72   25.67   26.64
     27.61     28.60   29.59   30.60   31.62   32.66   33.70   34.77   35.85   36.94
     38.06     39.20   40.37   41.56   42.80   44.07   45.40   46.79   48.25   49.81
     51.49     53.32   55.34   57.66   60.46   64.21   71.58   77.91
     83.77     90.59   94.08   96.71   98.92  100.86  102.62  104.25  105.76  107.19
    108.55    109.85  111.11  112.32  113.50  114.65  115.77  116.88  117.96  119.03
    120.09    121.13  122.15  123.16  124.17  125.16  126.14  127.10  128.06  129.01
    129.96    130.90  131.84  132.77  133.70  134.62  153.71
  REFLECTION HEIGHT=  286.536

11   0.1687497   2
       0.0     18.74   19.64   20.56   21.48   22.40   23.33   24.26   25.20   26.14
     27.10     28.06   29.04   30.03   31.04   32.05   33.08   34.12   35.18   36.26
     37.35     38.47   39.62   40.79   42.00   43.25   44.55   45.91   47.35   48.88
     50.53     52.32   54.30   56.57   59.30   62.96   69.93   76.38
     82.33     88.77   92.17   94.74   96.90   98.80  100.53  102.12  103.61  105.01
    106.34    107.62  108.84  110.03  111.19  112.32  113.42  114.51  115.57  116.62
    117.65    118.67  119.68  120.67  121.66  122.63  123.59  124.54  125.48  126.41
    127.34    128.26  129.18  130.10  131.01  131.91  150.65
  REFLECTION HEIGHT=  286.672

12   0.1703122   1
       0.0     18.92   19.83   20.75   21.68   22.61   23.55   24.49   25.44   26.39
     27.35     28.33   29.32   30.32   31.33   32.35   33.39   34.44   35.51   36.60
     37.71     38.84   39.99   41.18   42.40   43.66   44.97   46.35   47.80   49.35
     51.01     52.82   54.82   57.12   59.88   63.59   70.74   77.09
     83.01     89.66   93.10   95.70   97.89   99.81  101.55  103.16  104.66  106.08
    107.43    108.71  109.95  111.16  112.32  113.46  114.58  115.67  116.75  117.81
    118.85    119.88  120.89  121.90  122.89  123.87  124.84  125.80  126.75  127.69
    128.63    129.56  130.49  131.42  132.34  133.24  152.16
  REFLECTION HEIGHT=  286.599

13   0.1710933   1
       0.0     19.01   19.92   20.85   21.78   22.72   23.66   24.60   25.56   26.51
     27.48     28.46   29.46   30.46   31.48   32.50   33.55   34.61   35.68   36.77
     37.88     39.02   40.18   41.37   42.60   43.87   45.19   46.57   48.03   49.58
     51.25     53.07   55.08   57.39   60.17   63.91   71.15   77.49
     83.39     90.11   93.58   96.20   98.39  100.33  102.08  103.70  105.21  106.63
    107.98    109.28  110.52  111.73  112.90  114.05  115.17  116.27  117.35  118.41
    119.46    120.49  121.51  122.52  123.52  124.51  125.48  126.44  127.40  128.34
    129.28    130.22  131.16  132.09  133.01  133.92  152.93
  REFLECTION HEIGHT=  286.572
HORIZONTAL RANGE=  152.928
```

APPENDIX 6

HILBERT TRANSFORM METHOD OF DETERMINING THE PERIOD OF RAYLEIGH-ACOUSTIC WAVE GENERATED IONOSPHERIC DOPPLER RECORDINGS

I. Introduction

Well-dispersed earthquake generated Rayleigh waves launch acoustic waves into the atmosphere and cause oscillatory disturbances in the ionosphere. These acoustic waves are designated as Rayleigh-acoustic waves throughout this paper. By employing the Doppler sounding technique (Davies, 1969), these oscillatory disturbances at ionospheric height can be recorded. The purpose of this paper is to present a method, which employs the Hilbert transform and the analytic signal representation, for the determination of the period of the oscillatory disturbances recorded. This method is designated as the Hilbert transform method. Besides Rayleigh-acoustic waves, oscillatory disturbances in the ionosphere can be generated by other effects such as the geomagnetic sudden commencement (Davies, 1969). Complication in analysis may arise due to different nature of different disturbances. So we confine our discussion to records representing disturbances caused by Rayleigh-acoustic waves only. Throughout the paper, the term "Doppler record" denotes only those records displaying oscillations caused by Rayleigh-acoustic waves.

The Doppler record has been shown to be a faithful representation of the time rate of change of the displacement of the long-period Rayleigh waves (Yuen et al., 1969) and is equivalent to what an ideal long-period seismometer for measuring vertical component of a disturbance would record. At present, records of long-period Rayleigh waves from seismometers are not very satisfactory. Most of the time they are contaminated by Love waves and the seimometers are unstable due to violent oscillations caused by the strong body waves which arrive before the Rayleigh waves (Furumoto, 1970). On the other hand, ionospheric Doppler recordings do not have such serious drawbacks. So, Doppler records play a unique and important role in representing the long period seismic

Rayleigh waves.

Analysis of Doppler records gives valuable information for earthquake source mechanism investigations and other seismic studies. An example is the experimental tsunami warning system established at the Radioscience Laboratory of the University of Hawaii (Furumoto, 1970; Najita et al., 1974). In the process of analyzing a Doppler record, one essential and significant piece of information needed is the period of the oscillations. Traditionally, the period of the oscillations recorded by seismometers, as well as by Doppler technique, has been determined by the so-called "peak and trough" method (Pekeris, 1948; Ewing and Press, 1954). In this paper, the Hilbert transform method and the "peak and trough" method are compared by applying them to a Doppler record.

Before we go into the details of the Hilbert transform method, we first need to discuss the Doppler record.

II. The Doppler Record

The motion at one point of a dispersive medium due to a disturbance applied earlier at another point may be represented by a superposition of traveling plane waves of different wave number k (Brune et al., 1960)

$$u(x,t) = \frac{1}{2\pi}\int_0^\infty A(k)\cos(\omega t - kx + \phi(k))dk \qquad (1)$$

where $u(x,t)$ is a component of the displacement which is a function of the space coordinate x and the time t. $A(k)$ is an amplitude function, ω the angular frequency, and $\phi(k)$ the initial phase as a function of wave number. Furthermore, Brune (1960) utilized the calculations given by Pekeris (1948) to show that when a wave train, which is generated by the disturbance applied at one point, has become sufficiently dispersed, Equation 1 may be evaluated by the method of stationary phase and shown to be approximately

$$u(x,t) \simeq \left\{\frac{1}{2\pi t\left|\frac{d^2\omega}{dk^2}\right|_0}\right\}^{1/2} A(k_0)\cos(\omega_0 t - k_0 x + \phi(k_0) \pm \frac{\pi}{4}) \qquad (2)$$

provided ω_0 is not too near an extremum of group velocity and the

amplitude does not vary too rapidly as a function of frequency. Equation (2) then indicates that the motion at large x will consist of nearly sinusoidal oscillations whose frequency and amplitude slowly vary with time (essentially because ω_0 and k_0 are functions of (x/t)). Thus at remote points away from the source, the wave-train will be well-dispersed, and oscillation of frequency ω_0 will occur when traveling plane wave components with frequencies equal to and near ω_0 arrive at the point and interfere constructively with one another.

The above results can, and have, been used in the case of Rayleigh waves from large earthquakes (Brune et al., 1960). Since a Doppler record is a faithful representation of well-dispersed Rayleigh waves, they can also be applied to the case of Doppler record. In general, an oscillation recorded by using the Doppler technique at a certain time can be pictured as caused by a Rayleigh wave component x(t),

$$x(t) = A\cos(\omega t+\Phi) \tag{4}$$

where ω is the frequency, A is the amplitude, and Φ is the total phase shift. Actually, the amplitudes of the oscillations recorded are proportional to the particle velocity induced by the Rayleigh-acoustic waves. There is a $\pi/2$ phase difference between the peaks of displacement and the peaks of the Doppler frequency shift (Najita et al., 1974). This $\pi/2$ phase difference could be incorporated into the total phase shift Φ in (4). The ω in (4) is the frequency of the oscillation recorded, where reciprocal of ω gives the period of the oscillation.

III. The Hilbert Transform and The Analytic Signal

The Hilbert transform is frequently encountered in communication theory. The band-pass signals that are of interest in communication are signals that are generated by modulating a carrier signal by a narrow-band low-pass information-bearing signal. And the Hilbert transform provides an easy and elegant way to relate the band-pass modulated signal to the low-pass signal,

especially in single side-band modulation.

The Hilbert transform $\hat{x}(t)$ of a real-valued signal $x(t)$ is defined as (Kuo and Freeny, 1962; Schwarts et al., 1966)

$$\hat{x}(t) = \frac{1}{\pi} P \int_{-\infty}^{\infty} \frac{x(\tau)}{t-\tau} d\tau \tag{5}$$

and the inverse Hilbert transform as

$$x(t) = -\frac{1}{\pi} P \int_{-\infty}^{\infty} \frac{\hat{x}(\tau)}{t-\tau} d\tau \tag{6}$$

Where P denotes the Cauchy principle value of the integral at $\tau=t$. Let us demonstrate equation 5 by finding the Hilbert transform $\hat{x}(t)$ of the function in (4), $x(t) = A\cos(\omega t+\Phi)$. Substitute $\tau=t+\tau'$ in (5):

$$\hat{x}(t) = \frac{1}{\pi} P \int_{-\infty}^{\infty} (x(t+\tau')/-\tau')d\tau' \tag{7a}$$

$$= \frac{1}{\pi} P \int_{-\infty}^{\infty} (x(t+\tau)/-\tau)d\tau \quad . \tag{7b}$$

Then substitute (4) into the equation:

$$\hat{x}(t) = \frac{1}{\pi} P \int_{-\infty}^{\infty} (A\cos(\omega t+\omega\tau+\Phi)/-\tau)d\tau \tag{7c}$$

$$= \frac{A}{\pi} P \int_{-\infty}^{\infty} (\cos(\omega t+\Phi)\cos\omega\tau/-\tau)d\tau \tag{7d}$$

$$- \frac{A}{\pi} P \int_{-\infty}^{\infty} (\sin(\omega t+\Phi)\sin\omega\tau/-\tau)d\tau \quad . \tag{7e}$$

Since $\cos(\omega\tau)/\tau$ is and odd function, the first integral in the above equation is zero, and

$$\hat{x}(t) = \frac{A}{\pi} P \int_{\infty}^{\infty} (\sin(\omega\tau)/\tau)d\tau \cdot \sin(\omega t+\Phi) \tag{7f}$$

$$= A\sin(\omega t+\Phi) \tag{7g}$$

This result will be helpful in later analysis.

In another approach, $\hat{x}(t)$ may be regarded as the response of a (non-realizable) linear filter to $x(t)$. This Hilbert

transform filter has impulse response $1/\pi t$ and transfer function $-j\mathrm{sgn}(f)$ (Kuo and Freeny, 1962; Schwartz et al., 1966), where $j=\sqrt{-1}$ and sgn(f) is defined as

$$\mathrm{sgn}(f) = \begin{cases} 1 & f>0 \\ 0 & f=0 \\ -1 & f<0 \end{cases} .$$

So, if X(f) is the Fourier transform of x(t), then

$$\hat{X}(f) = -j\mathrm{sgn}(f)\cdot X(f) \tag{8}$$

and

$$\hat{x}(t) = (1/\pi t)*x(t) , \tag{9}$$

where * denotes the convolution.
Other properties of Hilbert transform are discussed in the literatures dealing with communication theory.

Now let us discuss the meaning of the analytic signal. The analytic signal representation of a real waveform was first introduced by Gabor (1946), and is now used widely in communication theory as a means of representing band-pass signals. The analytic signal z(t) of a real waveform x(t) - sometimes referred to as the pre-envelope and the complex signal - is defined as (Kuo and Freeny, 1962; Schwartz et al., 1966)

$$z(t) = x(t)+j\hat{x}(t) , \tag{10}$$

where $\hat{x}(t)$ is the Hilbert transform of x(t) ($\hat{x}(t)$ is sometimes called the quadrature function of x(t) in this case). Equation (10) can be expressed in another form,

$$z(t) = A(t)e^{j\theta} , \tag{11}$$

where

$$A(t) = |z(t)| = (x(t)^2+\hat{x}(t)^2)^{1/2} \tag{12}$$

and

$$\theta = \tan^{-1}(\hat{x}(t)/x(t)). \tag{13}$$

$A(t)$ is the amplitude, θ the instantaneous phase, and the time derivative of θ the instantaneous frequency of the analytic signal $z(t)$ (Schwartz et al., 1966).

IV. The Determination of Period by the Hilbert Transform Method

In section II, we have shown that an oscillation recorded by the Doppler technique is caused by a cosinusoid described by (4): $x(t) = A\cos(\omega t+\Phi)$. From (7g), the Hilbert transform of $A\cos(\omega t+\Phi)$ is $\hat{x}(t) = A\sin(\omega t+\Phi)$. Therefore, the analytic signal representation of $x(t)$ is, from (10)

$$z(t) = A\cos(\omega t+\Phi)+Aj\sin(\omega t+\Phi) \tag{14}$$

From (13) and (14), the instantaneous phase is

$$\theta = \tan^{-1}(\sin(\omega t+\Phi)/\cos(\omega t+\Phi))$$

$$= \tan^{-1}(\tan(\omega t+\Phi))$$

$$\therefore \theta = \omega t+\Phi \quad . \tag{15}$$

Differentiating both sides of (15) with respect to time t, we find that the frequency ω of $x(t)$ is equal to the instantaneous frequency of its analytic signal representation, since Φ is independent of t. That is, finding the frequency ω is the same as finding the instantaneous phase of the analytic signal, and then calculating its time derivative. So, the problem reduces to one of determining the instantaneous phase.

Now, let us transform the analytic signal into the frequency domain,

$$Z(f) = X(f)+j\hat{X}(f) \tag{16}$$

where $Z(f)$ is the Fourier transform of $z(t)$. From (8)

$$\hat{X}(f) = -j\,\mathrm{sgn}(f)\cdot X(f) \ ,$$

so $Z(f) = X(f)+j(-jsgn(f)\cdot X(f))$

$= X(f)+sgn(f)X(f)$

$$\therefore Z(f) = \begin{cases} 2X(f) & f>0 \\ X(f) & f=0 \\ 0 & f<0 \end{cases} \quad (17)$$

Therefore, it follows that the instantaneous phase of the analytic signal representation z(t) of a real signal x(t) can be determined using the following algorithm:

1. Transform x(t) into X(f),
2. Cancel the negative frequency terms and multiply the positive frequency terms by 2. This will give Z(f),
3. Transform Z(f) back into z(t) and plot θ, the instantaneous phase.

V. Practical Consideration

Since Fourier transform is involved in the computation of an analytic signal, a computer is convenient. At present, the most efficient way of doing Fourier transform is by using the Fast Fourier Transform (FFT) routine on a digital computer. Detailed description of writing and using the FFT routine is given by Brigham (1974).

In using a digital computer to calculate the analytic signal representation of a whole Doppler record, it is possible to input the whole Doppler record at one time and display the result by plotting the instantaneous phase as a function of time (i.e., using the same time axis as the Doppler record). Then, by taking the time derivative or the slope of the phase plot, the period at any time can be determined.

Techniques of proper handling a waveform in digital Fourier Transform analysis are discussed in many literatures. Since a continous Doppler record must be sampled discretely

in order to utilize a digital computer, the limitations due to the effect of sampling must be observed: The sampling theorem - a waveform x(t) should be sampled at a frequency of at least twice the largest frequency component of x(t) - must not be violated. Aliasing and leakage must be avoided. Two additional important points in finding the analytic signal are:

1. In the process of finding the analytic signal, the negative frequency terms are truncated. Discontinuity may occur at zero frequency and thus may violate the sampling theorem. So the zero frequency term should be filtered out or kept to a minimum before doing the inverse transform.
2. Since the calculation of the analytic signal of a waveform effectively involves convolution of the waveform with the slowly decaying kernel $1/\pi t$ of the Hilbert transform, the analytic signal representation will be unreliable near the beginning and end of the waveform (White and Cha, 1973).

Two examples of period determination by means of the analytic signal are given below. The first involves a sinusoid of a known period T, as shown in Figure 1. The instantaneous phase plot is given in Figure 2. By taking the time derivative of the phase plot, one can show that the instantaneous frequency found in Figure 2 is exactly equal to the frequency of the sinusoid in (1). The second example involves the 10 MHz. Doppler record obtained from the Radioscience Laboratory of the University of Hawaii at Manoa shortly after the Hachinohe, Japan earthquake of May 16, 1968. The Doppler record is shown in Figure 3 and its instantaneous phase plot is in Figure 4. One can determine the frequency at one time by measuring the slope of the phase plot at the time.

VI. Discussion

Without a digital computer, the determination of period by the Hilbert transform method becomes extremely difficult if not

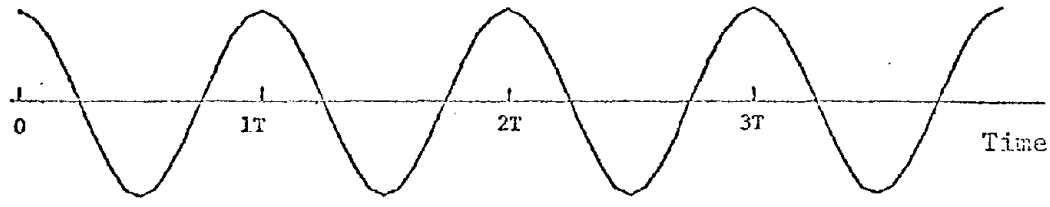

Figure 1. A Sinusoid with a constant Period T.

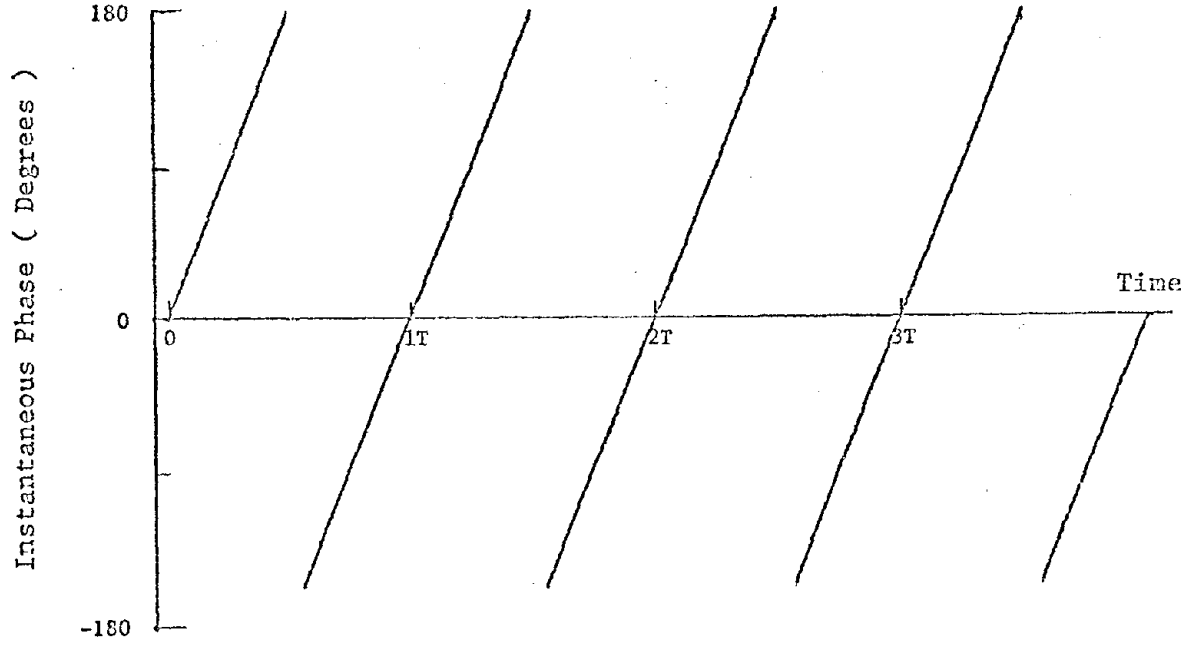

Figure 2. Instantaneous Phase Plot of the Sinusoid with Period T.

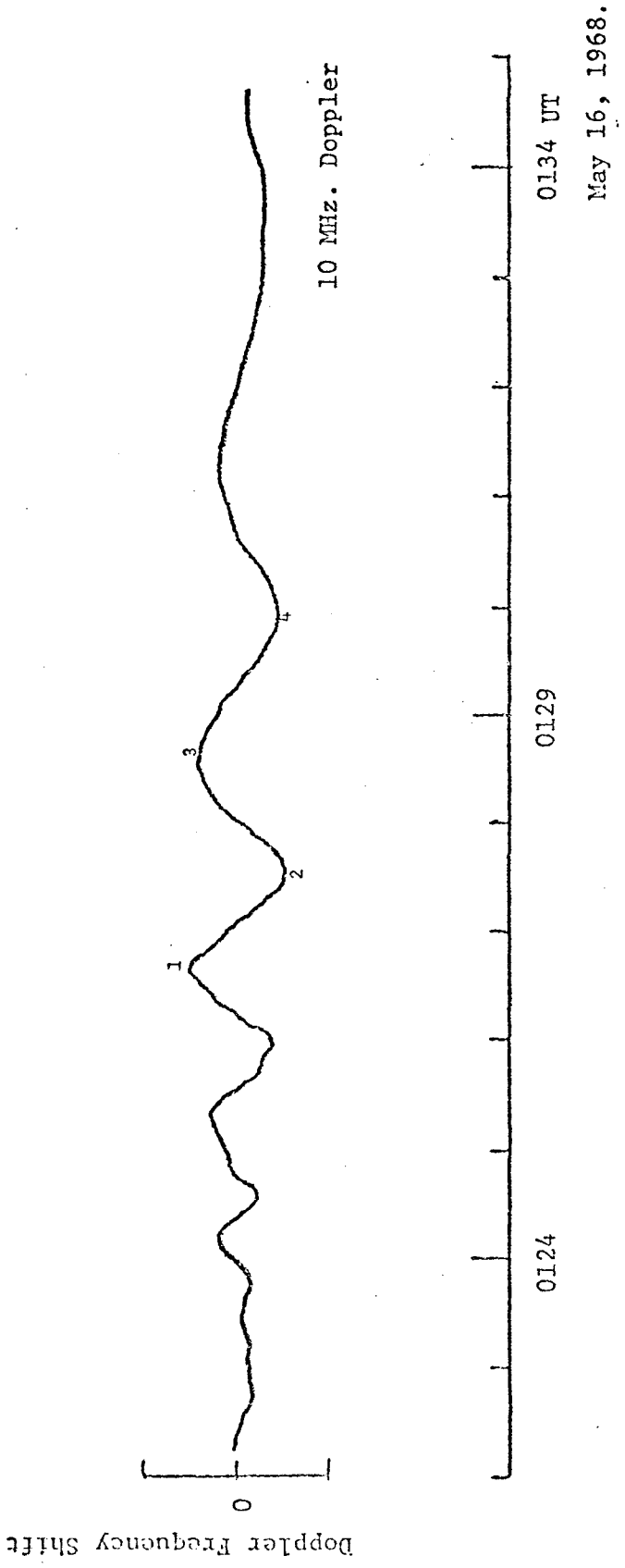

Figure 3. Doppler Shift Record from the Hachinohe, Japan Earthquake.

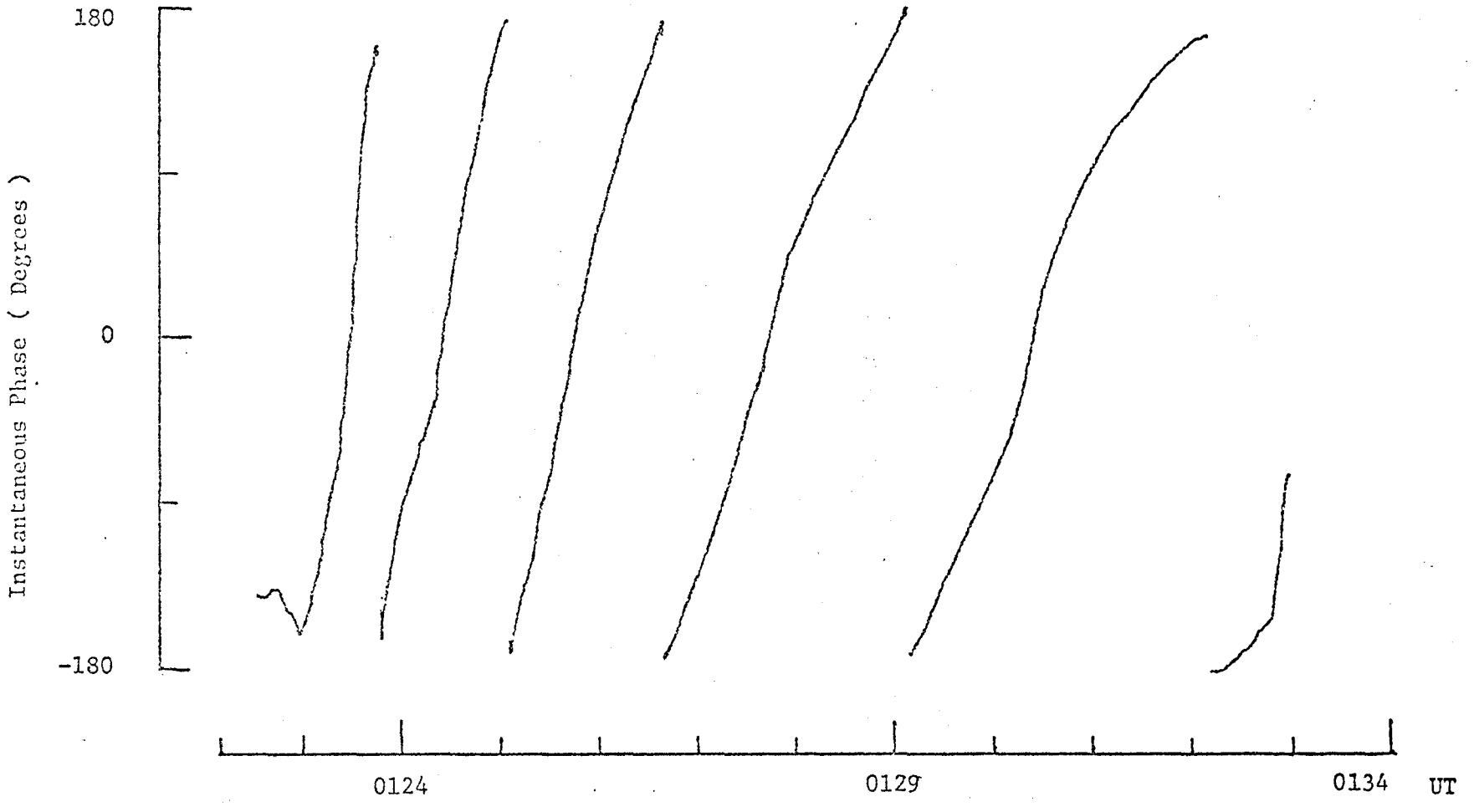

Figure 4. Instantaneous Phase Plot of the 10 MHz. Doppler Record from the Hachinohe, Japan Earthquake.

impossible. Although the analytic signal representation of a waveform was introduced many years ago, the expensiveness and the inefficiency of an early digital computer would certainly have hindered any attempt to use the analytic signal representation in time series analysis. With the introduction of FFT in 1965 and the unprecedented low price and high speed of mini-computers today, the determination of the period of a Doppler record by this method has become feasible. For example, the entire process from digitizing the Doppler record in Figure 3 to plotting the instantaneous phase in Figure 4 takes about 10 minutes using a Hewlett Packard programmable desk calculator system.

Traditionally, the period of the oscillations recorded by seismometers and by Doppler technique has been determined by the so-called "peak and trough" method. A description of this method may be found in Pekeris (1948) and Ewing and Press (1954). Briefly, one reads off the time T_n of the n-th maximum or minimum, and plots T_n against n. Then a smooth and continuous curve is drawn through the plotted points. The period at time T_n is obtained by measuring the slope of the curve at T_n. The crucial step in this method is the fitting of a curve to the plotted points. Since there is no standard way of fitting a curve (a least square fit may not be the best), error may be introduced. Figure 5 shows the curve obtained by applying the "peak and trough" method to the Doppler record in Figure 3. The periods of the labelled peaks and troughs obtained from Figure 4 together with those obtained from Figure 5 are entered into Table 1.

By comparing the two rows of values in Table 1, one can see that they are different for every event. There is no systematic error in going from Event 1 to Event 4: the values of Event 1 and Event 2 obtained by using the Hilbert transform method are smaller than those obtained by using the "peak and trough" method, but the values of Event 3 and Event 4 obtained by using the Hilbert transform method are greater than those obtained by using the "peak and trough" method. The differences between the values obtained from the two methods for Events 1, 2, and 4 are small and can be accounted for by errors introduced when measuring the slope

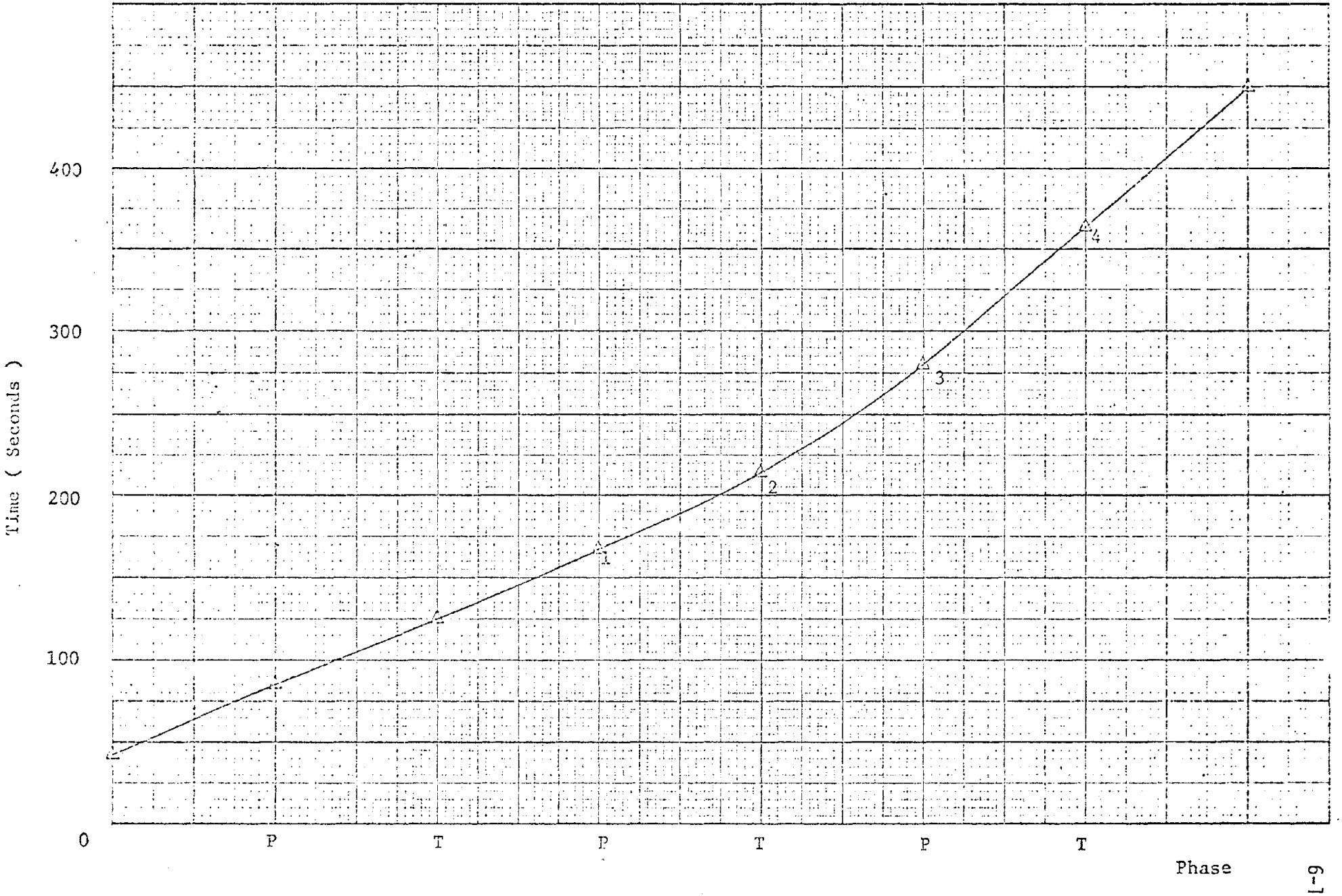

Figure 5. Arrival-time curve of the 10 MHz. Doppler Record from the Hachinohe, Japan Earthquake.

P = Peak, T = Trough.

Event		1	2	3	4
Period (seconds)	Hilbert Transform Method	80	108	170	173
	Peak and Trough Method	85	114	151	170

Table 1. Periods of labelled events obtained by using two different methods.

of the instantaneous phase plot. But there is a substantial difference between the values for Event 3. One possible explanation for this difference is the error introduced when fitting a curve to the plotted points in the "peak and trough" method as mentioned earlier in this section. Obviously, one advantage of the Hilbert transform method over the "peak and trough" method is that no curve fitting is necessary. But without exhaustive error analysis - which we shall not discuss in this paper due to its complexity - it is difficult and premature to judge which method gives the better result.

References

Brigham, E. O., The Fast Fourier Transform, Prentice-Hall Inc., 1974.

Brune, J. N., J. E. Nafe, and J. E. Oliver, A Simplified Method for Analysis and Synthesis of Dispersed Wave Trains, J. Geophys. Res., 65, 287, 1960.

Davies, K., Ionospheric Radio Waves, Blaisdell Publishing Company, 1969

Ewing, M., and F. Press, An Investigation of Mantle Rayleigh Waves, Bull. Seismol. Soc. Am., 44, 127, 1954.

Furumoto, A. S., Ionospheric Recordings of Rayleigh Waves For Source Mechanisms, Tsunamis in the Pacific Ocean, Proceedings of International Symposium on Tsunami and Tsunami Research, University of Hawaii, East-West Center Press, 1970.

Gabor, D., Theory of Communication, J.I.E.E., 93, 429, 1946.

Kuo, F. F., and S. L. Freeny, Hilbert Transforms and Modulation Theory, Proc. Nat. Electron. Conf., 51, Chicago, 1962.

Najita, K., P. F. Weaver, and P. C. Yuen, A Tsunami Warning System Using an Ionospheric Technique, Proc. IEEE, 62, 563, 1974.

Pekeris, C. L., Theory of Propagation of Explosive Sound in Shallow Water, Geol. Soc. Am. Mem., 27, 1948.

Schwartz, M., W. R. Bennett, and S. Stein, Communication Systems and Techniques, 29, McGraw-Hill, 1966.

White, O. R., and M. Y. Cha, Appendix to Analysis of the 5 Min. Oscillatory Photospheric Motion, Solar Physics, 31, 42, 1973.

Yuen, P. C., P. F. Weaver, and R. K. Suzuki, Continuous, Traveling Coupling between Seismic Waves and the Ionosphere Evident in May 1968 Japan Earthquake Data, J. Geophys. Res., 74, 2256, 1969.

APPENDIX 7
METHOD OF DETERMINING THE INITIAL PHASE OF THE SOURCE OF AN EARTHQUAKE FROM THE DOPPLER RECORDS

Introduction

Rayleigh waves from large earthquakes generate acoustic waves up into the atmosphere and cause delayed oscillations in the ionosphere. These oscillations were confirmed experimentally (Yuen et al., 1969) by employing the Doppler technique.

Doppler records obtained after the Kurile Island Earthquake on August 11, 1969, had been investigated in detail and a method was suggested by Dr. A. S. Furumoto (1970) relating data obtained from the Doppler record to the initial phase of the source.

In this report, a few modifications on the process of locating the initial phase of the source of an earthquake are discussed. Examples are given to illustrate the modifications.

Outline of Furumoto's Method

The details pertaining to Furumoto's method will not be reproduced here. The reader is referred to Furumoto's paper (1970) for a complete picture of the method. However, an outline of his method is given below for the purpose of comparison. The outline is divided into seven steps for easy identification:

1. Identify and label peaks and troughs on the Doppler record. For example, a trough that appeared first on the Doppler record is labelled as Event 1.
2. Find out the time of arrival of each event and determine the period associated with each event using the Peak and Trough method (Ewing and Press, 1954). The time of arrival of an event is the arrival time of the Rayleigh-acoustic waves at the ionospheric reflector.
3. From the data given by Ben-Menahem and Toksoz (1962), determine the phase velocity that corresponds to each event.
4. Tabulate the period, character, phase velocity and the time lag of each event. The time lag of an event is the difference in time between the event and Event 1.
5. Estimate the location where the Rayleigh-acoustic refraction from the ground took place. This location is called the launching point for the Rayleigh-acoustic wave. Also, find out the epicentral distance -

distance between the epicenter of an earthquake and the sub-ionospheric point.

6. Construct wave trains of all the events at the time when Event 1 reached the launching point. At that time, other events were behind Event 1 at a distance equal to the product of phase velocity and time lag. The wave trains are constructed from the launching point back towards the epicenter until a distance is found where the phases from all the trains are in agreement. This is the initial phase of the wave components.
7. When a wave leaves a source, there is an advance of $\pi/4$ in phase for normal branch of dispersion ($dV/dT > 0$, V = group velocity, T = period) (Brune et al., 1961). Hence, the initial phase of the source is $\pi/4$ behind the initial phase of the wave components.

Modifications

A. Estimation of travel time required and horizontal distance elapsed for the Rayleigh-acoustic wave to refract from the launching point up to the ionospheric reflector.

Ray tracing on the Rayleigh-acoustic wave was done by the staff of the Radioscience Laboratory using an IBM 360 computer. Phase velocities were used in the calculation. The results are displayed in Figure 1 and Figure 2. Figure 1 shows the delay time as a function of height and period. Figure 2 shows the horizontal range elapsed as a function of height and period. For a fixed height, a curve showing the relationship between the period and the horizontal range can be constructed using data from Figure 1 and Figure 2 respectively. For example, Figure 3 shows the delay time for different periods of Rayleigh-acoustic wave to reach an altitude of 300 kilometers, and Figure 4 shows the horizontal distance elapsed for that altitude. The curve showing the delay time as a function of period is used to correct the time lag in Step 4 of Furumoto's method, and the curve showing the horizontal range elapsed is used to determine the accurate location of the launching point in Step 5.

B. Location of the initial phase on a wave train plot.

A different approach is introduced here for locating the initial phase on a wave train. In the wave train plot in Step 6, the abscissa represents the straight line path on the earth's surface passing through the epicenter and the launching point. Since the wave train is plotted in a triangular

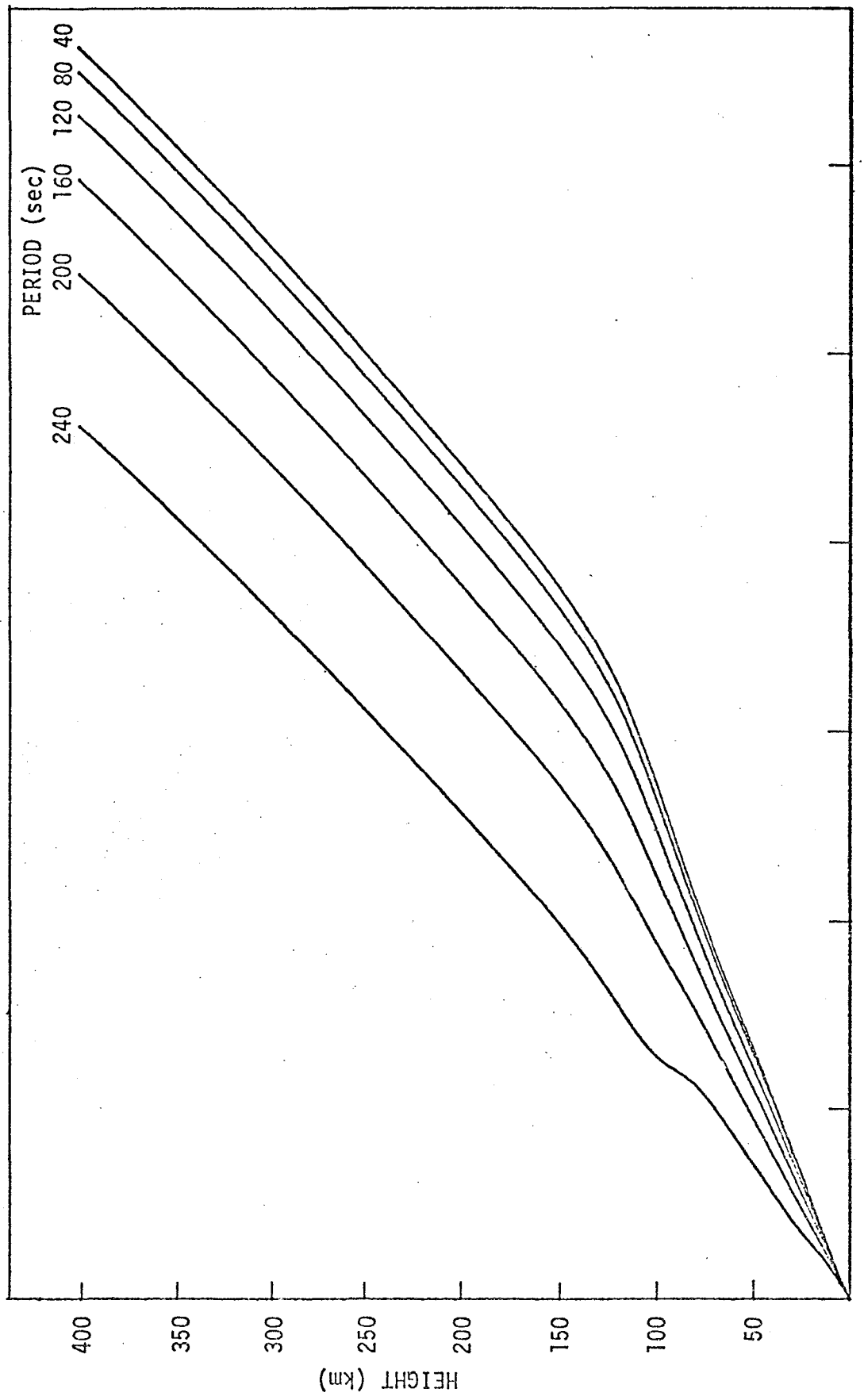

Figure 1. Travel time along ray-paths as a function of height and period.

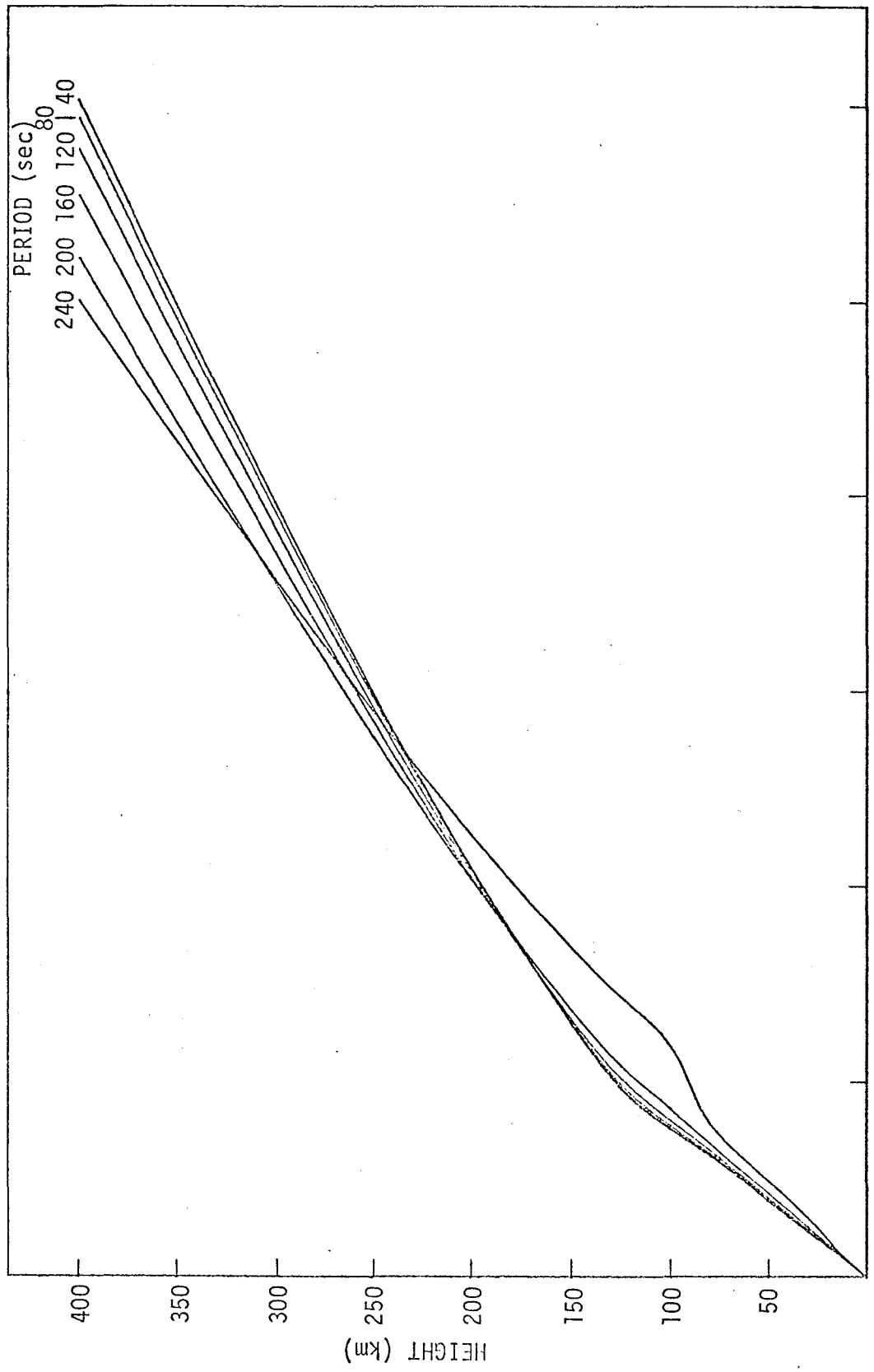

Figure 2. Ray-paths for infrasonic waves parameterized in terms of periods.

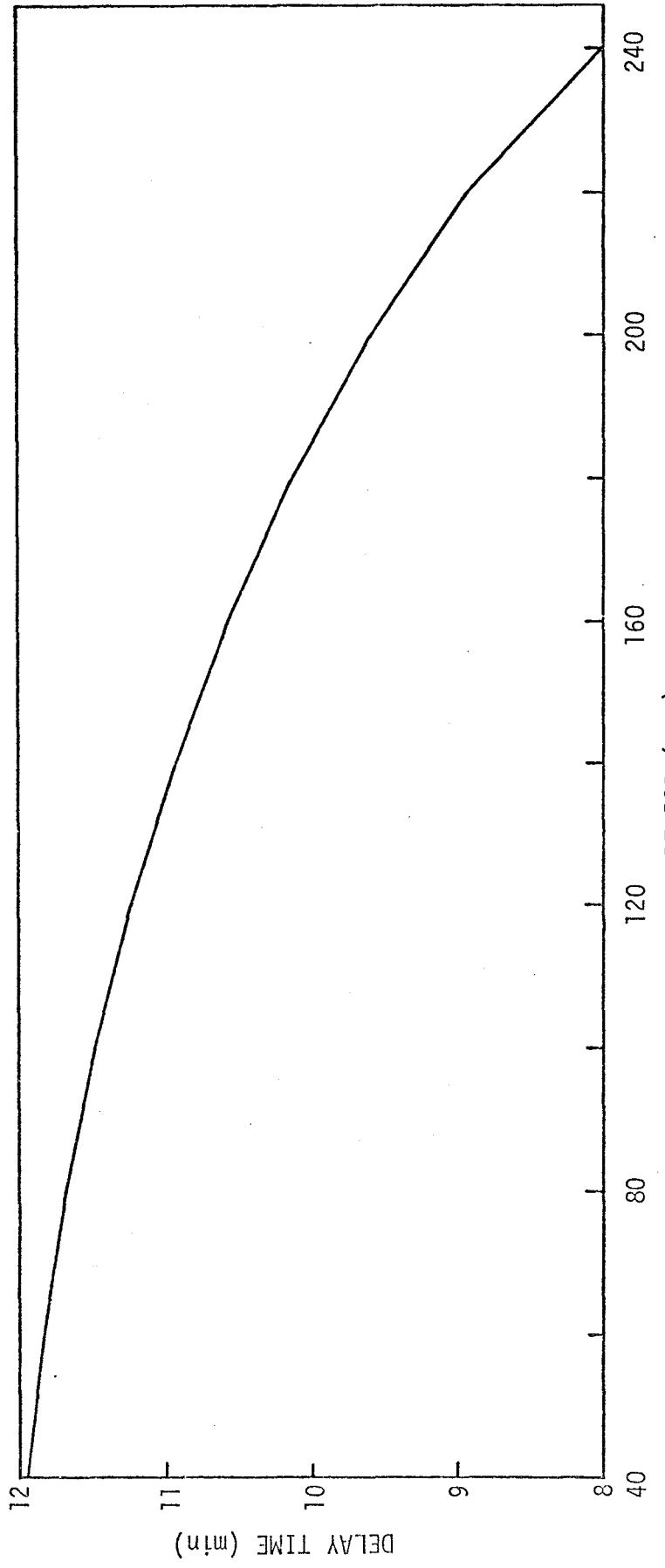

Figure 3. Delay time as a function of period.

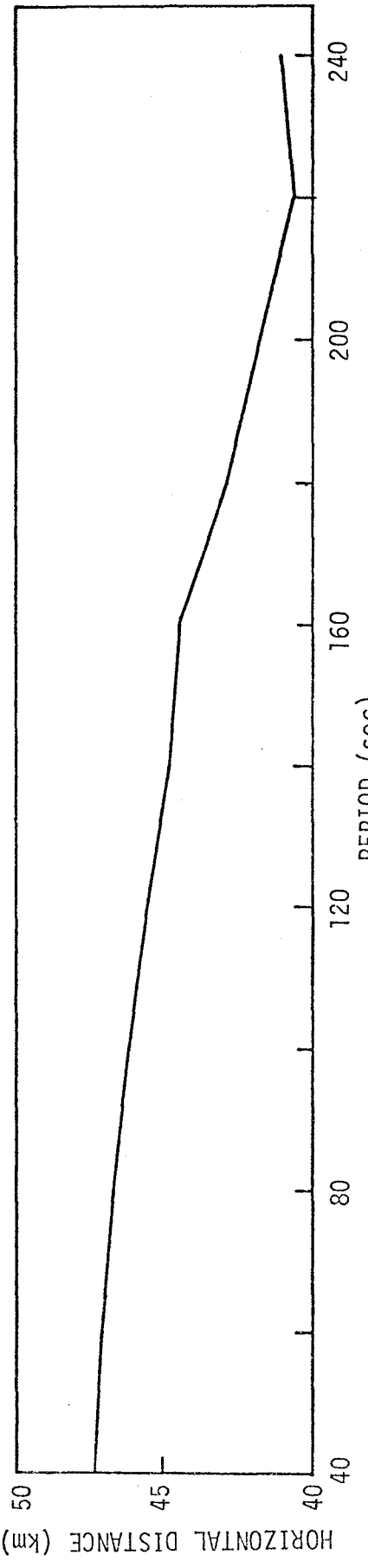

Figure 4. Horizontal displacement as a function of period.

wave pattern with constant amplitude, the ordinate has no meaning except in identifying the pase at a certain location. So, the wave train plot represents the phase variation with respect to distance of a component of the Rayleigh wave packet at a certain instant of time.

When an earthquake occurred, assume it occurred at time t_o, a Rayleigh wave packet was generated from the epicenter. This wave packet can be Fourier analyzed showing an infinite number of wave components with different periods but have the same initial phase. Since the medium is dispersive, they have different phase velocities. The phase velocity V_p of a wave component with certain period can be estimated readily from Figure 2 given in Dorman (1969) or from data given by Ben-Menahem and Toksoz (1962), it is therefore possible to calculate the distance d the initial phase has travelled in a certain period of time t by the simple equation

$$d = V_p t.$$

Since all the wave trains are plotted at the time when Event 1 reached the launching point, let this time be t_1, therefore $t = t_1 - t_o$, and the distance d of the initial phase from the epicenter can be determined:

$$d = V_p(t_1 - t_o).$$

Once the location of the epicenter is known, this distance can be located on the wave train plot to give the initial phase.

C. Initial phase of the source.

A Doppler record shows the Doppler frequency shift with respect to time. In order to apply the $\pi/4$ phase shift mentioned in Step 7, the Doppler record must be translated into a displacement curve. In translating the Doppler record into a displacement curve, there is an advance of $\pi/2$ in phase as shown in Figure 5. Together with the $\pi/4$ advance in phase when a wave leaves a source, the total change in phase is $\pi/4$ when relating the Doppler record to the source. Hence, the initial phase of the source is $\pi/4$ in advance of the initial phase obtained from a wave train plot.

Examples

The August 11, 1969 Kurile Earthquake was used by Dr. Furumoto to illustrate his method. So data from the same earthquake are used here to illustrate the suggested modifications.

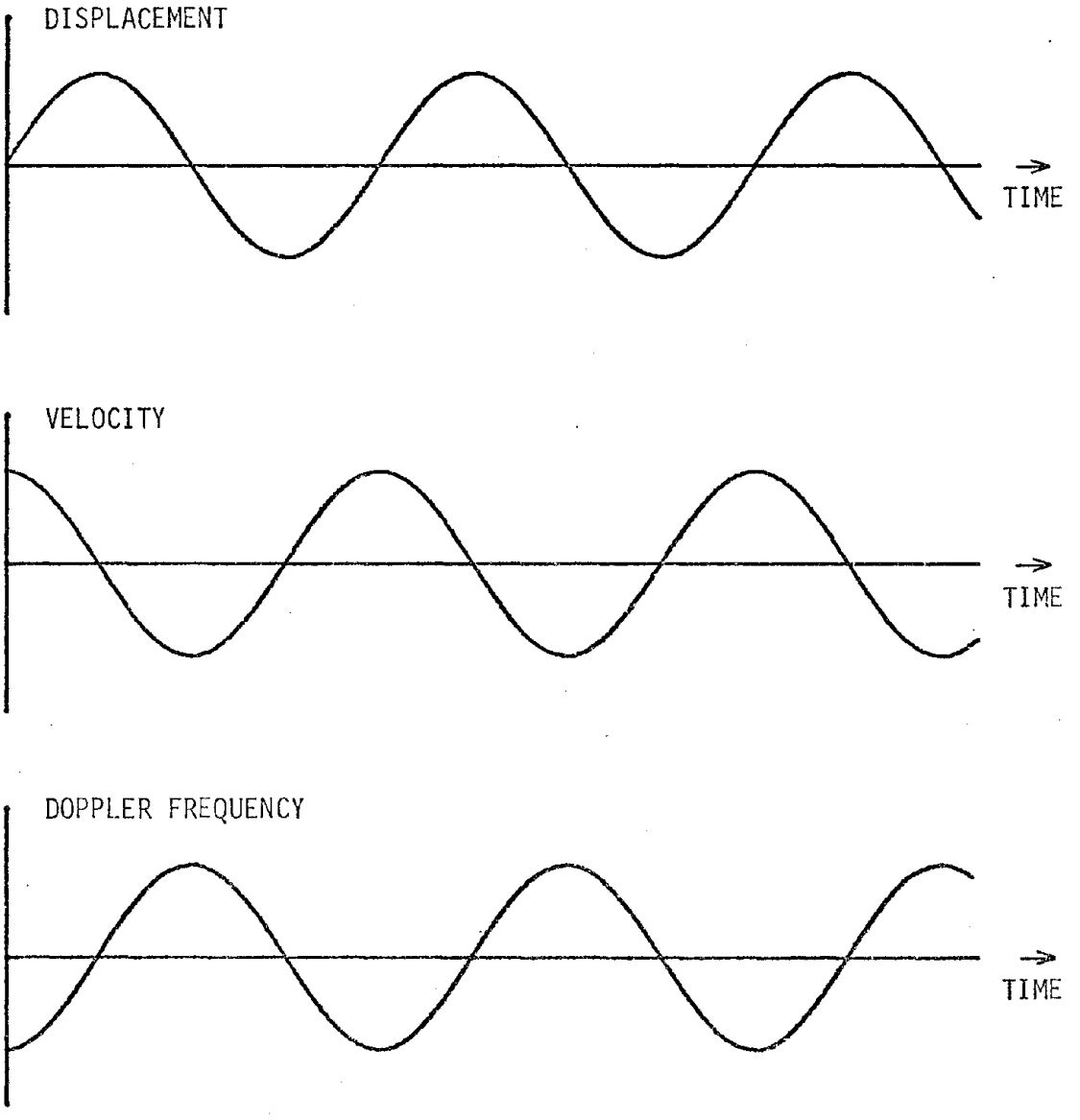

Figure 5. Phase difference between the displacement curve and the Doppler record.

The August 11, 1969 Kurile Earthquake was used by Dr. Furumoto to illustrate his method. So data from the same earthquake are used here to illustrate the suggested modifications.

The 10 MHz Doppler record obtained shortly after the Kurile Earthquake is shown in Figure 6. One can notice that the long period peaks and troughs are labelled. Table 1 shows all the data needed for constructing the wave trains and for locating the initial phase on each wave train. Values in column A through D of Table 1 are obtained directly from Table 1 found in Furumoto's paper (1970). In column E, values of the delay time are obtained from Figure 3. In column F, values of the horizontal distance elapsed are obtained from Figure 4. Time of arrival in column G is obtained directly from the Doppler record shown in Figure 6. Column H shows the time when the acoustic wave was launched. In column I, the distance compensation represents the distance of an event from the launching point of Event 1. Column J gives the wave length and column K the distance of initial phase from the epicenter of an event. Figure 7 is the wave train plot based on data from Table 1. In constructing the wave train plot, the epicenter is used as the reference point. The launching point for Event 1 is located by measuring the distance of the launching point from the epicenter. Triangular wave train is then constructed starting from the launching point. The location of the initial phase is then determined by measuring the distance between the initial phase and the epicenter. The above procedure is repeated for other events. The arrows in Figure 7 indicate the locations of the initial phase. All events except event 2 show good agreement in initial phase.

Another example is given here. Figure 8 shows the 10 MHz Doppler records from the Hachinohe, Japan Earthquake of May 16, 1968 with the peaks and troughs labelled. Table 2 gives all the data needed for the wave train plot. The plot is shown in Figure 9. Again, all the events show an astoundingly good agreement in initial phase.

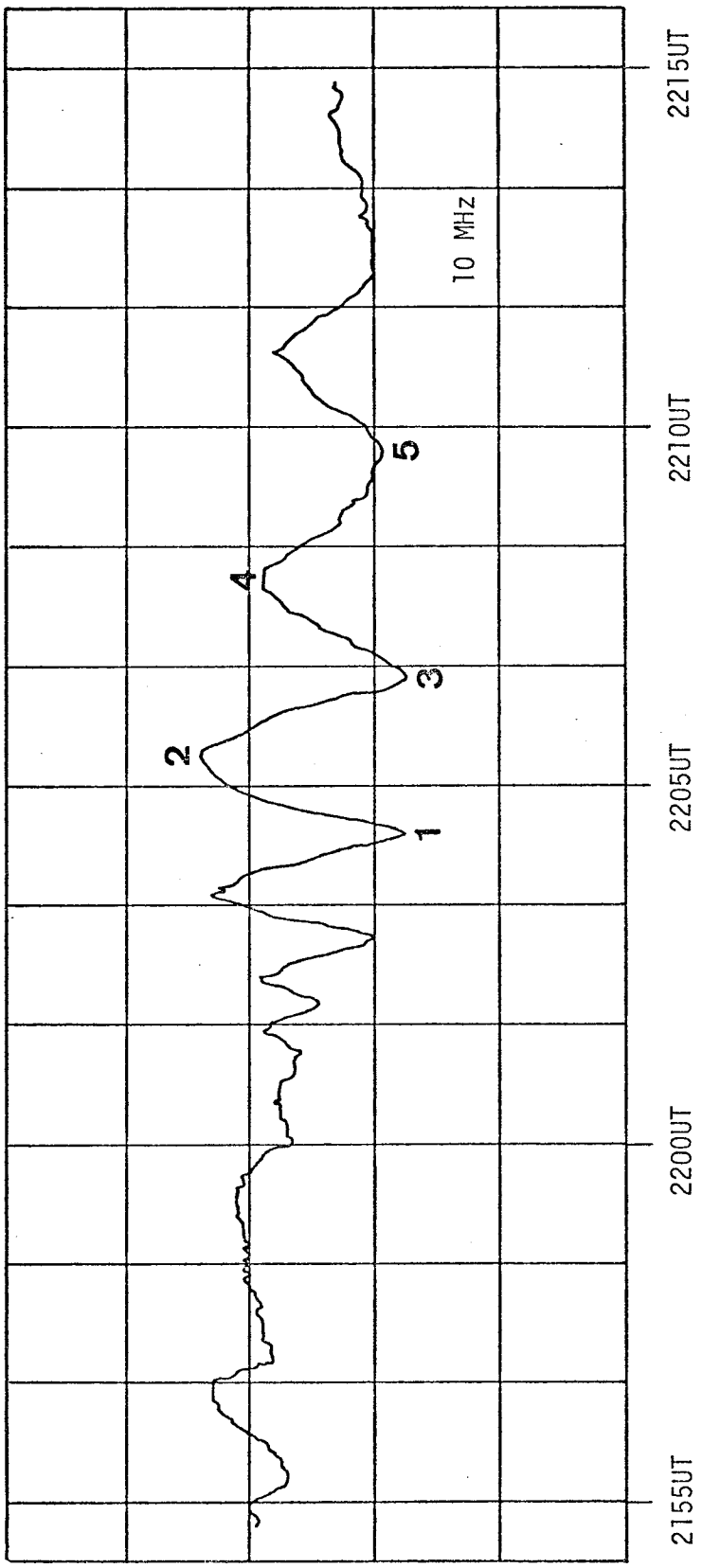

Figure 6. Doppler shift record from the Kurile Earthquake, August 11, 1969.

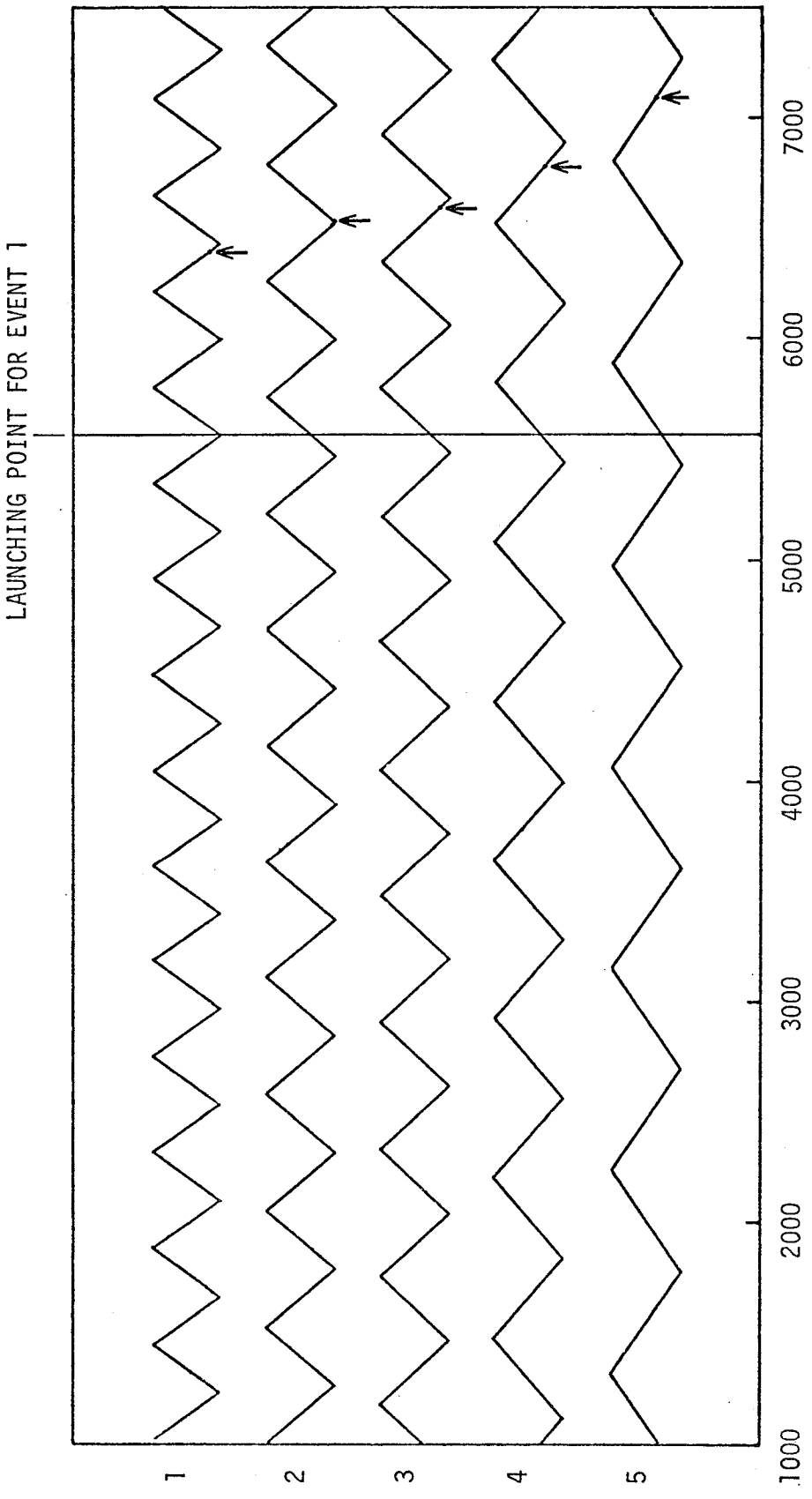

Figure 7. Wave trains from the Kurile Earthquake, August 11, 1969. The arrows indicate the locations of initial phase.

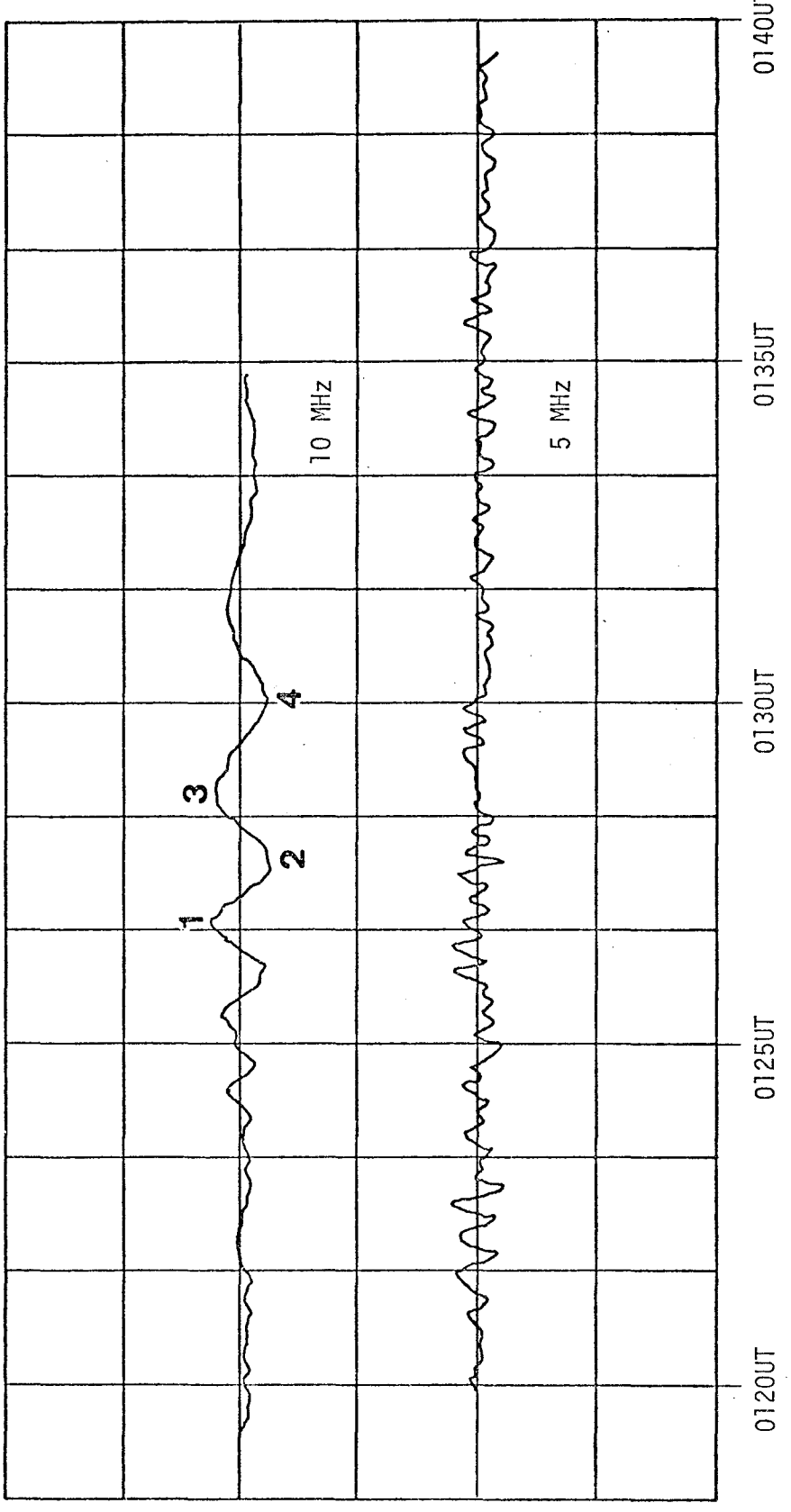

Figure 8. Doppler shift record from the Hachinohe, Japan Earthquake, May 16, 1968.

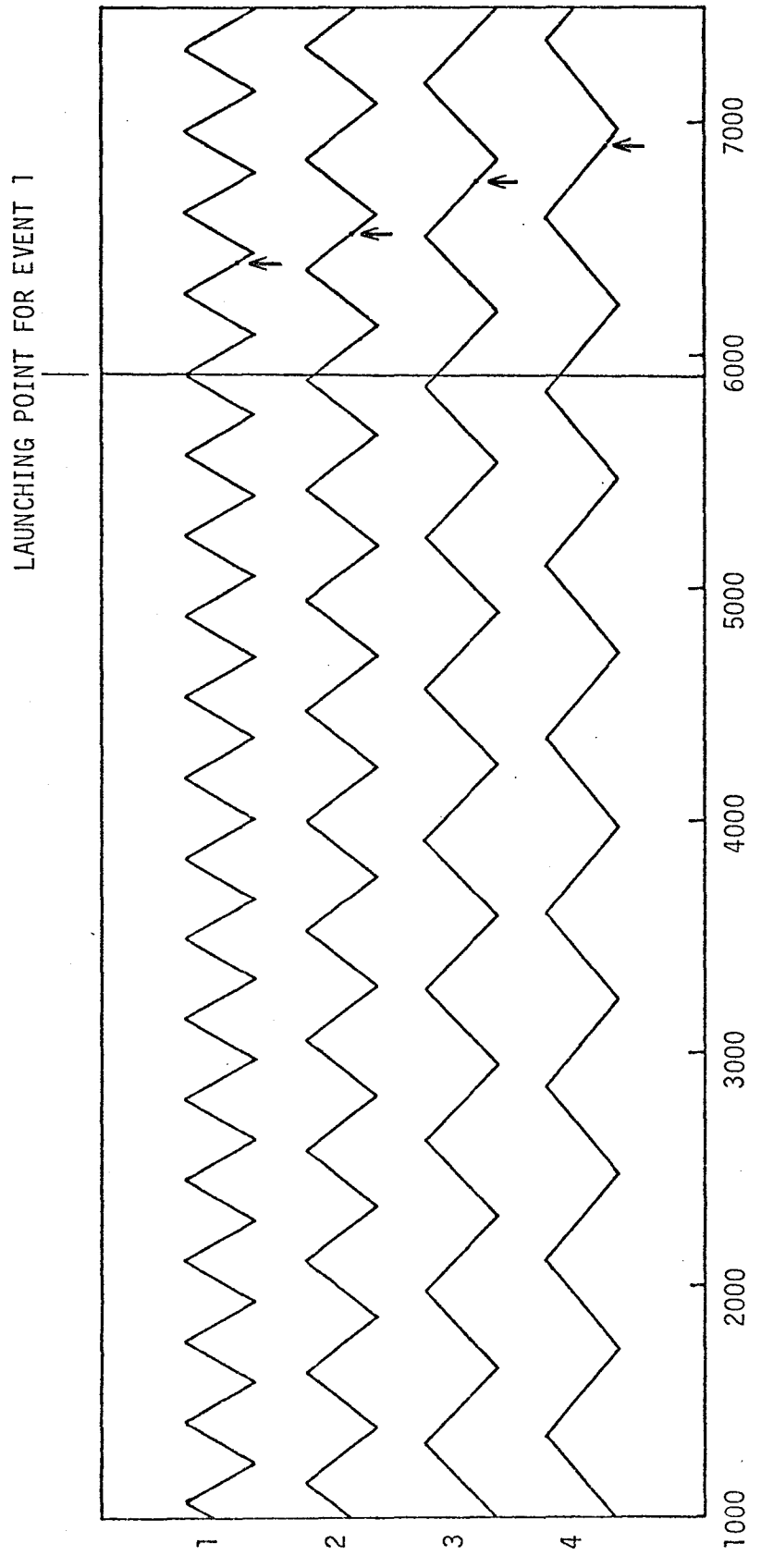

Figure 9. Wave trains from Hachinohe, Japan, Earthquake, May 16, 1968. The arrows indicate the locations of initial phase.

A	B	C	D	E	F	G	H	I	J	K
Event	Period (sec.)	Character	Phase Vel. (km/sec.)	Delay Time (min.)	Horizontal Distance (km)	Time of Arrival (UT)	Time Acoustic Wave Was Launched (UT)	Distance Compensation (km)	Wavelength (km)	Distance of Initial Phase
1	105	Trough	4.116	11.44	46.0	22:04:20	21:52:54	0	432.18	6396.26
2	125	Peak	4.205	11.18	45.3	22:05:30	21:54:19	356.73	525.63	6534.57
3	135	Trough	4.249	11.02	45.0	22:06:30	21:55:29	657.60	573.62	6602.94
4	165	Peak	4.365	10.47	44.0	22:08:00	21:57:32	1211.47	720.23	6783.21
5	200	Trough	4.566	9.60	41.7	22:09:40	22:09:40	1959.08	913.20	7095.56

Table 1. Data for constructing the wave trains of Rayleigh wave components from Kurile Earthquake, August 11, 1969.

Note: Time earthquake occurred 2127 UT.
Distance between epicenter and sub-ionospheric point: 5615 km.
H = G - E, I + D(H - 21:52:54) - (46.0 - F), J = BD, K = (21:52:54 - 21:27:00)D

A	B	C	D	E	F	G	H	I	J	K
Event	Period (sec.)	Character	Phase Vel. (km/sec.)	Delay Time (min.)	Horizontal Distance (km)	Time of Arrival (UT)	Time Acoustic Wave Was Launched (UT)	Distance Compensation (km)	Wavelength (km)	Distance of Initial Phase (km)
1	85	Peak	4.08	11.63	46.6	01:26:48	01:15:10	0	346.80	6405.60
2	114	Trough	4.16	11.32	45.7	01:27:33	01:16:14	263.80	474.24	6531.20
3	151	Peak	4.30	10.75	44.6	01:28:40	01:17:55	706.65	649.30	6751.00
4	170	Trough	4.40	10.36	43.6	01:30:05	01:19:43	1199.07	748.00	6908.00

Table 2. Data for constructing the wave trains of Rayleigh wave components from Hachinohe, Japan Earthquake, May 16, 1968.

Note: Time earthquake occurred: 0049 UT
Distance between epicenter and sub-ionospheric point: 5975 km.

REFERENCES

Ben-Mehahem, A., and M.N. Toksoz, Source-mechanism from spectra of long period seismic surface waves, J. Geophys. Res., 67, 1943, 1962.

Brune, J. et al., The polar shift of surface waves on a sphere, Bull. Am. Seism. Soc., 51(2), 247(1961).

Dorman, J. seismic surface wave data on the upper mantle, Geophys. Monog., 13, Am. Geophys. Union, 1969.

Ewing, M. and F. Press, An investigation of mantle Rayleigh waves, Bull. Seismol. Soc. Am., 44, 127, 1954.

Furumoto, A.S., Tsunamis in the Pacific Ocean, Proceedings of International Symposium on Tsunami and Tsunami Research, University of Hawaii, 1970.

Yuen, P.C., P.F. Weaver and R.K. Suzuki, Continuous, traveling coupling between seismic waves and the ionospheric evident in May 1968 Japan Earthquake data, J. Geophys. Res., 74, 2256, 1969.